Circuit mechanisms for encoding discriminative learning in the dorsal prefrontal cortex of behaving mice

Mattia Aime

université de BORDEAUX

THÈSE PRÉSENTÉE

POUR OBTENIR LE GRADE DE

DOCTEUR DE

L'UNIVERSITÉ DE BORDEAUX

ÉCOLE DOCTORALE

SCIENCES DE LA VIE ET DE LA SANTE

Neurosciences

Par Mattia AIME

Circuit mechanisms for encoding discriminative learning in the dorsal prefrontal cortex of behaving mice

Sous la direction de : Dr. Frédéric GAMBINO

Soutenue le 30 novembre 2017

Membres du jury :

M. FRICK, Andreas	DR	Bordeaux (FR)	Président
M. ADAMANTIDIS, Antoine	Prof	Bern (CH)	Rapporteur
Mme ROCHEFORT, Nathalie	Prof	Edinburgh (UK)	Rapporteur
M. FOSSAT, Pascal	MCF	Bordeaux (FR)	Examinateur
M. CHARLET, Alexandre	CR	Strasbourg (FR)	Examinateur

université de BORDEAUX

THÈSE PRÉSENTÉE

POUR OBTENIR LE GRADE DE

DOCTEUR DE

L'UNIVERSITÉ DE BORDEAUX

ÉCOLE DOCTORALE

SCIENCES DE LA VIE ET DE LA SANTE

Neurosciences

Par Mattia AIME

Circuit mechanisms for encoding discriminative learning in the dorsal prefrontal cortex of behaving mice

Sous la direction de : Dr. Frédéric GAMBINO

Soutenue le 30 novembre 2017

Membres du jury :

M. FRICK, Andreas	DR	Bordeaux (FR)	Président
M. ADAMANTIDIS, Antoine	Prof	Bern (CH)	Rapporteur
Mme ROCHEFORT, Nathalie	Prof	Edinburgh (UK)	Rapporteur
M. FOSSAT, Pascal	MCF	Bordeaux (FR)	Examinateur
M. CHARLET, Alexandre	CR	Strasbourg (FR)	Examinateur

Table of contents

1. Résumé en français

Codage neuronal de l'apprentissage discriminatif dans le cortex préfrontal des souris vigiles

Chez les mammifères, le néocortex constitue une structure remarquablement plastique assurant leurs multiples capacités d'adaptation et d'apprentissage. Par exemple, l'apprentissage associatif permet à chaque individu d'apprendre les relations entre un événement particulier (un danger par exemple) et les signaux environnementaux qui y sont associés, afin d'en anticiper les conséquences s'il se reproduit dans le futur. Dans le cas de la peur conditionnée, l'apprentissage associatif améliore les capacités de discrimination des signaux de menace et de sécurité, garantissant ainsi une représentation précise de l'environnement. Ce processus comportemental est en partie dépendent de l'interaction entre deux structures cérébrales: le cortex préfrontal (PFC) et le complexe basolatéral de l'amygdale (BLA). Bien que le PFC pourrait encoder à la fois les mémoires de menace et de sécurité qui seraient recrutées préférentiellement après l'apprentissage, on ignore toujours si une telle représentation discriminative existe réellement, et si oui, les mécanismes neuronaux et synaptiques qui en sont à l'origine.

Au cours de mon travail de thèse, en utilisant une approche de contrôle optogénétique de l'activité neuronale, j'ai démontré que l'activation des neurones excitateurs du PFC est nécessaire à la discrimination entre les signaux de menace et de sécurité. Ce résultat a été rendu possible grâce à la reproduction expérimentale de l'apprentissage associatif chez le rongeur. L'essence de l'apprentissage associatif repose sur le couplage de deux stimuli de nature différente. Le premier stimulus est qualifié de stimulus conditionnel (CS) car il ne produit généralement aucune réponse comportement manifeste. Le CS provoque parfois une faible réponse comportementale, mais, dans ce cas, elle reste sans rapport avec la réponse qui sera finalement apprise. Au contraire, le stimulus inconditionnel (US) provoque de façon systématique une réponse comportementale forte et cohérente (réponse inconditionnée). Les réponses inconditionnées sont innées; elles sont produites en l'absence de mécanismes d'apprentissage. La présentation répétée de CS suivie d'un US, induit progressivement une réponse nouvelle ou différente appelée « réponse conditionnée ». L'apprentissage associatif ou conditionnement classique permet aux animaux de distinguer les

événements qui se produisent de manière fiable de ceux qui sont associés de manière aléatoire, un processus mieux connu sous le nom d'apprentissage discriminatif. Cette forme d'apprentissage peut être reproduite expérimentalement en laboratoire grâce à un paradigme comportemental largement utilisé appelé conditionnement de la peur. Il s'agit d'un paradigme où un animal apprend à distinguer un stimulus conditionné (CS+) couplé à l'occurrence d'un événement aversif (US), avec un second stimulus neutre (CS-) qui ne prédit aucune sorte de menace ou de danger.

Le travail présenté dans cette thèse démontre le rôle prédominant du cortex préfrontal dans la discrimination entre des stimuli qui prédisent un danger et des signaux environnementaux similaires mais émotionnellement insignifiants. Les résultats obtenus dans cette thèse sont d'une importance primordiale, étant donné que l'incapacité à faire la distinction entre différents signaux environnementaux mène à des réponses inappropriées et peut entrainer de l'anxiété et des troubles post-traumatiques (TSPT). Notamment, les patients souffrant d'anxiété et de stress post-traumatique montrent une altération généralisée de leurs réactions face à des stimuli neutres/sécuritaires associée à des comportements inapproprié.

Le concept exposé dans ce manuscrit ne prive pas l'amygdale de son rôle central dans l'encodage de la peur. Le processus neuronal responsable de l'apprentissage et de la génération d'un comportement approprié est dirigé par l'amygdale. Cependant, conformément aux nombreuses études ultérieures, mon travail de thèse suggère un contrôle "top-down" des régions corticales sur les aires subcorticales impliquées dans l'acquisition et expression de la peur. Bien que le cortex préfrontal soit activée en aval de l'amygdale, il assure un rétrocontrôle sur l'activité de sortie des structures sous-corticales. Ces résultats sont en accord avec nombreux études cliniques identifiant le cortex préfrontal comme une région fonctionnelle qui régit l'attention accordée à certains stimuli, influence la mémoire, et façonne les plans mentaux conçus en réponse au stimuli environnementaux.

En outre, j'ai montré que le processus d'apprentissage discriminatif mené par l'activité d'une sous population de neurones du cortex préfrontal est associé à une réorganisation fonctionnelle qui semble être le résultat d'un phénomène de plasticité synaptique. Cette réorganisation se traduit par une décorrélation entre l'activité neuronale produite en réponse à des signaux neutres par rapport à des signaux qui prédisent un danger. Curieusement, ce remaniement présente des analogies avec un phénomène précédemment décrit dans la littérature dans le bulbe olfactif et dans le gyrus dentelé. Ce mécanisme de « *pattern separation* » semble être impliqué dans l'augmentation de la perception des signaux environnementaux. En effet, les résultats de ce travail indiquent que l'apprentissage

discriminatif réduit la similarité entre les patterns d'activité évoqués par le CS- (stimulus neutre/sécuritaire) ou le CS+ (danger).
En conclusion, nous proposons un modèle similaire à celui décrit dans le bulbe olfactif et l'hippocampe susceptible d'améliorer la perception de signaux environnementaux et donc permettant une meilleur précision de la discrimination. Cependant, ces régions distinctes du cerveaux montrent de différences. Tanis que la decorrelation des ensembles neuronaux dans le gyrus dentelé et dans le bulbe olfactif se développe principalement dans l'espace, nous montrons ici pour la première fois que le phénomène de « *pattern separation* » dans le cortex préfrontal semble se produire purement temporellement.

Pour pouvoir obtenir ces résultats, nous avons utilisé une technique de pointe qui nous a permis de suivre l'activité de la même population de neurones dans différentes sessions avant et après l'apprentissage discriminatif. En effet, l'un des majeurs défis de la neuroscience des systèmes concerne la façon dont les neurones rééquilibrent leur fonction et leur engagement à s'adapter aux stimuli saillants. Avec l'avènement de techniques permettant des enregistrements d'activité longitudinale à partir des mêmes populations de neurones, des études récentes ont fourni des nouvelles perspectives sur cette question. Des enregistrements longitudinaux des mêmes populations de neurones peuvent être obtenus en exploitant des techniques telles que l'imagerie calcique chronique à deux photons ou les enregistrements extracellulaires chroniques. Bien que les enregistrements extracellulaires chroniques fournissent une évaluation des mêmes neurones à travers plusieurs sessions différentes, cette technique montre quelques lacunes. Premièrement, le nombre de neurones enregistrés est généralement faible et diminue encore plus dans le temps. Deuxièmement, les enregistrements extracellulaires captent de préférence des informations provenant de neurones hautement actifs qui maintiennent leur activité stable, et par conséquent, les neurones silencieux qui deviennent actifs risquent d'être manqués. L'imagerie calcique à deux photons, au moyen des indicateurs calciques génétiquement codés (GECI), représente un outil puissant qui peut compenser les manques apparus dans d'autres techniques, pour fournir des mesures longitudinales fiables de neurones et de populations individuels. L'imagerie calcique à deux photons est aujourd'hui considérée comme l'outil le plus qualifié pour étudier la dynamique des populations neuronales in vivo avec une haute résolution dans le temps et dans l'espace.
Pour cette raison, nous avons exploité l'imagerie calcique chronique à deux photons chez l'animal évéillé qui a fourni des informations sur l'organisation fonctionnelle des neurones au cours du procès d'apprentissage durant tâche comportementale.

Enfin, j'ai démontré les mécanismes cellulaires et synaptiques à la base de la réorganisation fonctionnelle observée dans le PFC durant apprentissage discriminatif. Au cours de l'apprentissage, les neurones pyramidaux sont potentialisés et recrutés au sein de ses ensembles grâce l'association au niveau dendritique d'événements synaptiques non-linéaires issus des entrées sensorielles avec des entrées synaptiques provenant de la BLA. Ces résultats impliquent certains considérations : premièrement, le cortex préfrontal, de manière analogue aux régions corticales sensorielles facilite les mécanismes de plasticité synaptique à travers un phénomène d'intégration dendritique menée par l'association de deux (ou plus) projections neuronales. Une première dépolarisation dirigée par des entrées sensorielles est capable de s'associer à une deuxième menée par des entrées provenant de l'amygdale et de produire comme résultat une potentialisation durable dans le neurones pyramidaux du cortex préfrontal. Au cours de l'apprentissage associatif, les entrées sensorielles et émotionnelles (transmise par la BLA) coïncident sur les même réseaux neuronaux dans le PFC. Les neurones du PFC reçoivent et méta-associent ces entrées pour améliorer les compétences discriminatives entre différents signaux environnementaux au cours de la performance comportementale. Enfin, le présent travail démontre pour la première fois la pertinence du mécanisme d'intégration dendritique pour l'apprentissage et le comportement.

En conclusion, nos données fournissent la preuve d'un nouveau mécanisme synaptique qui associe, pendant l'apprentissage, l'expérience perçue avec l'état émotionnel transmise par la BLA permettant ainsi la formation d'ensembles neuronaux dans le cortex préfrontal. Cette réorganisation fonctionnelle du réseau pourrait renforcer la détection perceptuelle de signaux environnementaux.

Mots clés : Cortex Préfrontal, Conditionnement de la peur, Discrimination Perceptuelle

---

Unité de recherche

Interdisciplinary Institute for Neuroscience (IINS)

CNRS UMR 5297 – Centre Broca Nouvelle-Aquitaine

146, Rue Léo Saignat (33077) – Bordeaux

2. Abstract

Circuit mechanisms for encoding discriminative learning in the dorsal prefrontal cortex of behaving mice

The ability of an organism to predict forthcoming events is crucial for survival, and depends on the repeated contingency and contiguity between sensory cues and the events (i.e. danger) they must predict. The resulting learned association provides an accurate representation of the environment by increasing discriminative skills between threat and safety signals, most likely as a result of the interaction between the prefrontal cortex (PFC) and the basolateral amygdala (BLA). Although it suggests that local neuronal networks in the PFC might encode opposing memories that are preferentially selected during recall by recruiting specific cortical or subcortical structures, whether such a discriminative representation is wired within discrete prefrontal circuits during learning and by which synaptic mechanisms remain unclear. Here, the work at issue demonstrates that discrimination learning of both safe and fear-conditioned stimuli depends on full activity of the frontal association cortex, and is associated with the formation of cue-specific neuronal assemblies therein. During learning, prefrontal pyramidal neurons were potentiated through sensory-driven dendritic non-linearities supported by the activation of long-range inputs from the basolateral amygdala (BLA). Taken together, these data provide evidence for a new synaptic level mechanism that coincidently link (or meta-associate) during learning features of perceived experience with BLA mediated emotional state into prefrontal memory assemblies.

Keywords : Prefrontal Cortex, Fear Conditioning, Perceptual Discrimination

3. Acknowledgements

The doctorate has been one of the most significant academic challenges I have ever had to face. I can state, that when I came to Bordeaux, I was completely naïve in Neuroscience, with a poor theoretical and practical background, and not even aware of the existence of cranial windows, in vivo calcium imaging and in vivo electrophysiology. I was convinced that it was just science fiction. Nowadays, I know that we can replace a part of the skull with a small glass window to observe an intact brain thinking or insert a glass pipette to record neurons in a living animal. Even though I feel that my scientific background is still limited in science, during my PhD, I improved significantly my scientific background, and acquired practical experience and critical sensibility, and I owe it all to my advisor, Dr. Frédéric Gambino. I would like to highlight how precious he was during my doctorate, from the first surgery, the first imaging session, the first patch recording to the writing of the manuscript. He strongly dedicates himself in motivating me and the other coworkers and acts personally to help us to achieve our goals. I would like to express my deepest gratitude to him for all the fruitful discussions, his patience and dedication, and also the positive mood he brought to our lab, and I can state that if one day I will reach his level of knowledge and scientific ability, I will consider myself completely fulfilled.

Besides my advisor, I would like to thank the rest of my thesis committee: Prof. Antoine Adamantidis, Prof. Nathalie Rochefort, Dr. Pascal Fossat, Dr. Andreas Frick and Dr. Alexandre Charlet, for generously offering their time to examine my work.

My sincere thanks also goes to Dr. Yann Humeau, who provided me the opportunity to join his team by selecting my candidacy within the ENC – Erasmus Mundus project grant and also for having introduced me to the fascinating field of electrophysiology. His passion for neuroscience was the driving force that stoked the motivation for my first year's experiments. I am extremely grateful to him for the opportunities he gave to me to participate in numerous collaborations with several research teams. On the other hand, I am still waiting the wooden bird he promised me, and I will not leave Bordeaux without it.

By acknowledging Dr. Etienne Herzog, he will establish the new record of being quoted in all of my academic dissertations, before as a student supervisor (bachelor's manuscript) and then as a "spiritual adviser". He was always present in my career path to reach the right targets and discard the wrong choices. He helped me in choosing the good lab for my masters' thesis and strongly helped me in

taking the choice of joining Bordeaux Neurocampus for my doctorate, which turned out to be the right one.

I would like to thank Elisabeth Normand and Christelle Martin for having taught me the ethical conduct in the care and use of animals for research experimentation. In addition, I would like to thank Christelle for her help in managing our animal facility (MIND – Multimodal In vivo Neurophysiology Department). I do not feel I should thank Marilyn as a "health and safety manager", as her obsession with the rules was unbearable. I will keep performing my experiments without a lab coat! Instead, I would like to thank her for having been a good friend in the lab, and I wish her happiness and serenity in the future.

Life in lab would have been too hard and tough if I hadn't had special people around me sharing moments of happiness, joy, anger, frustration and madness. For this reason, I am extremely grateful to Tiago (Foda-se!), Vladimir (Dimitri), Elisabete (Morticia) and Hajer (Angela). I know I have met real friends I can count on in the future, especially to party, because, as we usually say: "work hard, party harder!".

I have to thank Florencia for having tolerated all my jokes and pranks over the past three years in the lab, and I would like to wish her and Ezequiel so much happiness for the baby they are about to have.

Finally, I want to thank my girlfriend, Antonella, for having supported me during my doctorate. People who work in Science have difficulties in separating job and private life, so I would like to thank her for having tolerated all my different moods. Working in Science also keep you moving quite often, but I am happy that for my next move I will not have to leave alone.

4. Abbreviations

2P two-photon

5HT-R 5-hydroxytryptamine receptors (serotonin receptor)

AAV adeno-associated virus

AC auditory cortex

ACC anterior cingulate cortex

AGl agranular cortex

AMPA α-amino-3-hydroxy-5-methyl-4-isoxazolepropionic acid

AP action potential

Arch archaerhodopsin

BA basal amygdala

BAC (firing) back-propagating action potential activated Ca^{2+} spike (firing)

BLA basolateral amygdala

CA cornu ammonis

CEA central amygdala

ChR2 channelrhodopsin 2

CNO clozapine-N-oxide

CR conditioned response

CREB cyclic AMP-responsive element-binding protein

CS conditioned stimulus

D-AP5 D(-)-2-amino-5-phosphonovaleric acidd

DG dentate gyrus

dPFC dorsal prefrontal cortex

DREADD designer receptor exclusively activated by designer drugs

FrA frontal association cortex

GABA gamma-aminobutyric acid

GAD65 glutamic acid decarboxilase 65

GECI genetically encoded calcium dye

GFP green-fluorescent protein

HPC hippocampus

IL infralimbic cortex

ITC intercalated cell

LA lateral amygdala

LTD long-term depression

LTP long-term potentiation

MD monocular deprivation

MGm medial geniculate body

mPFC medial prefrontal cortex

NMDA N-methyl-D-aspartate

OB olfactory bulb

PAG periacqueductal grey

ParS partial reinforcement schedule

PIN posterior intralaminar nucleus

PL prelimbic cortex

POm posterior medial nucleus

PPC posterior parietal cortex

PRh perirhinal cortex

PSD post synaptic density

PTSD post-traumatic stress disorder

PV parvalbumin

SG supragenicular nucleus

SOM somatostatin

SPFPC subparafascicular nucleus

UR unconditioned response

US unconditioned stimulus

VIP vasoactive intestinal polypeptide

VMH ventromedial hypothalamus

YFP yellow-fluorescent protein

5. Introduction

5.1 *Associative learning*

5.1.1. Classical or Pavlovian Conditioning

Well before the birth of modern psychology and neuroscience, philosophers suggested that the way the mind creates ideas is by forming associations between events. Distinct stimuli are associated because of their temporal and/or spatial synchrony, or perceived similarity. More complex thoughts would, in turn, be built upon these basal associations. Experience with two types of environmental relationship promotes association formation. One relationship is when two stimuli are experienced close in time (Pavlov, 1927); the other is when a behaviour is followed closely by a stimulus (Thorndike, 1898). Thus, we recognize two classes of associations: one caused by stimulus link between actions, and the other by the relationship between actions and the environment. This work focuses on the former class, stimulus based association.

Modern neuroscientific terminology refers to these behavioural phenomena as classical (pavlovian) conditioning or operating (instrumental) conditioning, respectively.

In his experiments, Pavlov observed that dogs were starting to salivate simply in the presence of the technician that normally fed them, before the presentation of the food (**Fig. 5.1**). Pavlov called the dogs' anticipatory salivation "psychic secretion". In an attempt to reproduce these observations in an experimental model, Pavlov presented a stimulus (e.g. the sound of a whistle), just before feeding the dogs. Interestingly, after a few repetitions, the stimulus itself was able to cause salivation. He concluded that if a particular stimulus in the dog's surroundings was occurring when the dog was given food, then this cue could become associated with the food and induce a behavioural response on its own. Hence, the stimulus was named the *conditioned stimulus* (CS) because the subsequent behavioural response depended on its association with food. In contrast, the food was defined as an *unconditioned stimulus* (US) because its effects did not rely on previous experience. Likewise, the behavioural responses to the CS and US were defined as the *conditioned* (CR) and *unconditioned responses* (UR), respectively. Accordingly, conditioning must be defined as an active learning process resulting in the ability to elicit CR whenever the CS is present, although both CR and UR behaviours are similar and innate by definition.

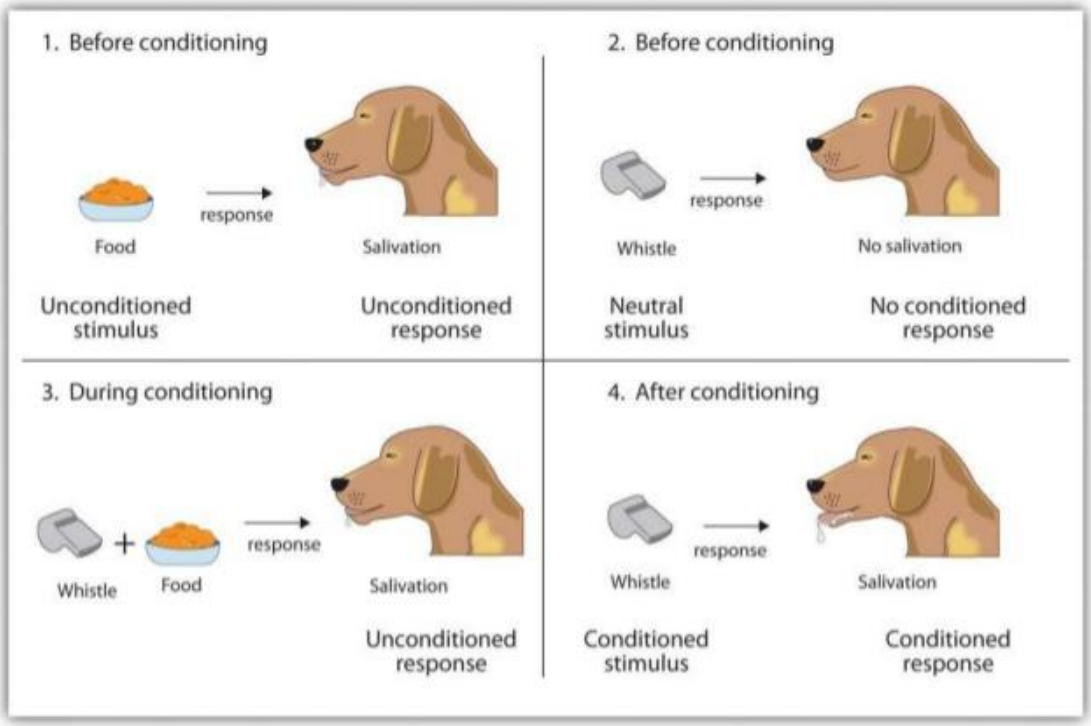

Figure 5.1. Schematic of Pavlov's experiments. Classical conditioning occurs when a neutral stimulus (e.g. whistle) is paired with an unconditioned stimulus (food). After associative learning, conditioned stimulus (CS) gains control of the conditioned response (salivation).

5.1.2 Fear Conditioning

One of the most widely used experimental models of classical learning is fear conditioning. This behavioural paradigm was developed 100 years ago by Watson and Rayner. Their famous "Little Albert's fear of rats" experiment demonstrated for the first time that a young kid learned to fear a previously attractive white rat when its visual presentation was associated with a disturbing loud noise (Watson & Rayner, 1917). In Pavlovian fear conditioning, an initially neutral conditional stimulus (CS; such as a tone) is paired with a fear-inducing, aversive unconditional stimulus (US; usually a foot-shock) in a novel chamber. After pairing, the animal develops a long-lasting fear of the discrete tone CS, known as tone or cued fear, as well as a fear of the environmental chamber, which has come to be known as contextual fear. The work presented in this dissertation mostly focuses on the first type of associative learning, cued or auditory fear conditioning (**Fig. 5.2**).

Learned fear is classically measured by the freezing response (defined as the suppression of movements but those required for breathing) (Anagnostaras et al., 2010;

Fanselow & Bolles, 1979). Freezing is the consequence of the activation of the functional behaviour system serving defence. In particular, fear conditioning activates the defensive post-encounter phase that occurs when a predator has been detected, but is not on the verge of contact. Freezing is effective at this point for two reasons: (1) stationary prey are more difficult to detect than moving prey, and (2) for many predators, the releasing stimulus for attack is movement. Many physiological aspects accompany freezing behavioural response: heart rate changes, blood pressure increases, and breathing becomes shallow and rapid (Fanselow & Wassum, 2015). Freezing behaviour is seen to be greatly impacted by levels of hormone (Llaneza & Frye, 2009). Pain sensitivity is also decreased (Fanselow & Bolles, 1979).

Owing to its simplicity and robust behavioural output (as described above), Pavlovian fear conditioning is a powerful model for studying the neural substrates of associative learning and the mechanisms of memory formation, as well as fear- and anxiety-related disorders (e.g. PTSD – Post traumatic stress disorders).

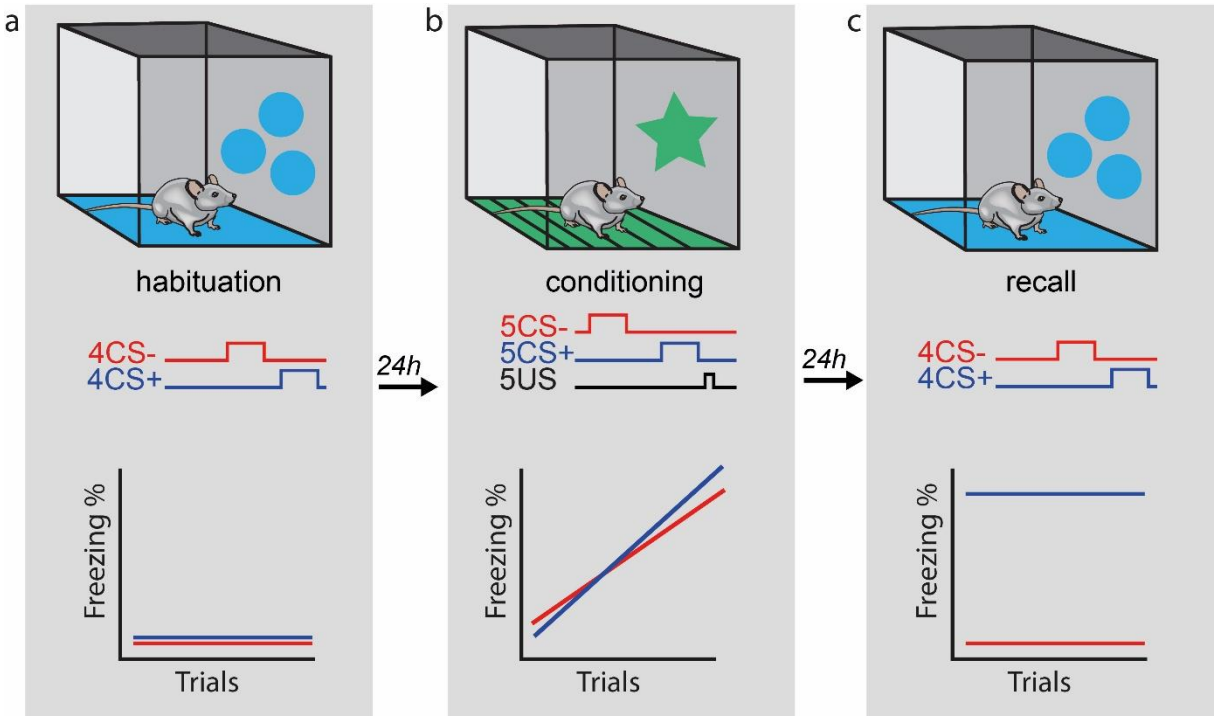

Figure 5.2. Schematic of cued or auditory fear conditioning paradigm. After a first day of habituation to two different auditory cues (CS- and CS+), the latter one is coupled to an unconditioned stimulus (e.g. foot-shock), whereas CS- is not. The association between CS+ and US bestows these stimuli with the ability to promote adaptive behaviour patterns that did not occur before the experience. Hence, a previous neutral stimulus (CS+), after conditioning gain a new emotional valence that produce an acquired conditioned response (freezing).

5.1.3 Neuronal circuits for fear conditioning

The circuitry of fear learning and memory has been extensively studied using fear conditioning. The progress, made on this topic, has leaded to a renaissance of interest of emotion within neuroscience. In many works, the fear system has been treated as a set of processing circuits that detect and respond to danger, rather than as a mechanism through which subjective states of fear are experienced. Through this approach, fear is operationalized, or made experimentally tractable.

a) Amygdala.

Researchers identified a collection of nuclei, situated in the temporal lobe, that is shown to be engaged in acquisition and expression of conditioned fear response. The term amygdala (from the latin-greek *amygdala*) was used by Burdach (Swanson and Petrovich, 1998), in the 19th century, to designate an almond-shaped structure in the deep temporal lobe of the human brain. In most mammals, including the mouse, the amygdala appears as a bump in the ventral surface of the cerebral hemispheres, just posterior to the lateral olfactory tract. There are several valid neuroanatomical classifications to label different regions composing the amygdala. The areas involved in fear conditioning can be distinguished between the lateral (LA), basal (B), accessory basal (AB), and central (CE) nuclei (Ledoux, 2000). However, other classifications consider B as basolateral, and AB as the basomedial nucleus. The basolateral complex frequently refers to LA and B together. Henceforth, in this dissertation, the basolateral amygdala (BLA) will refer to the complex encompassing lateral and basal nuclei (the target area of the experiments illustrated in the chapter "Results"). BLA is classically described as a cortex-like structure (Tovote et al. 2015), composed of approximately 80% of excitatory neurons while the fraction of inhibitory gamma-aminobutyric (GABA)-ergic neurons, which are probably involved in local neuronal circuitry, is relatively small. On the other hand, the central amygdala (CEA) is anatomically defined as a striatum-like structure and preferentially composed of GABAergic neurons (Sun & Cassell, 1993) (**Fig. 5.3**).

Many efforts have been devoted in different studies to identify the circuits that encode the CS. Much of the work has involved the auditory modality that is implicated in cued fear conditioning. The majority of sensory information of every modality (including auditory, visual and somatosensory input) that is conveyed to the amygdala is mainly targeting the LA nucleus (Ledoux et al., 1990), and damage of LA disrupts fear learning to conditioned auditory CS.

These observations are consistent with the suggestion that LA acts as an obligatory relay hub of sensory information from subcortical or cortical sensory structures (Ledoux, 1990; Campeau and Davis, 1995). Auditory inputs reach the lateral amygdala (LA) through two specific pathways. The first one conveys auditory information from the auditory and multimodal areas of the thalamus (Bordi & LeDoux, 1994; Linke et al., 2000). A second area carrying auditory information through its projections to LA, is the ventral auditory cortex. Both pathways are able to mediate fear conditioning to a simple auditory CS, although it has been suggested recently that the latter one is likely to be involved during complex, natural-like auditory stimulus (Letzkus, 2011). Nevertheless, more detailed studies are needed to better understand the exact conditions that require the cortex. In addition, a few studies have shown that the cortico-LA pathway is less effective over trial to promote fear learning than does the thalamic pathway, thus indicating that plasticity in the amygdala occurs, at least initially, through the thalamo-amygdalar projections (Quirk & Armony, 1997; Quirk et al., 1995).

As opposed to the CS encoding, much less is known about how the information about the aversive US reaches the amygdala to promote associative learning upon overlapping of the conditioned stimulus. However, it is generally believed that the amygdala is the centre of plasticity during conditioning, where convergence between CS and US occurs. Thalamic areas that receive information from the spino-thalamic tract are projecting, in turn, to LA (LeDoux, Cicchetti et al., 1990). In addition, LA neurons are responsible to nociceptive stimuli, and a subset of these cells is sensible to auditory input as well (Romanski et al., 1993). This leads to the conclusion that a population of neurons in LA is a potential proxy for fear conditioning (convergence of CS and US). Plasticity related to conditioning in the amygdala is controlled by neural circuitry originating from the midbrain periacqueductal gray region (PAG). Such a pathway is triggering plasticity by depolarizing neurons in the LA while CS inputs are active. Recent findings suggest that the US input is not invariant, but it is modulated by the expectation of the US during each learning trial (McNally et al., 2011; Shi Yuan Li & Mcnally, 2014). Therefore, when the occurrence or magnitude of the US is unexpected, strong teaching signals drive plasticity and learning in LA neurons. On the contrary, an expected stimulus is producing weak teaching signals, with unaltered LA synaptic strength.

A great variety of synaptic plasticity mechanisms have been associated to fear conditioning. However there is strong evidence to support a role for NMDA-dependent plasticity at the level of LA synapses. *In vitro* and *in vivo* blockade of NMDA receptors specifically in the lateral amygdala abolishes LTP and acquisition of fear learning (Bauer et al., 2002; Huang & Kandel, 1998).

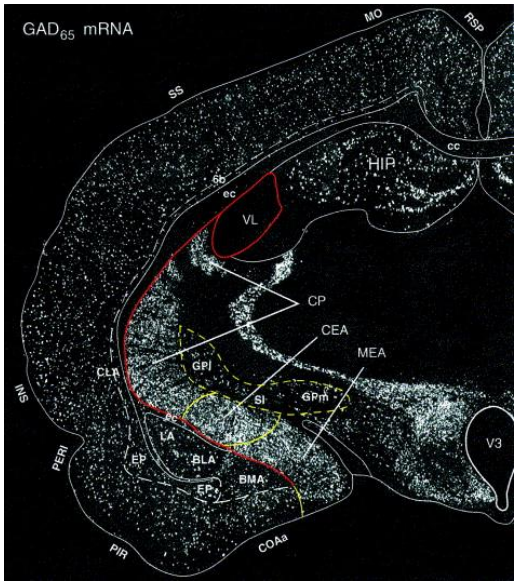

Figure 5.3. In situ hybridization, darkfield illumination of an autoradiograph. The picture is illustrating the distribution of glutamic acid decarboxilase (GAD65) – expressing neurons (the enzyme converting glutamate to GABA) in a coronal slice of the rat forebrain. These neurons are especially dense in the central nucleus of the amygdala (CEA), and to an approximately lesser extent in the medial nucleus of the amygdala (MEA). In contrast, other regions of the amygdala (BLA, BMA) contain only scattered GABA neurons (Swanson and Petrovich, 1998).

Even though compelling evidence has been shown a dominant role of the amygdala in acquisition and expression of fear learning (as debated above), the idea of multiple engrams that can be activated by separate or in unison at different times has been confirmed by recent studies (Herry & Johansen, 2014; Tovote et al., 2015). It appears likely that different aspects of a given memory are preferentially stored in different anatomical regions. Taking these observations together, it is now widely accepted that fear responses are mediated by distributed, highly interconnected forebrain regions.

b) Circuits for the conditioned stimulus (CS)

Thalamus. As discussed above, multimodal and auditory nuclei of the thalamus are engaged in processing the sensory information throughout associative learning. LeDoux was the first to describe the LA as the major recipient of auditory thalamo-amygdala projections (Ledoux et al., 1985). These projections originate directly from the medial division of the medial geniculate body (MGm), the posterior intralaminar nucleus (PIN), and the suprageniculate nucleus (SG) (**Fig. 5.4**). These thalamic regions are constituted of a subset of cells receiving convergent inputs from acoustic and somatosensory pathways, and these neuronal populations are projecting directly to LA (Bordi & LeDoux, 1994). To further complicate this issue, recent findings revealed a non-uniform distribution of the projections originating from these different thalamic nuclei to the amygdala (Linke et al., 2000). In particular, it was observed that SG, MGm and PIN predominantly projected to the laterodorsal and lateroventral portions of the lateral amygdala (LA). MGm afferents were located rather in

the dorsal part of the LA, whereas SG long-range connections were reaching mostly the ventrolateral part of the LA. PIN-projecting axons were found in the entire LA. In addition, PIN projections were observed in the anterior basomedial and central nuclei. Despite the high degree of anatomical superposition of these distinct afferents in the lateral nucleus of the amygdala, each thalamic nucleus seems to be differently involved in transmitting sensory information during associative learning.

It is generally believed that thalamo-amygdala projections act as a relay for the direct transmission of auditory stimuli in the amygdala. However recent work raised the issue of the content of information that is provided to the amygdala and the real role of thalamus during associative learning (Weinberger, 2011). The author argues that the thalamic MGm/PIN complex is a recipient of both auditory (CS) and nociceptive somatosensory (US) inputs that are able to promote associative plasticity (pairing-dependent increase of response to an acoustic CS). Therefore, this work revisited the role of the thalamus (MGm/PIN) during learning that should now be considered as a potential initial stage for CS-US convergence, and not merely as a sensory relay. In conclusion, although the belief that the amygdala is the locus of both acquisition and storage of learned fear remains dominant, further work should address the contribution provided by the thalamus during associative learning.

Auditory Cortex. The implication of the auditory cortex (AC) is contentious, with contrasting evidence arguing on one side an essential role of this cortical structure, and on the other side a secondary function in associative learning.

Anatomically, the cortico-amygdala projections are originating from the secondary (Te2/Te3) auditory cortex, and also from the perirhinal cortex (PRh), which receives information about multimodal sensory inputs. Each of these cortical regions is directly contacted by the thalamic medial portion (MGm) of the medial geniculate body (MGN) and the adjacent posterior intralaminar nucleus (PIN) (**Fig. 5.4**) (Ledoux et al., 1985; Deacon et al., 1983).

It has been debated above that information about auditory cues can be provided to the amygdala from two specific routes: a direct thalamo-amygdala pathway and an indirect thalamo-cortico-amygdala pathway. Nonetheless, whether it is widely accepted that the former has a leading role in associative learning, the engagement of the latter one is still unclear. Hence, plasticity of CS inputs to the thalamus and amygdala precedes circuit changes in the auditory cortex within and across trials, suggesting that associative learning relies predominantly on the thalamo-amygdala pathway, at least during early phases of learning (Quirk & Armony, 1997).

Interestingly, even though lesions of the auditory cortex performed prior to training does not alter learning, post-training lesions disrupt the expression of conditioned responses. Based on these results, some have hypothesized that post-training cortical lesions impair the expression of associative learning because AC is an obligatory relay for CS information to the amygdala (Campeau and Davis, 1995). Consistent with this hypothesis, recent findings suggest that a thalamo-cortical-amygdala pathway promotes auditory CS processing when auditory fear conditioning is acquired (Boatman & Kim, 2006). In fact, even though most studies have confirmed the leading role of the thalamo-amygdala pathway during fear conditioning, the fact that post-training cortical lesions completely disrupt associative memory highlights the importance of the thalamo-cortical-amygdala route during CS processing and expression of associative memory.

Recent findings proposed a potential role for the auditory cortex in cued fear conditioning. By exploiting trains of upward and downward frequency-modulated sweeps as the CS, they attributed a role for the AC in encoding complex tones (Letzkus et al., 2011). In this work, the authors identified a disinhibitory circuit required for associative learning. Layer 1 interneurons provided information about the aversive stimulus. This L1 activation promoted inhibition of L2-3 parvalbumin interneurons, which in turn controled the activation of pyramidal neurons through a feedforward inhibition. This footshock-evoked dishinibitory system in turn probably gated the induction of activity-dependent plasticity in the auditory cortex and at cortical afferents to the amygdala. Stimulus convergence and consequently aforementioned auditory cortex disinhibition was fundamental for associative learning. These observations emphasize the relevance of auditory cortex in encoding complex, naturalistic tones, in fear conditioning, as associative learning with pure tones is often unaffected by auditory cortical lesions.

In summary, plasticity to a simple tone depends predominantly on the direct projections from the auditory thalamus to the lateral amygdala. Surely, the thalamo-cortico-amygdala route is exploited for learning in situations involving complex sensory stimuli but not for the tasks typically used in simple fear conditioning. At the same time, the observation that a conditioned response persists in the auditory cortex upon extinction training, suggests that this cortical region is a site of long-term storage of some components of fear memory. Finally, a similar activation by footshocks has also been observed in the primary visual cortex, most probably underlying aspect of contextual fear learning. This finding indicates that the cue-evoked activation of L1 interneurons may be a general feature of neocortical organization underlying the formation of some aspects of fear memory traces.

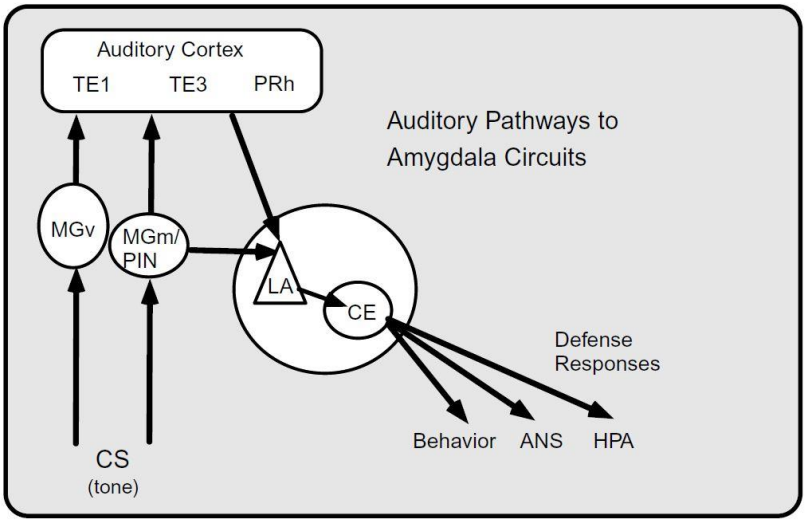

Figure 5.4. Schematic of the neural pathways involved in auditory information. Auditory inputs reach the lateral amygdala (LA) through two specific routes. The first one conveys auditory information from the auditory and multimodal areas of the thalamus (MGm/PIN) directly to LA. The thalamus can also project to the primary and secondary auditory cortices (Te1, Te2/Te3), that in turn, can contact the amygdala. Both pathways are able to mediate fear conditioning to a simple auditory CS, however it has been suggested that the latter one is involved with a more complex auditory stimulus pattern (J. E. Ledoux, 2000).

Primary sensory cortex. Up until now, the majority of studies on associative learning employed an auditory conditioned stimulus. However, the surrounding environment is characterized of stimuli of different modalities. Striving for a deeper understanding of how distinct brain regions are processing conditioned stimuli of different modalities, is an issue that has been recently addressed. In this line, a novel behavioural associative learning paradigm was developped to investigate this topic (Gdalyahu et al., 2012). This behavioural model exploited controlled whisker stimulation as a conditioned stimulus, that was paired with a foot-shock. The aim of this study was to probe how associative learning influences CS-evoked response in primary sensory cortex (Gdalyahu et al., 2012). This model was demonstrated to be effective as animals successfully learned the association between the somatosensory CS and the foot-shock and this memory was retained for weeks. The neuronal correlate of this behavioural acquired performance, was represented by functional reorganization of neural responses within the barrel cortex somato-topically corresponding the trained whisker. After training, the CS evoked responses in fewer neurons, yet these activity was stronger than in control mice in which the US was not paired with the CS. The sparse population coding reorganization and strengthening of neural responses observed in trained mice was proposed then as a strategy to improve metabolic efficiency of cortical processing.

Taken together, these data accounts for a model in which sparse network coding occurs in the sensory cortex as emotional value of a stimulus is learned. This example offers an insight into the complexity of the circuits that govern associative learning. Each structure of this network is involved in processing specific attributes (modality, contextual and emotional value, etc.) of an environmental stimulus. The aforementioned study (Gdalyahu et al., 2012)

illustrates, for example, how primary sensory cortices encode the physical, but also experience-dependent contextual attributes of a somatosensory conditioned stimulus.

c) Circuits for the unconditioned stimulus (US)

Periaqueductal Grey. Fear conditioning is a form of aversively motivated behaviour in which an initially neutral stimulus (CS) is paired with an aversive unconditioned cue (US) to produce a conditioned response (CR). This learning relies on the convergence of US and CS information that triggers *Hebbian* plasticity through amygdala neurons depolarizations. The pathway that conveys information about the CS to the lateral amygdala has been extensively discussed above, however the origin of US inputs to the amygdala remains to be debated.

It is widely accepted that the periaqueductal grey (PAG) is a structure involved in defensive responses, and many fear conditioning learning models define the PAG as a downstream target of the amygdala, promoting the appropriate behavioural response (e.g. freezing). This observation is confirmed by studies showing that stimulation of the periaqueductal grey (PAG) is an effective US in fear conditioning (Scala et al., 1987). Anatomically, the PAG can be subdivided into dorsolateral and dorsomedial columns (dPAG), and the ventrolateral column (vPAG), which are reciprocally separated by the lateral column. The PAG is regulating numerous physiological and behavioural aspects, such as regulating cardiovascular function, nociception, and vocalizations. Interestingly, the dorsal and ventral columns seem to trigger counteracting forms of defensive behaviours: escape and freezing, respectively.

Consistent with the idea that the PAG acts as an output structure, recent findings demonstrate that PAG inactivation reduced the expression of both conditioned fear responses and unconditioned reflexes following US foot-shock. Nonetheless, if PAG serves just as an output, its inactivation should only impair the expression but not the acquisition of fear learning. Contradicting this, it was shown that fear acquisition was disrupted by pre-training inactivation of PAG (Johansen et al., 2011). In line with these observations, another work suggests the key role of dPAG-BLA pathway to direct learned fear responses (Kim et al., 2013). Here, they showed that electrical stimulation of dPAG promoted robust freezing and vocalizations in rodents. However, differently from simple electrical stimulation of the amygdala, artificial activation of the dPAG supported fear conditioning. Importantly, this effect was completely abolished when the BLA was inactivated during dPAG stimulation, supporting the idea that dPAG-BLA pathway is essential to transmit the information about the US.

As previously outlined, compelling evidence suggests that fear conditioning may be instructed not by a simple sensory representation of the US, but instead by a US signal which is dampened by expectation (Tovote et al., 2015). Depolarization of LA neurons by an unconditioned stimulus instructs *Hebbian* plasticity that stores the CS-US engram during fear conditioning, and the US-evoked responses are dampened in time in both LA and PAG by expectation of the US (Johansen et al., 2011). Johansen and colleagues observed that US-evoked responses in LA and PAG decreased over the course of training in a manner that was inversely correlated with increased freezing behaviour. Following training, LA and PAG neurons were activated more strongly when the US were presented unexpectedly than when they were anticipated by the presence of the CS. These data provide evidence that expectation is negatively modulating LA and PAG responses to the US and indicate a mechanism through which PAG conveys expectancy-modulated US information to amygdala to promote associative neural plasticity and support the formation of fear memory traces.

Hypothalamus. As far as the periaqueductal grey is concerned, it was previously debated that this structure serves as an interface between limbic forebrain regions and execution of defensive behaviours. Projections from the PAG to the rostral ventromedial medulla trigger the autonomic reactions associated with defensive responses. The PAG is contacted by the amygdala, the best characterized modulator of defensive responding. In addition, glutamatergic projections are conveying information to the dPAG from the dorsomedial division of the ventromedial hypothalamus (dmVMH). These projections are activated by nociceptive input from the dmVMH (Borszcz, 2007). The dmVMH and interconnected medial hypothalamic nuclei are part of a mesolimbic circuit that is involved in the execution of defensive responses to threat. Borszcz and colleagues argue that the amygdala processes nociceptive inputs that are forwarded from the dmVMH. It is suggested that these regions may form a core limbic circuit that elaborates the affective aspects of the noxious stimuli during fear learning. The dmVMH together with other medial nuclei of the hypothalamus (dorsal premammillary nucleus and anteromedial hypothalamus-medial preoptic area) represents a behavioural check-point that controls the execution of defensive responses to environmental threats and dangers. Pain-induced plasticity in amygdala projections to both dmVMH and dPAG results in long-term increases in pain sensitivity and defensiveness to threatening/noxious stimuli.

To recapitulate, amygdala, PAG, and hypothalamus are forming a limbic circuit that accounts for a behavioural defensive response accompanied by the affective-motivational dimension of pain underlying suffering and disability associated with pain state.

Thalamus and Insular Cortex. The periaqueductal grey is not the only anatomical structure that has been described to transmit US (pain) information to the lateral amygdala. Shi and Davis, through a lesion approach, reported that the medial areas of the medial geniculate nucleus and the insular cortex might convey somatic pain input to LA as well (**Fig. 5.5**) (Shi & Davis, 1999). This study demonstrated that specific electrolytic lesion of either the insular cortex or the posterior intralaminar complex, including the posterior triangular nucleus (PoT), the posterior intralaminar nucleus (PIN or PIL), the suprageniculate nucleus (SG), the parvocellular part of the subparafascicular nucleus (SPFPC), and potentially the medial subdivision of the medial geniculate complex (MGM), did not affect fear conditioning. However, combined lesion of both thalamic and cortical structures impaired the acquisition of fear-potentiated startle. These data indicate that two parallel routes involving the cortex and thalamus process somatic noxious information. This is in line with the afferents conveyed to these regions. The posterior intralaminar complex receive US-inputs directly from the spinal cord, whereas the insular cortex is contacted by the primary and secondary sensory cortices and by the ventroposterior and intralaminar nuclei of the thalamus. Both structures, in turn, are forming thalamic-amygdala or insular-amygdala projections. Overall, this work provide evidence for the existence of two parallel pathways conveying US input to the amygdala (**Fig. 5.5**).

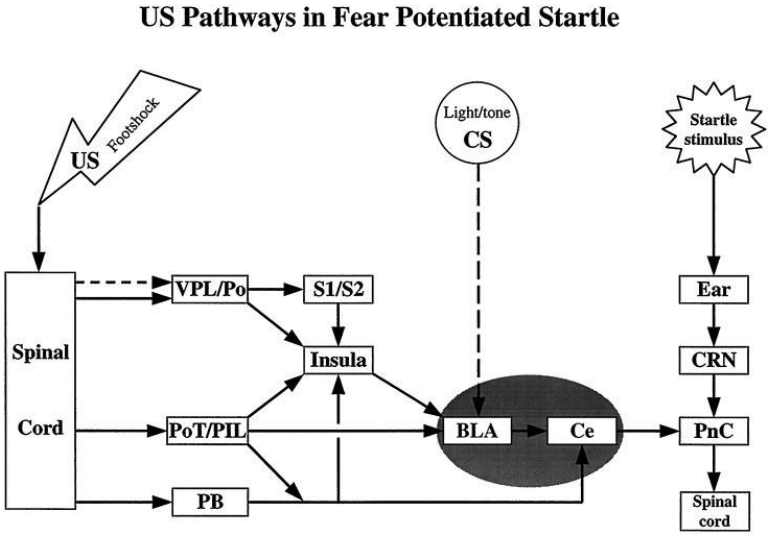

Figure 5.5. Schematic of the cortico-amygdala and thalamo-amygdala pathways involved in pain (US) information. Somatic noxious input from the spinal cord is conveyed directly to the ventroposterior and intralaminar nuclei of the thalamus. This information can be transferred directly to the amygdala through the thalamo-amygdala pathway, or relays input to the Insular Cortex, that, in turn, conveys this information to the LA (cortico-amygdala pathway). These two routes are supposed to be parallel and transmitting aversive information (e.g. foot-shock) to the amygdala to produce fear responding (Shi & Davis, 1999).

Anterior Cingulate Cortex. The implication of the anterior cingulate cortex (ACC) in the behavioural responses related to noxious stimuli, is of particular relevance for this work, because it allows the introduction of the key concept of "top-down" modulatory control from a prefrontal cortical area. Until recently, pain was largely considered as a sub-cortical

phenomenon. Consequently the involvement of cortical structure in pain processing has never been extensively investigated in animal models. However, few studies have highlighted recently the involvement of several cortical regions in processing pain experience including the ACC (Tang et al., 2005). In contrast to what has been observed in the somatosensory cortex, which has been associated with the discriminative aspects of pain experience, ACC seems to be involved in the emotional and affective features of pain. In particular, the work of Tang and colleagues argued that ACC contributes to pain "unpleasantness" (term extrapolated from Tang et al.). Early clinical studies showed that surgical ablation of this cortical structure significantly dampened pain unpleasantness without affecting the ability to process the intensity or location related to the noxious stimulus (Foltz, 1962). Tang and colleagues demonstrated a role of the ACC in the modulation of pain perception. However, which specific aspect of pain experience is encoded from this area remains unclear. It can be hypothesized that ACC neurons express pain affect, general unpleasantness, or even cognitive aspects. Hence, due to the implication of ACC in anticipation and attention, it is possible that this region alters learning through these processes. However, to date, investigation of cognitive processes in animal models remains problematic and clinical studies result more effective for such issues.

d) Modulation of fear expression

Hereinbefore, many subcortical and cortical regions have been encompassed within the fear network, and participate together in associative fear learning by processing the information about the conditioned and unconditioned stimuli. However, additional brain regions with no role during the acquisition of fear memories were shown to be important for the modulation of fear expression modulation. Amongst all these structures, the ventro-medial prefrontal cortex (vmPFC) is of particular interest. Its inactivation during post-training affects the expression of learned fear (Corcoran & Quirk, 2007). Post-conditioning infusion of Tetrodoxin (strategy adopted to block the activity of the vmPFC) specifically decreases freezing level during recall, demonstrating a critical role for this cortical region in fear expression. In addition, it was shown that vmPFC communicates directly with the basal amygdala (BA) through efferent excitatory projections (Likhtik et al., 2005).

The vmPFC implicated in fear learning can be anatomically distinguished into two areas: the infralimbic (IL) and prelimbic (PL) cortex. Recent findings observed that IL and PL display counteractive roles: the infralimbic subdivision has been shown to promote acquisition of fear extinction memory, whereas the prelimbic subdivision plays a role in fear expression

(Quirk & Mueller, 2008). However, the presumed conflicting roles exist only with regard to the resulting behavioural output. In fact, it is widely accepted that fear learning and extinction are not reverse events, but different learning processes with extinction memories being acquired and stored within disctinct neural circuits. For that reason, IL and PL should not be considered as counteractive structures, but rather as adjacent cortical regions involved in distinct pathways that interact with each other. In keeping with this idea, concinving data illustrated that within the amygdala, two subpopulations of overlapping neurons are projecting specifically to IL or PL (Senn et al., 2014). These two populations can be functionally subdivided into "extinction neurons" projecting to IL (activity increased after extinction), and "fear neurons" projecting to PL (activity increased upon presentation of a conditioned stimulus).

At the level of PL, a subpopulation of parvalbumin inhibitory neurons regulates the spiking activity of principal neurons, through phase resetting of local theta oscillations. This fine regulation of principal neurons, coordinated by parvalbumin (PV) interneurons, is critical for fear expression (Courtin et al, 2014). Likely, another local population of interneurons is responsible of inhibiting parvalbumin interneurons to promote fear expression through the aforementioned dishinibitory mechanism. The circuit is probably instructed by the projections conveyed from the amygdala. Notably, activation of PV interneurons do not abolish completely freezing response. This can be explained by the fact that the mPFC could act in concert with other brain structures responsible for fear expression. Converging evidence indicate that the mPFC is contacting both the amygdala and the periaqueductal grey. However, Courtin and colleagues observed that the basolateral amygdala is the preferential downstream target of the mPFC to control fear expression (**Fig. 5.6**).

Similarly to the prelimbic compartment, the infralimbic cortex, does not appear to have a significant role in the formation of fear extinction memories, but is required for their consolidation and recall. In fact, convincing results illustrated that the infralimbic cortex is responsive to tones after extinction, but not during extinction training, indicating that this area is probably storing long-term memories, but it is not involved in forming short-term memory traces (Milad et al., 2002). Consistent results showed that infusion of NMDAR antagonists (required for formation of long-term, but not for short-term memory) within the infralimbic cortex, prior or immediately after extinction training, impaired the expression of extinction memory (Burgos-Robles et al., 2007). Together, these results indicate the relevance of NMDA-dependent plasticity within the infralimbic cortex to promote consolidation of extinction memories.

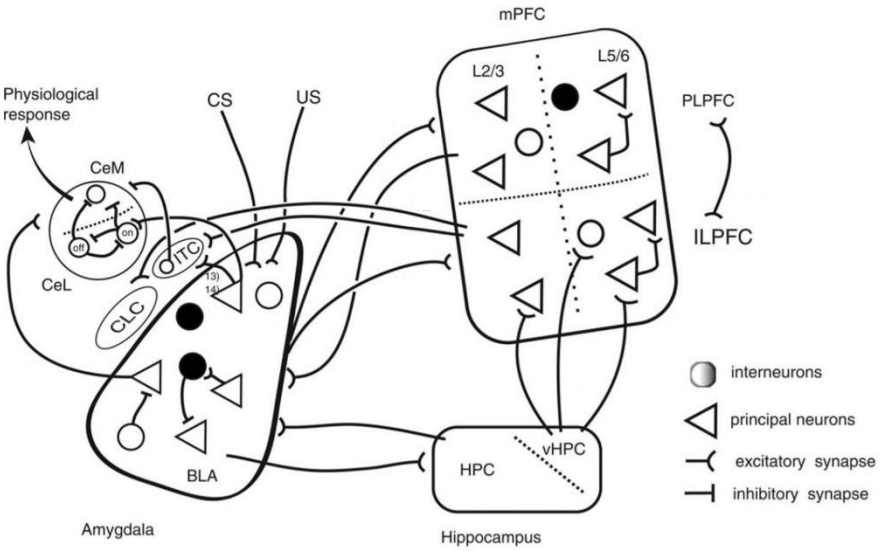

Figure 5.6. Schematic of the connections between the amygdala, hippocampus and prefrontal cortex. Triangles representing principal neurons and interneurons are shown as black or white circles, indicating the wide variety of these neurons. The simplified medial prefrontal cortex (mPFC) shows L2/3 and L5/6 of the prelimbic prefrontal cortex (PLPFC) and the infralimbic prefrontal cortex (ILPFC). The hippocampus (HPC) is lumped together as the HPC, except for the ventral hippocampal region (vHPC). The amygdala is divided into the input regions, the basolateral amygdala (BLA) where inputs from conditioned (CS) and unconditioned stimulus (US) converge. The output zone, the central amygdala is divided into three regions: the central capsular (CLC); central lateral (CeL); and central medial (Marek et al., 2013).

A proposed mechanism of extinction involves the intercalated cells of the amygdala (ITC), that represent a group of GABA neurons situated between the basolateral and central nuclei of the amygdalar complex. This population of neurons is responsible for feed-forward inhibition that negatively controls the central amygdala output nucleus (CeA). Numerous studies proposed that, after extinction training, ITC neurons are driven by infralimbic projections, resulting in the inhibition of CeA, and consequently to the abolishment of fear response (Marek et al., 2013).

5.2 *Implication of dPFC in associative learning*

Recent evidences suggest the crucial role of the dorsal region of the prefrontal cortex (dPFC or FrA) during associative learning, although its precise role is still ignored. The work presented in this dissertation principally focuses on this scientific issue.

In rodents, the prefrontal cortex is defined as the agranular part of the frontal lobe (for a review of the layered organization of the cortex, see **Table 5.1**). The medial areas of the dPFC are defined as the frontal association cortex, recently classified as Fr1 and Fr2 (Van De Werd & Evers, 2010). However, in the Paxinos & Franklin Atlas, Fr1 and Fr2 are considered as a unique anatomical site, named Frontal Association Cortex (FrA). The second frontal area (Fr2) borders on Fr1 cortex, on the medio-dorsal side of the frontal lobe. The progressive disappearance of layer 4 in Fr1, moves layer 5 to a more superficial position. The boundary Fr1-Fr2 is considered as the site where layer 5 has reached its most superficial position (Van De Werd & Evers, 2010). The second frontal area borders on the dorsal anterior cingulate area (ACCd). These two regions can be distinguished through distinct anatomical peculiarities. Firstly, layer 2 is much more irregular in the cingulate cortex compared to Fr2. Secondly, the typical columnar structure of the cortex is more densely packed in ACCd than Fr2. Finally, layer 3 is larger in Fr2 than ACCd (Van De Werd & Evers, 2010).

First evidence of the implication of the dorsal compartment in associative learning comes from the studies performed by Sacchetti and colleagues (Sacchetti et al., 2002, 2003). In the first study they demonstrated an important role of dorsal regions of the prefrontal cortex in auditory fear conditioning, but not contextual fear conditioning. These first preliminary results on this cortical structure underline that auditory and contextual cues are elaborated in different regions and that the dPFC may have a role in encoding the former category of stimuli. After demonstrating an implication of this area in fear acquisition, the following year, the activity of the same region was investigated during consolidation of fear memory (Sacchetti et al., 2003). This study provides new insights about the temporal activation of dPFC during fear learning. This cortical region seems more critical for acquisition than to the subsequent memory processing. It is probably involved in the early stages of consolidation but it does not seem to be a prominent site of engram elaboration during fear learning.

Recent convincing data proved the engagement of the frontal association cortex in fear learning and extinction (Lai et al., 2012). To investigate whether fear conditioning might shape FrA synaptic circuits, they performed transcranial two-photon imaging to assess experience-dependent structural plasticity in YFP-expressing transgenic mice. As opposed to control mice,

conditioned mice exhibited a robust increase in spine elimination in FrA 48h after fear acquisition. Strikingly, spine formation was not significantly affected after fear learning. This structural reorganization of the network resulted to be long-lasting as it was still present after 9 days. Interestingly, they observed that the increase of spine elimination significantly correlated with the degree of freezing in response to the CS, both 2 and 9 days after conditioning (**Fig. 5.7**). Subsequently, the same group of mice underwent to extinction learning and dPFC spine dynamics were compared before and after extinction training. They found that spine formation was significantly increased in parallel with freezing reduction in response to the CS. By contrast, spine elimination was not affected following extinction learning. Notably, freezing performance inversely correlated with spine formation, but not with spine elimination (**Fig. 5.7**). To sum up, spine elimination predicted fear learning, the degree of which was related to freezing performance. Conversely, fear extinction promoted new spine formation, which is inversely correlated with the degree of freezing responses.

Most importantly, they demonstrated that spine formation following extinction training occurred in the same dendritic branches on which fear conditioning previously caused spine pruning. These findings are extremely important, because they indicate the formation of memory traces within the dPFC and its partial erasure during fear extinction. This suggests that this region is directly involved in modulating fear behaviours. However, the specific role played by this cortical structure remains unclear.

Recent findings contribute to bring new insights into the understanding of the role of the dorsal prefrontal cortex in associative learning. To test whether dPFC was involved in the formation of fear memory traces in contextual fear conditioning they blocked both NMDA receptor activation and protein synthesis, and observed consequently the abolishment of freezing behaviour (Nakayama et al., 2015). Subsequently, they infused anisomycin (protein synthesis inhibitor) during either context exposure or shock delivery and detect a disruption of freezing performance in both cases, demonstrating that FrA is required for encoding both context and shock. By exploiting a protein synthesis analysis strategy in FrA, they furnished proof that FrA neurons receive convergent information about the context and foot-shock during fear learning. Finally, by taking advantage of a c-Fos approach, they provided evidence that information about the US was conveyed to the FrA through projections originating from the insular cortex (for an extensive review see "Neural circuits for fear conditioning – Circuits for the unconditioned stimulus"), whereas FrA-projecting perirhinal cortex neurons were activated by context exposure in fear conditioning.

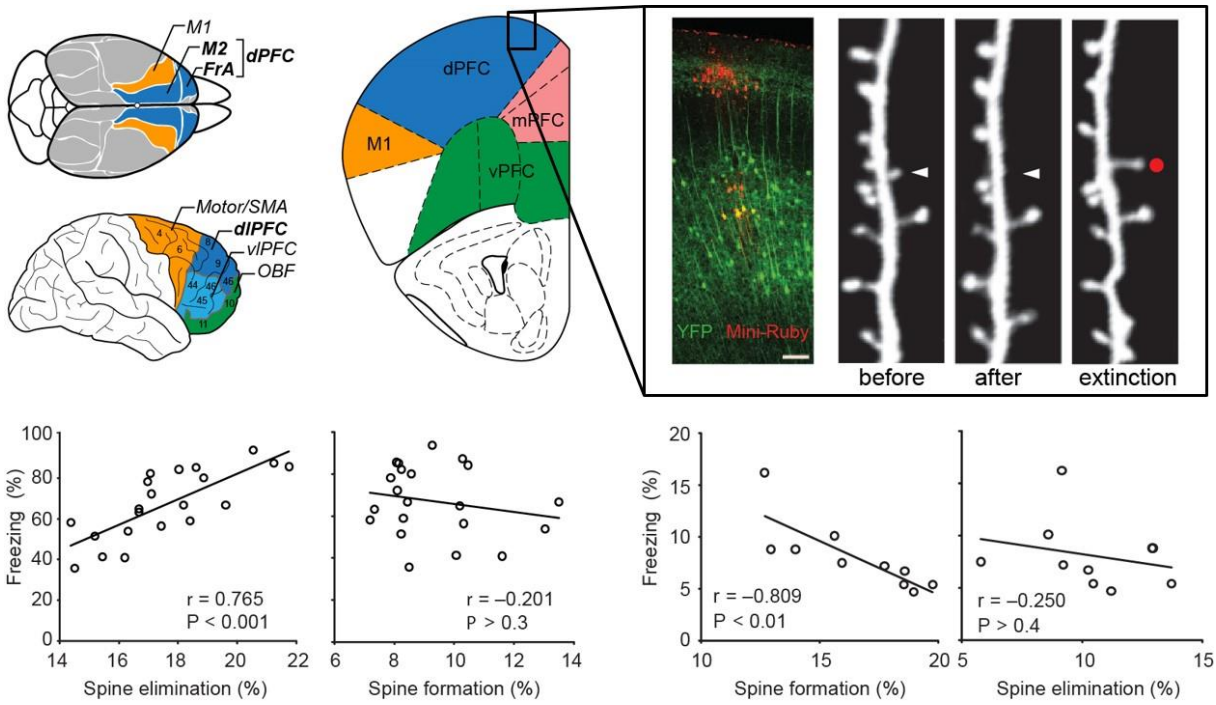

Figure 5.7. Summary of the main results obtained by Lai & colleagues. The dorsal prefrontal cortex (FrA) is a cortical structure engaged in neural processes critical to associative learning. Dendritic spine remodeling of FrA neurons is sensitive to paired sensory stimuli that produce associative learning. During fear learning, the degree of freezing responses is correlating with spine elimination, whether spine formation is not affected. Conversely, fear extinction promotes spine formation, and this spine dynamics is inversely correlated with freezing performances (adapted from Lai et al., 2012).

Together, all these studies provide evidence that a superficial cortical structure of the prefrontal cortex, defined as dorsal prefrontal cortex (dPFC) or frontal association cortex (FrA) is engaged in neural processes that are critical to associative learning. All these works agree with the fact that the FrA has a role during fear acquisition, whereas its implication in memory consolidation is less clear. Interestingly, this cortical structure seems to play a role in associative learning independently from the modality of the stimuli. In fact, both auditory and contextual fear conditioning require the activation of the dPFC neuronal circuits. Notably, it was observed that the dPFC is contacted by numerous cortical and subcortical regions that are involved in fear learning, such as the basolateral amygdala (Lai et al., 2012; Nakayama et al., 2015), the perirhinal cortex and the insular cortex. These regions are differently involved in fear network. In detail, the perirhinal cortex is involved in context discrimination (Howse et al., 2003), the insular cortex processes somatic noxious information, and the basolateral amygdala is directly responsible of the association between the conditioned and the aversive stimuli. The dorsal prefrontal cortex is defined as an associative area that is responsible of complex processing that goes on between the arrival of an input and the generation of behaviour. Therefore, it is reasonable to hypothesize that the dPFC integrates information about many aspects of fear

learning (shock, auditory, contextual and auditory inputs) and modulate, a posteriori, the behavioural response produced by the amygdala, through cognitive aspects (attention, working memory, etc.). In this view the amygdala circuit predominantly contributes to detect threat non-consciously and controlling subsequent behavioural and physiological fear responses, but it also sends information to the cognitive systems, such as the dPFC, that, in turn, integrate many inputs about the environment and eventually modulate, through cognitive functions, the behavioural output.

LAYER	NOMENCLATURE	CELL TYPE	PROJECTIONS	FUNCTION
I	External plexiform, molecular or superficial	Mainly inhibitory neurons	Apical dendrites of pyramidal neurons of the deeper layers	Centre for modulatory influences on the neurons in deeper layers. Modulation of arousal and attention of large parts of the cortex
II/III	Supragranular pyramidal	Small (lamina II) and medium-size (lamina III) pyramidal neurons, and stellate cells	Projections to adjacent and nearby areas of the cortex, as well as contralaterally through the corpus callosum	Local and cortico-cortical connectivity
IV	Granular	Different types of spiny stellate and pyramidal neurons	Thalamocortical fibres. Dendrites from layer VI neurons involved in feedback mechanisms to the thalamus	Sensory processing
V	Deep pyramidal	Large pyramidal neurons	Projections to a large array of subcortical and cortical targets	Output layer
VI	Polymorphic	Few large pyramidal neurons, many small spindle-like pyramidal and multiform neurons	Strong thalamic afference. Corticothalamic, corticocortical and distant ipsilateral cortical efferents, as well as projections to local cells in other layers	Output layer, Feedback control

Table 5.1. Layered organization in the cerebral cortex.

5.3 *Experience dependent learning plasticity*

When a brain region stores new information, it generally results into a reshaping of the wiring diagram. In agreement with this model, the dPFC undergoes a structural reorganization of the network during associative learning (Lai et al., 2012). It follows that neurons that adjust their reciprocal connections following experience, likely adapt their activity accordingly. Functional rearrangement in the dPFC represents a neural event that was extensively investigated in the work at issue.

5.3.1 Neuronal assemblies

The only way to know that an association has formed is to observe a change in behaviour following experience. This behavioural change underlies the acquisition of new knowledge, accompanied by a process of retaining and reconstructing the knowledge over time. These two mechanisms are better known as "learning" and "memory". Psychological conceptions of learning and memory identified the former as the acquisition or encoding processes, whereas the latter refers to the consolidation of trace storage that allows its maintenance in the brain and its selection during recall.

Although for contemporary neuroscience it seems obvious that the brain stores memories as physical alterations, this theme was hotly debated in the past. Indeed, researchers have been striving over the years to set out to translate the concepts of learning and memory into a neurobiological context. This resulted into the distinction between the ensemble of rapid events associated with memory encoding, and the successive occurrence of biochemical, biophysical and structural changes that represent the neural embodiment of memory storage.
Recent technological advances contributed to extensively and satisfactorily demonstrate that the neural circuits within the brain are adjusting to experience. Even though the brain represents an organ that does not contemplate cellular turnover (except few brain regions), connections among neurons are strongly dynamic. External inputs can trigger molecular and cellular modifications of individual synaptic connections and extend to multiple neurons whose interactions determine the expression of the behavioural response.

Memory is stored in the brain through the origin of chemical and structural changes that are embedded under the definition of "engram" (Holtmaat & Caroni, 2016; Tonegawa et al.,

2015). These biophysical and biochemical reactions are supposed to be maintained in the circuits to allow potential memory retrieval.

Pioneering attempts to investigate the localization of the engrams were carried out by the psychologist Karl Lashley that introduced different lesions in the cortex, trying to find a correlation between each of these damages and the performance of the lesioned animal to solve a maze task. The results indicated that memory was dependent on the amount of cortex removed, but independent on the location (Bruce, 2001). Lashley's theory was successively refuted by numerous studies. Lashley's failure to find the localization of the engram has to be attributed to two misinterpretations of his experiments. Firstly, the behavioural paradigm was too complex for the kind of issue that was planned to be investigated. Indeed, it is possible that the task was requiring multiple regions of the cerebral cortex. Secondly, memory storage could have occurred mostly in subcortical areas that were not taken into account in those experiments. Nevertheless, this study allowed to introduce a new concept, the engram pathway, defined as the ensemble of engram cells connected by specific neuronal circuits. As a matter of fact, it is important to notice that the engram, or neuronal assembly, is not located necessarily in a specific brain region, but can be distributed between numerous interconnected areas (Holtmaat & Caroni, 2016; Tonegawa et al., 2015).

The concept that specific circuits in the brain are storing memory allowed researchers to hypothesize that artificial reactivation of those engram neurons could simulate internal representations and recall memory. The creation of synthetic traces in behaving animals could indicate that activation of engram pathways is sufficient for memory to take place (Kandel et al., 2014). Different approaches can be adopted for this inquiry. One useful approach involves the exploitation of cfos promoter (a marker of recent neuronal activity) to select the neurons that are activated during the encoding of a memory. This strategy allowed Liu et al., 2012 to demonstrate that artificial stimulation of engram neurons in the dentate gyrus is sufficient for the recall of the memory. To select and reactivate the engram formed during the encoding process, they expressed channelrhodopsin (ChR2) in the neuronal assembly using the cfos-based genetic tagging approach. Subsequent optogenetic activation of this neuronal sub-population was sufficient to produce memory retrieval.

An alternative approach consists in using a chemical genetic approach, through designer receptors exclusively activated by designer drugs (DREADDs). The designer receptor (hM3Dq) is a Gq-coupled muscarinic receptor mutated in order to respond to an exogenous ligand (clozapine-N-oxide, CNO), but not to the endogenous acetylcholine. The strategy entails the employment of transgenic animals in which hM3Dq receptor is selectively expressed in sensory

experience-activated neurons. Animals are conditioned in a context A and hM3Dq-expressing neurons can be artificially activated with CNO in a context B. This approach induces the formation of neural hybrid representations incorporating elements from both contexts A and B (Garner et al., 2012).

Taken together, these results suggest that the activation of sparse neural circuits composing an engram or memory trace, is sufficient to induce the recall of a specific memory. However, these studies are not providing information about the mechanisms that recruit neurons into the engram. In other words, what are the requirements that a neurons should meet to make part of an engram? The process that selects neurons and synapses that will store a given memory is called "memory allocation" (Holtmaat & Caroni, 2016; Kandel et al., 2014; Rogerson et al., 2014). There is now increasing evidence that memory allocation is not a random process, but instead dedicated mechanisms establish the exact sites were memories are stored. This process is necessary as unoptimized storage of memories within brain regions leads to inefficient use of storage space.

Many studies have shown that the transcription factor cyclic AMP-responsive element-binding protein (CREB) is the principal responsible of neuronal allocation. CREB controls neuronal allocation by modulating neuronal excitability (Zhou et al., 2009). Neurons that express higher CREB levels are more excitable and, consequently, more reactive to sensory inputs. Higher excitability levels in such neurons result in an increase of probability to be recruited by inputs and culminate in synaptic strengthening that underlie formation of memory traces. Evidence for this hypothesis derive from numerous studies performed in the lateral amygdala upon fear learning. In fact, even though the majority of neurons composing LA is receiving information from the conditioned or unconditioned stimulus, very few are then involved in forming associative traces. Changing the proportion of CREB levels within neurons was inducing an alteration of the selection probability to for memory traces. Increased levels of CREB in few LA neurons, was increasing the chances of these neurons to contribute to the engram, whereas decreased levels had the opposite outcome (**Fig. 5.8**) (Han et al., 2007; Jin-Hee et al., 2009).

In parallel with neuronal allocation that selects the neurons implicated in forming the memory traces, an equivalent mechanism exists for synapses. Synaptic allocation establishes which synapses will go on to encode the memory. Numerous mechanisms determine how synapses are recruited to the memory trace. For example, synapses are not equally responding to a given stimulus, but their activation is dependent on prior events, a phenomenon known as metaplasticity. Furthermore, the potentiation of a given synapse can shape the response to a

plasticity-inducing input and give rise to mechanisms defined as synaptic tagging and capture. However, neuronal and synaptic allocations are not independent processes, but they are strictly cooperating. Indeed, neuronal excitability, that drives neuronal allocation, also determines whether a given synapse will be selected to encode a memory or not. Enhanced neuronal excitability increases the chance of a given synapse to undergo plasticity (Han et al., 2007; Jin-Hee et al., 2009; Rogerson et al., 2014).

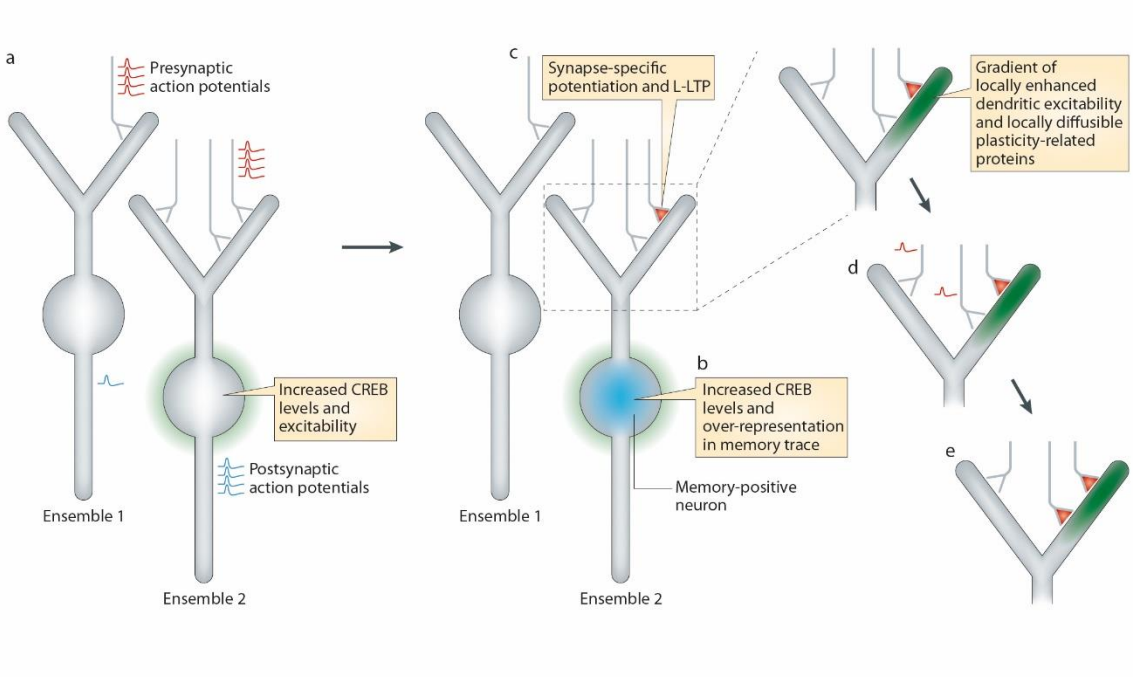

Figure 5.8. Schematic of the mechanisms underlying memory allocation. a) In neural circuits few cells hold higher levels of CREB, thus resulting in increased excitability and increased probability of firing in response to presynaptic action potentials. b) This increase their chance to be committed to form memory traces. c) Synapse-specific potentiation occurs through release of plasticity-related proteins and enhances excitability. d) Increased excitability promotes plasticity among neighbouring spines for a brief period of time. e) Neighbouring spines can finally be potentiated at long-term (Rogerson et al., 2014).

Neuronal and synaptic allocation can reciprocally influence each other. For example, the formation of a strong memory can promote LTP in a subset of synapses in a specific neuronal ensemble, but not in a second one (Han et al., 2007; Rogerson et al., 2014). This induces recruitment of plasticity related proteins responsible of consolidation mechanisms, resulting into conversion from a weak to a strong memory in a neuronal ensemble, but not in a second one. Thus, synaptic allocation mechanisms can define which neurons would encode a given memory. If mechanisms associated with synaptic allocation can influence neuronal allocation, the opposite circumstance is also true. For instance, enhancement of neuronal excitability might bias in favour of a few dendrites to dominate memory allocation processes.

In addition, formation of neuronal assemblies depend on the involvement of interneurons, that have central roles in shaping network activity (Isaacson & Scanziani, 2011).

In addition, recent studies have provided compelling evidence that various form of inhibition, but also dishinibition, could regulate learning and synaptic plasticity (Cichon & Gan, 2015; Letzkus et al., 2011). Disinhibition is a process that can be guided by vasoactive intestinal polypeptide (VIP)-expressing cells, a specific class of interneurons. VIP neurons modulate the activity of somatostatin (SOM)- or parvalbumin (PV)-expressing neurons, that, in turn, target their inhibition to principal excitatory neurons. During behavioural models associated with incremental learning (Trial- and Error-type paradigms), disinhibition guides the formation of neuronal assemblies. In detail, VIP interneurons potentiate their inhibitory control over SOM- and PV-interneurons. This leads to a disinhibition of the principal excitatory neurons, and eventually facilitates the recruitment of neurons into the forming assembly. Assembly modifications occur as far as VIP activity is protracting along the encoding process. After that, VIP inhibitory control dampens and PV and SOM neurons restore their inhibition on excitatory neurons (**Fig. 5.9**) (Holtmaat & Caroni, 2016). However, a second model of assembly shaping achieved by inhibitory control has been observed in rapid associative learning. Under these conditions, the induction of assemblies is relatively powerful and PV neurons reinforce their inhibition over pyramidal neurons. These high levels of inhibitions select only the neurons that are most strongly activated, whereas weakly activated neurons are excluded from the neuronal assembly (**Fig. 5.9**) (Holtmaat & Caroni, 2016).

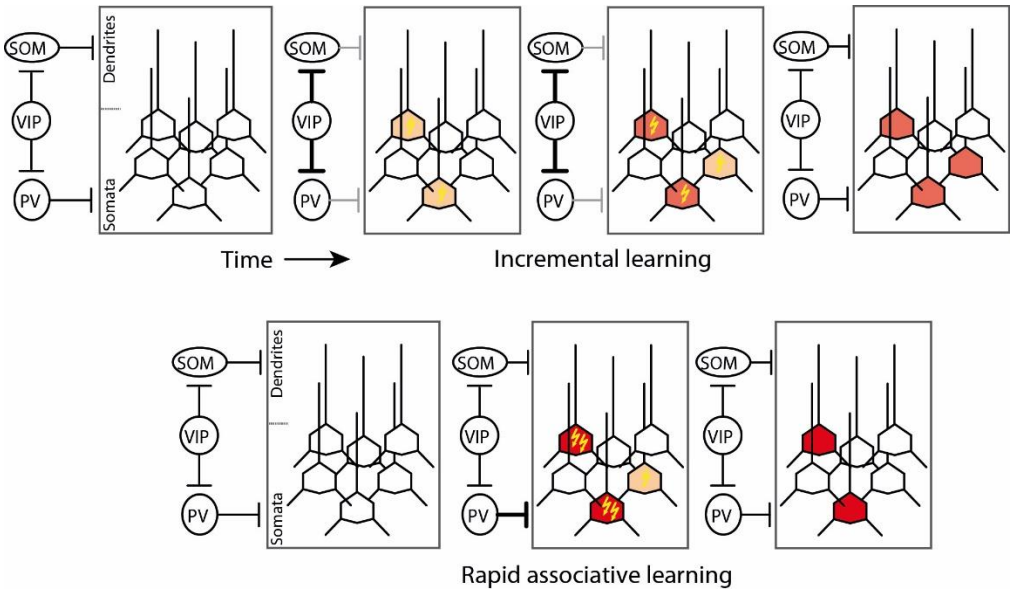

Figure 5.9. Schematic of assembly formation under the control of disinhibition and inhibition. In the upper part of the panel, during incremental learning VIP neurons promote disinhibition allowing recruitment, within the assembly, of weakly activated neurons. In the panel above, during rapid associative learning, PV interneurons induce widespread inhibition along the neuronal circuit, allowing just strongly activated neurons to be committed to the neuronal assembly (Holtmaat & Caroni, 2016).

5.3.2 Experience-dependent structural plasticity

The previous paragraph extensively illustrates the mechanisms by which memory is stored in a specific group of neurons called engram or neuronal ensemble. The selection of the neurons embodied in the engram does not occur randomly, but it involves a process that takes into account the excitability levels of neurons in a given circuit. However, another question that should be addressed regards the mechanisms that underlie the modifications between neuronal contacts, that occur during encoding processes. Over the last few decades bulk of evidence indicate that dendritic spines are engaged in synaptic signalling, integration and plasticity. Dendritic spines are small dynamic protrusions emerging from the dendritic shaft that can be subjected to numerous modifications in shape and size (Sorra & Harris, 2000). Dendritic spines are generally consisting of a head (up to a micron in length) connected to the dendritic shaft via a neck. Spines can vary in size, likely correlating with the strength of the synapses they form. Spines have been classified into several types based on their morphology, such as stubby, thin or mushroom-shaped. However, this distinction reflects temporary stages of spine maturation or function, and each spine can rapidly switch from one stage to another one on a time scale of minutes (Lippman & Dunaevsky, 2005). Spines constitute the favourite site of synaptic input: more than 90% of electrical excitatory stimuli flow in dendritic spines, although not all spines are forming synapses (Arellano et al., 2007). Indeed, experience-driven plasticity in adult neuronal circuits may involve different mechanisms that result into a morphological reshaping of the synapses between neurons. These adjustments can involve a strengthening or weakening of existing synapses, as well as synapse formation or elimination.

In vivo studies pointed out that volume of spines is a reliable indication of synaptic strength. In fact, spine volume is proportional to the area of the PSD, which in turn is proportional to synaptic AMPA receptor content and to the post-synaptic sensitivity to glutamate release (Holtmaat & Svoboda, 2009). As a matter of fact, spines are observed to increase in volume after long-term potentiation (LTP) (Kopec et al., 2009), whereas long-term depression (LTD) is associated with head shrinkage (Zhou et al., 2004). These assessments can be experimentally achieved *in vivo* by measuring the intensity of fluorescent markers integrated in dendritic spines. Changes in fluorescence are a trustworthy parameter to signal changes in synaptic strength (**Fig. 5.10A**) (Svoboda, 2004). In addition to modifications in the strength of pre-existing synapses, structural plasticity also encompasses formation of new spines, as well as elimination of previously established ones (Holtmaat et al., 2005; Holtmaat & Svoboda, 2009). Such structural modifications significantly increase the storage capacity within the brain

because they allow formation of a large number of synaptic connections. D*e novo* appearance and elimination of pre-established spines were firstly described by *in vitro* imaging experiments, which revealed the occurrence of such structural dynamics over timeframes of hours to days (Portera-Cailliau et al., 2003).

In vivo long-term imaging in the somatosensory and visual cortices have revealed that some spines might appear and disappear over days, whereas the majority of spines remains stable. The fraction of persistent spines grows progressively from young stages to adulthood, even though spine turnover endures. These data provide the first evidence that cortical networks remain dynamics at different developmental stages (Holtmaat et al., 2005). Although several studies have reported different measurements regarding spine dynamics, possibly depending on different cortical structures and methods, it is now accepted that the majority of spines (70-90%) remains stable over long time, whereas a small fraction appears and disappears. The vast majority of new-born spines are transient, and eliminated after few days. On the other hand, spines that persist for more than 4 days are very likely to stabilize and be present for much longer times (**Fig. 5.10B**) (Holtmaat et al., 2005). In general, *in vivo* imaging studies have classified spines based on their lifespan: 1) *transient spines* are newly formed but present for less than 4 days; 2) *new persistent spines* (NP) are new born protrusions that last more than 4 days; 3) *lost persistent spines* (LP) are composed of long-lastingly spines that disappear; 4) *always persistent spines* are observed over the entire imaging period. As previously mentioned, spine morphology seems to be correlated with spine function. Accordingly, transient spines generally consist in dynamic and short life-time filipodia-like protrusions, whereas the majority of persistent spines are characterized by big mushroom-type morphologies (Knott et al., 2006). The consensus is that there is a link between spine size and stability; transient spines are typically tiny, whereas persistent ones are bigger with a defined spine head. However, this relationship between stability and structure is not always trustworthy. Indeed, small spines can also persist, whereas large spines can disappear.

In addition to spine growth and retraction, spines can react to developmental and experience-driven plasticity, through head motility (a process also called twitching) (Majewska et al., 2003). It has been proposed that actin rearrangements are recurring and are modulating synaptic function. These changes in spine motility may be dependent on synaptic inputs that forerun salient phases of structural plasticity, such as spine retraction and stabilization (Majewska et al., 2006). On the same line, *in vivo* studies performed in the mouse barrel cortex indicated that thalamocortical axonal branches are stable over months. However, their relative boutons were subjected to structural rearrangement (De Paola et al., 2006). These results

indicate that axonal boutons, together with dendritic spines, contribute to rewire neuronal circuits. However, it is important to note that the turnover of *en passant* boutons is lower than dendritic spines, allowing to hypothesize that these two processes are not strictly coupled. A recent study found that *en passant* boutons and dendritic spines densities increase throughout adult life. However, this increased density is counterbalanced by a lower long-term spine stabilization in old mice. Aging is also associated with a smaller size of dendritic spines. Thus, these results suggest that aging-related deficits to store long-term memories can be linked to alterations in size and stability of spines and boutons (Mostany et al., 2013).

Most of our knowledge about experience-dependent structural plasticity come from studies that were performed in sensory cortices upon gross sensory manipulation. The rodent barrel cortex represents a pertinent model to investigate structural plasticity upon sensory stimulation or whisker trimming. During early post-natal stages dendritic protrusions in the barrel cortex are highly motile, and sensory experience drives these dynamics. Indeed, whisker trimming considerably decreases such motility during a critical period, without affecting density, length or shape (Lendvai et al., 2000). Accordingly, unilateral chessboard whisker plucking, an experimental paradigm that promotes adaptive functional changes in the neocortex, results into an increase of spine turnover in the barrel cortex (Holtmaat et al., 2006a). In detail, while the vast majority of spines is stable under baseline conditions, chessboard whisker trimming stabilizes new-born spines and increases pruning for previously-established ones. Intriguingly, structural changes are observed mainly in a subset of layer 5 cortical neurons with a complex apical tuft (Holtmaat et al., 2006a). In agreement, novel sensory experience and learning are associated with structural re-organization of the network resulting into stabilization of new formed spines and pruning of a subset of stable ones (Yang et al, 2009). Those results indicate that memory storage leads to long-term marks in the cortical network.

Similarly, sensory manipulation of visual inputs also affects spine dynamics and morphology in the visual cortex. Cortical activity manipulation through dark-rearing of mice from birth negatively correlates with dendritic spine structural dynamics (Tropea et al., 2010). Dark-reared mice display significant upregulation of spine motility and immature spine morphology. However, a few days of light stimulation are sufficient to promote spine stabilization and restore mature spine morphology. Interestingly, when mice undergo to short light stimulation (2 h), cortical networks are subjected to a rapid NMDA-dependent reorganization associated with an untimely emergence of sensory evoked cortical activation and enhanced spine dynamics. These results indicate that structural and functional dynamics are linked *in vivo*, but can undergo rapid and transient changes when perturbed before their

relationship is settled (Tropea et al., 2010). Focused retinal lesion in the adult mouse induces an adaptation to the altered visual input (Keck et al., 2008). The deafferented cortical region displays an almost complete spine turnover within 2 months from the time of the lesion. Furthermore, monocular deprivation (MD) provokes long-lasting structural changes, such as increase of spine formation and consequently enhanced spine density (Hofer et al., 2009). Interestingly, such effect was specific to layer 5 pyramidal neurons located in the binocular cortex.

Recent studies in the mouse motor cortex provide further evidence about the correlation between learning and structural changes of cortical networks. By training mice in a forelimb reaching task, rapid but long-lasting formation of post-synaptic dendritic spines of L5 pyramidal neurons occurred in the contralateral forelimb cortex (T. Xu et al., 2009). Rapid spine formation upon training, is subsequently followed by enhanced spine elimination, resulting in a similar overall spine density to that observed before learning. However, learning-induced new formed spines are preferentially maintained and stabilized during subsequent training. Furthermore, learning of a different forelimb motor task induces synaptogenesis in a different subset of synapses, leaving the first-task dependent set of synapses unaltered (T. Xu et al., 2009). This finding indicates that structural changes upon learning are restricted to discrete subsets of synapses or neurons that are storing memory related to a specific acquired motor skill, and different motor skills are most probably encoded by different subpopulations of synapses.

More recently, spine elimination and formation have been shown to occur also in high cognitive functions areas, such as the frontal association cortex (Lai et al., 2012). Fear conditioning enhances the rate of spine elimination in L5 pyramidal neurons, whereas fear extinction increases the degree of spine formation. Notably, fear extinction-induced synaptogenesis occurs in the same dendritic sites where spines were eliminated upon fear learning. Furthermore, reconditioning preferentially induces pruning of dendritic spines that were formed after extinction (Lai et al., 2012). Taken together, despite the absence of large-scale remodelling of dendrites, these studies clearly indicate that restructuring of cortical connections provides a physical substrate for experience-dependent plasticity.

Unlike changes in synaptic strength, spine formation serves as an efficient strategy to increase the memory storage capacity of the brain. *De novo* spine growth supplies a structural substrate to store new memory. In this model, transient spines may be engaged in optimizing rapid adaptation to sensory inputs. In baseline conditions, transient filopodia-like spines sample available pre-synaptic partners. However, the majority of these attempts fail to produce new

functional synapses and transient spines are subsequently eliminated. Nonetheless, this constant sampling would facilitate rapid synaptogenesis in response to sensory inputs, allowing prompt adaptation to experience (**Fig. 5.10C**). Structural changes outlast the triggering sensory inputs and serve as a substrate for memory storage, preparing the brain for prompt adaptation to equivalent experiences in the future. In addition, different experiences are retained in different subsets of neurons or in different subsets of synapses from the same neuron.

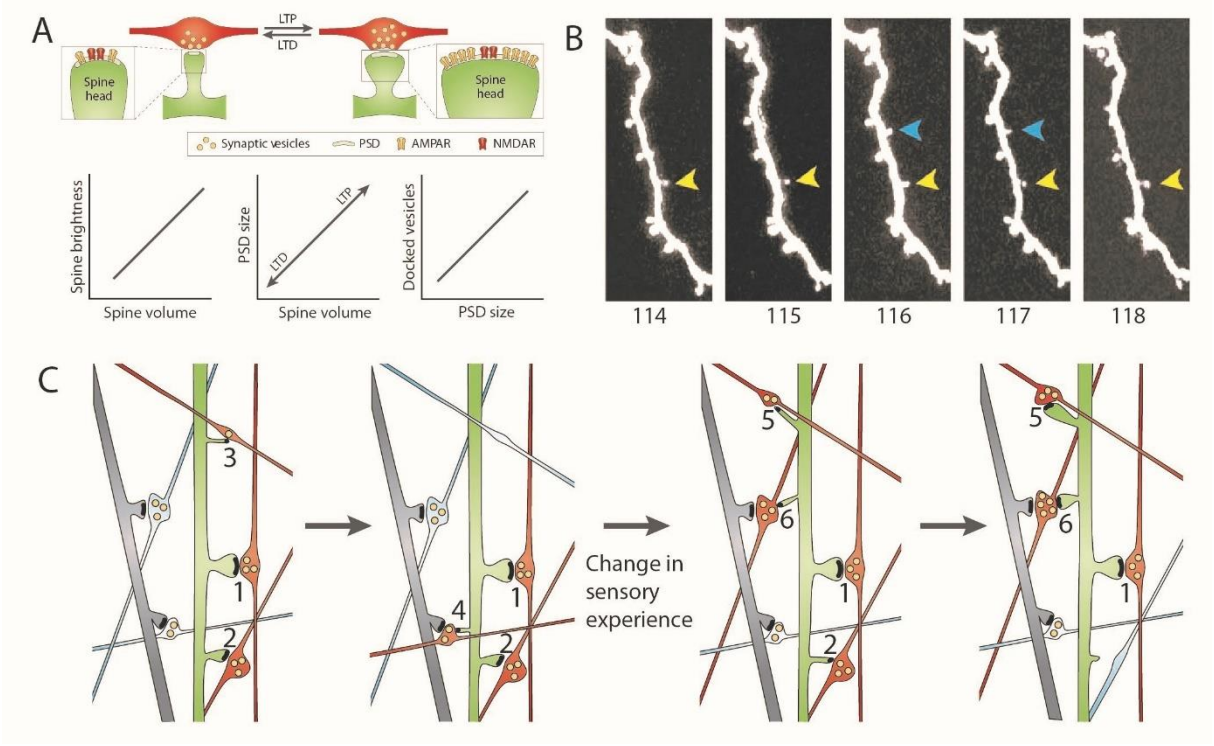

Figure 5.10. (A) Schematic of the structural correlates of synaptic strength (adapted from Holtmaat & Svoboda, 2009). (B) Chronic imaging (post-natal days 114-118) of persistent (yellow arrowheads) and transient (blue arrowheads) spines (Holtmaat et al., 2005). (C) Schematic of structural plasticity upon experience. The majority of spines is stable (e.g. 1, 2), whereas transient spines sample available pre-synaptic partners (3). A change in sensory experience promotes stabilization of newborn spines (5, 6), whereas some pre-established one are eliminated (2) (Holtmaat & Svoboda, 2009).

5.3.3 Experience-dependent functional plasticity

The mechanisms underlying structural plasticity have been extensively investigated in the last two decades. Modifications in strength, formation, stabilization and pruning of synaptic connections potentially change the way circuits compute signals. Surprisingly, how neurons are rebalancing their function and commitment to adapt to salient stimuli has been largely disregarded in the past. Information processing depends on the coordinated activity of large distributed neuronal circuits. Cortical neuronal patterns are supposed to account for sensory perception, memory storage, and decision making, as well as motor execution (e.g., Euston et al., 2012; Komiyama et al., 2010; Sachidhanandam et al., 2013). These patterns have to manage to reach a compromise between stable operating function and dynamic adaptation to environmental changes. In the previous paragraph, it has been extensively reviewed the ability of neural wiring diagrams to adjust to experience, through structural reshuffle of the network. However, how and to what extent these modifications impact processing and computational features of neuronal populations is less clear. With the advent of techniques allowing longitudinal activity recordings from the same populations of neurons, recent studies have provided new insight into this issue.

Longitudinal recordings of the same populations of neurons can be achieved by exploiting techniques such as chronic two-photon calcium imaging or chronic extracellular recordings. Although chronic extracellular recordings provides assessment of same neurons across several different sessions, this technique shows some shortcomings (Lütcke et al., 2013). Firstly, the number of recorded neurons is usually small and further drops in time. Secondly, extracellular recordings preferentially capture information from highly active neurons that maintained their activity stable, and consequently silent neurons that become active are likely to be missed.

Two-photon calcium imaging, through genetically encoded calcium dyes (GECIs), represents a powerful tool that can compensate for the lacks emerged in other techniques, to provide reliable longitudinal measurements of individual neurons and populations. Two-photon calcium imaging is nowadays considered as the most qualified tool to investigate *in vivo* neural population dynamics with high resolution in time and space (Lütcke et al., 2013).

Recently, chronic two-photon calcium imaging has been exploited to unravel the dynamics of neuronal activity in the mouse whisker-related motor cortex (Huber et al., 2012). Within motor cortex, somatosensory information reaches L2/3 pyramidal neurons, which, in turn, project to

layer 5B neurons to produce a motor output. L2/3 neurons undergo to plasticity upon learning. It has been observed that the motor cortex contains numerous spatially intermingled sensory and motor representations. These populations of neurons coding for singles features of a motor task, are stabilized across learning. Population-representations are pre-existing before learning, suggesting that neurons are preferentially pre-wired. Learning modifies the dynamics of activation of neuronal ensembles by reducing the temporal jitter following a stimulus, and consequently increasing the response performances of the motor cortex (**Fig. 5.11A**) (Huber et al., 2012).

Similar longitudinal studies were performed on sensory cortices upon sensory manipulation. Local cortical populations are shown to be considerably heterogeneous in sensory-evoked activity (Brecht et al., 2003), however to what extent functional properties of individual neurons are preserved across time, remains poorly understood. To longitudinally record the activity of single neurons in the intact brain, chronic two-photon calcium imaging has been performed above the barrel cortex prior and following sensory deprivation (Margolis et al., 2012). In agreement with reports carried out in the motor cortex, somatosensory neurons display a sparse distribution of neurons with different tuning properties within the same region and this regime of responsiveness is maintained across time under baseline conditions. Increasing evidence suggests that cortical populations of neurons display a typical sparse population activity (Barth & Poulet, 2012; Huber et al., 2012; Margolis et al., 2012). For instance, Margolis and colleagues identified at least three different groups of cells with distinct tuning properties under baseline conditions in the somatosensory cortex. On the same line, Huber and colleagues highlighted intermingled subsets of L2/3 motor neurons responding to different sensory or motor representations. Finally, evidence of the accuracy of such model derives from studies performed in the posterior parietal cortex (PPC) upon perceptual and working memory decision (Harvey et al, 2012). The PPC is a brain structure important for perceptual decision-making and movement planning. During a navigation-based decision task, PPC neurons have been recorded and their activity assessed. Cells with prolonged activity pattern and significant synchronized events during the task are not observed. On the contrary, neurons are forming cortical sequences of activity in such a way that each neuron is active for only a fraction of the task duration before transferring the information to the following one (Harvey et al., 2012). In line with previous reports showing functionally distinct cortical subsets of neurons anatomically intermingled (Huber et al., 2012; Lütcke et al., 2013; Margolis et al., 2012), cells in the PPC, participating in different choice-specific sequences, are shuffled in the cortical network (Harvey et al., 2012).

Cortical neurons in the somatosensory or motor cortex preserve their functional properties across time, however, experience dependent plasticity can retune their responses. In the barrel cortex, for example, sensory deprivation (e.g. single whisker experience) rebalance neuronal response in favour of the spared whisker (**Fig. 5.11B**). This phenomenon is the result of differential modes of plasticity across functionally distinct neural subsets. Indeed, sensory experience recruits silent or low-responsive neurons by increasing their response magnitude, whereas high-responsive cells exhibit decreased responsiveness to both the spared and the trimmed whisker (Margolis et al., 2012).

In conclusion, chronic recordings of neuronal activity, using electrodes or, more recently, two-photon imaging technologies, has just started to provide insights about the functional organization of neurons upon experience and learning. In line with reports on the structure of the neuronal patterns, functional studies reveal a prominent stability of the regime of responsiveness and functional across the cortical networks. Intriguingly, within cortical areas, neighbouring neurons hold distinct functional properties likely underlying different roles within the cortical tasks. Experience and learning affect this stability by retuning the responsiveness properties of such neurons. The precise mechanisms, pathways and molecular players of experience-dependent functional re-organization of the cortical networks remain to be identified. However, with the advent of optical technologies able to record longitudinally high-dimensional populations of neurons, upcoming studies will be able to tackle the unresolved questions.

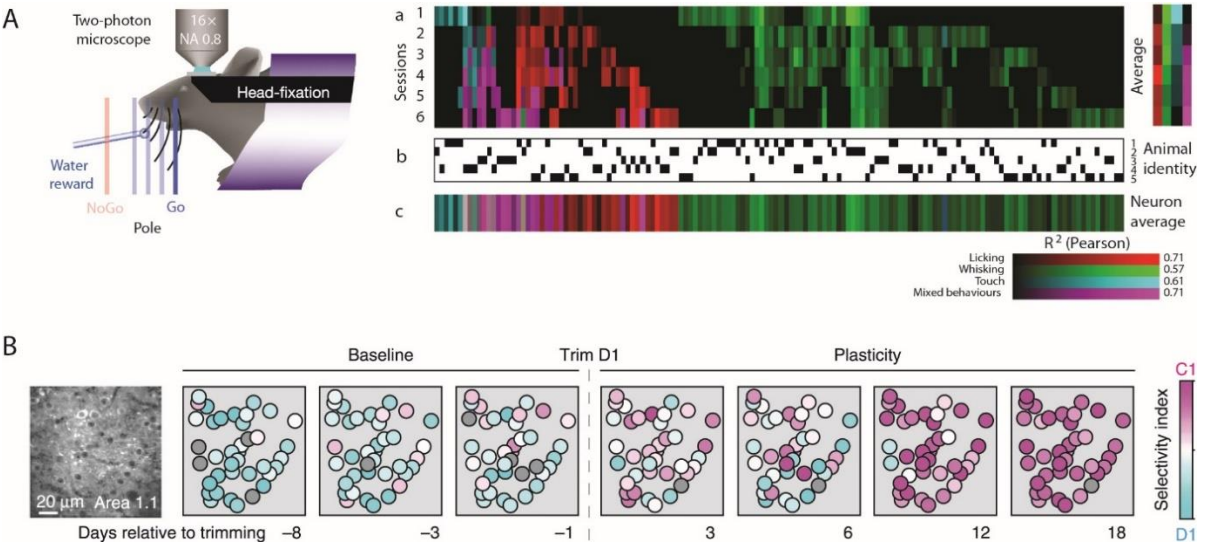

Figure 5.11. (A) Left, schematic of two-photon calcium imaging of the vibrissal motor cortex during a sensorimotor task. Right, a) Classification of single neuron (columns) representations (licking, whisking, touch, mixed) across multiple sessions. Dynamics of single neurons was determined through a decision tree-based classification algorithm and quantified as correlation between data and model (R^2). b) Animal identity. Black squares correlate the animal with the corresponding cell. c) neuron averaged representation across sessions (adapted from Huber et al., 2012). (B) Re-adjustment of neuronal selectivity upon D1 whisker trimming (Margolis et al., 2012).

5.4 *The role of dPFC in fear learning and the underlying mechanisms of plasticity*

The introduction of this dissertation revolves around three main themes: associative learning, the structural and functional mechanisms of plasticity, and the dorsal prefrontal cortex (dPFC). The essence of associative learning is the pairing of two stimuli. A first one, defined conditioned stimulus (CS) produces either no overt response or a weak response usually unrelated with the response that eventually will be learned. The reinforcement, or unconditioned stimulus (US), normally elicits a strong and consistent response (unconditioned response). Unconditioned responses are innate; they are produced in absence of learning mechanisms. Repeated presentation of CS followed by an US, progressively induces a new or different response called "conditioned response". Associative learning or classical conditioning enables the animals to distinguish events that reliably occur together from those that are only randomly associated, a process that is known as discriminative learning. This form of learning can be experimentally reproduced in laboratory through a widely used behavioural paradigm named cued fear conditioning. During this task, an animal learns to discriminate between a conditioned stimulus (CS+) paired with the occurrence of an aversive event (US), with a second neutral stimulus (CS-) that is not predicting any kind of threat or danger. The neuronal correlates and mechanisms involved in associative fear learning have been extensively investigated in the past (for a review see paragraph 5.1 Associative Learning). It is now widely accepted that the amygdala represents the neural embodiment of fear conditioning. The lateral nucleus of the amygdala (LA) is thought to be a site of synaptic change during stimulus association. The CS and US signals converge in the lateral amygdala; when the CS and the US are temporally paired, the effectiveness of the CS is enhanced.

Surprisingly, whether fear learning is a process widely investigated, how an animal learns to discriminate between threatening and surrounding neutral/safe stimuli remains poorly understood. Dissociating stimuli that predict danger from ones that do not is crucial for survival and self-preservation. Inability to discriminate between emotionally distinct environmental cues leads to inappropriate responses and may result into anxiety and post-traumatic disorders (PTSDs). Notably, anxiety and PTSD patients display generalization and unfitting behavioural response to neutral/safe stimuli. Therefore, finding an answer to such scientific question is of primary importance. **The work presented in this thesis aimed at demonstrating a prominent**

role of the dorsal prefrontal cortex in discriminating fearful stimuli from the surrounding similar yet emotionally meaningless environmental cues.

Previous attempts at unraveling the functional engagement of the dorsal prefrontal cortex in fear conditioning adopted rough strategies of pharmacological inactivation of the investigated area (Lai et al., 2012; Sacchetti et al., 2002, 2003). Unfortunately this approach does not allow temporal and spatial precise control of the functional neuronal blockade. Even though these studies indicated a potential role in fear acquisition, they failed to accurately understand the exact role of such cortical structure in fear learning. By exploiting a more refined and elegant optogenetic approach in behaving animals, the results illustrated in this dissertation clearly indicate a pivotal role of the dPFC in discriminative learning. Inhibition of dPFC at precise time frames and exclusively during the association between the CS and the US, resulted into overgeneralized response to safe stimuli.

The concept expounded in this manuscript does not deprive amygdala from its central role in fear encoding. The neural processing responsible for fear learning and generation of an appropriate behavioural output is led by the amygdala. However, in line with numerous studies that have implicated the anterior cingulate cortex, the insular cortex and the ventromedial prefrontal cortex in various aspects of emotional processing, the present work provides new insights into a potential top-down control of cortical regions upon subcortical areas involved in fear acquisition and expression. The dorsal prefrontal cortex intervenes after amygdala activation by refining the behavioural outcome triggered by subcortical activity. These results are in agreement with different clinical studies identifying the prefrontal cortex as a functional region that governs attention accorded to certain stimuli, influences the content retrieved from memory, and shapes mental plans conceived as a response to the triggering stimulus. Furthermore, the current study characterizes the functional properties that subtend a reorganization of the network upon experience. Compelling evidence indicates structural plasticity upon fear learning in this cortical region (Lai et al., 2012). Consistently, the work presented in this manuscript illustrates generation of temporally non-overlapping neuronal assemblies that define stimulus discrimination after pavlovian conditioning.

Finally, this study distinctly unravels the mechanisms by which experience-dependent functional plasticity occurs in the dorsal prefrontal cortex. *In vivo* plasticity events are relying upon the convergence of at least two distinct pathways (Gambino et al., 2014; Gambino & Holtmaat, 2012; M. Larkum, 2013; Pouchelon et al., 2014). The simultaneous activation of two projections upon the same dendritic branches in the cortical network promotes plastic events. Such plasticity can results into a reshape of cortical maps. However, whether this model holds

to be true in high cognitive areas remains poorly understood. Accordingly with previous studies performed in the somatosensory e motor cortex, this work describes the existence of analogous experience-dependent functional plasticity in higher functional cortical areas, and this process is governed by convergence of at least two long-range pathways conveying distinct information. Indeed, dPFC receives pre-processed sensory information that triggers non-linear dendritic activation of cortical neurons. Emotional information conveyed from the amygdala, during pavlovian conditioning, superimposes on the former input selecting the neurons that will aggregate to the neuronal assemblies encoding for stimulus discrimination.

To recapitulate, this manuscript illustrates results that associate the dorsal prefrontal cortex to stimulus discrimination during associative learning. This function relies upon functional restructuring of cortical maps that depends on the convergence of sensory and emotional information on dPFC primary neurons.

6. Materials and Methods

6.1 Animals

All experiments were performed in accordance with the Guide for the Care and Use of Laboratory Animals (National Research Council Committee (2011): Guide for the Care and Use of Laboratory Animals, 8th ed. Washington, DC: The National Academic Press.) and the European Communities Council Directive of September 22th 2010 (2010/63/EU, 74). Experimental protocols were approved by the institutional ethical committee guidelines for animal research (N°50DIR_15-A) and by the French Ministry of Research (N°02169.01). We used male C57Bl6/J 6-weeks old mice from Charles River that were housed with littermates (3-4 mice per cage) in a 12-h light-dark cycle. Cages were enriched and food and water were provided *ad libitum*.

6.2 Surgery and virus injection

Mice were anesthetized with an intraperitoneal (i.p.) injection of a mix containing medetomidine (sededorm, 0.27 mg kg^{-1}), midazolam (5 mg kg^{-1}) and fentanyl (0.05 mg kg^{-1}) in sterile NaCl 0.9% (MMF-mix). Analgesia was achieved by local application of 100 µl of lidocaine (lurocaine, 1%) and subcutaneous (s.c.) injection of buprenorphine (buprécare, 0.05 mg kg^{-1}). 40 µl of dexamethasone (dexadreson, 0.1mg ml^{-1}) was administrated intramuscularly (i.m.) in the quadriceps to prevent inflammation potentially caused by the friction of the drilling. A heating-pad was positioned underneath the animal to keep the body temperature at 37ºC. Eye dehydration was prevented by topical application of ophthalmic gel. The skin above the skull was disinfected with modified ethanol 70% and betadine before an incision was made. Stereotaxic injections were done as previously described (Gambino et al., 2014) . Briefly, the bregma and lambda were aligned (x and z) and a hole for injection was made using a pneumatic dental drill (BienAir Medical Technologies, AP-S001). The injections were targeted either to the layer 2/3 of the FrA (from bregma: AP, +2.8 mm; DV, -0.2-0.3 mm; ML ±1.0 mm) or to the BLA (from bregma: AP, -1.3 mm; DV, -4.5 to 4.8 mm; ML, ±2.9 mm), or to both at the same time. 200 nl of virus were injected at a maximum rate of 60 nl/min, using a glass pipette (Wiretrol, Drummond) attached to an oil hydraulic manipulator (MO-10, Narishige).

The following viruses were used depending on the experiments. AAV-ChR2 (AAV9.CamKIIa.hChR2(H134R).eYFP.WPRW.SV40, 1.03 x 10^{14} GC ml^{-1}, Penn Vector Core, provided by K. Deisseroth) was unilaterally injected in the right BLA, whereas AAV-ArchT (AAV9.CAG.ArchT.GFP.WPRE.SV40, 5.66 x 10^{12} GC ml^{-1}, Penn Vector Core, provided by Ed

Boyden and the MIT), AAV-ArchT-Flex (AAV2/9.CBA.flex.Arch-GFP.WPRE.SV40, Penn Vector Core, provided by Ed Boyden and the MIT), Cav-Cre (Cav2.CMV.Cre, IGMM BioCampus Montpellier) were bilaterally injected into the BLA or FrA. Control experiments were performed using an AAV containing the DNA construct for only GFP (AAV9.CamKII0.4.eGFP.WPRE.rBG, 5.27 x 10^{13} GC ml^{-1}, Penn Vector Core) or GFP-DIO (AAV2/9.EF1a.DIO.eYFP.WPRE.hGH 2.46 x 10^{13} GC ml^{-1}, Penn Vector Core, provided by K. Deisseroth). For somatic and dendritic calcium imaging, AAV-GCaMP5G (AAV1.hSyn.GCAMP5g.(GCAMP3.T302L.R303P.D380Y).WPRE. SV40, Penn Vector Core, 2.13x10^{13} GC ml^{-1}) and AAV-GCaMP6-Flex (AAV9.Syn.Flex.GCaMP6s. WPRE.SV40, Penn Vector Core, 7.28x10^{13} GC ml^{-1}) combined with AAV-Cre (AAV1. hSyn.Cre.WPRE.hGH, Penn Vector Core, 5.048x10^{13} GC ml^{-1}), diluted 1/10000, were injected to the FrA immediately after the craniotomy was made. The same virus was used for the calcium imaging of BLA-FrA boutons, but the injection was targeting the right BLA. After injections, the viruses were allowed to diffuse for at least 10 min before the pipette was withdrawn. Mice were then either prepared for cranial window implantation or waked-up by a sub-cutaneous injection of a mixture containing atipamezole (revertor, 2.5 mg kg^{-1}), flumazenil (0.5 mg kg^{-1}), and buprenorphine (buprécare, 0.1 mg kg-1) in sterile NaCl 0.9% (AFB-mix).

To evaluate the viral expression profiles in BLA and dPFC, fixed brain slices were imaged post-hoc using a wide-field epifluorescence microscope (Nikon, Eclipse N-iU). Illumination was set such that the full dynamic range of the 16-bit images was utilized. A two-dimensional graph of the intensities of pixel was plot using Fiji Software. 16-bit images' brightness was processed and masks were registered to the corresponding coronal plates (ranging from -1.94 to -2.70 mm) of the mouse brain atlas(Paxinos & Watson, 2007) using Illustrator (Adobe), at various distances antierior (FrA) or posterior (BLA) to the bregma.

6.3 *Behavior*

At least 5 days before starting behavior, mice went through handling with the same experimenter that performed the experiments in order to decrease stress. On the first day of the protocol, mice were placed on the conditioning compartment (context A, consisting on a squared box with grid floor that allows the release of a foot shock and with home cage litter under; cleaned between individuals with 70% ethanol) for habituation, where two conditional stimuli (CS) (CS+: 8 kHz; CS-: white noise pips; composed of 27 pips, 50 ms, 0.9 Hz for 30 s) were presented 4 times with a 80 dB sound pressure level and variable inter stimulus interval (ISI). The freezing time during

each CS presentation was measured and the mice returned to their home cage. 24 hours later mice were exposed to context A and 5 CS+ were paired with the unconditional stimulus (US, 1s foot shock at 0.6 mA) with the onset coinciding with the CS+ offset. 5 CS- presentations were intermingled with CS+ presentations with a variable (10-60 s) ISI during the test. Recall tests were carried out 24 hours after the conditioning phase by measuring the freezing time during the presentation of 2 CS+ and 2 CS- in a new context (context B, consisting of a cylindrical white compartment with home cage litter on the floor; cleaned between individuals with septanios MD 2%). Freezing behavior was quantified automatically in each behavioral session using a fire-wire CCD-camera connected to automated freezing detection software (AnyMaze, Ugo Basile, Italy).
For the experiments in which the conditioning phase was taken place under the 2 photon microscope, the behavior context consisted on the microscope box in which the mice were head-restrained in a custom tube containing with a shocking grid at the bottom. CS and US presentations were triggered by a MATLAB routine, associated to a pulse-stimulator (Master-8, A.M.P.I) capable of triggering the foot shock. For optogenetic experiments using *archeorhodopsin* (ArchT) or GFP controls, mice were subjected to the same behavioral protocol described above, but light-induced neuronal network inhibition of the FrA during conditioning phase was obtained by applying a 3 second-lasting yellow laser stimulation during the pairings between CS+ and US (since the last second of CS+ presentation until 2 seconds after US termination). Optogenetic inhibition of BLA-to-FrA projections during the CS- presentation of the conditioning phase was achieved by synchronizing the 50 ms laser pulses with the 50 ms pip of the CS- presentations.

6.4 *2-photon laser-scanning microscope (2PSLM)-based calcium imaging*

The cranial windows were made as previously described(F. Gambino et al., 2014). Briefly, after skull's exposure a ~5 mm plastic chamber was attached on the area of interest and a 3 mm craniotomy was made on the right hemisphere above FrA and M2, with a pneumatic dental drill, leaving the dura intact. The craniotomy was covered with sterile saline (0.9% NaCl) and sealed with a 3 mm glass cover slip after viral injection (for imaging experiments). The chamber, the cover slip and a custom-made stainless steel head stage were well attached to the skull using dental acrylic and dental cement (Jet Repair Acrylic, Lang Dental Manufacturing).
Head-fixed awake mice were placed and trained under the microscope every day for at least 7 days prior to the experiment, and then imaged 21 to 35 days after virus injection using an *in vivo* non-

descanned FemtoSmart 2PLSM (Femtonics, Budapest, Hungary) equipped with a ×16 objective (0.8 NA, Nikon). The MES Software (MES v.4.6; Femtonics, Budapest, Hungary) was used to control the microscope, the acquisition parameters, and the TTL-driven synchronization between the acquisition and auditory/footshock stimuli. The GCaMPs were excited using a Ti:sapphire laser operating at λ=910 nm (Mai Tai DeepSee, Spectra-Physics) with an average excitation power at the focal point lower than 50 mW. Time-series images were acquired within a field-of-view of 300 x 300 µm (for axons and somas, 256 lines, 1ms/line). Each imaging session consisted of 30 s of baseline recording followed by 8 gaussian and 8 pure (8kHz)-tone auditory stimuli delivered in a pseudorandom order. We imaged on average 3500 frames (~900 s) per session, and no visible photo-bleaching was observed. Images were then analyzed as previously described(F. Gambino et al., 2014) using custom routines written in Fiji and Matlab (Mathworks). We registered images over time and corrected XY motion artifacts within a single imaging session by using cross-correlation based on rigid body translation (Stack aligner, Image J, NIH, USA). Motion corrections were then assessed by computing pair-wise 2D correlation coefficient (Image correlation, Image J, NIH, USA), and frames were discarded from the analysis if lower than 0.7. Similar rigid body translation was used to align inter-sessions images with the session 4 (first session post learning) selected as a reference template. Regions of interest (ROIs) for pyramidal neurons and putative axonal boutons were selected and drawn manually. All pixels within each ROI were first averaged providing a single time-series of raw fluorescence. To limit the effect of fluorescence drift over time, peaks of fluorescence were first detected, and the baseline fluorescence (F_0) was calculated as the mean of the lower 50% of previous 10 s fluorescence values. Change in fluorescence ($\Delta F_t/F_0$) was defined as $(F_t-F_0)/F_0$, were F_t is the fluorescence intensity at time t (time of the first pixel in each frame). Calcium events were then detected using a template-based method with a custom library of calcium transients. Each detected event was inspected visually and analysis was restricted to detected events rather than on raw fluorescence. To measure correlations between neurons within a single population, the activity of each recorded neuron was normalized to the activity during baseline prior to auditory stimulation. Detected events ($\Delta F/F_0$) upon 30 s-lasting auditory stimulation were binned (1 sec), averaged over 8 trials, and organized in a n x 30 two-dimensional matrix (n=number of ROIs per animal). Pearson's coefficient of correlations were then computed between CS+ and CS- related matrices.

6.5 *In vivo whole cell recordings*

Isoflurane (4% with ~0.5 l min^{-1} O_2) combined with an i.p. injection of urethane (1.5 g kg^{-1}, in lactated ringer solution containing in [mM] 102 NaCl, 28 Na L Lactate, 4 KCl, 1.5 $CaCl_2$) was used to induce anesthesia and prolonged by supplementary urethane (0.15 g kg^{-1}) if necessary. To prevent risks of inflammation, brain swelling and salivary excretions, 40 µl of dexamethasone (dexadreson, 0.1 mg ml^{-1}, i.m.) and glycopyrrolate (Robinul-V, 0.01 mg kg^{-1}, s.c.) were injected before the surgery. Adequate anesthesia (absence of toe pinch and corneal reflexes, and vibrissae movements) was constantly checked and body temperature was maintained at 37°C using a heating-pad positioned underneath the animal. Ophthalmic gel was applied to prevent eye dehydration. Analgesia was provided as described for viral injection (with lidocaine and buprenorphine). After disinfection of the skin (with modified ethanol 70% and betadine), the skull was exposed and a ~3mm plastic chamber was attached to it above the prefrontal cortex using a combination of super glue (Loctite) and dental acrylic and dental cement (Jet Repair Acrylic, Lang Dental Manufacturing). A small ~1 x 1 mm craniotomy centered above the FrA (+2.8 mm from bregma, ±1.0 mm midline) was made using a pneumatic dental drill, leaving the dura intact.

Whole-cell patch-clamp recordings of L2/3 pyramidal neurons were obtained as previously described (Gambino et al., 2014) Briefly, high-positive pressure (200–300 mbar) was applied to the pipette (5–8 MΩ) to prevent tip occlusion, when passing the pia. Immediately after, the positive pressure was reduced to prevent cortical damage. The pipette resistance was monitored in the conventional voltage clamp configuration during the descendent pathway through the cortex (until -200 µm from the surface) of 1 µm steps. When the pipette resistance abruptly increased, the 3–5 GΩ seal was obtained by decreasing the positive pressure. After break-in, Vm was measured, and dialysis was allowed to occur for at least 5 min before launching the recording protocols. Current-clamp recordings were made using a potassium-based internal solution (in mM: 135 potassium gluconate, 4 KCl, 10 HEPES, 10 Na2-phosphocreatine, 4 Mg-ATP, 0.3 Na-GTP, and 25 µM, pH adjusted to 7.25 with KOH, 285 mOsM), and acquired using a Multiclamp 700B Amplifier (Molecular Devices). Spontaneous activity was recorded prior, during and after the presentation of the CS- and the CS+. Spiking pattern of patched cells was analyzed to identify pyramidal neurons. dAP5 (1 mM, Tocris) was topically applied to the dura mater, before whole cell recordings. Offline analysis was performed using custom routines written in Sigmaplot (Systat), IGOR Pro (WaveMetrics) and Matlab (Mathworks).

6.6 *In vivo optogenetics*

After virus injection for ChR2 or ArchT expression, mice were subsequently implanted with fiber optic cannula for optogenetics (CFML22U, Thorlabs) in the FrA or BLA. The optic fibers were previously cleaved with a fiber optic scribe (S90R, Thorlabs) at 4.5mm for BLA, or 0.4-0.5 mm for superficial implantation in FrA. The cannula were guided and stereotaxically inserted inside the brain with the help of a cannula holder (XCL, Thorlabs) through the same burr hole used for the viral injections (FrA coordinates from bregma: AP, +2.8 mm; DV, -0.5 mm; ML, ±1.0 mm; BLA coordinates from bregma: AP, -1.3mm; DV, -4.5 mm; ML, ±2.9mm) and secured in place with a mix of super glue (Loctite) and dental acrylic and dental cement (Jet Repair Acrylic, Lang Dental Manufacturing). Anesthesia was reversed using AFB-mix for mice assigned to behavioral experiments. For *in vivo* photostimulation of ChR2-expressing BLA neurons, the fiber optic cannula and the optogenetic patch cable (M83L01, Thorlabs) were connected through a ceramic split mating sleeve (ADAL1, Thorlabs). The patch cable was then coupled to a blue DPSS laser (SDL-473-050MFL, Shanghai Dream Lasers Technology) which was triggered by a pulse-stimulator (Master-9, A.M.P.I), able to synchronize 50 ms laser pulses with 50 ms sound pips composing the CS. For inhibition of FrA or BLA-to-FrA projections during learning, *in vivo* bilateral optic stimulation of ArchT-expressing neurons was achieved by coupling the optic fibers implanted in FrA or BLA, respectively to a multimode fiber optic coupler (FCMH2-FCL, Thorlabs), with a ceramic split mating sleeve, and subsequently connected to a yellow DPSS laser (SDL-LH-1500, Shanghai Dream Lasers Technology).

6.7 *In vitro whole-cell recordings*

Mice were anesthetized with a mixture of ketamine/xylazine (100mg/kg and 10mg/kg respectively) and cardiac-perfused with ice-cold, oxygenated (95% O2, 5% CO2) cutting solution (NMDG) containing (in mM): 93 NMDG, 93 HCl, 2.5 KCl, 1.2 NaH2PO4, 30 NaHCO3, 25 Glucose, 10 MgSO4, 0.5 CaCl2, 5 Sodium Ascorbate, 3 Sodium Pyruvate, 2 Thiourea and 12mM N-Acetyl-L-cysteine (pH 7.3-7.4, with osmolarity of 300-310 mOsm). Brains were rapidly removed and placed in ice-cold and oxygenated NMDG cutting solution (described above). Coronal slices (300 µm) were prepared using a Vibratome (VT1200S, Leica Microsystems, USA) and transferred to an incubation chamber held at 32°C and containing the same NMDG cutting solution. After this incubation (9-11 min), the slices were maintained at room temperature in

oxygenated modified ACSF containing (mM): 92 NaCl, 2.5 KCl, 1.2 NaH_2PO_4, 30 $NaHCO_3$, 20 HEPES, 25 Glucose, 2 $MgSO_4$, 2 $CaCl_2$, 5 Sodium Ascorbate, 3 Sodium Pyruvate, 2 Thiourea and 12mM N-Acetyl-L-cysteine (pH 7.3-7.4, with osmolarity of 300-310 mOsm) until recording. Whole-cell recordings of layer 2/3 FrA principal neurons were performed on coronal slices (from bregma: +2.58 mm to +3.08 mm) at 30-32ºC in a superfusing chamber. Patch electrodes (3-5 MΩ) were pulled from borosilicate glass tubing and filled with a K-gluconate-based intracellular solution (in mM: 140 K-gluconate, 5 QX314-Cl, 10 HEPES, 10 phosphocreatine, 4 Mg-ATP and 0.3 Na-GTP (pH adjusted to 7.25 with KOH, 295 mOsm). BLA-to-dPFC monosynaptic EPSCs were elicited by 1-50 ms light stimulations delivered by an ultrahigh power 460 nm LED (Prizmatix Ltd, Israel). Data were recorded with a Multiclamp700B (Molecular Devices, USA), filtered at 2 kHz and digitized at 10 kHz. Data were acquired and analysed with pClamp10.2 (Molecular Devices).

6.8 *uDISCO*

Animals, previously infected in the right BLA with an AAV-CaMKII-GFP, were anaesthetized by administration of MMF-mix via intraperitoneal injection. After having checked for complete anaesthetic state, mice were perfused for 5-10 min, at room temperature, with heparinized (10U/ml of Heparin, ratiopharm GmbH, N68542.03) 0.1 M PBS, and subsequently for 20 min with 4% paraformaldehyde in 0.1 M PBS for 20 min at a speed of 3 ml/min, using a peristaltic pump. After removal of the intact brain from the skull, tissue post-fixation was performed over-night in 4% PFA at 4°C (long post-fixation should be avoided to prevent auto-fluorescence artefacts) and thereafter washed 2-3 time with PBS at room temperature.

The clearing process required the preparation of different clearing solutions. Serial dilutions of tert-Butanol (Sigma 360538) (30%, 50%,70%, 80%, 90%, 96%) were obtained in distilled water. Pure solutions of Tert-Butanol and Dichloromethane (DCM, Sigma 270997) were also used for the dehydration and lipid dissolution processes, respectively. The clearing process consisted into different steps of incubation in serial dilutions of tert-Butanol at 35°C (30% over night, 50% for 10h, 70% over night, 80% for 10h, 90% over night, 96% for 10h, 100% over night) and subsequently the samples were incubated at room temperature in DCM for 50-70min. Finally brain tissues were incubated at room temperature in BABB-D (benzyl alcohol (BA, Sigma 24122), benzyl benzoate (BB, Sigma W213802) and diphenyl ether (DPE, Alfa aesar A15791)) for at least 2-3h.

Images were acquired using a Nanozoomer 2.0HT or via light-sheet microscopy using the Ultramicroscope II (Lavision Biotech). Image processing steps were performed using the Fiji software and 3D reconstruction was realized via the software Arivis Vision 4D.

7. Results

Discriminative learning is an evolutionary important survival strategy that depends on the repeated contingency and contiguity between sensory cues (conditioned stimuli, CS) and the events (i.e. danger) they must predict (unconditioned stimuli, US) (LeDoux, 2000; Likhtik & Paz, 2015a). The resulting learned association provides an accurate representation of the environment by increasing discriminative skills between aversive (threat) and non-aversive (safety) environmental signals (LeDoux, 2000; Likhtik & Paz, 2015a). Many anxiety-related behaviors such as post-traumatic stress disorder (PTSD) are associated with a loss of cue discrimination that may result in fear overgeneralization to harmless environment (LeDoux, 2000; Peri et al., 2000). Therefore, further exploration of the neural circuits that encode and compare aversive *vs.* non-aversive signals is critical for our understanding of PTSD and related affective disorders. However, while previous work has mostly focused on how the CS generate fear responses (e.g. (Dejean et al., 2016; Courtin et al., 2014; Karalis et al., 2016)), it remains unclear how the brain learns to discriminate between CS and similar yet meaningless stimuli (Li et al., 2008; Resnik et al., 2011).

The medial prefrontal cortex (mPFC) appeared over the past decade as a critical region that shapes behaviors in response to both aversive and non-aversive environmental cues (Likhtik & Paz, 2015; Likhtik et al., 2014; Stujenske et al., 2014). These antagonistic effects of mPFC possibly develop through specific interaction between its different subdivisions (i.e prelimbic (PL) and infralimbic (IL) cortices) and the basolateral complex of the amygdala (BLA) (Courtin et al., 2014; Likhtik et al., 2014; Senn et al., 2014; Sierra-Mercado et al., 2011; Vidal-Gonzalez et al., 2006). However, the idea that higher neuronal networks above the mPFC might encode opposing memories that are later preferentially selected during recall by recruiting downstream cortical (e.g. PL or IL mPFC) or subcortical structures (e.g. BLA) (Kitamura et al., 2017; Lai et al., 2012; Manita et al., 2015; Otis et al., 2017; Rajasethupathy et al., 2015; Reijmers et al., 2007) has never been challenged. In keeping with this idea, it has been shown that the superficial frontal association cortex (FrA) contributes to memory formation during associative learning in rodents (Komiyama et al., 2010; Lai et al., 2012; Nakayama et al., 2015; Sacchetti et al., 2002; Sul et al., 2011). This region of the lateral part of the agranular cortex (AGl) (Paxinos & Watson, 2007; Uylings et al., 2003) is reciprocally connected with the medial PFC (mPFC), the BLA, and the mediodorsal thalamic nucleus (Lai et al., 2012; Mátyás et al., 2014; McDonald, 1987; Rajasethupathy et al., 2015), and its inactivation alters both fear learning and extinction (Lai et al., 2012; Sacchetti et al., 2002). Recently, fear conditioning and extinction have been shown to induce in FrA dendritic spine elimination and formation, respectively (Lai et al., 2012). Importantly, this occurred within the same dendrite supporting the idea that a unique FrA circuit might be well suited to control discrimination by computing opposite memories.

Theoretically, the existence of a dynamic high-dimensional cortical state (Delamater, 2012; Hall, 2002; Salzman & Fusi, 2010) could increase memory storage capabilities and facilitate perceptual acuity (Briggman & Kristan, 2008; Dejean et al., 2016; Harvey et al., 2012; Pastalkova et al., 2008). Whether such a learned discriminative representation is wired within discrete FrA circuits during conditioning and by which synaptic mechanisms remain unknown. To address these questions, we used *in vivo* whole-cell recordings (Gambino et al., 2014) and optogenetic conditional strategies (Kitamura et al., 2017; Rajasethupathy et al., 2015), together with two-photon (2P) calcium imaging in head-restrained mice to explore the dynamics of layer (L) 2/3 FrA pyramidal neurons (Harvey et al., 2012; Kitamura et al., 2017; Komiyama et al., 2010; Rajasethupathy et al., 2015) and long-range projections from the BLA (Gambino et al., 2014) during the acquisition and recall of discriminative memories. We found that classical fear conditioning is associated with the creation of cue-specific FrA activity patterns whose decorrelation predicted the level of discrimination between threat and safety signals. In naive mice, sensory auditory stimulation produced frequency-specific, NMDARs-dependent, plateau-like depolarizations that potentiated FrA L2/3 neurons when combined with the channelrhodopsin-2-mediated activation of BLA neurons projecting to the FrA. During conditioning, those long-range projecting BLA neurons conveyed integrated information about the CS/US association that were critical to threat *vs.* safety discriminative learning. In conclusion, our study reveals a new circuit and synaptic mechanism for cue discrimination and provides a new cortical framework for our understanding of predictive learning and related disorders.

7.1 *Chronic imaging of FrA pyramidal neurons during auditory cue discrimination*

To examine whether cue discrimination might be encoded within specific prefrontal circuits, mice were injected with a virus encoding the calcium indicator GCaMP5 (Tian et al., 2012) and implanted with a cranial window (Gambino et al., 2014; Harvey et al., 2012) above the frontal association cortex (FrA) (**Fig. 7.1 and Methods**). The same population of putative pyramidal neurons was imaged longitudinally in head-fixed awake mice before (sessions 1-3) and

after (sessions 4-6) differential fear conditioning while discriminative performance was tested at least 6 hours after each imaging session (**Fig. 7.1d**).

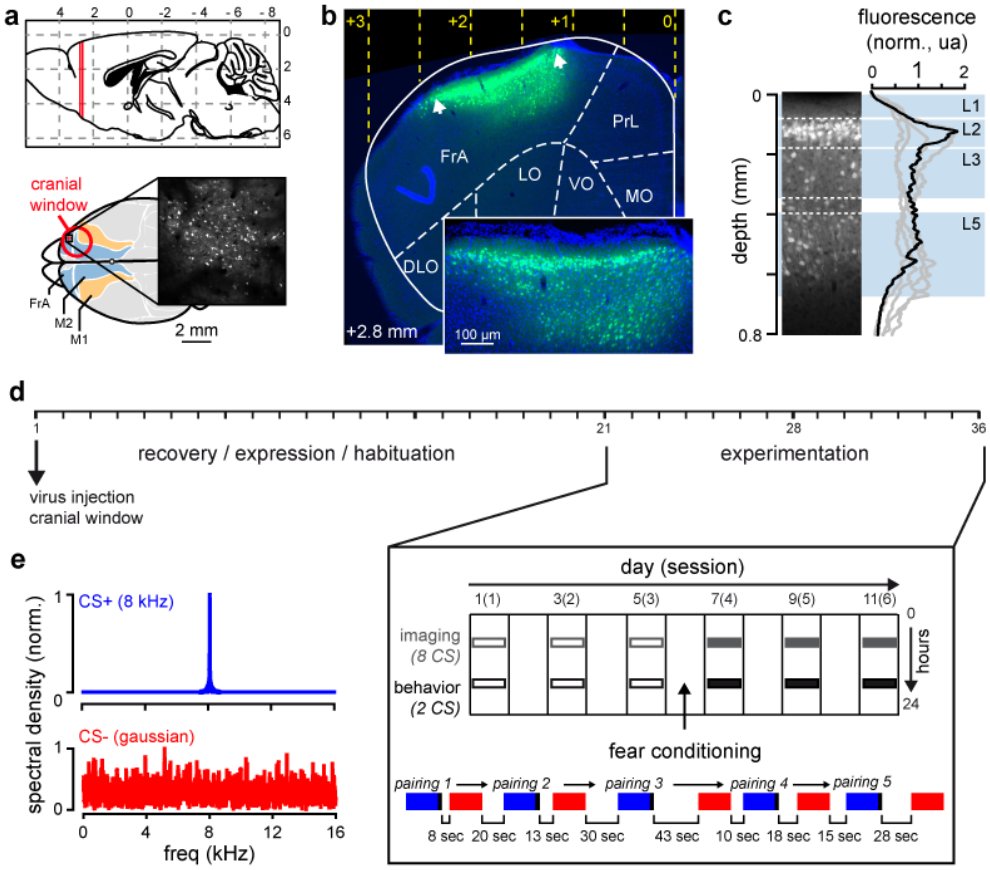

Figure 7.1. Experimental protocol. a, Injection sites (AAV-GCaMP5) and position of cranial window are depicted in red. **b**, Representative example of the GCaMP5G expression profile in the mouse FrA (+2.8 mm from bregma). FrA, *frontal association cortex*; PrL, *prelimbic cortex*; MO, *medial orbital cortex*; VO, *ventral orbital cortex*; LO, *lateral orbital cortex*; DLO, *dorsolateral orbital cortex*. **c**, Plot comparing the intensity profiles as a function of cortical depth of 5 different animals (4 mice were used for imaging experiments). Black line represents the example from the left (same as in **b**). Putative layers (L) are indicated in light blue. **d**, Schedule of experiments. Head-fixed awake mice were placed and trained under the microscope every day for at least 7 days prior to the experiment, and then imaged 21 to 35 days after virus injection. Fear conditioning protocol is represented below. Five auditory stimuli (each consisting of 27 pure (8 kHz)-tone or white noise pips, 50 ms, 0.9 Hz for 30 s) were positively (blue, CS+, 8 kHz) or negatively (red, CS-, gaussian noise) paired with the delivery of a mild electrical shock (black, 0.6 mA) to the paws in a pseudorandom order. Delays between stimuli are indicated below. **e**, Spectral properties of auditory stimulation.

During conditioning, five auditory stimuli (each consisting of 27 pure (8 kHz)-tone or white noise pips, 50 ms, 0.9 Hz for 30 s) were positively (CS+, 8 kHz) or negatively (CS-, gaussian noise) (see **Fig. 7.1e**) paired with the delivery of a mild electrical shock (0.6 mA) to the paws in a pseudorandom order (**Fig. 7.1d**). During recall in a new context, mice froze significantly more in response to CS+ as compared to the habituation period (session 3: 10.1 ± 3% *vs.* session 4: 64.5 ± 2.4 %; n=5; $p<0.001$; *paired t-test*) while freezing responses upon CS- presentation remained

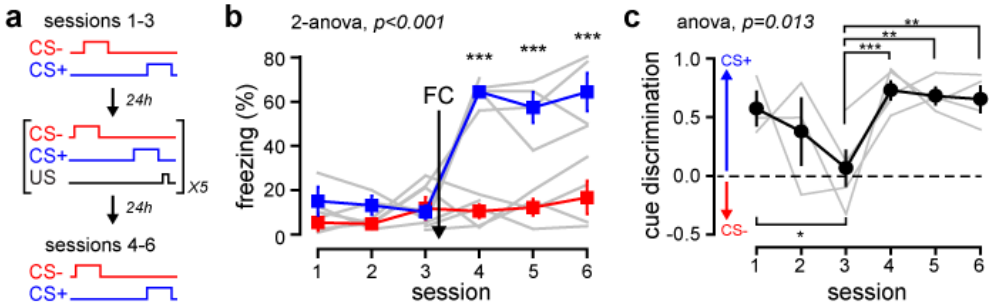

Figure 7.2. Fear conditioning increases cue discrimination. a, Fear conditioning protocol. US, unconditioned stimulus. **b**, Fear behaviors in response to CS+ (blue) and CS- (red) were measured as percentage of freezing after each imaging session. FC, Fear conditioning (FC). **c**, Fear conditioning increases the index of cue discrimination between CS+ and CS-. Only GCaMP5 mice that went through 6 imaging sessions are represented (n=4; p=0.013, one-way anova; *p<0.05, **p<0.01, ***p<0.001; post-hoc Holm-Sidak test). Grey lines indicate individual mice. Black line and circles indicate mean ± sem.

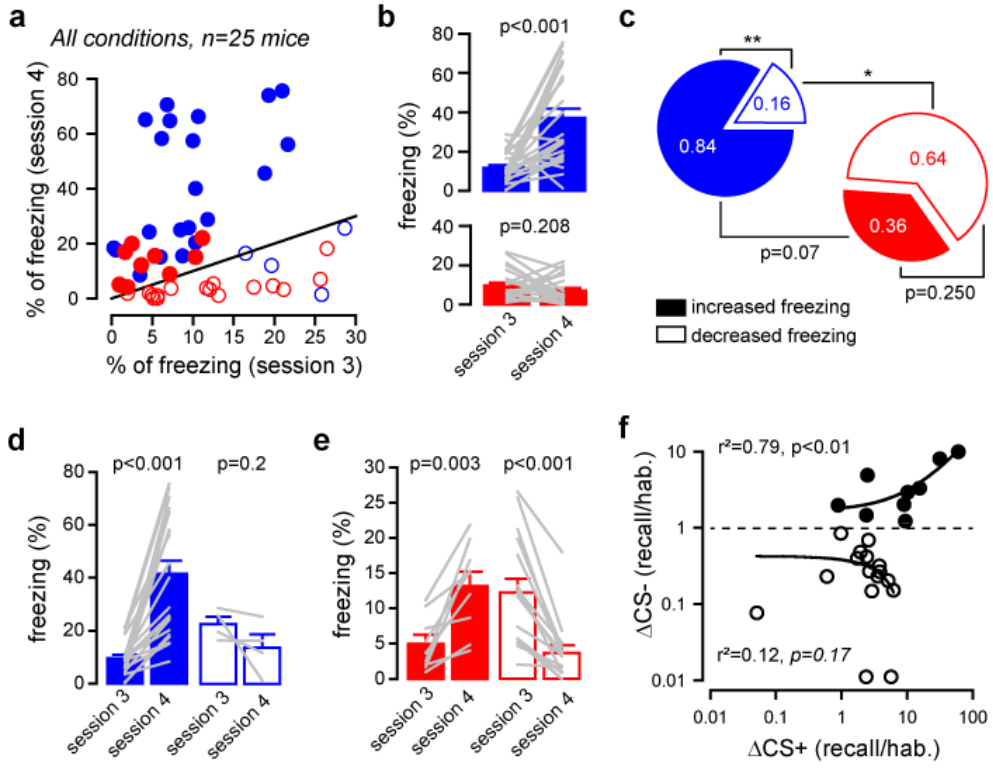

Figure 7.3. Effect of fear conditioning on behavioral parameters among all mice. a, Relation between the level of freezing before (session 3) and after (session 4) fear conditioning. Each circle represents the freezing response upon CS+ (blue) and CS- (red) stimuli. Filled and open circles indicate increased and decreased freezing responses, respectively (*i.e* above and below the unity black line). **b**, Effect of fear conditioning on fear responses evoked by the presentation of CS+ (top, blue; n=25; p<0.001; paired t-test) and CS- (bottom, red; n=25; p=0.208; paired t-test). Grey lines indicate pairs. **c**, Proportions of mice with increased (filled pie, n=21 and 9) or decreased (open pie, n=4 and 16) fear responses evoked by CS+ (blue, n=25; **p=0.0044; χ^2=8.12) and CS- (red, n=25; p=0.25; χ^2=1.32). The proportion of mice that showed decreased fear responses are significantly different between CS+ and CS- (n=4 and 16; *p=0.0213; χ^2=5.23). **d**, Mice were categorized depending on whether they showed increased (filled bars, n=21; p<0.001; Wilcoxon Signed Rank Test) or decreased (open bars; n=4; p=0.199; paired t-test) fear responses evoked by the presentation of CS+. **e**, Same presentation as in **g** but for CS- (increase, n=9, p=0.003; decrease, n=16, p<0.001; paired t-test). **f**, Relation between fear index (ΔCS) upon CS+ and CS- (freezing responses after learning were normalized to freezing responses before learning). Each circle represents a mouse. Learning-dependent decreased freezing behaviors in response to CS- do not depend on the freezing behaviors observed upon CS+ (white circle, ΔCS- <1; n=16; r^2=0.12; p=0.1758; one way anova).

unchanged (session 3: 11.7 ± 5 % *vs.* session 4: 10.5 ± 2.9 %; n=5; p=0.827; *paired t-test*) (**Fig. 7.2**). The index of cue discrimination (cd) was then calculated as follow :

$$cd = \frac{\%\ \text{freezing}\ \ \text{CS}^{+}\ - \%\ \text{freezing}\ \ \text{CS}^{-}}{\%\ \text{freezing}\ \text{CS}^{+} + \ \%\ \text{freezing}\ \text{CS}^{-}}$$

Fear conditioning eventually resulted in increased behavioral cue discrimination (session 3: +0.064 ± 0.14 *vs.* session 4: +0.73 ± 0.04, n=5; p=0.013; *paired t-test*) (**Fig. 7.2c**).

Importantly, when all experimental conditions were pooled together, most animals froze less to the presentation of CS- as compared to the habituation period (**Fig. 7.3**), indicating that sensory cues that were not explicitly paired to the footshock might acquire relative safety properties (Likhtik & Paz, 2015a; Likhtik et al., 2014; Stujenske et al., 2014a).

7.2 *FrA computes both paired and unpaired sensory cues during learning*

7.2.1 Global tuning properties of FrA upon fear learning

We recorded simultaneously over 6 imaging sessions the activity (ΔF/F0) of ~100 identified neurons per mouse (n=4 mice), among which ~40 % displayed significant calcium transient evoked by the presentation of CS+ and/or CS- stimuli (8 trials per CS with pseudo-random delay) (**Fig. 7.4a-c**). We found that fear learning increased non-specifically the activity of neurons in response to both CS+ and CS- (pooled sessions; CS+, before: 0.93 ± 0.16 Hz, after: 2.82 ± 0.51 Hz; CS-, before: 0.96 ± 0.10 Hz, after: 2.48 ± 0.49 Hz; *2-ways anova: before vs. after*, p<0.001; *CS+ vs. CS-*, p=0.684) (**Fig. 7.4d**).

First, neurons were categorized as non responding, CS+ specific, CS- specific, and non-specific (i.e, responding to both CS+ and CS-). Neurons were considered responding if at least one calcium transient was detected in at least 1 out of 8 trials, and all neurons from all recorded mice (n=4) were pooled. Then we calculated the weighted responding probabilities [w*P*(CS) = averaged responding probabilities over 8 consecutive trials weighted by the mean of peaks of detected ΔFF0].The selectivity index was then computed as follows :

$$selectivity = \frac{\text{wP}(\text{CS}^{+})\ - \text{wP}(\text{CS}^{-})}{\text{wP}(\text{CS}^{+}) + \text{wP}(\text{CS}^{-})}$$

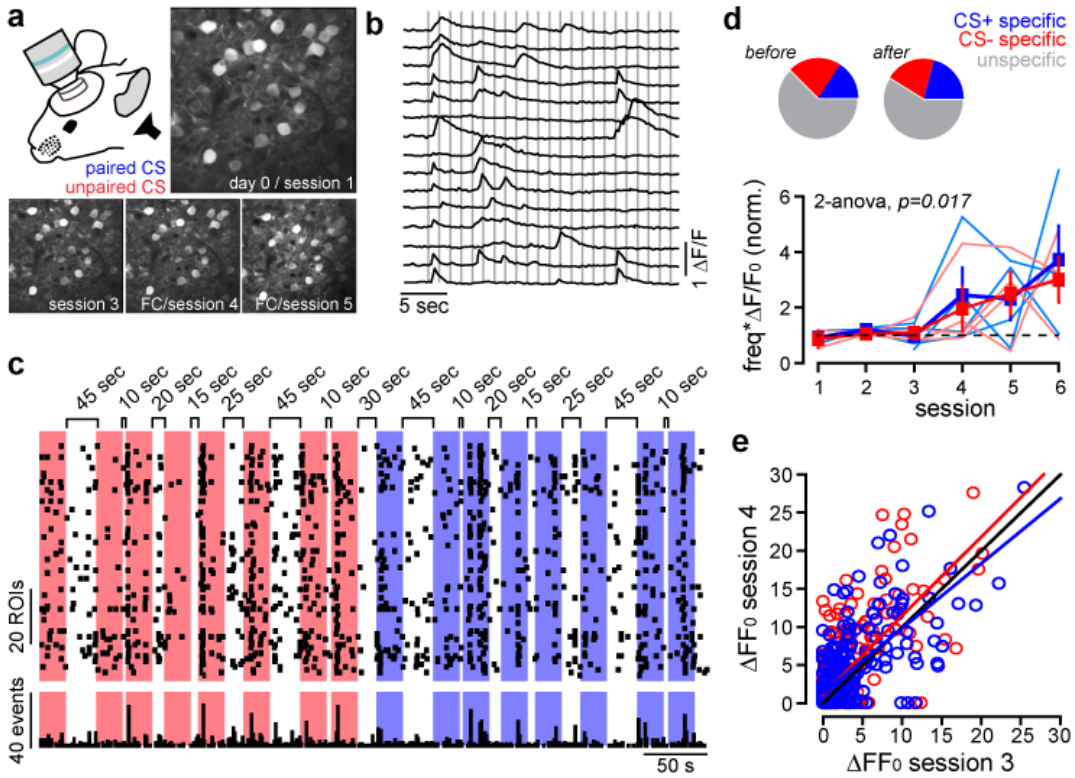

Figure 7.4. Chronic 2-photon calcium imaging of FrA pyramidal neurons. a, Chronic 2P imaging of GCaMP5-expressing FrA neurons over 6 sessions during the presentation of paired (CS+, 8kHz) and unpaired (CS-, gaussian) auditory tones. CS, conditioned stimulus. **b**, Examples of somatic calcium transients (ΔF/F0) from individual neurons recorded during one CS composed of 27 pips (grey bars: 50 ms, 0.9 Hz for 30 s). **c**, Example raster plots (top) and peri-stimulus time histograms (bottom, bin size: 1 s) showing the heterogeneity of neuronal activity among successive auditory stimuli. Each square represents a detected calcium transient. Red and blue bars represent CS- and CS+ epochs, respectively. Pseudo-random delays between epochs are indicated. **d**, Fear learning does not affect the global tuning properties of FrA network (top, CS+ *vs.* CS- specific, before *vs.* after, p=0.7103, χ^2=0.1380) but significantly increases the activity (bottom, frequency*ΔF/F0 of detected events normalized to the baseline activity before auditory stimulation) of individual neurons in response to both CS+ (blue) and CS- (red) (n=4; p=0.017; two way analysis of variance (anova). **e**, Relationship between the activity before and after fear conditioning. For each responding neuron, all detected ΔFF0 events within a single trial were first summed and then averaged among all trials. Blue and red circles represent the activity of neurons in response to CS+ and CS-, respectively. Blue and red lines represent linear regression line. Black line represents the identity line.

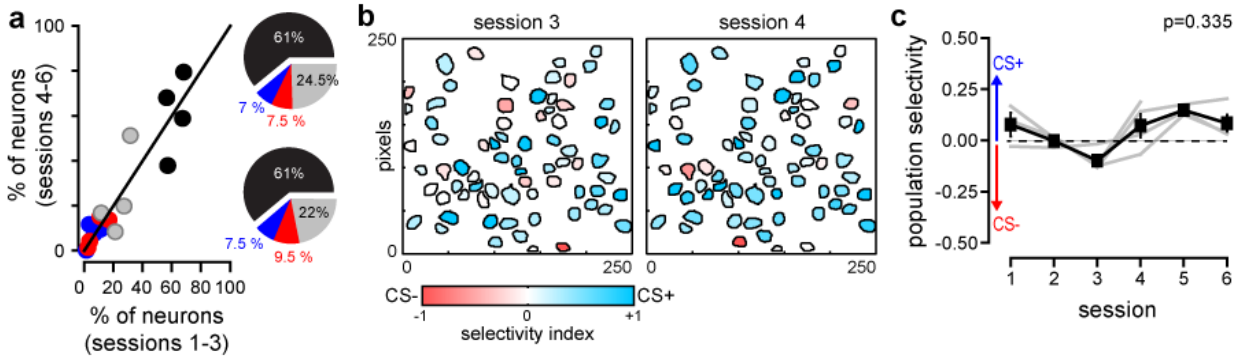

Figure 7.5. Fear conditioning does not alter neuronal network selectivity. a, Relationship between the proportion of neurons in different categories (black=non responding, grey=unspecific; blue=CS+; red=CS- before (sessions 1-3) and after (sessions 4-6) fear conditioning. **b**, Example of FrA population selectivity. Responding neurons are outlined and color-coded as a function of their selectivity index. Values close to 1 and -1 indicate higher activity upon CS+ and CS- presentation, respectively. Values close to 0 indicate equal activity. **c,** Average selectivity index as a function of imaging session. Grey lines represent individuals (n=4), black line and squares, mean ± sem. Fear conditioning occurred between sessions 3 and 4 (p=0.335; n=4; Friedman repeated measures anova on ranks).

Intriguingly, we observed that fear conditioning altered neither the proportion of active neurons nor the neuronal selectivity (**Fig 7.5**), indicating that the global tuning properties of active networks were not affected upon fear conditioning.

7.2.2 Decorrelation of cue-specific activity patterns predicts cue discrimination

In addition, the temporal activity patterns during cue presentation were highly heterogeneous and we did not observe any stable gains in coincident activity between pairs of neurons that were reported previously (Cheng & Frank, 2008; Komiyama et al., 2010; Rajasethupathy et al., 2015) (**Fig. 7.6**). Instead, we found that learning reduced the similarity between activity patterns evoked by the CS+ and the CS- (Pearson correlation coefficient; session 3: 0.13 ± 0.06 *vs.* session 4: -0.022 ± 0.04; n=4; p=0.048 *paired t-test*), indicating that learning may create specific cortical representations by increasing the separation of activity patterns evoked by similar yet distinct sensory inputs (**Fig. 7.6**). Because activity decorrelation has been proposed to facilitate memory storage (Wiechert et al., 2010) and to predict learning performance (Leutgeb et al., 2007; Gschwend et al., 2015), we plotted the Pearson correlation coefficient computed in sessions 3 to 6 as a function of perceptual discrimination (**Fig. 7.6**). We observed a linear negative relation between the level of CS+ *vs.* CS- correlated activity and the behavioral performance (r^2 = 0.63; n=4; p<0.01), indicating that the degree of activity separation in the FrA might predict the ability to discriminate between fear and relative safe sensory cues.

7.2.3 FrA is required during learning for safety detection

To test whether population activity in the FrA was indeed required for cue discrimination rather than for fear acquisition (Lai et al., 2012), we injected mice bilaterally with an AAV expressing the light-activated proton pump *archaerhodopsin* (AAV9-CAG-ArchT-GFP, or AAV9-CamKII-eGFP) into the FrA and suppressed the activity of layer 2/3 neurons with light through implanted optical fibers during the presentation of US (Chow et al., 2010) (**Fig. 7.7b-e**). *Ex-vivo* slice recordings confirmed that photostimulation of ArchT-GFP-expressing FrA pyramidal neurons reliably suppressed action potentials (**Fig. 7.7a**). The light-driven inactivation of FrA during CS+/US pairings (**Fig. 7.7c-e**) significantly impaired the ability to discriminate sensory cues during recall as compared to controls (GFP: 0.67 ± 0.11, n=5; ArchT: 0.08 ± 0.13, n=5; p=0.008; *t-test*). FrA inactivation did not affect CS+-evoked fear behavior (normalized to habituation; GFP: 2.2 ± 0.4, n=5; ArchT: 2.04 ± 0.6, n=5; p=0.828; *t-test*) (**Fig. 7.7e**), confirming

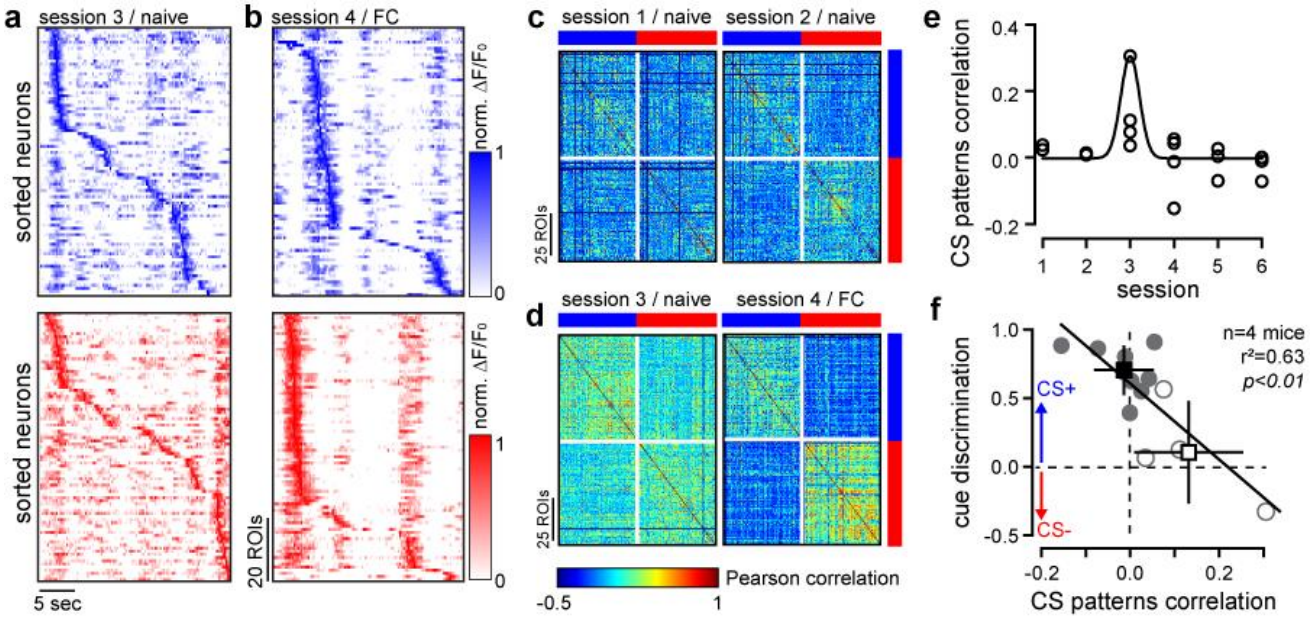

Figure 7.6. Learning-dependent neuronal assemblies in the FrA are associated with improved cue discrimination. a, b, Color-coded ΔF/F0 of sorted neurons from one example mouse before (**a**) and after (**b**) fear conditioning (FC). Each raw ΔF/F0 trace during CS presentation (30 s; CS+, blue; CS-, red) was normalized to the peak and sorted by its relative peak time. **c, d**, Example of correlation matrices (same mouse as in **a** and **b**). Blue, CS+; Red, CS-. To minimize bias, neurons were not categorized according to their tuning properties and matrices were computed over 30 s time window based on detected events rather than on raw fluorescence. **e**, Pearson's coefficients of correlation among all imaging sessions. **f**, Linear relationship (n=4 mice; r^2=0.63; p<0.01; anova) between mean correlation coefficients and behavioural performance before (session 3, white circles) and after (sessions 4-6, grey circles) fear conditioning. Each circle represents a mouse. Squares represent averages.

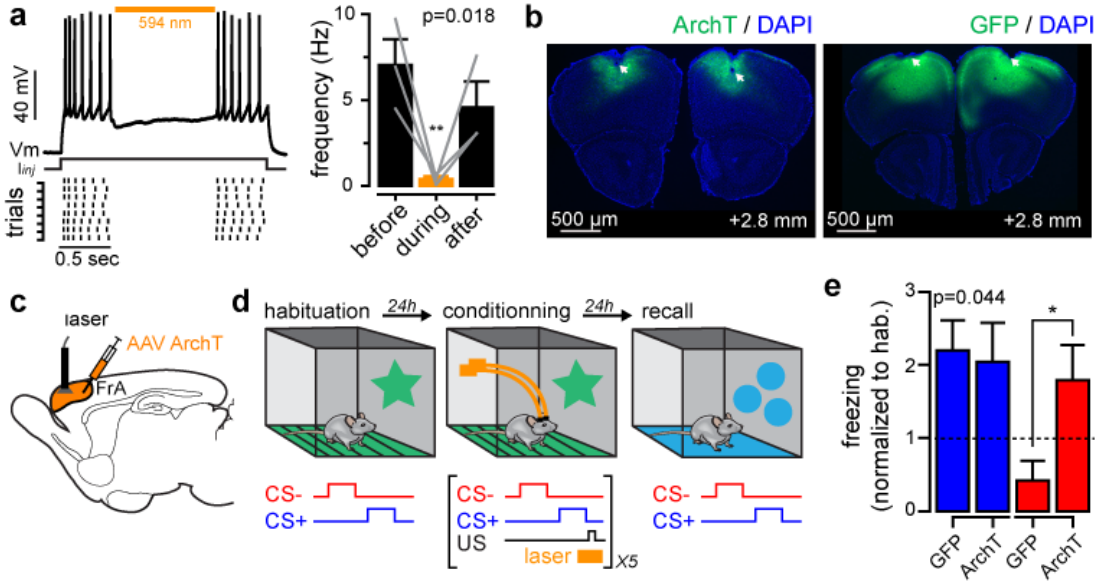

Figure 7.7 Optogenetic inhibition of FrA during conditioning decreases cue discrimination. a, Left, example of the effect of photo-inhibition on the spiking pattern of L2/3 pyramidal neurons expressing ArchT. Right, Average spike frequency before, during and after illumination (n=3; p=0.018, one way repeated measures anova; **p=0.007, Holm-Sidak method multiple comparisons versus condition "before"). **c**, Examples of mice expressing bilaterally ArchT (left) and GFP (right) in FrA. Arrows, positions of cannulas. **c,** Schematic of fear conditioning with ArchT (n=5) and GFP (n=5) expressing mice. Virus injections and optical fibers implantations in the FrA were confirmed *post-hoc* with coronal brain sections (**b**). **d**, Modified fear conditioning protocol. FrA neurons were photo-inhibited during the delivery of the footshock. **e**, Effect of light on freezing responses upon auditory stimuli (GFP, n=5; ArchT, n=5; one way anova; *,p<0.05, post-hoc Holm-Sidak test).

that the decrease in cue discrimination performance was not due to a deficit in fear learning acquisition. Rather, we observed an overgeneralization of fear learning with excessive freezing behaviors in response to the neutral CS- (normalized to habituation; GFP: 0.42 ± 0.26, n=5; ArchT: 1.81 ± 0.47, n=5; p=0.032; *t-test*) (**Fig. 7.7e**), confirming that safety detection is an active process that develops during conditioning (Likhtik et al., 2014) and requires FrA L2/3 pyramidal neurons.

7.3 *Auditory stimulation generates dendritic plateau potentials*

The above results indicate that the FrA actively participates in learning-induced cue discrimination and guides behaviors by computing both paired (fear) and unpaired (safety) stimuli during conditioning. To further explore the underlying circuit and synaptic mechanisms, we performed somatic whole-cell recordings of FrA L2 pyramidal cells *in vivo* during anesthesia to limit the effects of attention. Isoflurane (4% with ~0.5 l min^{-1} O_2) combined with an i.p. injection of urethane (1.5 g kg^{-1}, in lactated ringer solution containing in [mM] 102 NaCl, 28 Na L Lactate, 4 KCl, 1.5 $CaCl_2$) was used to induce anesthesia and prolonged by supplementary urethane (0.15 $g.kg^{-1}$) if necessary. Whole-cell patch-clamp recordings of L2/3 pyramidal neurons were obtained as previously described (Gambino & Holtmaat, 2012).

7.3.1 Subthreshold activation of FrA pyramidal neurons

Consistent with previous *in vivo* recordings of L2/3 pyramidal neurons in anesthetized animals (Gambino & Holtmaat, 2012), membrane potential spontaneously fluctuated between up and down states (**Fig. 7.8a, b**), and spontaneous overshooting spikes were observed only during up states. Spontaneous activity was recorded prior, during and after the presentation of the CS- and the CS+ (each consisting as previously described of 27 pips, 50 ms, 0.9 Hz, 30 s). The effect of both stimuli was tested on the same cell. However, to reduce the variability related to spontaneous activity, the cumulative PSPs were computed and subtracted by the linear regression during the baseline period (0-30 s) (see **Methods** and **Fig. 7.8**).

In contrast to a pure auditory tone (used during conditioning as a CS+) that failed to activate frontal pyramidal neurons, gaussian tone (used during conditioning as a CS-) alone evoked a long-lasting subthreshold depolarization in naive animals (i.e. before conditioning; **Fig. 7.9**). It indicates

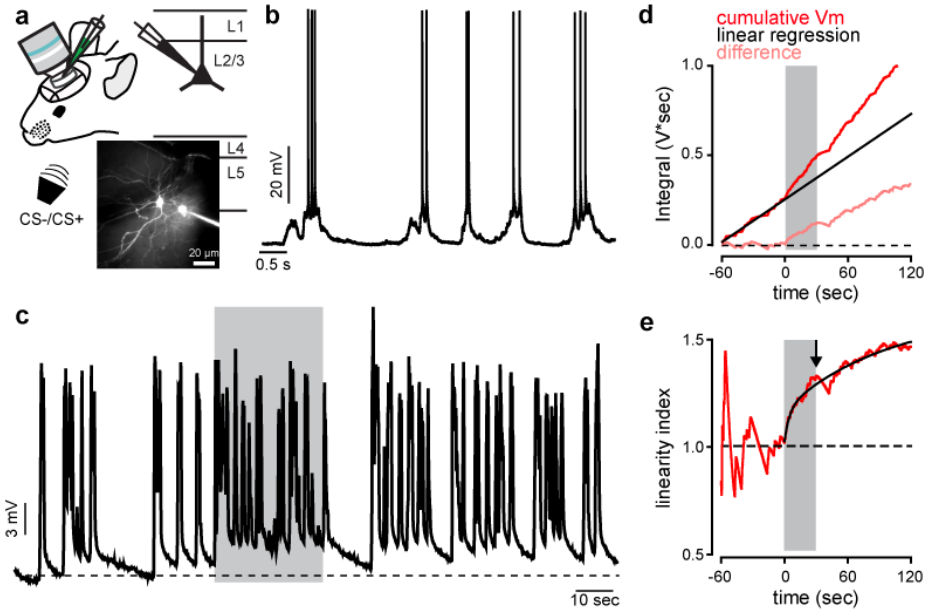

Figure 7.8. Whole-cell recordings during anesthesia. a, Sensory-evoked PSPs were recorded from L2/3 pyramidal neuron under anesthesia with 2P guidance. **b**, Typical spontaneous fluctuations. **c**, Example traces of PSP recorded from an individual FrA L2/3 pyramidal neuron upon gaussian auditory stimulation (grey bar). **d**, The cumulative PSPs (red) were subtracted by the linear regression (black line) during the baseline period prior to auditory stimulation (grey bar). The difference (pink) represents stimulus-induced cumulative change. **e**, Linearity was computed by dividing cumulative depolarization by the linear regression. Grey bar, auditory stimulation; arrow, analysis time point.

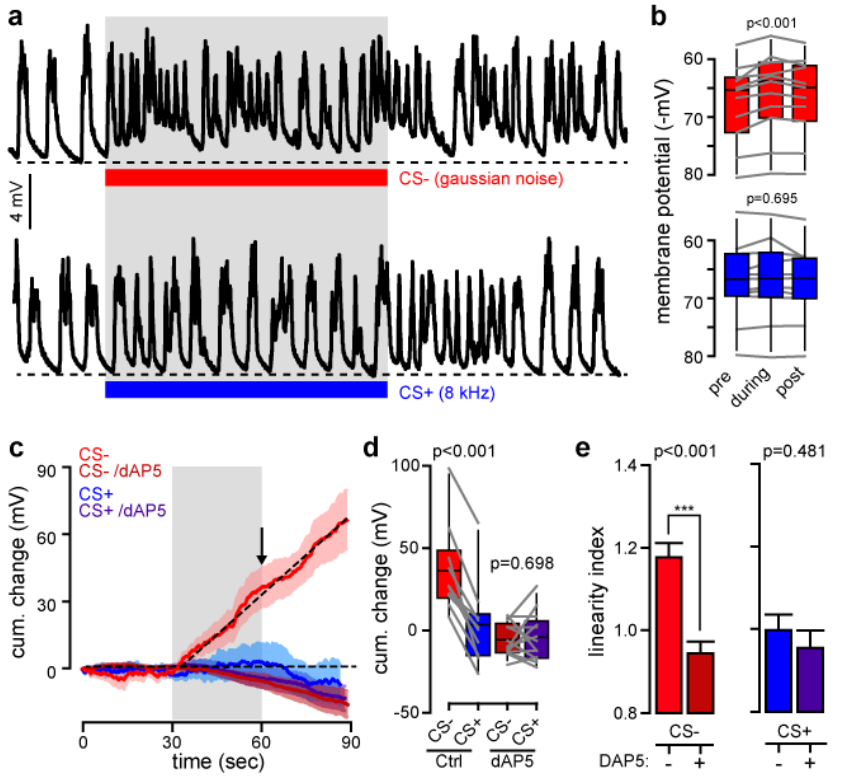

Figure 7.9. Gaussian stimulation evokes NMDAR-dependent, plateau potentials. a, Example traces of PSPs upon gaussian (top, CS-, red) and pure (bottom, CS+, blue) auditory stimulation. **b**, 30 s-averaged membrane potential before, during, and after auditory stimulation (top, gaussian noise, n=11, p<0.001, one way repeated measures anova; bottom, 8 kHz tone, n=10, p=0.695, one way repeated measures anova on ranks). Grey lines between bars indicate pairs. **c**, Averaged change (± sem) in cumulative PSP with or without dAP5. Grey bar, auditory stimulation; arrow, analysis time point. **d**, Effect of dAP5 on cumulative PSPs change at the end of the stimulation (Ctrl, n=10, p<0.001, paired t-test; dAP5, n=13, p=0.698, paired t-test). Grey lines between bars indicate pairs. **e**, Effect of dAP5 on CS- (left) and CS+ (right) evoked PSP linearity (CS-, p<0.001, one-way anova; CS+, p=0.484, Kruskal-Wallis one way anova on ranks).

that FrA pyramidal neurons are capable to categorize auditory stimuli based on their spectral properties during anesthesia (see **Fig. 7.1e** for spectral properties of auditory tones). Multiple convergent inputs from successive or parallel cortical regions that are involved in complex sound processing (e.g. auditory cortex) likely drive this process (LeDoux, 2000; Mizrahi et al., 2014; Pai et al., 2011), although we cannot rule out that FrA neurons were directly activated through a subcortico-FrA route.

7.3.2 NMDARs-dependent dendritic plateau potentials

The gaussian tone-evoked increase in cumulative potential was essentially supra-linear (**Fig. 7.9**) and bore similarities with evoked cortical up-states which were shown to depend on NMDA receptors (NMDARs) (Gambino et al., 2014). Accordingly, the topic application of the specific NMDAR antagonist D(-)-2-Amino-5-phosphonovaleric acid (dAP5; 1 mM) efficiently and selectively suppressed the sustained depolarization evoked by the gaussian auditory stimulation (CS-: 36.3 ± 8 mV, CS+: 3.5 ± 8 mV, n=10; CS-/dAP5: -5.6 ± 3 mV, CS+ /dAP5: -4.1 ± 4 mV, n=13; $p<0.001$, *anova*) (**Fig. 7.9**). In line with previous studies *in vivo* (Gambino et al., 2014; Palmer et al., 2014), it suggests that auditory-evoked sustained depolarizations recorded at the soma were likely to be mediated by local dendritic Ca^{2+} events through the recruitment of active NMDARs-dependent conductances.

To test this hypothesis, we infected mice with a combination of AAVs (AAV9-Syn-Flex-GCaMP6s, and 1/10000 dilution of AAV1-hSyn-Cre). This strategy was used in order to obtain sparse labeling with only a limited number of GCaMP-expressing neurons (**Fig 7.10a**), and consequently allow imaging of isolated dendritic branches (**Fig 7.10b**). The activity of superficial dendrites was recorded in response to both gaussian (CS-) and pure-tone (CS+) auditory stimulations (**Fig. 7.10c**). As opposed to whole-cell recordings, this was done in awake head-restrained mice. Clear auditory-evoked dendritic calcium activities were visible (**Fig. 7.10c**). For extracting spatial and temporal properties of dendritic calcium events, a Gaussian function was fitted to the fluorescence intensities of the ROIs in a visually 'active' region. All Gaussian fits were then normalized to their maximum value and full-width half max (FWHM) of the gaussian fit was calculated. Interestingly, when all dendritic events were pooled together, CS- evoked on average smaller events than those evoked upon CS+ presentation (median ± sem: CS-, 13.8 ± 3.2 µm, n=25; CS+, 22.5 ± 4.9 µm, n=26; p=0.026, *Mann-Whitney rank sum test*) (**Fig. 7.10d**), suggesting that gaussian stimulations were likely to be more efficient in producing small, local dendritic events.

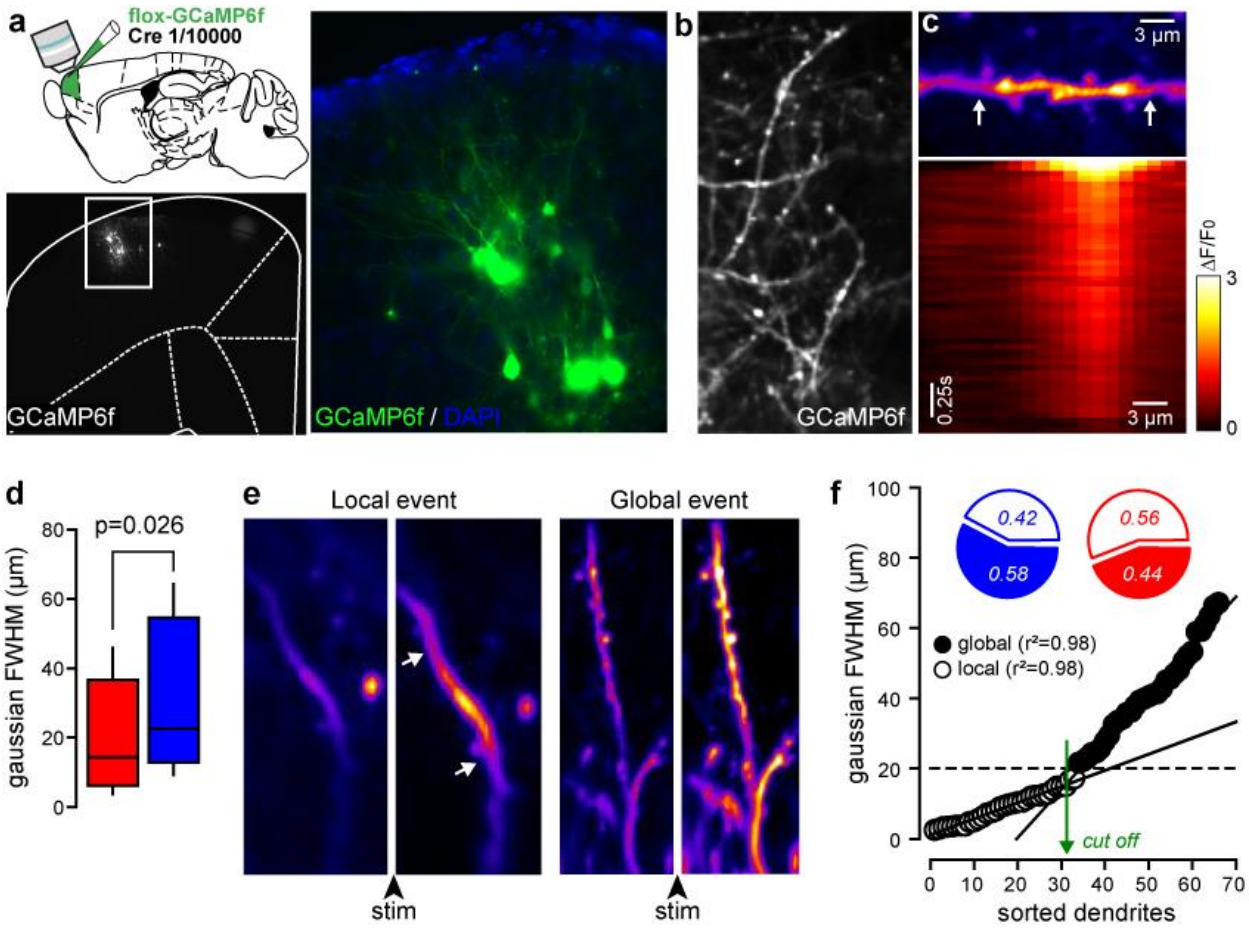

Figure 7.10. Both gaussian and pure-tone auditory stimulation evoke dendritic local events in awake animals. a, top left, scheme of the experimental strategy. Mice were double-infected with flex-GCaMP6s and 1/10000 diluted Cre viruses. Right and bottom left, representative coronal slice of GCaMP6s sparse labelling in the dPFC. **b**, representative enlargement of dendritic branches obtained with 2-photon imaging. **c**, Examples of dendritic calcium event upon auditory stimulation. **d**, Comparison of all dendritic events in response to CS- (red) and CS+ (blue). **e**, representative examples of local and global dendritic events. **f**, fraction of local (open symbols) *vs.* global (filled symbols) events categorized according to the value of their FWHM.

Dendritic calcium events were then classified in local or global events, based on its spread along the dendritic branches: events with a full-width half max (FWHM) of the gaussian fit equal or lower than 30 µm (cut-off value defined experimentally, see **Fig. 7.10e**) were categorized as a local event or plateau potential (**Fig. 7.10e, f**) (Gambino et al., 2014). Events with a full-width half max (FWHM) higher than 30 µm were categorized as a global event and presumably reflected back-propagating action potentials (Gambino et al., 2014) (**Fig. 7.10e, f**). Intriguingly, the fraction of local *vs.* global dendritic events were similar upon CS+ and CS- auditory stimulations (CS+: 42.3% *vs.* 57.7%, CS-: 56 % vs. 44 %; p=0.3238, χ^2 = 0.9561), indicating that both tones were capable of evoking dendritic plateaus. It contrast with our whole-cell recordings (see **Fig. 7.9**), where pure-tone (CS+) stimulation failed to evoke somatic plateau potentials presumably because of anesthesia. Altogether, our data indicate that both CS+ and CS- might evoke dendritic local depolarization during wakefulness.

7.3.3 Fear learning occludes NMDA plateau potentials

Importantly, those auditory-evoked plateau potentials were strongly attenuated in conditioned animals (naive: 36.3 ± 8 mV, n=10; conditioned: 5.4 ± 9 mV, n=8; p=0.008; *anova*) and correlated with learned behaviors (**Fig. 7.11**), suggesting that they might overlap mechanistically with learning-dependent plasticities during memories acquisition (Basu et al., 2016; Rioult-Pedotti et al., 2000). Altogether, our data suggest that specific synaptic mechanisms within the FrA might associate salient value to sensory cues that were not explicitly paired with the footshock during conditioning.

7.4 Co-activation of convergent inputs reinforces FrA L2/3 pyramidal neurons

Given that the activation of BLA neurons instructs prefrontal circuits during conditioning and memory recall (Genud-Gabai et al., 2013; Likhtik & Paz, 2015; Likhtik et al., 2014; Nakayama et al., 2015; Sangha et al., 2013), we hypothesized that BLA axons, along with the synaptic non-linearities evoked by gaussian auditory stimuli, could reinforce L2/3 FrA pyramidal neurons through their projections in L1 (Lai et al., 2012; M. Larkum, 2013; Mátyás et al., 2014) (see **Fig. 7.12e**). To address this question, we expressed the recombinant light-gated ion channel

channelrhodopsin-2-YFP (ChR2; AAV9-CamKIIa-hChR2-eYFP) into the BLA and performed intracellular recordings in L2/3 FrA neurons of naive mice (n=6) (**Fig. 7.12a, b**).

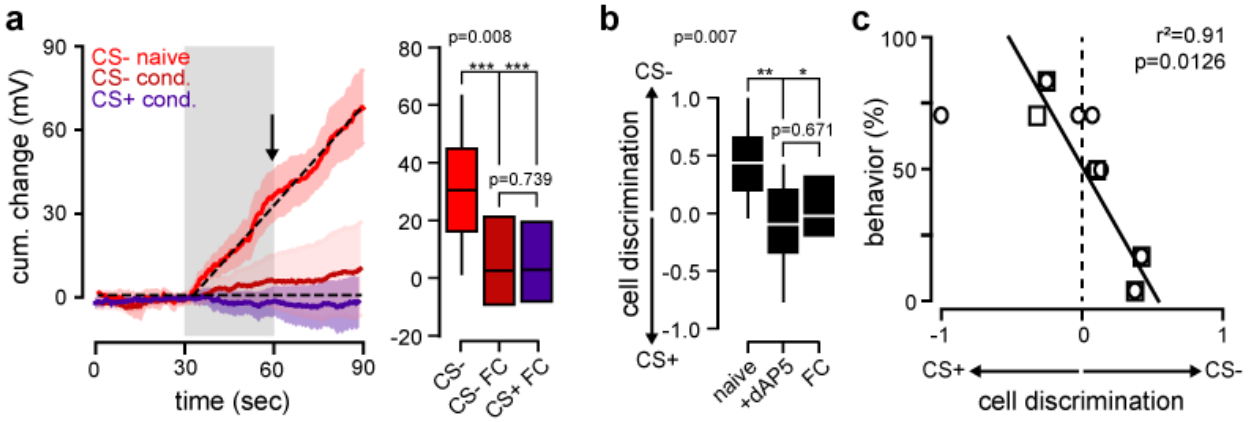

Figure 7.11. Fear conditioning occludes auditory-evoked plateau potentials. a, Effect of fear conditioning (FC) on cumulative PSPs change. Same representation as in e (left) and f (right). (CS- naive, n=10; CS- FC, n=8; CS+ FC, n=8; p=0.005, one way anova; ***, p<0.001, post-hoc Holm-Sidak test). **b**, Effect of dAP5 and fear conditioning (FC) on cellular discrimination between CS- and CS+ (naive, n=10; naive+dAP5, n=13; FC, n=8; p=0.007, one way anova; *, p<0.05, **, p<0.001, post-hoc Holm-Sidak test). **c**, Linear relationship between mean cellular discrimination and CS+ evoked freezing response following fear conditioning (n=5 mice; r²=0.91; p=0.0126; anova). Each circle represents a cell (n=8), each square represents a mouse (n=5).

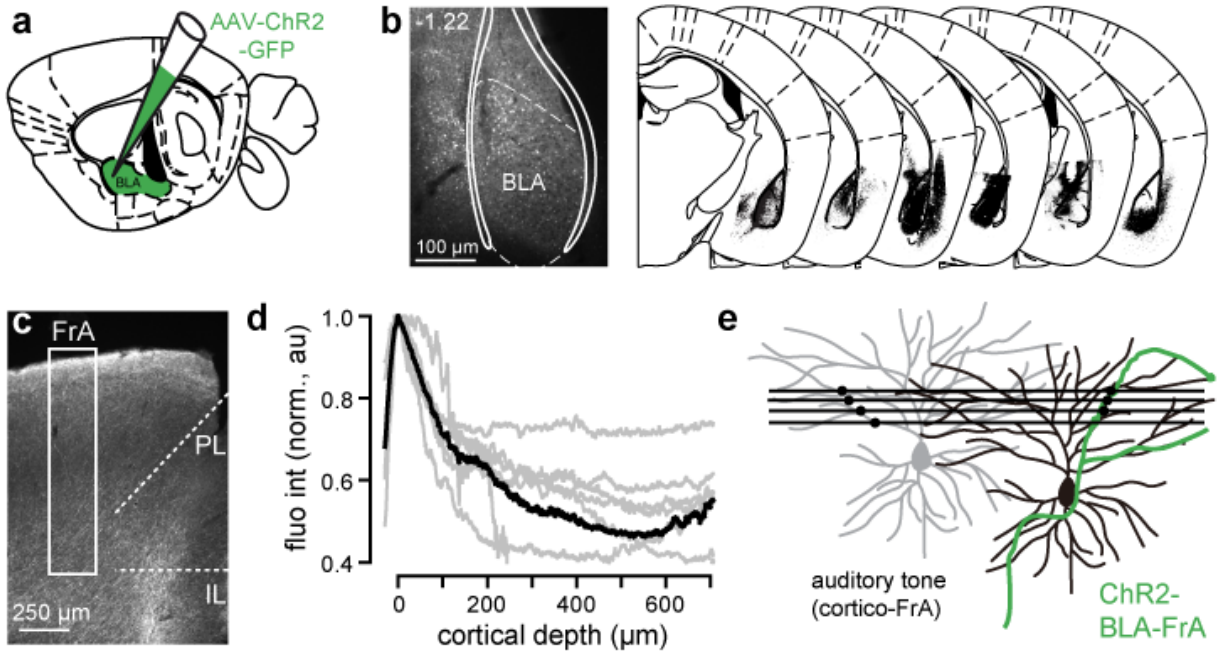

Figure 7.12. Expression of ChR2-GFP in the BLA and its afferents. a, Schematic of the viral injection in the BLA. Neurons were transfected with AAV9-CamKIIa-hChR2-eYFP. **b**, Representative example of the ChR2-GFP expression profile in the mouse BLA (Left). The coronal diagrams of the brains from 6 mice showing the expression profiles (in black) of ChR2-GFP are depicted on the right. Diagrams were adapted from the Paxinos atlas. **c**, Example of a cortical slice with ChR2-GFP fluorescence in the FrA. *PL, prelimbic cortex; IL, infralimbic cortex*. **d**, plot comparing the intensity profiles measured in the FrA (white bow on the left) of 6 different animals in which injections targeted BLA. **e**, Co-activation protocol. ChR2-expressing BLA neurons were photo-stimulated during auditory stimulation.

7.4.1 Long-range connection between BLA and FrA pyramidal neurons

First, we confirmed that ChR2-expressing BLA neurons were projecting to the superficial layers of the prefrontal cortex (**Fig. 7.12**). Then we used the recently described uDISCO protocol after transparisation (Becker et al., 2012) to precisely describe the trajectories used by BLA axons to innervate FrA pyramidal neurons (**Fig 7.13**).

As described above, the amygdala is a collection of nuclei located in the temporal lobe that generate appropriate behavioural strategies particularly in response to conditioned external stimuli. For instance, the amygdala is supposed to mediate through direct or indirect pathways classical fear conditioned responses such as 1) the immobilization of the animal, 2) the potentiation of startle reactions, 3) the release of stress hormones, and 4) changes in blood pressure and heart rate (Davis er al., 1994). Accordingly, we observed that the amygdalar complex massively and ipsilaterally projects to an array of nuclei of the hypothalamus and brain stem, that are directly affecting these behavioural responses (**Fig. 7.13a**) (Ledoux et al., 1988). These projections most likely use both cerebral peduncles and internal capsules to target 3 specific areas: 1) the *periaqueductal gray* matter (PAG) that is activated during vocalizations, startle reactions, analgesia and cardiovascular changes (Behbehani, 1995); 2) the *parabrachial nucleus* (PBN) that has been shown to contribute to pain processing (Moga et al., 1990) and fear memories acquisition (Sato et al., 2012); and 3) the *nucleus tractus solitarius* (NTS) which projects towards the vagal system (Van der Kooy et al., 1984) (**Fig. 7.13a-c**).

In addition to those direct projections to the presumed anatomical and functional correlates of fear responses, we identified other projections targeting structures that has been shown to control learning itself rather than behavioral responses. For instance, the *anterior commissure* provides projections to the contralateral amygdala. In addition, the amygdala projects via the *stria terminalis* (ST) to the *bed nucleus of the stria terminalis* (BNST) (**Fig. 7.13a**), which participates in encoding the context in which conditioned learning occurred, rather than conditioning itself (Sullivan et al., 2004). Those regions are probably connected through indirect projections to the hypothalamus and ascending monoaminergic neurons (Russchen et al., 1987). Indeed, we do not observe any projection of the amygdala towards the *locus coerulus* (LC), the *substantia nigra* (SN) or the *ventral tegmental area* (VTA). The amygdala also projects towards subcortical structures that are involved in several aspects of emotional learning. For example, we observed a direct projection between the amygdala and the *ventral hippocampus* (vHPC) (**Fig. 7.13b**), which is supposed to regulated social and defensive behaviours, including social avoidance (Felix-Ortiz et al., 2013). We also observed a direct projection via the *ventral striatum* towards the *nucleus*

accumbens (nAC), the role of which is essential during reward-seeking behaviors (Otis et al., 2017).

As opposed to subcortical projections, projections of the amygdala to the cortex are relatively exiguous and heterogeneously diffused. Although those pathways were poorly visible, we identified, in agreement with previous studies, marked projections to the entorhinal cortex (EC) via the *amygdalar capsule* (amc). In a similar way to the role of BNST, it has been shown that the optogenetic inhibition of these projections prevents the acquisition of conditioned contextual fear. Finally, we observed, in accordance with our hypothesis, dense projections to the medial prefrontal cortex (infralimbic and prelimbic mPFC) via the external capsule as well as widespread projections towards the dorsal prefrontal cortex (dPFC) (**Fig. 7.13d**) (uDISCO experiments were performed, in collaboration with the BIC – Bordeaux Imaging Center, by Christel Poujol and Nathalie Piette).

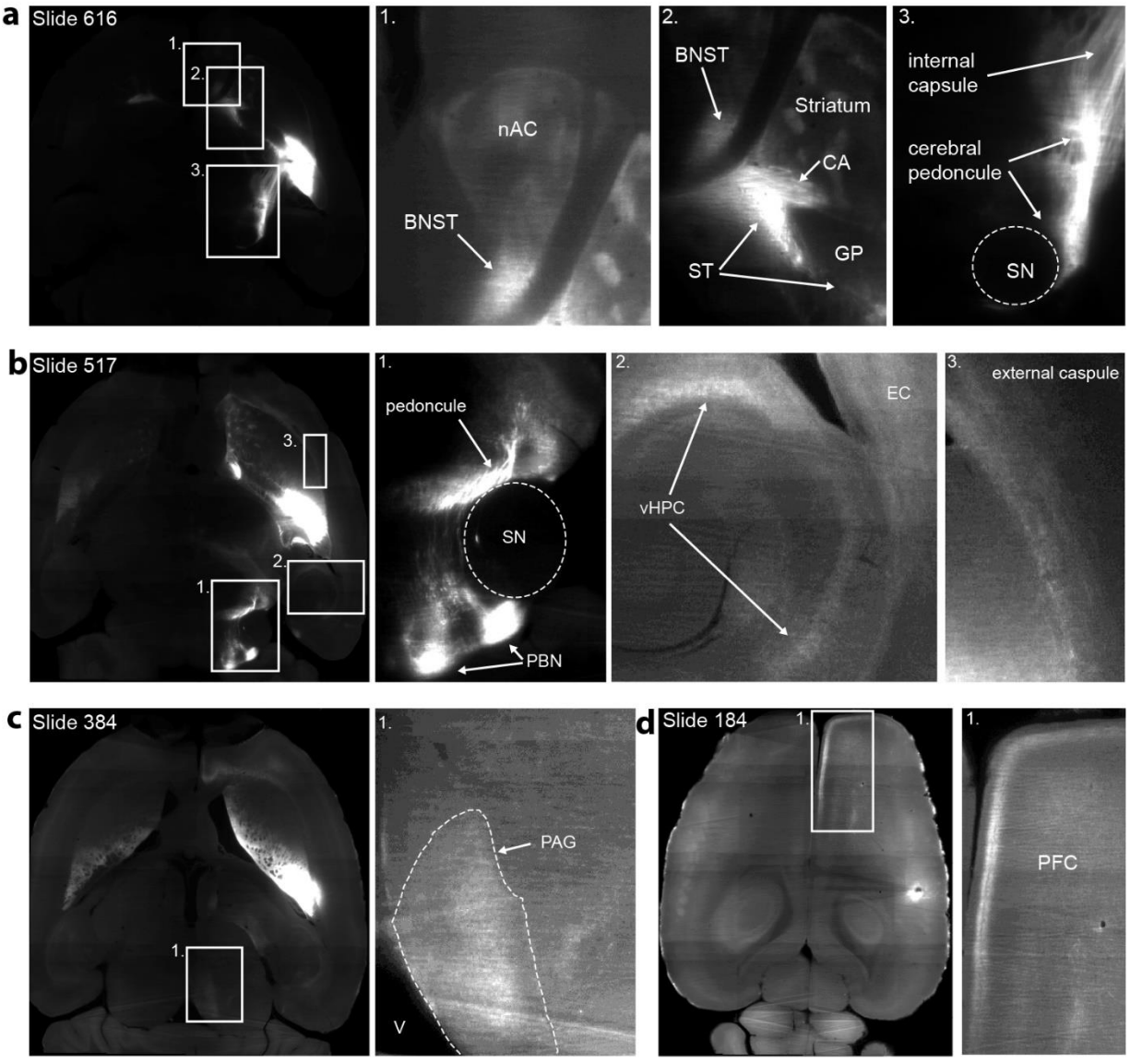

Figure 7.13. BLA communicates with many sub-cortico and cortical areas involved in fear learning.

7.4.2 BLA photostimulation produces NMDARs plateau-like depolarization

Local photostimulation of ChR2-BLA axons in acute slices produced excitatory postsynaptic current (EPSC) in FrA pyramidal neurons with short latencies (3.5 ± 0.36 ms, n=9) and low jitter (0.289 ± 0.04 ms, n=9), suggesting that a fraction of BLA neurons are directly and monosynaptically connected to FrA pyramidal neurons (**Fig. 7.14**) (Klavir et al., 2017). Similar to the cortical responses evoked by long-range thalamic projections (Gambino et al., 2014), we found that the *in vivo* photostimulation of BLA neurons with an implanted optical fiber produced plateau-like depolarizations in all recorded neurons (averaged integral: 6.5 ± 1 mV*sec, n=13) (**Fig. 7.14**) that were suppressed by artificial hyperpolarization (pre: 6.15 ± 1.6 mV*sec, hyper: 3.9 ± 1.5 mV*sec, post: 5.56 ± 1.4 mV*sec; n=4; p=0.004; *anova repeated measures*) or ectopic dAP5 application (Ctrl: 6.5 ± 1 mV*sec, n=13: dAP5: 1.57 ± 0.7 mV*sec, n=3; p=0.022; *Mann-Whitney test*) (**Fig. 7.14**).

7.4.3 Activation of BLA inputs during auditory stimulation potentiate FrA neurons

BLA-mediated plateau-like depolarizations likely emerge from dendritic NMDARs-mediated conductances which might amplify and facilitate the potentiation of coincident sensory-driven inputs (Brandalise et al., 2016; Gambino et al., 2014; Lavzinet al., 2012; Palmer et al., 2014; Xu et al., 2012). Therefore, we next investigated the effect of BLA activation during auditory cue presentation (see **Fig. 7.12e**). ChR2-expressing BLA neurons were photo-stimulated during 30 s at 0.9 Hz with 27 square light pulses (50 ms), a protocol that precisely overlapped the pattern of auditory stimuli (**Fig. 7.15**). The coincident activation of BLA (Johansen et al., 2010) produced no difference during the stimulation as compared to the presentation of the CS- alone (CS-: 12.4 ± 13 mV *vs.* CS-/light: 32 ± 10 mV; n=6; p=0.245; *paired t-test*), but significantly altered later on-going spontaneous slow-wave fluctuations (**Fig. 7.15**). The increase in cumulative potential observed 30 sec after the end of the co-stimulation (CS-: 9.5 ± 14 mV *vs.* CS-/light: 76 ± 20 mV; n=6; p=0.023; *paired t-test*) (**Fig. 7.12**) possibly reflects synaptic plasticity and might be critical for shaping future sensory perception and learning (Buzsaki & Draguhn, 2004). Together, our data confirmed the existence of functional and relevant BLA synaptic inputs to frontal L2/3 pyramidal neurons.

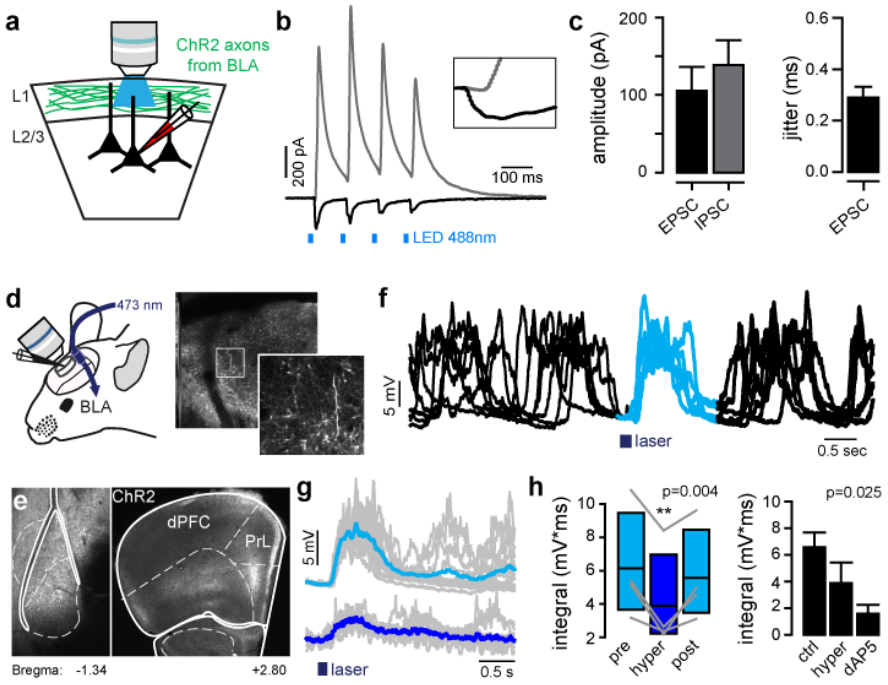

Figure 7.14. BLA-mediated plateau-like depolarization in FrA pyramidal neurons. a, schematic of the slice experiment. **b**, Excitatory and inhibitory post-synaptic current (E/IPSCs) were evoked with a 488 nm LED. **c**, amplitude and jitter of light-evoked EPSCs. **d**, Left, schematic of the *in vivo* photostimulation of ChR2-BLA neurons. Right, examples of ChR2-expressing axons. **e**, Expression profiles of ChR2-eYFP in the BLA (left) and cortex (right). **f**, Photostimulation of BLA neurons evoked sustained depolarizations in FrA neurons. **g**, Examples of photostimulus-evoked PSPs in L2/3 neuron at resting membrane potential (top) and upon hyperpolarization (bottom). Grey, single trials; blue, averaged traces. **h**, Left, BLA-mediated PSP integrals before (pre), during (hyper) and after (post) hyperpolarization (n=4, p=0.004, repeated measures anova; **, p=0.002, post-hoc Holm-Sidak test). Grey lines between bars indicate pairs. Right, Effect of hyperpolarization (n=4) and dAP5 (n=3) on *in vivo* FrA PSPs evoked by the photostimulation of BLA (control, n=13; p=0.025, Kruskal-Wallis anova on ranks).

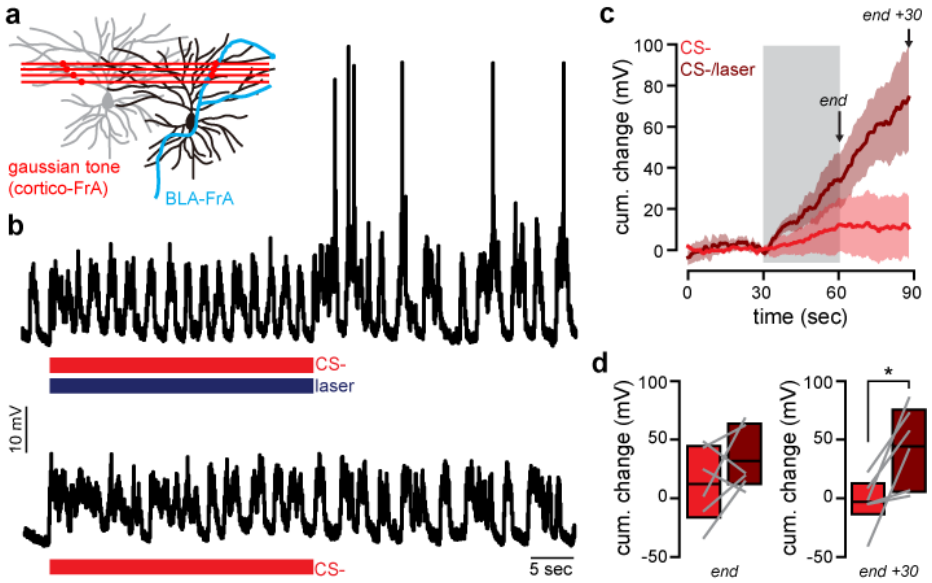

Figure 7.15. Coincident activation of BLA excitatory inputs to the FrA reinforces L2/3 pyramidal neurons. a, activation protocol. **c**, Examples of membrane potential upon auditory stimulation paired (top) or not (bottom) with BLA photoactivation. Red and blue bars below the traces indicate the duration of the stimulation. **c**, Averaged change (± sem) in cumulative PSP (n=6) upon paired (dark red, CS-/laser) and unpaired (red, CS-) auditory stimulation. The analysis was restricted to the end of the (co-) stimulation (end arrow) and 30 s later (end+30 arrow). **d**, Effect of photostimulation on CS-evoked cumulative change (left; n=6, p=0.245, paired t-test; right; n=6, *, p=0.023, paired t-test). Grey lines between bars indicate pairs.

7.5 *BLA-to-PFC long-range axons are required for discriminative learning*

The results above provide a possible cooperative, *Hebbian*-like mechanism for safety encoding that temporally integrates converging inputs from both BLA and cortex into neuronal assemblies during associative learning (**Fig. 7.12e**) (Buzsaki & Draguhn, 2004; Johansen et al., 2010, 2014; M. Larkum, 2013; Nakayama et al., 2015). To test this hypothesis, we questioned the functions of BLA projecting axons to FrA during conditioning (**Fig. 7.16** and **Fig. 7.17**).

7.5.1 Activation of BLA inputs to FrA during conditioning

First, we injected a virus expressing GCaMP5 into the right BLA and imaged axonal Ca^{2+} responses (Gambino et al., 2014) in superficial L1 of the right FrA of awake head-restrained mice during fear conditioning (**Fig. 7.16a-c**). GCaMP5 calcium transients ($\Delta F/F_0$) provided a direct measure of the activation of BLA neurons projecting to the FrA. While the activity of 242 individual BLA boutons (n=3 mice) was relatively low at rest, it increased significantly upon successive CS-US pairings (baseline: 1.1 ± 0.5 Hz; pairings: 1.73 ± 0.63 Hz; n=3; +71 ± 20 %; p=0.0042, χ^2=8.2) (**Fig. 7.16d-f**).

Importantly, the activation of BLA axons was non-specific and independent of the nature of the CS presented (CS+: 1.46 ± 0.14 Hz; CS-: 1.72 ± 0.26 Hz; n=3; p=0.19, χ^2=1.7) (Rotem Genud-Gabai et al., 2013; Likhtik & Paz, 2015a; S. Sangha et al., 2013). However, it never occurred before the end of the first CS+/US pairing (baseline: 1.1 ± 0.5 Hz; first CS+: 1.02 ± 0.02Hz; n=3; p=0.49, χ^2=0.46) (**Fig. 7.16f**).

Altogether, it supports the idea that BLA projecting axons likely passively conveyed information about the learning, i.e. the CS+/US association itself rather than (or in addition to) auditory cues alone (Nakayama et al., 2015), that must be further combined in the FrA with auditory-evoked non-linearities to recruit prefrontal neurons into cue-specific memories.

7.5.2 Photo-inhibition of BLA-to-FrA neurons decreases cue discrimination

This hypothesis was tested by specifically silencing BLA-to-FrA axons during fear conditioning but only during the presentation of the unpaired CS- (**Fig. 7.17**). Mice were injected bilaterally with a retrograde Cav-2-CMV-Cre (Hnasko et al., 2006) into the FrAs together with an

AAV9-flex-CBA-ArchT-GFP (or AAV1-CAG-flex-eGFP) into both BLAs (**Fig. 7.17a**). This resulted in the expression of the light-driven inhibitory proton pump ArchT only in BLA neurons that project to the FrA (**Fig. 7.17b**). Similar to the effect of FrA photo-inhibition (**Fig. 7.7**), the specific inactivation of BLA-to-FrA neurons during the presentation of the CS- (**Fig. 7.17a**) increased freezing behaviors during recall in response to the CS- while leaving the CS+-evoked fear behaviors unaltered (**Fig. 7.17c**). Consequently, discriminative performance was strongly attenuated as compared to controls (GFP: 0.98 ± 0.08 *vs.* ArchT: 0.33 ± 0.17; n=4; p=0.016; *paired t-test*) (**Fig. 7.17d**). Taken together, our data revealed that the coincident activation of BLA projecting neurons and FrA pyramidal neurons during conditioning drives cue discrimination most likely by encoding safety.

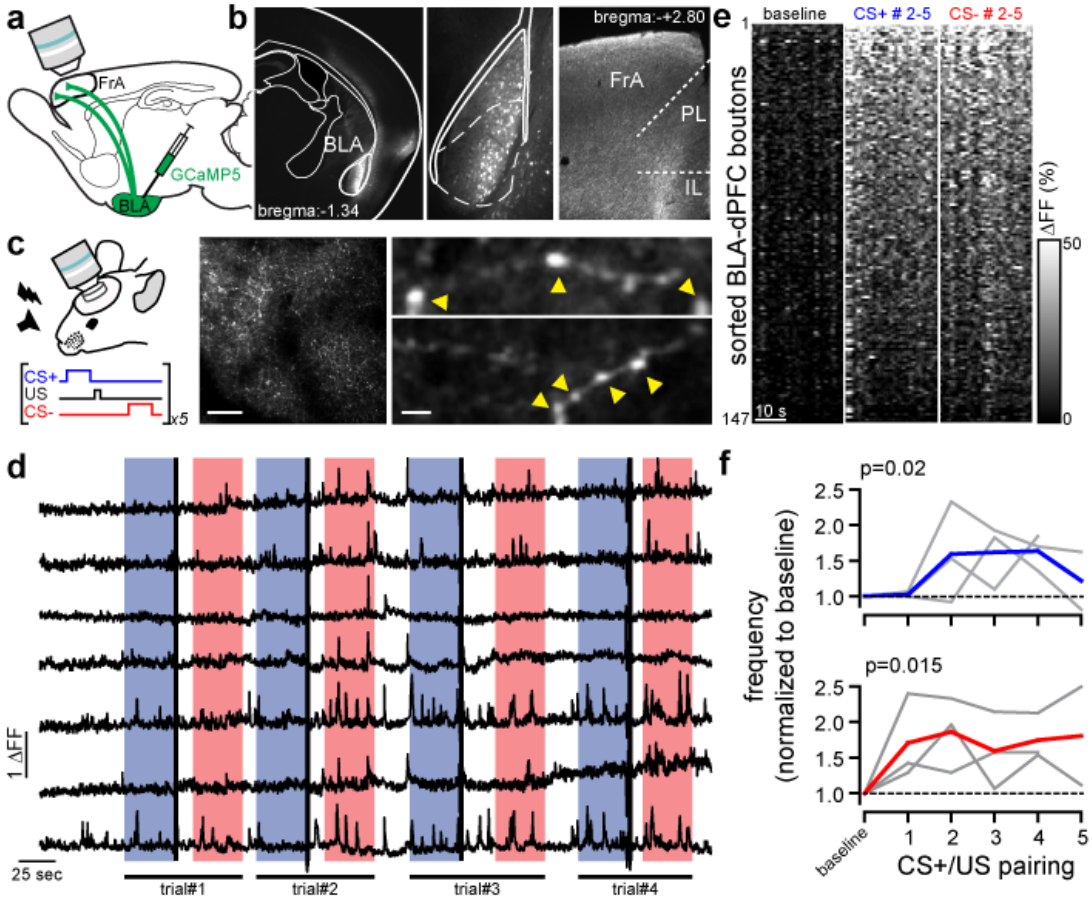

Figure 7.16. Activation of BLA-to-FrA projecting axons during conditioning. a, Schematic of the experimental protocol. BLA neurons were transfected with AAV1-hSyn-GCAMP5G and their boutons were imaged in the superficial layer of the FrA. **b**, Expression profiles of GCaMP5 in the BLA (left) and FrA (right). PL, prelimbic cortex; IL, infralimbic cortex. **c**, GCaMP5-expressing mice were fear conditioned under the microscope (left), and GCaMP5-expressing axons (middle) and individual presynaptic boutons (right, yellow arrowheads) were imaged in the FrA during conditioning. Scale bars, 50 µm (middle), 2 µm (right). **d**, Examples of calcium transients (ΔF/F0) from individual boutons recorded from one mouse upon 4 consecutive CS+ / US pairings. Blue bars, CS+; red bars, CS-; black bars, footshock (US). Each CS is composed of 27 pips (50 ms in duration at 0.9 Hz for 30 s). **e**, Color-coded ΔF/F0 of 147 individual boutons from one example mouse during baseline, CS+ (blue) and CS- (red) auditory stimuli. ΔF/F0 from trials 2 to 5 were averaged. **f**, Frequency of detected calcium events during CS+ (top, blue; baseline *vs.* CS+#2-4, p=0.019, χ^2=5.5) and CS-(bottom, red; baseline *vs.* CS-#2-4, p=0.0153, χ^2=5.8) presentation. Grey lines indicate individual mouse. Color lines represent mean.

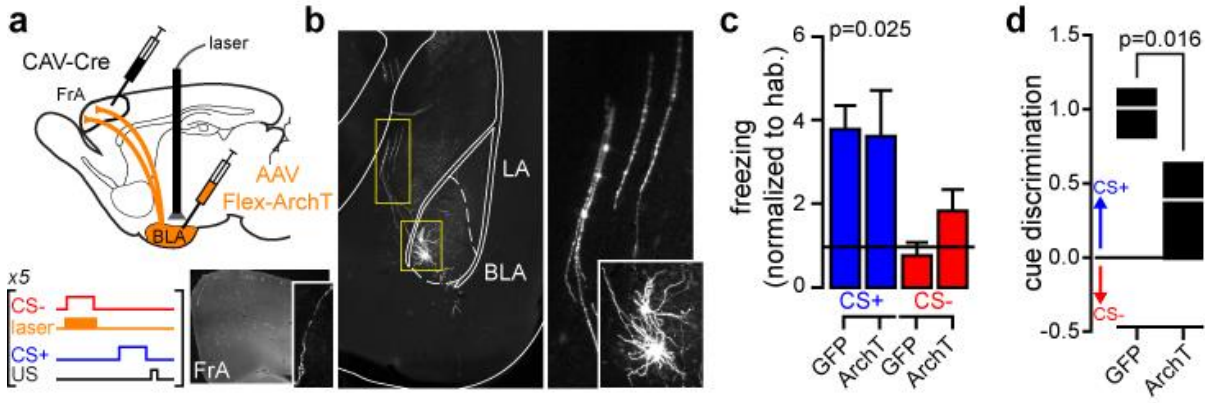

Figure 7.17. BLA-to-FrA projecting neurons mediate discriminative learning. a, Schematic of fear conditioning with ArchT (n=4) and GFP (n=4) BLA-to-FrA expressing mice. BLA axons were visible in the FrA (bottom right). BLA neurons that project to FrA were specifically photo-inhibited during the presentation of the CS- (bottom left). **b**, Examples of neurons and axons projecting from the BLA to the FrA. LA, lateral amygdala. **c, d**, Effect of light on freezing responses (**c**) and cue discrimination (**d**) upon auditory stimuli (GFP, n=4; ArchT, n=4; one way anova).

7.6 *Data availability and statistics*

All data generated or analysed during this study are included in the manuscript. All statistics were performed using Matlab (Mathworks) and Sigmaplot (Systat) with an α significant level set at 0.05. Normality of all value distributions and the equality of variance between different distributions were first assessed by the Shapiro-Wilk and Levene median tests, respectively. Standard parametric tests were only used when data passed the normality and equal variance tests ($p>0.05$). Non-parametric tests were used otherwise. Only two-sided tests were used. When applicable, pair-wise multiple post-hoc comparisons were done by using the Holm-Sidak method. Randomization and blinding methods were not used. No statistical methods were used to estimate sample size, but β-power values were calculated for parametric tests and are provided in the tables below.

Figure 7.2b

Group	**N**	**Missing**	**Mean**	**Standard deviation**	**Standard error**
CS+, Session1	5	2	15.111	11.108	6.413
CS+, Session2	5	2	13.167	7.485	4.322
CS+, Session3	5	0	10.100	6.866	3.071
CS+, Session4	5	0	64.467	5.275	2.359
CS+, Session5	5	1	57.333	13.738	6.869
CS+, Session6	5	1	64.333	17.159	8.580
CS-, Session1	5	2	5.333	6.405	3.698
CS-, Session2	5	2	4.778	2.417	1.396
CS-, Session3	5	0	11.733	11.267	5.039
CS-, Session4	5	0	10.500	6.669	2.982
CS-, Session5	5	1	12.250	7.377	3.688
CS-, Session6	5	1	16.667	14.875	7.438
Shapiro-Wilk test : p=0.805 (normality passed)			**Levene median test: p=0.312 (equality of variance passed)**		
Two-way analysis of variance (general linear model):					
Source of variation	**Degrees of freedom**	**Sum of squares**	**Mean squares**	**F-ratio**	***P-value***	**Significant ?**	**β power**
CS	1	8505.499	8505.499	82.427	<0.001	yes	1
Session	5	9082.340	1816.468	17.603	<0.001	yes	1
Interaction	5	6308.417	1261.683	12.227	<0.001	yes	1
Residual	36	3714.765	103.188				
Total	47	28942.981	615.808				
Multiple comparison procedures (Holm-Sidak method):							

Comparison	Difference of means	t-value	*P-value*	Significant ?
CS+, session 4 vs session 3	54.367	8.462	<0.001	yes
CS+, session 5 vs session 3	47.233	6.932	<0.001	yes
CS+, session 6 vs session 3	54.233	7.959	<0.001	yes
CS-, session 4 vs session 3	1.233	0.192	0.849	no
CS-, session 5 vs session 3	0.517	0.0758	0.940	no
CS-, session 6 vs session 3	4.933	0.724	0.474	no

Figure 7.2c

Group	N	Missing	Mean	Standard deviation	Standard error
Session 1	5	2	0.571	0.247	0.143
Session 2	5	2	0.375	0.488	0.282
Session 3	5	0	0.0641	0.330	0.148
Session 4	5	0	0.727	0.167	0.0747
Session 5	5	1	0.679	0.140	0.0699
Session 6	5	1	0.652	0.218	0.109
Shapiro-Wilk test : p=0.991			**Levene median test: p=0.100**		

One-way analysis of variance (general linear model):

Source of variation	Degrees of freedom	Sum of squares	Mean squares	F-ratio	*P-value*	Significant?	β power
Between Groups	5	1.491	0.298	3.987	0.013	yes	0.731
Residual	18	1.347	0.0748				
Total	23	2.838					

Multiple comparison procedures (Holm-Sidak method):

Comparison	Difference of means	t-value	*P-value*	Significant?
Session 3 vs. Session 4	0.663	3.834	0.001	yes
Session 3 vs. Session 5	0.615	3.354	0.004	yes
Session 3 vs. Session 6	0.588	3.204	0.005	yes
Session 3 vs. Session 1	0.507	2.540	0.021	yes
Session 3 vs. Session 2	0.311	1.556	0.137	no

Figure 7.3b

Group	N	Missing	Mean	Standard deviation	Standard error
CS+ naive	25	0	11.630	7.735	1.547
CS+ FC	25	0	37.025	23.654	4.731
Difference CS+	25	0	-25.395	24.488	4.898
CS- naive	25	0	9.617	7.479	1.496
CS- FC	25	0	7.067	6.806	1.361
Difference CS-	25	0	2.550	9.850	1.970

Shapiro-Wilk test : p=0.157 (CS+); p=0.721 (CS-)							
Student paired t-test							
Source of variation	**Degrees of freedom**	**Difference of means**	**t-value**	**95% confidence interval**	***P-value***	**Significant?**	**β power**
CS+ Naive vs FC	24	-25.395	-5.185	-35.503 to -15.286	<0.001	yes	0.999
CS- Naive vs FC	24	2.550	1.294	-1.516 to 6.616	0.023	no	0.116

Figure 7.3d (left)

Treatments	**N**	**Missing**	**Median**	**25%**	**75%**
CS+ naive	21	0	8.750	5.662	10.958
CS+ FC	21	0	40.000	19.700	64.750

Shapiro-Wilk test : p<0.05						
Wilcoxon Signed Rank Test:						
Source of variation	**W**	**T+**	**T-**	**Z-statistic (positive ranks)**	***P-value***	**Significant?**
Between treatments	231	231	0	4.015	<0.001	yes

Figure 7.3d (right)

Group	**N**	**Missing**	**Mean**	**Standard deviation**	**Standard error**
CS+ naive	4	0	22.667	5.569	2.785
CS+ FC	4	0	13.750	10.043	5.021
Difference	4	0	8.917	10.857	5.429

Shapiro-Wilk test : p=0.282							
Student paired t-test							
Source of variation	**Degrees of freedom**	**Difference of means**	**t-value**	**95% confidence interval**	***P-value***	**Significant?**	**β power**
CS+, naive vs FC	3	8.917	1.643	-8.360 to 26.193	0.199	no	0.153

Figure 7.3e

Group	N	Missing	Mean	Standard deviation	Standard error
CS- naive (increase)	9	0	4.981	3.798	1.266
CS+ FC (increase)	9	0	13.148	6.286	2.095
Difference (increase)	9	0	-8.167	5.659	1.886
CS- naive (decrease)	16	0	12.224	7.853	1.963
CS+ FC (decrease)	16	0	3.646	4.286	1.072
Difference (decrease)	16	0	8.578	5.521	1.380
Shapiro-Wilk test : p=0.501 (increase); p=0.319 (decrease)					

Student paired t-test							
Source of variation	**Degrees of freedom**	**Difference of means**	**t-value**	**95% confidence interval**	***P-value***	**Significant?**	**β power**
naive vs FC (increase)	8	-8.167	-4.330	-12.516 to -3.817	0.003	yes	0.965
naive vs FC (decrease)	15	8.578	6.215	5.636 to 11.520	<0.001	yes	1

Figure 7.4d

Group	N	Missing	Mean	Standard deviation	Standard error
CS+, Session1	4	2	0.919	0.339	0.240
CS+, Session2	4	1	1.195	0.0721	0.0416
CS+, Session3	4	0	0.971	0.443	0.221
CS+, Session4	4	0	2.443	1.987	0.994
CS+, Session5	4	0	2.301	1.517	0.758
CS+, Session6	4	0	3.723	2.437	1.219
CS-, Session1	4	2	0.858	0.453	0.320
CS-, Session2	4	1	1.053	0.0454	0.0262
CS-, Session3	4	0	1.092	0.428	0.214
CS-, Session4	4	0	1.951	1.587	0.793
CS-, Session5	4	0	2.503	1.558	0.779
CS-, Session6	4	0	2.999	1.625	0.812
Shapiro-Wilk test : p<0.05 (normality failed)				**Levene median test: p=0.503 (equality of variance passed)**	

Two-way analysis of variance (general linear model):							
Source of variation	**Degrees of freedom**	**Sum of squares**	**Mean squares**	**F-ratio**	***P-value***	**Significant?**	**β power**
CS	1	0.327	0.327	0.161	0.691	no	-
Session	5	33.402	6.680	3.296	0.017	yes	-
Interaction	5	1.273	0.255	0.126	0.985	no	-

Residual	30	60.800	2.027				
Total	41	95.878	2.338				

Multiple comparison procedures (Holm-Sidak method):				
Comparison	**Difference of means**	**t-value**	***P-value***	**Significant?**
session 3 vs session 1	0.143	0.164	0.871	no
session 3 vs session 2	0.0926	0.120	0.905	no
session 3 vs session 4	1.165	1.637	0.112	no
session 3 vs session 5	1.371	1.926	0.064	no
session 3 vs session 6	2.330	3.273	0.003	yes
session 3 vs session 1	0.143	0.164	0.871	no

Figure 7.5c

Treatments	**N**	**Missing**	**Median**	**25%**	**75%**
session 1	4	1	0.0949	0.00108	0.149
session 2	4	1	0.0107	-0.0249	0.0155
session 3	4	0	-0.123	-0.130	-0.0684
session 4	4	0	0.0837	-0.0210	0.164
session 5	4	1	0.140	0.129	0.166
session 6	4	0	0.0504	0.0330	0.134

Shapiro-Wilk test : p<0.05				
Friedman repeated measures analysis of variance on Ranks				
Source of variation	**Degrees of freedom**	**χ^2**	***P-value***	**Significant?**
Between treatments	5	5.714	0.335	no

Figure 7.6f

Group	**[pearson correlation coefficient; cue discrimination]**	
Session 3	[0.3047;0.3298], [0.1111;0.1233], [0.0351;0.0638], [0.0753; 0.5636]	**Shapiro-Wilk test : p=0.8771**
Session 4	[0.0543; 0.9087], [0.0422; 6427], [-0.0134; 0.6883], [-0.1544; 0.8835]	
Session 5	[0.0254; 0.5506], [2.7958e-3; 0.6242]	**Levene median test: p=0.2212**
Session 6	[-6.9924e-4; 0.3931], [-0.0725; 0.8608], [-0.0112; 0.8018]	

Non-linear regression (polynomial, y = a*x+b):				
	Coefficient	**Standard error**	**t-value**	***P-value***
a	-2.7852	0.6341	-4.3925	0.0011
b	0.6065	0.0674	9.0003	<0.0001
R	0.7981	0.2326		

Analysis of variance (corrected for the mean of the observations):							
Source of variation	**Degrees of freedom**	**Sum of squares**	**Mean squares**	**F-ratio**	***P-value***	**Significant?**	**β power**

Regression	1	1.0442	1.0442	19.2937	0.0011	yes	-
Residual	11	0.5954	0.0541				-
Total	12	1.6396	0.1366				

Figure 7.7b

Treatments	**N**	**Missing**	**Mean**	**Standard deviation**	**Standard error**
Frequency before	3	0	7.046	2.609	1.506
Frequency during	3	0	0.393	0.301	0.174
Frequency after	3	0	4.566	2.603	1.503
Shapiro-Wilk test : p=0.817			**Levene median test: p=0.649**		

One-way repeated measures analysis of variance:							
Source of variation	**Degrees of freedom**	**Sum of squares**	**Mean squares**	**F-ratio**	***P-value***	**Significant?**	**β power**
Between Subjects	2	16.867	8.434				
Between Treatments	2	67.812	33.906	12.943	0.018	yes	1
Residual	4	10.479	2.620				
Total	8	95.158					

Multiple comparison procedures (Holm-Sidak method):				
Comparison	**Difference of means**	**t-value**	***P-value***	**Significant?**
Before vs during	6.652	5.034	0.007	yes
Before vs after	2.480	1.876	0.134	no

Figure 7.7e

Group	**N**	**Missing**	**Mean**	**Standard deviation**	**Standard error**
CS+ GFP	5	0	2.204	0.923	0.413
CS+ ArchT	5	0	2.046	1.278	0.571
CS- GFP	5	0	0.418	0.587	0.262
CS- ArchT	5	0	1.813	1.053	0.471
Shapiro-Wilk test : p=0.671			**Levene median test: p=0.667**		

One-way analysis of variance (general linear model):							
Source of variation	**Degrees of freedom**	**Sum of squares**	**Mean squares**	**F-ratio**	***P-value***	**Significant?**	**β power**
Between Groups	3	10.022	3.341	3.394	0.044	yes	0.486
Residual	16	15.750	0.984				
Total	19	25.772					

Multiple comparison procedures (Holm-Sidak method):				
Comparison	**Difference of means**	**t-value**	***P-value***	**Significant?**
CS+ GFP vs CS- GFP	1.786	2.846	0.012	yes
CS+ ArchT vs CS- GFP	1.628	2.594	0.020	yes
CS- ArchT vs CS- GFP	1.395	2.223	0.041	yes
CS+ GFP vs CS- ArchT	0.391	0.624	0.542	no
CS+ ArchT vs CS- ArchT	0.233	0.372	0.715	no
CS+ GFP vs. CS+ ArchT	0.158	0.252	0.804	no

Figure 7.9b (top)

Treatments	**N**	**Missing**	**Mean**	**Standard deviation**	**Standard error**
CS- pre	11	0	67.556	6.869	2.071
CS- during	11	0	65.966	7.160	2.159
CS- post	11	0	66.432	6.955	2.097
Shapiro-Wilk test : p=0.506			**Levene median test: p=0.792**		

One-way repeated measures analysis of variance (general linear model):							
Source of variation	**Degrees of freedom**	**Sum of squares**	**Mean squares**	**F-ratio**	***P-value***	**Significant?**	**β power**
Between Subjects	10	1460.046	146.005				
Between Treatments	2	14.716	7.358	18.109	<0.001	yes	1
Residual	20	8.127	0.406				

Multiple comparison procedures (Holm-Sidak method):				
Comparison	**Difference of means**	**t-value**	***P-value***	**Significant?**
pre vs during	1.591	5.853	<0.001	yes
pre vs post	1.125	4.139	<0.001	yes
post vs during	0.466	1.714	0.102	no

Figure 7.9b (bottom)

Treatments	**N**	**Missing**	**Median**	**25%**	**75%**
CS- pre	11	0	66.711	63.108	69.482
CS- during	11	0	66.604	62.517	69.525
CS- post	11	0	66.522	63.077	69.912
Shapiro-Wilk test : p<0.05					

Friedman repeated measures analysis of variance on ranks:					
Source of variation	**Degrees of freedom**	**χ^2**	***P-value***	**Significant?**	**β power**

Between treatments	2	0.725	0.698	no	-

Figure 7.9d

Group	N	Missing	Mean	Standard deviation	Standard error
CS- ctrl	10	0	36.268	26.714	8.448
CS+	10	0	3.485	25.384	8.027
Difference ctrl	10	0	32.783	12.934	4.090
CS- dAP5	13	0	-5.592	9.972	2.766
CS+ dAP5	13	0	-4.122	14.737	4.087
Difference dAP5	13	0	-1.471	13.324	3.695
Shapiro-Wilk test : p=0.345 (ctrl); p=0.858 (dAP5)					

Student paired t-test							
Source of variation	**Degrees of freedom**	**Difference of means**	**t-value**	**95% confidence interval**	***P-value***	**Significant?**	**β power**
CS- vs CS+ ctrl	9	32.783	8.016	23.531 to 42.035	<0.001	yes	1
CS- vs CS+ dAP5	12	-1.471	-0.398	-9.522 to 6.581	0.698	no	0.05

Figure 7.9e (left)

Group	N	Missing	Mean	Standard deviation	Standard error
End, control	10	0	1.176	0.110	0.0349
End, dAP5	13	0	0.944	0.102	0.0284
End+30, control	10	0	1.063	0.0361	0.0114
End+30, dAP5	13	0	0.895	0.151	0.0418
Shapiro-Wilk test : p=0.324			**Levene median test: p<0.05**		

One-way analysis of variance (general linear model):							
Source of variation	**Degrees of freedom**	**Sum of squares**	**Mean squares**	**F-ratio**	***P-value***	**Significant?**	**β power**
Between Groups	3	0.532	0.177	14.355	<0.001	yes	1
Residual	42	0.519	0.0124				
Total	45	1.051					

Multiple comparison procedures (Holm-Sidak method):				
Comparison	**Difference of means**	**t-value**	***P-value***	**Significant?**

End, control vs dAP5	0.233	4.972	<0.001	yes
End+30, control vs dAP5	0.168	3.590	<0.001	yes

Figure 7.9e (right)

Treatments	**N**	**Missing**	**Median**	**25%**	**75%**
End, control	10	0	1.014	0.951	1.033
End, dAP5	13	0	0.929	0.838	1.056
End+30, control	10	0	0.977	0.947	1.004
End+30, dAP5	13	0	0.945	0.917	0.986
Shapiro-Wilk test : p<0.05					

Kruskal-Wallis one way analysis of variance on ranks:					
Source of variation	**Degrees of freedom**	**H**	***P-value***	**Significant?**	**β power**
Between treatments	3	2.468	0.481	no	-

Figure 7.10f

Treatments	**N**	**Missing**	**Median**	**25%**	**75%**
CS-	25	0	13.802	6.060	34.112
CS+	26	0	22.580	12.825	53.152

Mann-Whitney U Statistic=206.000					
Source of variation	***P-value***	**Significant?**	**β power**		
Between treatments	0.026	yes	1		

Figure 7.11a

Group	N	Missing	Mean	Standard deviation	Standard error
CS- naive	10	0	36.268	26.714	8.448
CS- FC	8	0	5.410	26.650	9.422
CS+ FC	8	0	1.441	14.016	4.955
Shapiro-Wilk test : p=0.268			**Levene median test: p=0.305**		

One-way analysis of variance (general linear model):

Source of variation	Degrees of freedom	Sum of squares	Mean squares	F-ratio	*P-value*	Significant?	β power
Between Groups	2	6700.554	3350.277	6.034	0.008	yes	0.767
Residual	23	12769.564	555.198				
Total	25	19470.118					

Multiple comparison procedures (Holm-Sidak method):

Comparison	Difference of means	t-value	*P-value*	Significant?
CS- (naive) vs. CS+ (FC)	34.826	3.116	0.005	yes
CS- (naive) vs. CS- (FC)	30.858	2.761	0.011	yes
CS- (FC) vs. CS+ (FC)	3.969	0.337	0.739	no

Figure 7.11b

Group	N	Missing	Mean	Standard deviation	Standard error
Naive	10	0	0.436	0.327	0.104
Naive+dAP5	13	0	-0.0977	0.383	0.106
FC	8	0	-0.0235	0.449	0.159
Shapiro-Wilk test : p=0.086			**Levene median test: p=0.880**		

One-way analysis of variance (general linear model):

Source of variation	Degrees of freedom	Sum of squares	Mean squares	F-ratio	*P-value*	Significant?	β power
Between Groups	2	1.756	0.878	5.944	0.007	yes	0.770
Residual	28	4.137	0.148				
Total	30	5.893					

Multiple comparison procedures (Holm-Sidak method):

Comparison	Difference of means	t-value	*P-value*	Significant?
Naive vs Naive + dAP5	0.533	3.300	0.003	yes
Naive vs FC	0.459	2.519	0.018	yes
FC vs Naive + dAP5	0.0742	0.430	0.671	no

Figure 7.11c

Group	**[cell discrimination index; % of freezing]**	
Mouse 1	[0.0784; 49.5000], [0.1364; 49.5000]	**Shapiro-Wilk test : p=0.0653**
Mouse 2	[0.3764; 3.6667]	
Mouse 3	[-0.2504; 83.1667]	**Levene median test: p=0.05**
Mouse 4	[-1.0000; 70.1667], [-0.0266; 70.1667], [0.0743; 70.1667]	
Mouse 5	[0.4235; 16.6667]	

Non-linear regression (polynomial, y = a*x+b):				
	Coefficient	**Standard error**	**t-value**	***P-value***
a	-94.0741	17.5060	-5.3738	0.0126
b	51.0207	5.5140	9.2530	0.0027
R	0.9518	12.0397		

Analysis of variance (corrected for the mean of the observations):

Source of variation	**Degrees of freedom**	**Sum of squares**	**Mean squares**	**F-ratio**	***P-value***	**Significant?**	**β power**
Regression	1	4185.9899	4185.9899	28.8778	0.0126	yes	-
Residual	3	434.8657	144.9552				-
Total	4	4620.8556	1155.2139				

Figure 7.14h (left)

Treatments	**N**	**Missing**	**Mean**	**Standard deviation**	**Standard error**
pre	4	0	6.138	3.291	1.645
hyper	4	0	3.891	3.021	1.510
post	4	0	5.566	2.822	1.411
Shapiro-Wilk test : p=0.950			**Levene median test: p=0.674**		

One-way repeated measures analysis of variance:

Source of variation	**Degrees of freedom**	**Sum of squares**	**Mean squares**	**F-ratio**	***P-value***	**Significant?**	**β power**
Between Subjects	3	81.651	27.217				
Between Treatments	2	10.910	5.455	15.563	0.004	yes	0.964
Residual	6	2.103	0.351				
Total	11	94.664					

Multiple comparison procedures (Holm-Sidak method):

Comparison	**Difference of means**	**t-value**	***P-value***	**Significant?**
Pre vs hyper	2.247	5.368	0.002	yes
Pre vs post	0.573	1.369	0.220	no

Figure 7.14h (right)

Treatments	N	Missing	Median	25%	75%
Area-CTRL	13	0	5.400	3.121	8.088
Area-HYPER	13	9	2.488	2.268	5.514
Area-DAP5	3	0	0.951	0.863	2.432
Shapiro-Wilk test : p<0.05					
Kruskal-Wallis one way analysis of variance on ranks:					
Source of variation	**Degrees of freedom**	**H**	***P-value***	**Significant?**	**β power**
Between treatments	2	7.358	0.025	yes	-

Figure 7.15d

Group	N	Missing	Mean	Standard deviation	Standard error
CS- / end	6	0	12.336	32.015	13.070
CS- laser / end	6	0	31.804	26.351	10.758
Difference end	6	0	-19.468	36.246	14.797
CS- / end+30	6	0	9.333	36.675	14.973
CS- laser / end+30	6	0	75.969	50.697	20.697
Difference end+30	6	0	-66.636	50.398	20.575
Shapiro-Wilk test : p=0.66 (endl); p=0.24 (end+30)					
Student paired t-test					
Source of variation	**Degrees of freedom**	**Difference of means**	**t-value**	**95% confidence interval**	***P-value***	**Significant?**	**β power**
CS- vs CS- laser End	5	-19.468	-1.31	-57.505 to 18.570	0.245	no	0.105
CS- vs CS- laser End+30	5	-66.636	-3.23	-119.525 to -13.747	0.023	yes	0.698

Figure 7.17c

Group	N	Missing	Mean	Standard deviation	Standard error
CS+ GFP	4	0	3.800	1.127	0.563
CS+ ArchT	4	0	3.630	2.200	1.100
CS- GFP	4	0	0.772	0.614	0.307
CS- ArchT	4		1.842	1.009	0.505
Shapiro-Wilk test : p=0.236			**Levene median test: p=0.578**		

One-way analysis of variance (general linear model):							
Source of variation	**Degrees of freedom**	**Sum of squares**	**Mean squares**	**F-ratio**	***P-value***	**Significant?**	**β power**
Between Groups	3	25.547	8.516	4.538	0.024	yes	0.633
Residual	12	22.519	1.877				
Total	15	48.066					

Multiple comparison procedures (Holm-Sidak method):				
Comparison	**Difference of means**	**t-value**	***P-value***	**Significant?**
CS+ GFP vs CS- GFP	3.028	3.126	0.009	yes
CS+ ArchT vs CS- GFP	2.858	2.951	0.012	yes
CS+ GFP vs CS- ArchT	1.958	2.022	0.066	no
CS+ ArchT vs. CS- ArchT	1.788	1.846	0.090	no
CS- ArchT vs CS- GFP	1.070	1.105	0.291	no
CS+ GFP vs CS- ArchT	0.170	0.175	0.864	no

Figure 7.17d

Group	**N**	**Missing**	**Mean**	**Standard deviation**	**Standard error**
GFP	4	0	0.982	0.168	0.0839
ArchT	4	0	0.337	0.348	0.174
Shapiro-Wilk test : p=0.765			**Levene median test: p=0.494**		

Student t-test							
Source of variation	**Degrees of freedom**	**Difference of means**	**t-value**	**95% confidence interval**	***P-value***	**Significant?**	**β power**
GFP vs ArchT	6	0.645	3.340	0.172 to 1.117	0.016	yes	0.763

7.7 Conclusions

Our data describe a new critical role for the prefrontal cortex during behavioral discrimination of threat *vs*. safety environmental signals. Compared to the other prefrontal regions, the frontal association area (FrA) of rodents has long been neglected presumably because of a lack of a standardized anatomical definition (Uylings et al., 2003). However, despite different names accross the literature (e.g. Fr2 (Uylings et al., 2003), PrCm (Vidal-Gonzalez et al., 2006), agranular medial and lateral cortices (Sul et al., 2011), frontal cortex (Sacchetti et al., 2002), dorsal frontal cortex (Barrett et al., 2003), secondary motor area (Mátyás et al., 2014)), the implication of FrA in classical conditioning has constantly been reported (Barrett et al., 2003; Lai et al., 2012; Sacchetti et al., 2002; Vidal-Gonzalez et al., 2006). For example, the pharmacological inactivation of FrA before fear conditioning or extinction impaired the consolidation of fear or extinction memories, respectively (Lai et al., 2012; Sacchetti et al., 2002), indicating that FrA promotes both the expression and suppression of fear memory traces. Here, we provide the first experimental evidence that the formation of segregated FrA neuronal assemblies that are specific for threatening and non-threatening cues is associated upon learning with increased discriminative performance (**Fig. 7.7**), providing a possible circuit mechanism for the opposing behavioral output of FrA.

Over the last decade, neuronal assemblies have become the favorite physical substrate for memory traces in brain circuits (A. Holtmaat & Caroni, 2016). They are supposed to be formed during learning and further consolidated into long-term memories through the strengthening of synaptic connections between pairs of neurons with similar input selectivity (A. Holtmaat & Caroni, 2016). For instance, increased temporal correlated activity among similar neurons has been recently reported in the hippocampus during learning (Cheng & Frank, 2008), which might help subsequent *Hebbian*-like synaptic plasticity mechanisms and promote the selection of the same pattern of neural activity upon memory recall of a particular event (Cheng & Frank, 2008; A. Holtmaat & Caroni, 2016; Komiyama et al., 2010; Rajasethupathy et al., 2015). In contrast, in FrA we found that fear learning increased non-specifically the activity evoked by distinct auditory stimulations (**Fig. 7.4d**). In addition, neither the auditory-cue selectivity nor the temporal correlation between the activity of FrA pyramidal neurons evoked by the same auditory stimulus were affected (**Fig. 7.5**). Instead, we observed a decrease in the correlation of activity patterns evoked by paired and unpaired CS after learning (**Fig. 7.6**), suggesting the formation of an higher-order representation between paired and unpaired CS that might differ from the formation of individual CS representations. Likewise, our data are consistent with the increase of sparse

population coding reported in the somatosensory cortex after fear learning (Gdalyahu et al., 2012), which might support activity pattern decorrelation (Wiechert et al., 2010). Pattern decorrelation has been observed in different divergent neuronal networks. It has been proposed to make stimulus representations more distinct, which in turn may facilitate learning performance (Leutgeb et al., 2007; Gschwend et al., 2010). In agreement, we observed that the level of fear learning-induced separation of CS activity patterns was associated with a better discrimination of paired (aversive) *vs.* non-paired (non-aversive) auditory stimuli (**Fig. 7.6f**).

The above results imply that sensory cues that were not positively or explicitly paired with the delivery of the footshock must have been encoded within FrA into safety-related representation. In agreement with this hypothesis, we showed that optogenetic inactivation of the FrA during learning resulted in fear overgeneralization with bias towards encoding neutral, unpaired cues as threat (**Fig. 7.7**). This indicates that the FrA is required for safety *vs.* threat discrimination rather than for fear acquisition. It contrasts however with previous lesion studies (Lai et al., 2012; Sacchetti et al., 2002), which might be explained by the high temporal and spatial precision of our optogenetic inhibition. Besides, our data are consistent with recent studies showing an increase of theta synchronization between mPFC and BLA during safety and CS discrimination that possibly inhibits fear response and anxiety-related behaviors (Likhtik & Paz, 2015a; Likhtik et al., 2014; Stujenske et al., 2014a).

The learning-driven synaptic mechanisms that underlie the encoding of unpaired sensory cue into safety-related cortical assembly remain unclear. Beyond its classical role during CS+/US association (Likhtik & Paz, 2015a; McGaugh, 2013), the BLA has emerged as a key structure during recall of the CS- (S. Sangha et al., 2013; Senn et al., 2014). In addition it provides massive cortical inputs that critically influence safety encoding and long-lasting memory consolidation (Likhtik & Paz, 2015a; Likhtik et al., 2014; Mátyás et al., 2014; Stujenske et al., 2014a) presumably through synaptic plasticity (McGaugh, 2013). Here, we confirmed that BLA neurons projecting to the FrA participated in the acquisition of safety memory traces as well (Fig. 6.15). However, only a limited fraction of BLA neurons were required (Johansen et al., 2014; Reijmers et al., 2007) (**Fig. 7.17**) and their activation during conditioning was not cue-specific (**Fig. 7.16**), indicating that neuronal target specificity of BLA-to-FrA long-range projections is likely to be necessary though not sufficient for cue discrimination (Senn et al., 2014). Indeed, we showed that, in addition to the presumed spatial specificity, temporal coincident activation of convergent inputs from both BLA and cortex was required to potentiate FrA pyramidal responses evoked by unpaired, gaussian auditory stimulation (**Fig. 7.15**). This possibly occurred at the level of distal dendrites with the help of BLA-induced NMDARs-dependent dendritic plateau potentials

(Brandalise et al., 2016; Gambino et al., 2014; Lavzin et al., 2012; Palmer et al., 2014; Xu et al., 2012) (**Fig. 7.14d-h**). Together, it indicates that long-range BLA projections in superficial layer of FrA might produce strong local dendritic depolarization and gain control over synaptic plasticity of coincident cortical inputs and thus recruit neurons into safety-related assembly (Gambino et al., 2014; Larkum, 2013; McGaugh, 2013).

Taken together, our results provide a new *Hebbian* cortical framework for our understanding of discriminative learning, during which BLA long-range inputs actively instruct intra-cortical cue-specific inputs, likely resulting in the emergence of discriminative neuronal patterns that is associated during recall with a normal cue-discrimination behavior, in particular during the non-threat (safe) periods. Whether a similar synaptic mechanism is involved during the formation of fear-related assembly remains to be determined. We found that during anesthesia only gaussian tone (CS-) evoked long-lasting subthreshold depolarization in naive animals (i.e. before conditioning) while pure auditory tones had no effect (**Fig. 7.9**), suggesting a frequency-specific mechanism. Although convergent inputs from successive or parallel cortical regions that are involved in complex sound processing (e.g. auditory cortex) likely drive this process (LeDoux, 2000; Mizrahi et al., 2014), we cannot exclude an effect of anesthesia and future experiments in awake animals will further clarify the synaptic role of tone frequencies in the formation of cue-specific assemblies (see **Fig. 7.10**).

8. General Discussion

8.1 *The dPFC encodes stimulus discrimination during associative learning*

The present work demonstrates a prominent role of the dorsal prefrontal cortex, in discriminating fearful stimuli from the surrounding similar yet emotionally meaningless environmental cues. So far, fear conditioning studies have mostly focused on fear learning, whereas how an animal learns to dissociate threatening from neutral/safe remains poorly investigated. The novelty of the results presented in this dissertation comes from the fact that this work describes, for the first time, the brain circuits and the synaptic and neuronal mechanisms by which an animal discriminates environmental stimuli.

Fear is classically defined as a physiological reaction meant to protect a person from harm. Fear triggers numerous reactions in the body, whose purpose is to help defend against danger or to avoid it. However, the environment is composed of both dangerous and safe cues and the ability to distinguish between them is crucial for survival. Safety signals are defined as "learned cues that predict the non-occurrence of an aversive stimulus" (Christianson et al., 2012). This topic has become more and more relevant due to traumatized individuals characterized by the inability to take advantage of safety cues to inhibit fear responses. This pathological state is also known as "post-traumatic stress disorders", and is defined as amplified expression of fear in contexts where it is not appropriate, and usually develops in people who have experienced a scary, shocking or dangerous situation.

Learning of safety cues is distinct from extinction learning. During extinction, the encounter with a previously learned danger cue is repeated without the occurrence of an aversive reinforcement, and this results into an alteration of the danger cue value that becomes predictive of the absence of the aversive event. Thus, fear extinction establishes a new memory that competes with the previously learned danger association, which results into inhibition of fear (Bouton, 2004; Christianson et al., 2012). Differently, learned safety signals are counterposing fear responses to cues that are still paired with an aversive event. In this view, safety signals can be learned just when the subjects predicts danger but it does not occur. Fear extinction cannot be considered as safety learning, because the fear memory trace that was previously formed is not erased, but is maintained within the fear circuits. This is confirmed by behavioural data indicating that fear can easily recover following extinction (Schiller et al. 2008). Likewise, "safety signals" are not innate, but might predict safe environment by inhibiting fear behaviour upon associative learning. As such, discriminative learning allows

subjects to distinguish between stimuli that are "positively" associate with an aversive event to produce a conditioned response, and stimuli that are "negatively" paired with the aversive event and prevent or reduce the expression of fearful behaviours. Inability to discriminate between danger and safety results into "fear generalization", a process that hastens fear responses to a stimulus, but that also induces overreaction to non-dangerous cues. Lack of fear inhibition in presence of safe stimuli results into generalized fear, that is associated with post-traumatic stress disorders (PTSDs).

8.1.1 The Amygdala instructs both danger and safety

Recent evidences indicate a main role of the basolateral complex of the amygdala in mediating discrimination among cues signifying safety or danger (Sangha et al. 2013). In this study, they developed a protocol to investigate fear and safety learning in parallel. To do so, animals were subjected to the presentation of a safety cue (no foot-shock), and fear cue (paired with foot-shock). Trials with fear and safety cues together (Fear+Safety) were also included. Simultaneously, the activity of basal amygdala single units was recorded. Animals were significantly decreasing their freezing behaviour in Fear+Safety trials compared with Fear alone, indicating that the safety cue was acting as a danger inhibitor. In parallel, single unit recordings revealed that a population of BA neurons was changing its firing rates to combined Fear+Safety, but not Fear alone. These findings suggest the presence of "safety" neurons in the basal amygdala. In addition, by presenting a reward-expecting cue, they observed that the BA neuronal population activated was overlapping with safety-encoding neurons. This introduces the concept according to which the absence of an aversive outcome is encoded as a reward itself.

Similar results were obtained by recordings of BLA neurons in nonhuman primates during complex discriminative aversive-conditioning (Genud-Gabai et al. 2013). This behavioural paradigm encompasses two different modalities, auditory and visual, where the CS+ was paired with an air-puff to the eye, and two other stimuli (CS-) were unpaired. The study confirms the robust encoding of safety cues in the amygdala, described by Sangha et al., and adds to it in several aspects. First of all, they confirmed that amygdala signals not only cues that predict threat, but also cues that predict safety, in a different animal model, suggesting the wide evolutionary conservation of this neural mechanism in different species. Secondly, differently conceived behavioural paradigms, exploited by Genud-Gabai et al. and Sangha et al., equally lead to the isolation of subpopulations of amygdala neurons responding to positive (safety)

predicting cues. Finally, using single unit recordings, they found that “safety” neurons displayed similar neural properties to “fear” neurons. Indeed, the proportion of responsive neurons, the magnitude of responses, increases and decreases, onsets, and anatomical positions were analogous.

8.1.2 PFC-BLA synchronization suppresses fear behaviour during safety

The above results indicate that amygdala instructs both danger and safety. However, as mentioned in the paragraph 5.1.3. "Neuronal circuits for fear conditioning", many brain regions can be involved in the control and modulation of emotion. Hence, the amygdala safety signalling can be driven by other structures, and the prefrontal cortex as emerged as an ideal candidate. Indeed, it was recently established that reciprocal communication between mPFC and BLA has a crucial role for successful discrimination between safety and threat (Likhtik & Paz, 2015b). For instance, it has been shown that vmPFC is subdivided into two distinct compartments supporting counteracting behavioural outcomes. The activity of the prelimbic cortex (PL) is enhanced during fear conditioning and expression, whereas the infralimbic cortex (IL) increases its activity during fear extinction (Quirk & Mueller, 2008). More recently, this view of the vmPFC has been replaced by a more advanced and comprehensive theory that reconsiders the role of IL and PL. These two subregions are more likely co-operating in sharpening discrimination of distinct environmental cues. On one side, this concept is consistent with the initial notion that IL-BLA is involved in diminishing fear and anxiety, but extend the role of the mPFC as a co-operating unit (prelimbic and infralimbic cortex together), assisting the amygdala during discriminating tasks (Likhtik & Paz, 2015b; Likhtik, Stujenske, Topiwala, Harris, & Gordon, 2013). In line with this model, simultaneous recordings of BLA and mPFC revealed that mice able to successfully discriminate between an aversive CS+ and an anxiolytic CS-, were displaying higher synchrony than in mice that were generalizing (Stujenske, Likhtik, Topiwala, & Gordon, 2014b).

Synchronous activity in the theta (4-12 Hz) and fast gamma (70-120 Hz) range, is highly relevant to the signalling of discriminative learning in the mPFC-BLA circuit (Likhtik & Paz, 2015b; Stujenske et al., 2014b). Synchronous theta frequency oscillations is a major mechanism of communication between these two regions in response to aversive cues. This synchronous activity is significantly enhanced in animals able to correctly discriminate CS- versus CS+, whereas no changes in synchrony is associated with fear generalization.

It has been extensively demonstrated that the amygdala is sufficient to generate fear memories. However, it is less clear to what extent amygdala sustains more complex forms of learning. Probabilistic paradigms, such as partial reinforcement schedules (ParS), have been extensively used to investigate this issue. These models are not affecting the final memory (acquired under probabilistic regime), but they are dramatically slowing down the extinction process. mPFC-BLA interactions are elevated during the first pairings in simple associative tasks (e.g. continuous reinforcement schedule), but then it drops down. It is likely that the involvement of the mPFC instructs the amygdala about uncertainty and its activity is dampened by the increase of predictability. In line with this theory, in probabilistic schedules (ParS), the degree of mPFC-BLA synchronization remains elevated, due to the fact that prediction error is not reduced in time (Livneh & Paz, 2012). The retention of the synchronized discharge of mPFC and BLA, displayed in ParS, predicts a higher resistance to extinction. Likely, if memory is actively maintained by PL-BLA pathway, IL would take longer to inhibit fear response and promote extinction behaviour. During recall of discriminative learning acquired during continuous reinforcement schedules, BLA is phase-locked to mPFC theta rhythms only during the safe CS-. In generalizing animals mPFC-BLA synchronization is not observed, and this indicates a direct involvement of those theta oscillations in discrimination. In addition to theta activity, two distinct bands of gamma-frequency coexist in BLA. Intriguingly, fast gamma (70-120 Hz) power and synchrony are enhanced during safety, whereas low range gamma oscillations (30-80 Hz) are increasing with fear. mPFC theta oscillations are believed to coordinate local gamma activity within BLA and leading to strong local theta/gamma coupling during the occurrence of the aversive CS+. In contrast, during the presentation of the safe CS-, mPFC-BLA inputs predominate and suppress fear response, through fast gamma circuit (Stujenske et al., 2014b). Given the fact that in numerous structures inhibitory interneurons are able to generate gamma and pace theta rhythms, it is likely that a subpopulations of interneurons in the BLA, can support this role during safe conditions.

8.1.3 The relevance of dPFC to perceptual acuity

Taken together, these observations lead to conclude that mPFC-BLA communication actively suppresses fear behaviour during safety, by synchronizing theta oscillations with local fast gamma generating inhibitory neurons, which ultimately modulate fear response.

In summary, great efforts have been made to set out to unravel the circuits involved in fear learning (Tovote et al., 2015). Recently, a few studies have also started to focus on the circuits

implicated in encoding for safety (Likhtik & Paz, 2015b; Likhtik et al., 2014). Animals are able to take advantage of sources of security and protection offered in the environment. Disruption of this ability leads to hyperarousal, hypervigilance and, consequently, stimulus generalization, related to the symptomatology of PTSD. The amygdala was shown to be sufficient to support fear responses. However, the ability to discriminate between aversive versus anxiolytic cues seems to require the intervention of cortical structures (Likhtik & Paz, 2015b; Likhtik et al., 2013; Livneh & Paz, 2012; Quirk & Mueller, 2008). Notably, the activity of BLA is instructed by the mPFC, that plays a role during both the encounter of negative and positive cues. The activity of the dorsal prefrontal cortex, that has been investigated in this work, comes into this framework. Indeed, it is reasonable to expect the existence of higher function cortical structures that could facilitate perceptual acuity and control downstream areas, such as vmPFC and BLA. Indeed, these regions have been shown to be reciprocally connected (Lai et al., 2012; Manita, Suzuki, Larkum, et al., 2015; Mátyás et al., 2014).

To address these questions, the current study exploited chronic *in vivo* two-photon calcium imaging, together with whole cell recordings and optogenetic approaches, to assess dPFC neuronal population and BLA-dPFC long-range projection dynamics during acquisition and retrieval of discriminative memories. First, to investigate the involvement of prefrontal circuits in discriminative learning, mice were implanted with cranial windows over the PFC upon injection of the genetically encoded calcium indicator GCaMP5g. The activity of the same population of neurons was assessed before and after fear conditioning. This protocol allowed monitoring of neuronal activity and potential functional plasticity after learning. Behavioural tests performed at least 6h after imaging sessions revealed that mice froze significantly more in response to conditioned aversive stimuli (CS+) compared to habituation. On the other hand, the neutral stimulus (CS-) produced equal or less freezing response after learning compared as before, supporting the idea that negatively paired cues acquire safety properties, as previously discussed. Fear conditioning is therefore associated with gain of cue discrimination performances.

Interestingly, in baseline sessions, ~ 40% of dPFC neurons displayed significant enhancement of their activity upon encounter of both CS- and CS+. Within this group the majority of neurons were nonspecific, whereas the remaining ones were cue-specific. At that stage, those cues emerged as classical auditory stimuli, since associative learning did not take place yet. These observations suggest that the dPFC receives auditory sensory information probably conveyed from the auditory thalamus or the auditory cortex. Further investigation is needed to identify the pathway carrying sensory input to the dorsal prefrontal regions.

During habituation, the activity patterns evoked by CS- or CS+ were similar, indicating that prefrontal neurons failed to dissociate distinct sensory inputs prior discriminative learning. This hypothesis was confirmed by a positive correlation between activity pattern similarity and discriminative performance. After learning, the activities evoked by the neutral and aversive stimulus respectively were not correlating anymore. In addition, neuronal pattern de-correlation was predicting gain of behavioural discriminative performances. Such de-correlation was essentially time-related, as neuronal specificity to cues remains unvaried after learning. Nonetheless, fear learning increased non-specifically the activity of neurons in response to both the aversive and safe stimuli. Together, these results indicate that dPFC neurons underwent functional rewiring resulting into temporally distinct neuronal assemblies upon discriminative learning. Learning give rise to specific cortical representations through temporal dissociation of activity patterns triggered by similar yet emotionally distinct cues.

Safe (CS-) and aversive (CS+) cues seem to be encoded within temporally specific neuronal assemblies within the dorsal prefrontal cortical networks. However, whether this region was required for discrimination of emotionally relevant cues remained unclear. To address this question an optogenetic strategy was adopted. During fear acquisition, dPFC was inhibited in behaving mice coincidentally with CS-US pairings. When the activity of dPFC was suppressed, animals displayed impaired ability to discriminate affective sensory signals. On the contrary, associative learning was not affected. Indeed, animals showed similar degrees of freezing upon presentation of the paired stimulus (CS+) compared to the control group. This indicated that optogenetically-induced deficiency of discrimination performance was not related to impairment of fear learning acquisition. These results highlight the relevance of dPFC in perceptual acuity. In this model fear acquisition depends on the activity of the amygdala, and this is confirmed by the fact that dPFC inhibition does not impact fear learning. However, suppression of dPFC activity impairs ability of animals to take advantage of sources of security offered in the environment. Disruption of this ability leads to hyperarousal and stimulus generalization. These results offer a new point of view that confers to the FrA a predominant role in discrimination performance. In addition, for the first time, the function of a cortical region has been clearly associated with the encoding of safety related signals. Some studies have demonstrated the presence of safety-specific neurons in the amygdala circuits, and their activity seems to be driven by vmPFC activity. However, the existence of a brain region able to enhance perceptual acuity and store cue discrimination memory was hypothesized but never proved. The results illustrated in this dissertation suggest a top-down control of the dPFC

over the activity of vmPFC and the amygdala to facilitate discernment of environmental stimuli.

The present study does not demonstrate a causal relationship between acquisition of discrimination performance and formation of distinct temporal assemblies. However, these two events seem to be strictly correlated. Additional investigation using models for anxiety and PTSD, could establish a direct link between these two events. PTSD is generally diagnosed through typical symptoms: re-experiencing, avoidance and hyperarousal. The former manifests itself through involuntary re-live of the traumatic event. Avoidance is characterized by escaping people, circumstances or environments that could remind the situation triggering the trauma. Finally, hyperarousal refers to amplified physiological responses such as hypervigilance and exaggerated startle response (Goswami et al., 2013). PTSD is characterized by frequent re-live of the fear response caused by the traumatic event. In addition, as aforementioned, PTSD results into overgeneralization to other stimuli and situations. To understand the neural basis of PTSD, classical fear conditioning provides a coherent tool to understand how animals learn to predict danger and, at the same time, benefit from sources of security encountered in the environment. Compelling evidence indicates that fear dysregulation exhibited in PTSD derives from inability to discern safe from threatening contexts (Grillon, 2002; Grillon, Morgan, Davis, & Southwick, 1998). These findings suggest that PTSD patients and models display unrealistic danger expectations, which converge into a state of anxiety that induces fear to generalize to safe stimuli. Notably, the dorsal prefrontal cortex of PTSD models should be investigated as the results presented in this dissertation support a predominant role in cue discrimination and inhibition of that cortical regions leads to PTSD-like symptoms. In this scenario, it could be hypothesized a dysfunction of dPFC activity or abnormal origin of temporally de-correlated cue specific assemblies, within this cortical area, in PTSDs.

8.2 *Pattern separation in dPFC improves perceptual discrimination*

Perceptual discrimination is an essential function that is required to have an appropriate overview of the surrounding environment. Facing the external world demands continuous comparison between present and past experience, to assess any similarities/differences compared to experienced situations. This strategy allows individuals to recall previously stored memories to deal with partially analogous circumstances or store new information about similar yet distinct events from previously encountered. This balance between maintaining similar episodes separate and recalling previously stored memories based on environmental signals relies on two counterposed processes, pattern completion and pattern separation. The former involves the retrieval of complete previously stored representations from incomplete inputs. Pattern separation entails the ensemble of mechanisms responsible of processing overlapping inputs into distinct memory representations.

Pattern completion and separation are computational processes that have been extensively studied over the years in different brain regions. Many studies have focused their attention on pattern separation computation particularly in the dentate gyrus (e.g. McHugh et al. 2007; Gilbert et al. 2001) or the olfactory bulb (e.g. Wilson 2009; Barnes et al. 2008). The dentate gyrus is a subregion of the hippocampus that is thought to pre-process activity patterns representing complex, multisensory information for storage and classification in other hippocampal areas, such as CA3. There are many reasons to consider pattern separation as a function of the dentate gyrus (Deng et al. 2010). First of all, the dentate gyrus (DG) owns an optimal anatomical structure to fulfil for pattern separation: it is, indeed, composed of five to ten times more neurons than its main input, the entorhinal cortex. This neuronal scheme support theoretical algorithms in machine learning where information is projected into higher-dimensions spaces to promote input separation and discrimination. Secondly, the dentate gyrus, similarly to other brain regions, is made up of sparse coding neurons that receive feedforward and feedback inhibition from local interneurons and *in vivo* recordings have demonstrated that those neurons are rarely activated during behaviour. This suggests that dentate gyrus neurons are finely tuned allowing even to similar inputs to be encoded by distinct neuronal subpopulations. Finally, DG granule cells are able to depolarize downstream CA3 pyramidal neurons, revealing their ability to drive memory encoding in the hippocampus, despite their sparse coding scheme (Deng et al. 2010).

Similarly to the dentate gyrus, the olfactory bulb (OB) is capable of undergoing pattern decorrelation mechanisms. Interestingly, one of the main recipients of the OB, the piriform cortex, shares some similarities with the CA3, the principal downstream region of the DG. Indeed, the piriform cortex has a similar architecture compared to the CA3, and analogous function. Like CA3, the piriform cortex acts as an associative memory system for the storage of information encoded by distributed activity patterns. Taken together, these observations suggest that pattern separation may carry out similar general functions in both the OB and DG. As a matter of fact, it is generally agreed that pattern decorrelation is engaged in reducing interference with overlapping information. The DG plays a role in increasing discrimination acuity between overlapping spatial or contextual information. Analogously, the olfactory system succeeds in discriminating numerous complex spatial and temporal patterns. In both structures pattern separation likely constitutes an adaptive strategy to optimally encode stimulus discrimination. In line with this hypothesis, recent evidence in zebrafish suggests that odour stimuli evoking highly correlated glomerular inputs initially induce correlated activity patterns across mitral cells in the olfactory bulb (Miklavc et al. 2012; Friedrich 2013). However, correlation between mitral cell activity patterns evoked by similar yet distinct cues decreases in time. Intriguingly, when fish fail to discriminate between different cues, neuronal activity patterns remain highly correlated in time. This data allows to hypothesize an association between discrimination performance and decorrelation of neuronal activity patterns. A recent study has provided clear evidence for an important role of pattern separation in discrimination learning in mice (Gschwend et al. 2015). Gschwend and colleagues firstly confirmed the ability of the olfactory bulb in rapidly reformatting overlapping odour representations through pattern separation. Successively, the authors demonstrated a causal relationship between pattern separation and perceptual discriminative performance in a behavioural task. Notably, it was shown that the extent of pattern decorrelation predicted the degree of discrimination accuracy. Finally, by taking advantage of optogenetic and pharmacogenetic strategies, they proposed a potential circuit-level mechanism that could modulate the decorrelation of overlapping mitral cell activity patterns, which ultimately helps the animals to disambiguate similar odorants and improve discrimination learning. Basing their experiments on previous theoretical work (Giridhar et al. 2011; Arevian et al. 2008) suggesting an engagement of lateral inhibition in pattern separation, they found that enhancement of inhibitory activity in the granule cell layer of OB, was facilitating odour-evoked output pattern separation and consequently improving discrimination accuracy.

Interestingly, computational models of pattern separation predicted that similar experiences would be encoded by non-overlapping populations of neurons, and thus DG and OB would separate signals anatomically. However, in vivo electrophysiology recordings in awake-behaving rodents suggest that the same population of neurons disambiguate subtle differences between similar inputs (Alme et al., 2010; Leutgeb et al., 2007). In agreement with what was observed in DG and OB, the work presented in this dissertation revealed a pattern separation-like computation within the dPFC. Indeed, the results of the current work indicate that learning reduced the similarity between activity patterns evoked by similar yet distinct stimuli, suggesting that learning may underlie origin of specific cortical representations by enhancing pattern separation. Decorrelation of activity patterns can be assessed by computing the Pearson product-moment correlation coefficient. A neuronal activity pattern at a precise time t, can be represented by a vector in which each element stand for the firing rate of one neuron measured at the time t. In this model, highly overlapping neuronal activity patterns are depicted by vectors that score high Pearson correlation coefficients, e.g., they project in comparable directions within the high-dimensional coding space. Pattern decorrelation results into reduced similarity between activity patterns so that the Pearson correlation coefficient of the corresponding activity vectors decreases and their angular separation is enhanced. Consequently, this process facilitates the selection of a procedure, a classifier, to discern between activity vectors. Notably, the work at issue demonstrates that pattern decorrelation is thus useful for pattern classification, a key operation in discriminative learning operated by the dPFC. Intriguingly, by plotting the Pearson correlation coefficient computed in sessions before *vs* after learning as a function of perceptual discrimination, it has been observed a linear negative relationship between the extent of CS+ *vs* CS- correlated activity and the behavioural performance. This suggests that the extent of pattern decorrelation, in the dPFC, might predict the discrimination accuracy between aversive and safe sensory stimuli.

Interestingly, the pattern separation that has been described in the dPFC, similarly to DG and OB, likely contributes to improve discrimination accuracy. However, these distinct brain regions show some dissimilarities. The dPFC displays a purely temporal pattern separation, whereas decorrelation of activity patterns in DG and OB seems to develop mainly spatially. Indeed, in the frontal association cortex, after learning, the same population of neurons reorganizes its activity in order to respond, with temporally distinct patterns, to safe *vs* aversive sensory cues. Conversely, even though some studies performed in rodent OB and DG indicate that the same population of neurons could disambiguate subtle differences between similar inputs, compelling evidence proved that pattern separation occurs through recruitment of new

neuronal assemblies in such brain regions. Remarkably, the continuous modification of OB and DG neuronal circuits through adult neurogenesis has been recently associated to pattern separation (Sahay et al. 2011a). Two alternative models have been proposed to elucidate the role of neurogenesis in pattern separation. The first model asserts a cell autonomous commitment of new-born neurons as encoding units. The new-integrated neurons become a preferred substrate to be recruited in the newly activated assemblies. The second model opts for a modulatory role of new-born neurons in pattern separation (Sahay et al. 2011a). A recent work demonstrated that neurogenesis is required for disambiguate between similar contextual representations (Sahay et al. 2011b). By using a contextual fear discrimination task, previously shown to rely upon pattern separation in DG, they observed that blocking neurogenesis impaired the ability of mice to discriminate between an aversive and safe stimulus-associated context. Conversely, when neurogenesis was enhanced in the DG, mice exhibited increased ability in the discriminative task. Therefore, it may be assumed that in auditory fear conditioning the dPFC could play a role commensurate with the DG in contextual fear learning. However, whether DG can take advantage of neurogenesis processes in adult organisms, the dPFC exploits different strategies to overcome a lack of adult neurogenesis. Likely for that reason, frontal regions improve perceptual discrimination by increasing the temporal separation between activity patterns encoding for fear and safe sensory cues, respectively. This hypothesis leaves some unresolved questions. For example, if adult neurogenesis is so effective in sensory and context discrimination by promoting spatial pattern separation, why it is not widespread in the brain? It can be hypothesized that the DG and OB can afford such a strategy because the neural circuits composing these regions are mostly encoding rather than storing information, whereas memory storage mainly occurs in downstream pathways, such as CA3 and piriform cortex, respectively. Conversely, the dPFC is probably storing associative memory traces within its cortical layers and potential integration of new neurons could erode memory traces. This is presumably the main reason why frontal regions preclude neurogenesis process inclusion within their circuits. However, it can also be possible that adult neurogenesis in OB and DG represents an evolutionary holdover, not present in other brain regions.

The work at issue mainly focuses on layer 2/3 pyramidal neurons in the dorsal prefrontal cortex. However, it is widely accepted that inhibitory neurons are engaged in cortical computation and behaviour. In detail, cortical interneurons can be implicated in two distinct task during discriminative learning within the frontal regions. Firstly, formation of neuronal assemblies can depend upon the involvement of interneurons, that recruit neurons through numerous processes (Holtmaat and Caroni 2016). Secondly, they seem to be involved in pattern

separation to improve discrimination performances, through a process known as lateral inhibition (Arevian et al. 2008; Arruda et al. 2013; Gschwend et al. 2015). Lateral inhibition is the capacity of an excited neuron to reduce the activity of its neighbours. It results into a dampening of action potential spreading from excited neurons to connected ones in the lateral direction. Compelling evidences indicate that inhibitory neurons alone are able to shape the local activity in order to improve stimulus discrimination (Arruda et al. 2013; Gschwend et al. 2015).

Cortical interneurons can be grossly classified into three non-overlapping groups based on their expression of the molecular markers parvalbumin (PV), somatostatin (SOM), or serotonin receptor (5HT-R) (Rudy, Fishell, Lee, & Hjerling-Leffler, 2011). These groups of GABAergic interneurons account for 30-40% each, although the distribution varies across different cortical laminae. 5HT-R-expressing interneurons are mostly concentrated in superficial layers, whereas PV- and SOM-expressing neurons are predominant in deep laminae. For instance, layer 1 expresses mainly 5HT-R neurons, whereas deep layers are composed almost of 50% PV and 50% SOM.

5HT-R can be further subdivided into VIP- and non-VIP-expressing neurons. Recent data revealed that an important disinhibitory microcircuit is represented by vasoactive intestinal polypeptide (VIP)-expressing neurons, which inhibit SOM- and PV-expressing interneurons that, in turn, target their inhibitory activity to excitatory cell dendrites or perisomatic regions (David, Schleicher, Zuschratter, & Staiger, 2007). In contrast, PV activity enhancement induces widespread inhibition along cortical circuits. Inhibitory and disinhibitory microcircuits likely have important roles in learning-related neuronal assembly formation and remodeling (e.g. pattern separation). Therefore, these findings lead to the hypothesis that inhibitory interneurons, within the dorsal prefrontal cortex, could play a key role in shaping the neuronal activity and promote pattern separation underlying the enhancement of perceptual acuity during discriminative learning.

8.3 *A circuit-level mechanism underlying perceptual discrimination*

One of the greatest challenges in neuroscience is the understanding of how brain drives behaviour. To achieve this, researchers need to be able to link different levels of brain function. In the last few decades neuroscientists have made great progress in using functional imaging techniques to identify which brain areas are active in the brain during behaviour. But these techniques lack the temporal and spatial resolution to provide an understanding on the level of the underlying machinery of the brain: the level neural circuits, the level of single neurons, the level of synapses and the level of underlying molecules.

To understand the neural code, scientists need to be able to measure activity in neural circuits and to be able to clarify how that activity drives behaviour. To do so, they need to implement two basic ingredients: the timing of activity and the spatial dimension in the neural circuits. In other words, they need to unravel which neurons are active at specific times. In summary, to understand the neural code researchers need to measure activity in neural circuits and understand the precise sequence of activity as it spreads through neural circuits during behaviour. Unfortunately, the link between neural activity and behaviour is being incredibly complicated by the complexity that characterizes brains circuits. Indeed, neurocircuits are constituted of many different cell types and, at present, their interconnectivity is largely ignored. In addition, during behaviour, neuronal activation involves the implication of thousands to millions of cells. Consequently, making the link between neuronal computation and behavioural output turns out to be extremely challenging. A way to cut through this complexity and to set out to understand the neural code, is the investigation of the physical hub where computation is implemented. Most computational models of cortical function treat the pyramidal neurons as simple compartment units. However, models that do not take into account the shape and orientation of pyramidal neurons coupled with the laminar architecture of the cortex turn out to be incomplete (M. Larkum, 2013). As a matter of fact, there is increasing evidence that cellular intrinsic properties and the architecture of the cortex are tightly correlated, suggesting the existence of a characteristic *modus operandi* of the cortex. A key finding supporting this view is represented by the pyramidal neuron dendritic arbour, which seems to be the main site where computation is implemented in the cortex. Indeed, inputs in the cortex follow a basic rule that sensory information (feed-forward stream) reaches the middle cortical laminae, whereas information from other cortical areas (feedback stream)

terminate in the output layers (supra- or infra-granular layers) (Larkum, 2013). In this scenario, the cortex acts by integrating feedforward and feedback information, and this computation seems to occur predominantly at the dendritic level. The computational power of pyramidal cell dendrites has been hotly debated. Emerging evidence suggests that dendrites, do not simply collect and transmit information to the cell body, but they function as non-linear, decision-making computational units (Schiller et al. 2000; Major et al. 2013). A key finding matching with this view was the discovery of supra-linear events in the dendritic machinery, defined as dendritic spikes (Schiller et al. 2000; Major et al. 2008; Schiller et al. 1997). Although dendritic spikes differ to some extent from classical sodium action potentials (APs) recorded at the soma, they share some similarities with them. Indeed, dendritic spikes are thresholded (all-or-none) events, displaying a refractory period and are able to propagate actively for some distance (Schiller et al. 1997). There is now general agreement regarding the NMDA receptor (NMDAR) as the predominant depolarization-activated conductance in thin dendrites of neocortical excitatory neurons (Larkum et al. 2009; Schiller et al. 2000; Major et al. 2008). The function of NMDA dendritic spikes (also known as dendritic plateaus) can be various depending on the cortical region. For instance, they could play a role in maintaining network upstates and persistent firing associated with working memory. They could also potentially refine receptive fields in primary cortices and be engaged in top-down/bottom-up interactions. An interesting feature associated with dendritic spikes (Ca^{2+}-sustained) concerns its influence with axonal action potentials (Na^{+}-sustained) (Larkum et al. 1999; Larkum 2013). Sodium-dependent action potentials can propagate back from the soma to the dendrites where coincident distal dendritic input, within a time window of several milliseconds, could facilitate the initiation of calcium action potentials (Larkum et al. 1999). Dendritic spikes, in turn, enhance axonal response by inducing a burst of axonal APs. This electrophysiological phenomenon, named "back-propagating action potential activated Ca^{2+} spike" (BAC) firing, might represent a mechanism by which cortical pyramidal neurons can associate inputs reaching different cortical layers, such as feed-forward information, reaching the middle cortical laminae, and feedback information terminating in the output layers. In this scenario, the feed-forward input around the soma compartment can be significantly potentiated by sub-threshold input to the distal compartment. This entails that, when the pyramidal neuron is activated by feed-forward input, it becomes much more susceptible to feedback input. The relevance of this mechanism lies in the fact that pyramidal neurons, in the neocortex, represent a computational unit that, through a sophisticated dendritic machinery, is able to detect and associate coincident input to proximal and distal dendritic regions, potentially combining feed-

forward (external representation) with feed-back (internal representations) information (Larkum 2013). This hypothesis may conceivably explain the reason why the cortex owns a laminar organization with inputs reaching different layers, and the mechanism by which the cortical neurons can integrate sparse inputs instantaneously.

In vivo evidence of the BAC firing mechanisms comes from a study that demonstrated how feedback and feedforward information is integrated in somatosensory cortical neurons to produce Hebbian-like forms of plasticity (Gambino et al., 2014). In the rodent somatosensory cortex (or barrel cortex), sensory information flows in parallel pathways from whiskers to cortex. Sensory fibres from the whisker follicles reach the contralateral thalamus, through the trigeminal nerve, that in turn project to the barrel cortex. The lemniscal pathway runs, via the principal nucleus and the dorsomedial section of the ventrolateral medial nucleus (VPMdm) to barrels in layer 4 of the somatosensory cortex. By contrast, the paralemniscal pathway reaches L2/3 cells directly or indirectly through thalamic posterior nucleus (POm) efferents that target pyramidal cell dendrites in L5A and L1. The authors demonstrated that coincident activation of these two pathways induced synaptic LTP in layer 2/3 pyramidal cells and this event was mediated by NMDA dendritic spikes/plateaus. *In vivo*, dendritic plateau-mediated LTP could be engaged in strengthening connections between neurons that spike scatteredly and infrequently, preparing the circuit for the potential arrival of a sensory input.

In summary, the structure and the precise function of the cortex are still debated. Increasing evidence suggest that the cerebral cortex possesses a unique ability of associating perceived experience with an internal representation of the world. This capability conceivably derives from computational units represented by pyramidal neurons, which own a sophisticated dendritic apparatus able to integrate external and internal information. This cellular mechanism, involving dendritic processing, can match the internal representation/prediction with ongoing external reality. This process envisages plasticity phenomena in order to adapt internal predictions to environmental changes. However, whether this associative mechanism is relevant for learning and behaviours has never been clearly demonstrated. To set out to achieve this aim the study presented in this dissertation investigated the cellular/synaptic mechanisms by which the dorsal prefrontal cortex improves stimulus discrimination performances during a pavlovian conditioning task. The results obtained provide evidence that long-range projections from the basolateral amygdala, combined with cue-evoked non-linearities, are able to potentiate layer 2/3 pyramidal neurons within the dorsal prefrontal cortex during associative learning. These observations imply a few considerations. Firstly, the dorsal prefrontal cortex, analogously to sensory cortical regions (Gambino et al. 2014), functions to

facilitate, perhaps hebbian, forms of synaptic plasticity, through BAC firing-like mechanisms, *in vivo*. Indeed, the dPFC receives auditory sensory information able to promote NMDA-dependent long lasting depolarizations, which bear similarities to dendritic spikes/plateaus (Schiller et al. 2000, 1997; Major et al. 2008). Those NMDA-dependent dendritic spikes serve as a first depolarization that, associated with BLA long-range excitatory inputs, provoke long-lasting potentiation in L2/3 pyramidal neurons. Secondly, this BAC firing-like mechanism is engaged in cortical areas, such as the dPFC, that are not receiving direct sensory feed-forward information (agranular cortex). This suggests that the brain is composed of check-point regions that receive and integrate pre-processed information from several sub-cortical and cortical regions to sharpen the behavioural output during sensory-motor/cognitive tasks. As a matter of fact, the dPFC is receiving pre-processed sensory information, most probably from the thalamus or the auditory cortex, that converges into the dendritic tuft of prefrontal pyramidal neurons, by inducing NMDA spikes. During associative learning, these inputs coincidently merge with associative information from the amygdala. Prefrontal neurons receive and meta-associate those inputs to improve stimulus discrimination skills during the behavioural performance.

Finally, as already touched briefly, the present work demonstrate for the first time the relevance of the BAC firing mechanism proposed by Larkum, for learning and behaviour. These data suggest that coincident activity of BLA long-range inputs and pre-processed sensory information converging to the superficial layers of the dPFC, induce Hebbian-like forms of synaptic plasticity that can underlie a functional reorganization of the network. This experience-dependent functional plasticity sharpen perceptual performance via formation of temporally separated neuronal assemblies (**Fig. 8.12**).

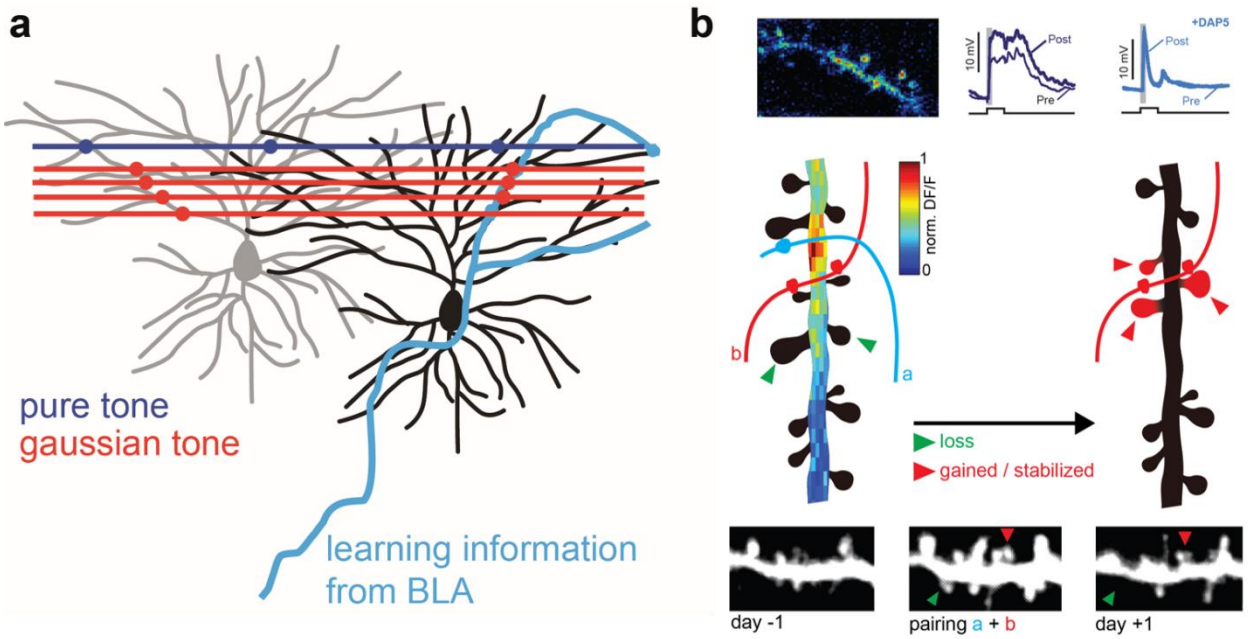

Figure 8.12. (a) Proposed model for meta-association during learning. Specific layer 2/3 dPFC pyramidal neurons (black) are recruited within cue-specific assemblies by integrating associative information from BLA projections with non-linearities evoked by specific auditory stimulation (e.g. gaussian tone). (b) Schematic of NMDA dendritic spikes evoked by long-range projections. Coincident activation of at least two pathways upon a single dendritic arbour promotes Hebbian-like plasticity (adapted from Gambino et al. 2014).

8.4 dPFC: conscious perception of unconscious fear responses

Neuroscientists and psychologists are using the term “fear” to describe two distinct phenomena, with different underlying brain systems. These different brain states, elicited by fear-asouring stimuli, refers to conscious feelings and behavioural and physiological response to a threat, respectively. Joseph LeDoux proposed to restrict the meaning of the work “fear” to conscious feelings, whereas the nonconscious mechanism that produce a behavioural and physiological response to a threat shoud not be described in terms of “fear”.

Among fear conditioning researchers, the question of what exactly a fear system does has turned out to be tricky. In fact, differents views were developed in time. In its manuscript “the expression of the emotions in Man and Animals” in 1872, Charles Darwin gave the most obvious answer to this issue: he proposed that the occurrence of a threat activates a fear system in the brain and the result is simply the feeling of fear. At a later time, this affective state is triggering the expression of a behavioural defensive outcome. This view of the fear system was defined as the “commonsense view of fear” and, although it is nowadays put aside, it thrived in the past years.

Many fear conditioning researchers, defined fear as a state that takes place between the occurrence of a threat and the generation of a defensive response. However, this definition differs substantially, from the commonsense view, as these researchers avoided any kind of reference to conscious state and feelings (Bolles & Fanselow, 1980; Masterson & Crawfor, 1982; Miller, 1948; Rescorla & Solomon, 1967). They typically claimed that fear was a central state, specifically a “defensive motivational state” (central state view). Proponents of this view, considered fear as a physiological state that controls fear responses.

LeDoux, proposed a different approach from the aforementioned ones. Due to the fact that he was considering misleading both the commonsense view, as it based too much on conscious fear, and the central state view, as it ignored conscious fear, he gave a new interpretation of fear processing. He highlighted the existence of both conscious and nonconscious pathways, playing independent roles (Ledoux 2014; Ledoux 2012). He proposed that emotional signals are transmitted to the central nervous system through sensory pathways that are acting nonconsciously. Threat stimuli, for example, are processed in the amygdala that is eliciting fear response. This flow is automatic and is not requiring either conscious perception of the stimulus, or conscious modulation of the behavioural output. This theory is confirmed by

clinical studies performed on healthy humans or patients with different brain lesions (Bechara et al., 1995; Labar et al. 1995; Olsson & Phelps, 2004). It was observed that a threat stimulus produces a conditioned response even without the person perceiving consciounsly the stimulus and without feeling fear. Research on patients with brain damage revealed that fear conditioning promotes the formation of implicit (nonconscious) memories, without affecting explicit/declarative (conscious) memories. For instance, damage to the hippocampus in humans perturbs the conscious recall of having been conditioned but has no effect on fear conditioning itself, whereas disruption of the amygdala abolishes fear conditioning but does not affect the conscious memory of having been conditioned.

This thesis promoted by Joseph Ledoux agrees also with our daily life experience of accidentally respond to a stimulus and just subsequently realizing that a threat occurred.

The unconscious processing of threat signals is probably a strategy preserved even among higher species as it give raise to prompt defensive responses. Indeed, the neural processes that enable organisms to consciounsly realize about the presence of a danger are considerably slower compared to the unconscious process that are responsible of generating defensive responses.

In the model proposed by Ledoux, following the encounter of an aversive event, sensory processing follows two distinct flows of information, one that detects the emotional significance of stimuli and drives the expression of appropriate behavioural responses and physiological accompaniments, and a second one that triggers cognitive processes and results in the formation of conscious feelings. What is defined as the conscious feeling of fear, is due to the representation in consciousness, through cognitive functions (e.g. attention), of unconscious dynamics that are consequences of the activation of the amygdala defensive circuit. The view of the amygdala as a central neural embodiment of defensive responses persists. However, its activity is split into two distinct functions, it has a direct role in perceiving threats nonconsciously and producing an appropriate behavioural outcome, but it also conveys information to cognitive systems to induce the emergence of conscious feelings of fear. As a result, the experience of feelings, is probably able to influence decision-making and produce conscious modulation of underway behavioural responses.

To sum up, the evolutionary function of an organism to detect and respond to threatening events, is not to generate feelings and emotions, but to ensure survival. The capacity to consciously perceive emotional states depends on the activity of neocortical cognitive areas, and allows organisms to adapts underway behavioural responses to environmental dynamics and past experience.

In agreement, the work at issue identified a cortical regions that could intervene to consciounsly modulate a behavioural fear response in progress. Indeed, the dorsal prefrontal cortex activates later than the amygdala, and it is responsible of modulating the behavioural output triggered by the amygdala defensive system. dPFC is defined as an association cortex, or rather a region responsible of complex processes that combines information from sensory areas to generate planification, modulation, memory and cognitive processes.

Consistently, when an organism encounters a threat, the amygdala promptly produces a behavioural response combined with physiological accompaniments. Indeed, the basolateral complex of the amygdala, receives sensory information and controls, through the central nucleus, the behavioural output, as well as activation of the sympathetic system (shortness of breath, increase of blood pressure and heart beat, release of hormones). In parallel, as shown in the current work, the BLA conveys information to the frontal association cortex. This region integrates inputs from BLA and sensory areas (most likely thalamus or sensory cortices) and provide an accurate representation of the environment. Notably, FrA seems to facilitate perceptual acuity by dissociating threatening and safe/neutral aspects of the surrounding environment.

If it is essential for an animal to adequately react to a danger, it is equally important to recognise and benefit from sources of security offered in the environment. Coherently, although fear response can be merely triggered by subcortical activity, perceptual discrimination requires the participation of cortical structures. In this regard, the dPFC intervenes during behavioural execution and, after having integrated information about the surroundings, activates a top-down control over subcortical areas to adapt the behavioural action to the circumstances. Confirmation of this theory comes from many evidences illustrated in this dissertation. Firstly, the BLA and dPFC are reciprocally connected through massive excitatory projections. The BLA conveys input to the frontal cortex during fear encoding and receives, in turn, a feedback control (Karalis et al., 2016a). Secondly, the dPFC receives simultaneously sensory and BLA-mediated information that produces functional plasticity, resulting into cue discrimination. Thirdly, the cortex activates after amygdala, when the fear response has already started. This observation suggests that the dPFC has predominantly a modulatory rather than triggering role. Finally, inactivation of dPFC impairs the ability of perceiving safety information from the environments and arrange the behavioural output accordingly.

In conclusion, even though the mechanisms by which the dPFC controls the fear output remain poorly understood, many evidences lead to hypothesize a prominent role of this cortical region in conscious perception and control of fear responses.

9. Bibliography

Alme, C. B., Buzzetti, R. A., Marrone, D. F., Leutgeb, J. K., Chawla, M. K., Schaner, M. J., Barnes, C. A. (2010). Hippocampal granule cells opt for early retirement. *Hippocampus*, *20*(10), 1109–1123.

Anagnostaras, S. G., Wood, S. C., Shuman, T., Cai, D. J., LeDuc, A. D., Zurn, K. R., … Herrera, G. M. (2010). Automated assessment of Pavlovian conditioned freezing and shock reactivity in mice using the VideoFreeze system. *Frontiers in Behavioral Neuroscience*, *4*, 158.

Arellano, J. I., Espinosa, A., Fairén, A., Yuste, R., & Defelipe, J. (2007). Non-synaptic dendritic spines in the neocortex. *Neuroscience*, *145*, 464–469.

Arevian, A. C., Kapoor, V., & Urban, N. N. (2008). Activity-dependent gating of lateral inhibition in the mouse olfactory bulb. *Nat Neurosci*, *11*(1), 80–87.

Arruda, D., Publio, R., & Roque, A. C. (2013). The Periglomerular Cell of the Olfactory Bulb and its Role in Controlling Mitral Cell Spiking: A Computational Model. *PLoS ONE*, *8*(2).

Barnes, D. C., Hofacer, R. D., Zaman, A. R., Rennaker, R. L., & Wilson, D. A. (2008). Olfactory perceptual stability and discrimination. *Nature Neuroscience*, *11*, 1378–1380.

Barrett, D., Shumake, J., Jones, D., & Gonzalez-Lima, F. (2003). Metabolic mapping of mouse brain activity after extinction of a conditioned emotional response. *The Journal of Neuroscience : The Official Journal of the Society for Neuroscience*, *23*(13), 5740–9.

Barth, A. L., & Poulet, J. F. A. (2012). Experimental evidence for sparse firing in the neocortex. *Trends in Neurosciences*, *35*, 345–355.

Basu, J., Zaremba, J. D., Cheung, S. K., Hitti, F. L., Zemelman, B. V, Losonczy, A., & Siegelbaum, S. A. (2016). Gating of hippocampal activity, plasticity, and memory by entorhinal cortex long-range inhibition. *Science*, *351*(6269), aaa5694-aaa5694.

Bauer, E. P., Schafe, G. E., Ledoux, J. E., & Keck, W. M. (n.d.). NMDA Receptors and L-Type Voltage-Gated Calcium Channels Contribute to Long-Term Potentiation and Different Components of Fear Memory Formation in the Lateral Amygdala.

Bechara, A., Tranel, D., Damasio, H., Adolphs, R., Rockland, C., & Damasio, R. A. (1995). Double dissociation of conditioning and declarative knowledge relative to the amygdala and hippocampus in humans. *J. Wildl. Manage. Can. J. Zool. J. Anim. Ecol. Oecologia Ecology*, *90143963194*(0), 1115–395.

Becker, K., Mauch, C. P., Hojer, C. D., Egen, J. G., Hellal, F., Bradke, F., … Ert, A. (2012). Three-dimensional imaging of solvent-cleared organs using 3DISCO. *Nature Protocols*, *7*(11).

Behbehani, M. M. (1995). Functional characteristics of the midbrain periacqueductal grey. *Progress in Neurobiology*, *46*, 575–605.

Boatman, J. A., & Kim, J. J. (n.d.). A thalamo-cortico-amygdala pathway mediates auditory fear conditioning in the intact brain.

Bolles, R. C., & Fanselow, M. S. (1980). A perceptual-defensive-recuperative model of fear and pain. *The Behavioral and Brain Sciences*, *3*, 291–323.

Bordi, F., & LeDoux, J. E. (1994). Response properties of single units in areas of rat auditory thalamus that project to the amygdala I1. Cells receiving convergent auditory and somatosensory inputs and cells antidromically activated by amygdala stimulation. *Exp Brain Res*, *98*, 275–286.

Borszcz, G. S. (n.d.). Contribution of the Ventromedial Hypothalamus to Generation of the Affective Dimension of Pain.

Bouton, M. E. (2004). Context and Behavioral Processes in Extinction. *Learning & Memory*, *11*(5), 485–494.

Brandalise, F., Carta, S., Helmchen, F., Lisman, J., & Gerber, U. (2016). Dendritic NMDA spikes are necessary for timing-dependent associative LTP in CA3 pyramidal cells. *Nature Communications*, *7*, 13480.

Brecht, M., Roth, A., & Sakmann, B. (2003). Dynamic Receptive Fields of Reconstructed Pyramidal Cells in Layers 3 and 2 of Rat Somatosensory Barrel Cortex. *The Journal of Physiology*, *553*(1), 243–265.

Briggman, K. L., & Kristan, W. B. (2008). Multifunctional pattern-generating circuits. *Annual Review of Neuroscience*, *31*, 271–94.

Bruce, D. (2001). Fifty Years Since Lashley's In Search of the Engram: Refutations and Conjectures. *Journal of the History of the Neurosciences*, *10*(3), 308–318.

Burgos-Robles, A., Vidal-Gonzalez, I., Santini, E., & Quirk, G. J. (2007). Consolidation of Fear Extinction Requires NMDA Receptor-Dependent Bursting in the Ventromedial Prefrontal Cortex.

Buzsaki, G., & Draguhn, A. (2004). Neuronal Oscillations in Cortical Networks. *Science*, *304*(5679), 1926–1929.

Cheng, S., & Frank, L. M. (2008). New experiences enhance coordinated neural activity in the hippocampus. *Neuron*, *57*(2), 303–13.

Chow, B. Y., Han, X., Dobry, A. S., Qian, X., Chuong, A. S., Li, M., … Boyden, E. S. (2010). High-performance genetically targetable optical neural silencing by light-driven proton pumps. *Nature*, *463*(7277), 98–102.

Christianson, J. P., Fernando, A. B. P., Kazama, A. M., Jovanovic, T., Ostroff, L. E., & Sangha, S. (2012). Inhibition of Fear by Learned Safety Signals. *Journal of Neuroscience*, *32*(41), 14118–14124.

Cichon, J., & Gan, W.-B. (2015). Branch-specific dendritic Ca 21 spikes cause persistent synaptic plasticity. *Nature*, *520*, 180–185.

Corcoran, K. A., & Quirk, G. J. (2007). Activity in Prelimbic Cortex Is Necessary for the Expression of Learned, But Not Innate, Fears. *Journal of Neuroscience*.

Courtin, Chaudun, Rozeske, Karalis, Gonzalez-Campo, Wurtz, Abdi, Baufreton, Bienvenu, Herry. (2014). Prefrontal parvalbumin interneurons shape neuronal activity to drive fear expression. *Nature*, *505*, 92–96.

David, C., Schleicher, A., Zuschratter, W., & Staiger, J. F. (2007). The innervation of parvalbumin-containing interneurons by VIP-immunopositive interneurons in the primary somatosensory cortex of the adult rat. *European Journal of Neuroscience*, *25*(8), 2329–2340.

Davis, M., Rainnie, D., & Cassell, M. (1994). Neurotransmission in the rat amygdala related to fear and anxiety. *Trends in Neurosciences*, *17*(5), 208–214.

De Paola, V., Holtmaat, A., Knott, G., Song, S., Wilbrecht, L., Caroni, P., & Svoboda, K. (2006). Cell Type-Specific Structural Plasticity of Axonal Branches and Boutons in the Adult Neocortex. *Neuron*, *49*, 861–875.

Deacon T., Eichenbaum H., Rosenberg, P. (1983). Afferent Connections of the Perirhinal Cortex in the Rat. *Journal of Comparative Neurology*, *220*, 168–190.

Dejean, C., Courtin, J., Karalis, N., Chaudun, F., Wurtz, H., Bienvenu, T. C. M., & Herry, C. (2016). Prefrontal neuronal assemblies temporally control fear behaviour. *Nature*, *535*(7612), 420–4.

Delamater, A. R. (2012). On the nature of CS and US representations in Pavlovian learning. *Learning & Behavior*, *40*(1), 1–23.

Deng, W., Aimone, J. B., & Gage, F. H. (2010). New neurons and new memories: how does adult hippocampal neurogenesis affect learning and memory? *Nature Reviews. Neuroscience*, *11*(5), 339–50.

Eldon l. Foltz, lowell E. W. (1962). Pain "relief" by frontal cingulumotomy. *Journal of Neurosurgery*, *251*, 1355–1358.

Euston, D. R., Gruber, A. J., & McNaughton, B. L. (2012). The Role of Medial Prefrontal Cortex in Memory and Decision Making. *Neuron*, *76*(6), 1057–1070.

Fanselow, M. S., & Bolles, R. C. (1979). Naloxone and Shock-Elicited Freezing in the Rat. *Journal of Comparative and Physiological Psychology*, *93*(4), 736–744.

Fanselow, M. S. F., & Bolles, R. C. (1979). Triggering of the endorphin analgesic reaction by a cue previously associated with shock: Reversal by naloxone. *Bulletin of the Psychonomic Society*, *14*(2), 88–90.

Fanselow, M. S., & Wassum, K. M. (2015). The Origins and Organization of Vertebrate Pavlovian Conditioning. *Cold Spring Harbor Perspectives in Biology*, *8*(1), a021717.

Felix-Ortiz, A. C., Beyeler, A., Seo, C., Leppla, C. A., Wildes, C. P., & Tye, K. M. (2013). BLA to vHPC Inputs Modulate Anxiety-Related Behaviors. *Neuron*, *79*, 658–664.

Friedrich, R. W. (2013). Neuronal Computations in the Olfactory System of Zebrafish. *Annu. Rev. Neurosci*, *36*, 383–402.

Gambino, F., & Holtmaat, A. (2012). Spike-Timing-Dependent Potentiation of Sensory Surround in the Somatosensory Cortex Is Facilitated by Deprivation-Mediated Disinhibition. *Neuron*, *75*, 490–502.

Gambino, F., Pagès, S., Kehayas, V., Baptista, D., Tatti, R., Carleton, A., & Holtmaat, A. (2014). Sensory-evoked LTP driven by dendritic plateau potentials in vivo.

Garner, A. R., Rowland, D. C., Hwang, S. Y., Baumgaertel, K., Roth, B. L., Kentros, C., & Mayford, M. (2012). Generation of a Synthetic Memory Trace. *Science*, *335*, 1513–1516.

Gavan P. McNally, Joshua P. Johansen, H. T. B. (2011). Placing prediction into the fear circuit. *Cell Review*, *34*, 283–292.

Gdalyahu, A., Tring, E., Polack, P.-O., Gruver, R., Golshani, P., Fanselow, M. S., … Trachtenberg, J. T. (2012). Associative Fear Learning Enhances Sparse Network Coding in Primary Sensory Cortex. *Neuron*, *75*, 121–132.

Genud-Gabai, R., Klavir, O., & Paz, R. (2013). Safety Signals in the Primate Amygdala. *Journal of Neuroscience*, *33*(46), 17986–17994.

Gilbert, P. E., Kesner, R. P., & Lee, I. (2001). Dissociating hippocampal subregions: A double dissociation between dentate gyrus and CA1. *Hippocampus*, *11*(6), 626–636.

Giridhar, S., Doiron, B., & Urban, N. N. (2011). Timescale-dependent shaping of correlation by olfactory bulb lateral inhibition. *Proceedings of the National Academy of Sciences of the United States of America*, *108*(14), 5843–5848.

Goswami, S., Rodríguez-Sierra, O., Cascardi, M., Paré, D., Sandi, C., Wotjak, C. T., … Quirk, G. (2013). Animal models of post-traumatic stress disorder: face validity. *Frontiers in Neuroscience*, *7*.

Grillon, C. (2002). Startle Reactivity and Anxiety Disorders: Aversive Conditioning, Context, and Neurobiology. *Biological Psychiatry*, *52*, 958–975.

Grillon, C., Morgan, C. A., Davis, M., & Southwick, S. M. (1998). Effects of Experimental Context and Explicit Threat Cues on Acoustic Startle in Vietnam Veterans with Posttraumatic Stress Disorder. *Biol Psychiatry*, *44*, 1027–1036.

Gschwend, O., Abraham, N. M., Lagier, S., Begnaud, F., Rodriguez, I., & Carleton, A. (2015). Neuronal pattern separation in the olfactory bulb improves odor discrimination learning. *Nature Neuroscience*, *18*, 1474–1482.

Hall, G. (2002). Associative Structures in Pavlovian and Instrumental Conditioning. In *Stevens' Handbook of Experimental Psychology*. Hoboken, NJ, USA: John Wiley & Sons, Inc.

Han, J., Kushner, S. a, Yiu, A. P., Cole, C. J., Matynia, A., Brown, R. a, … Josselyn, S. a. (2007). Neuronal Competition and Selection During Memory Formation. *Science*, *316*(April), 457–460.

Harvey, C. D., Coen, P., & Tank, D. W. (2012). Choice-specific sequences in parietal cortex during a virtual-navigation decision task. *Nature*, *484*(7392), 62–68.

Herry, C., & Johansen, J. P. (2014). Encoding of fear learning and memory in distributed neuronal circuits. *Nat Neurosci*, *17*, 1644–1654.

Hnasko, T. S., Perez, F. A., Scouras, A. D., Stoll, E. A., Gale, S. D., Luquet, S., … Palmiter, R. D. (2006). Cre recombinase-mediated restoration of nigrostriatal dopamine in dopamine-deficient mice reverses hypophagia and bradykinesia. *Proceedings of the National Academy of Sciences of the United States of America*, *103*(23), 8858–63.

Hofer, S. B., Mrsic-Flogel, T. D., Bonhoeffer, T., & Hubener, M. (2009). Experience leaves a lasting structural trace in cortical circuits. *Nature*, *457*, 313–317.

Holtmaat, A., & Caroni, P. (2016). Functional and structural underpinnings of neuronal assembly formation in learning. *Nature Neuroscience*, *19*(12), 1553–1562.

Holtmaat, A. J. G. D., Trachtenberg, J. T., Wilbrecht, L., Shepherd, G. M., Zhang, X., Knott, G. W., & Svoboda, K. (2005). Transient and persistent dendritic spines in the neocortex in vivo. *Neuron*, *45*(2), 279–291.

Holtmaat, A., & Svoboda, K. (2009). Experience-dependent structural synaptic plasticity in the mammalian brain. *Nature Reviews. Neuroscience*, *10*(9), 647–658.

Holtmaat, A., Wilbrecht, L., Knott, G. W., Welker, E., & Svoboda, K. (2006). Experience-dependent and cell-type-specific spine growth in the neocortex. *Nature*, *441*, 979–983.

Holtmaat, A., & Caroni, P. (2016). Functional and structural underpinnings of neuronal assembly formation in learning. *Nature Neuroscience*, *19*(12).

Howse, D. J., Squires, A. S., Martin, G. M., & Skinner, D. M. (2003). Perirhinal Cortex Lesions Impair Context Aversion Learning. *Learning & Memory*, *10*, 161–167.

Huang, Y.-Y., & Kandel, E. R. (1998). Postsynaptic Induction and PKA-Dependent Expression of LTP in the Lateral Amygdala. *Neuron*, *21*, 169–178.

Huber, D., Gutnisky, D. A., Peron, S., O 'connor, D. H., Wiegert, J. S., Tian, L., … Svoboda, K. (2012). Multiple dynamic representations in the motor cortex during sensorimotor learning. *Nature*, *484*, 473–478.

Isaacson, J. S., & Scanziani, M. (2011). How Inhibition Shapes Cortical Activity. *Neuron*, *72*, 231–243.

Jin-Hee, H., Kushner, S. A., P. Yiu, A., Hsiang, H.-L. (Liz), Buch, T., Waisman, A., … Josselyn, S. A. (2009). Selective Erasure of a Fear Memory. *Science*, *323*(March), 1492–1496.

Johansen, J. P., Diaz-Mataix, L., Hamanaka, H., Ozawa, T., Ycu, E., Koivumaa, J., … LeDoux, J. E. (2014). Hebbian and neuromodulatory mechanisms interact to trigger associative memory formation. *Proceedings of the National Academy of Sciences*, *111*(51), E5584–E5592.

Johansen, J. P., Hamanaka, H., Monfils, M. H., Behnia, R., Deisseroth, K., Blair, H. T., … Bruce McEwen, (2010). Optical activation of lateral amygdala pyramidal cells instructs associative fear learning. *PNAS*, *107*, 12692–12697.

Johansen, J. P., Tarpley, J. W., Ledoux, J. E., & Blair, H. T. (2011). Neural substrates for expectation-modulated fear learning in the amygdala and periaqueductal gray, *Nature Neuroscience 13*(8), 979–986.

Kandel, E. R., Dudai, Y., & Mayford, M. R. (2014). The Molecular and Systems Biology of Memory. *Cell*, *157*, 163–186.

Karalis, N., Dejean, C., Chaudun, F., Khoder, S., Rozeske, R. R., Wurtz, H., … Herry, C. (2016a). 4-Hz oscillations synchronize prefrontal-amygdala circuits during fear behavior. *Nature Neuroscience*.

Keck, T., Mrsic-Flogel, T. D., Afonso, M. V., Eysel, U. T., Bonhoeffer, T., & Hübener, M. (2008). Massive restructuring of neuronal circuits during functional reorganization of adult visual cortex. *Nature Neuroscience*, *11*, 1162–1167.

Kim, E. J., Horovitz, O., Pellman, B. A., Tan, L. M., Li, Q., Richter-Levin, G., & Kim, J. J. (n.d.). Dorsal periaqueductal gray-amygdala pathway conveys both innate and learned fear responses in rats.

Kitamura, T., Ogawa, S. K., Roy, D. S., Okuyama, T., Morrissey, M. D., Smith, L. M., … Tonegawa, S. (2017). Engrams and circuits crucial for systems consolidation of a memory. *Science (New York, N.Y.)*, *356*(6333), 73–78.

Klavir, O., Prigge, M., Sarel, A., Paz, R., & Yizhar, O. (2017). Manipulating fear associations via optogenetic modulation of amygdala inputs to prefrontal cortex. *Nature Neuroscience*, *20*(6), 836–844.

Knott, G. W., Holtmaat, A., Wilbrecht, L., Welker, E., & Svoboda, K. (2006). Spine growth precedes synapse formation in the adult neocortex in vivo. *Nature Neuroscience*, *9*, 1117–1124.

Komiyama, T., Sato, T. R., O'Connor, D. H., Zhang, Y.-X., Huber, D., Hooks, B. M., … Svoboda, K. (2010). Learning-related fine-scale specificity imaged in motor cortex circuits of behaving mice. *Nature*, *464*(7292), 1182–6.

Kopec, C. D., Li, B., Wei, W., Boehm, J., & Malinow, R. (2009). Glutamate Receptor Exocytosis and Spine Enlargement during Chemically Induced Long-Term Potentiation. *Journal of Neuroscience*, *26*(7), 2000–2009.

Labar, K. S., Ledoux, J. E., Spencer, D. D., & Phelps, E. A. (1995). Impaired Fear Conditioning Following Unilateral Temporal Lobectomy in Humans. *The Journal of Neuroscience*, *15*(10).

Lai, C. S. W., Franke, T. F., & Gan, W.-B. (2012). Opposite effects of fear conditioning and extinction on dendritic spine remodelling. *Nature*, *483*(7387), 87–91.

Larkum, M. (2013). A cellular mechanism for cortical associations: an organizing principle for the cerebral cortex. *Trends in Neurosciences*, *36*, 141–151.

Larkum, M. E., Sandler, M., Polsky, A., & Schiller, J. (2009). Synaptic Integration in Tuft Dendrites of Layer 5 Pyramidal Neurons: A New Unifying Principle. *Science*, *663*(August), 756–760.

Larkum, M. E., Zhu, J. J., & Sakmann, B. (1999). A new cellular mechanism for coupling inputs arriving at different cortical layers. *Nature*, *398*(March), 2–5.

Lavzin, M., Rapoport, S., Polsky, A., Garion, L., & Schiller, J. (2012). Nonlinear dendritic processing determines angular tuning of barrel cortex neurons in vivo. *Nature*, *490*(7420), 397–401.

Ledoux, J. (2012). Perspective Rethinking the Emotional Brain. *Neuron*, *73*, 653–676.

Ledoux, J. E. (2014). Coming to terms with fear. *PNAS*, *111*(8), 2871–2878.

Ledoux, J. E. (2000). Emotion Circuits in the Brain. *Annual Review of Neuroscience*, *23*(1), 155–184.

Ledoux, Cicchetti, Xagoraris, and Romanski*. (1990). The lateral amygdaloid nucleus: sensory interface of the amygdala in fear conditioning. *The Journal of Neuroscience*, *10(4)*, 1062–1069.

Ledoux, J. E., Farb, C., & Ruggiero, D. A. (1990). Topographic Organization of Neurons in the Acoustic Thalamus That Project to the Amygdala. *The Journal of Neuroscience*, *fO*(4), 1043–54.

Ledoux, J. E., Iwata, J., Cicchetti, P., & Reis, D. J. (1988). Different Projections of the Central Amygdaloid Nucleus Mediate Autonomic and Behavioral Correlates of Conditioned Fear. *The Journal of Neuroscience*, *8*(7), 2517–2529.

Ledoux, J. E., Ruggiero, D. A., & Donald Reis, A. J. (1985). Projections to the Subcortical Forebrain From Anatomically Defined Regions of the Medial Geniculate Body in the Rat. *THE JOURNAL OF COMPARATIVE NEUROLOGY*, 242–182.

Lendvai, B., Stern, E. A., Chen, B., & Svoboda, K. (2000). Experience-dependent plasticity of dendritic spines in the developing rat barrel cortex in vivo. *Nature*, *404*, 876–880.

Letzkus J., Wolff SB, Meyer EM, Tovote P, Courtin J, H. C. & L. A. (2011). A disinhibitory microcircuit for associative fear learning in the auditory cortex. *Nature*, *480*, 331–335.

Leutgeb, J. K., Leutgeb, S., Moser, M.-B., & Moser, E. I. (2007). Pattern Separation in the Dentate Gyrus and CA3 of the Hippocampus. *Science*, *315*(5814), 961–966.

Li, W., Howard, J. D., Parrish, T. B., & Gottfried, J. A. (2008). Aversive Learning Enhances Perceptual and Cortical Discrimination of Indiscriminable Odor Cues. *Science*, *319*(5871), 1842–1845.

Likhtik, E., & Paz, R. (2015). Amygdala-prefrontal interactions in (mal)adaptive learning. *Trends in Neurosciences*.

Likhtik, E., Pelletier, J. G., Paz, R., & Paré, D. (2005). Prefrontal Control of the Amygdala.

Likhtik, E., Stujenske, J. M., Topiwala, M. A., Harris, A. Z., & Gordon, J. A. (2013). Prefrontal entrainment of amygdala activity signals safety in learned fear and innate anxiety. *Nature Publishing Group*, *17*(1).

Linke R., Braune, G. H. S. (2000). Differential projection of the posterior paralaminar thalamic nuclei to the amygdaloid complex in the rat. *Exp Brain Res, 134*, 520–532.

Lippman, J., & Dunaevsky, A. (2005). Dendritic spine morphogenesis and plasticity. *Journal of Neurobiology*, *64*(1), 47–57.

Liu, X., Ramirez, S., Pang, P. T., Puryear, C. B., Govindarajan, A., Deisseroth, K., & Tonegawa, S. (2012). Optogenetic stimulation of a hippocampal engram activates fear memory recall. *Nature*, *484*, 381–385.

Livneh, U., & Paz, R. (2012). Amygdala-Prefrontal Synchronization Underlies Resistance to Extinction of Aversive Memories.

Llaneza, D. C., & Frye, C. A. (2009). Progestogens and Estrogen Influence Impulsive Burying and Avoidant Freezing Behavior of Naturally Cycling and Ovariectomized Rats. *Pharmacol Biochem Behav*, *93*(3), 337–342.

Lütcke, H., Margolis, D. J., & Helmchen, F. (2013). Steady or changing? Long-term monitoring of neuronal population activity. *Trends in Neurosciences*, *36*(7), 375–384.

Majewska, A. K., Newton, J. R., & Sur, M. (2006). Remodeling of Synaptic Structure in Sensory Cortical Areas In Vivo. *Journal of Neuroscience*, *26*(11), 3021–3029.

Majewska, A., & Sur, M. (2003). Motility of dendritic spines in visual cortex in vivo: Changes during the critical period and effects of visual deprivation. *PNAS*, *100*(26), 16024–16029.

Major, G., Larkum, M. E., & Schiller, J. (2013). Active properties of neocortical pyramidal neuron dendrites. *Annual Review of Neuroscience*, *36*, 1–24.

Major, G., Polsky, A., Denk, W., Schiller, J., & Tank, D. W. (2008). Spatiotemporally graded NMDA spike/plateau potentials in basal dendrites of neocortical pyramidal neurons. *Journal of Neurophysiology*, *99*(5), 2584–2601.

Manita, S., Suzuki, T., Homma, C., Matsumoto, T., Odagawa, M., Yamada, K., … Murayama, M. (2015). A Top-Down Cortical Circuit for Accurate Sensory Perception. *Neuron*, *86*(5), 1304–1316.

Marek, R., Strobel, C., Bredy, T. W., & Sah, P. (2013). The amygdala and medial prefrontal cortex: partners in the fear circuit. *J Physiol*, *59110*, 2381–2391.

Margolis, D. J., Lütcke, H., Schulz, K., Haiss, F., Weber, B., Kügler, S., … Helmchen, F. (2012). Reorganization of cortical population activity imaged throughout long-term sensory deprivation. *Nature Neuroscience*, *15*(11), 1539–1546.

Masterson, F. A., & Crawfor, M. (1982). The defense motivation system: A theory of avoidance behavior. *The Behavioral and Brain Sciences*, *5*, 661–696. Retrieved from

Mátyás, F., Lee, J., Shin, H. S., & Acsády, L. (2014). The fear circuit of the mouse forebrain: Connections between the mediodorsal thalamus, frontal cortices and basolateral amygdala. *European Journal of Neuroscience*, *39*(11), 1810–1823.

McDonald, A. J. (1987). Organization of amygdaloid projections to the mediodorsal thalamus and prefrontal cortex: a fluorescence retrograde transport study in the rat. *The Journal of Comparative Neurology*, *262*(1), 46–58.

McGaugh, J. L. (2013). Making lasting memories: remembering the significant. *Proceedings of the National Academy of Sciences of the United States of America*, *110 Suppl*(Supplement_2), 10402–7.

McHugh, T. J., Jones, M. W., Quinn, J. J., Balthasar, N., Coppari, R., Elmquist, J. K., … Tonegawa, S. (2007). Dentate Gyrus NMDA Receptors Mediate Rapid Pattern Separation in the Hippocampal Network. *Science*, *317*, 94–99.

Miklavc, P., Valentinčič, T., & Valentinč, T. (2012). Chemotopy of Amino Acids on the Olfactory Bulb Predicts Olfactory Discrimination Capabilities of Zebrafish Danio rerio. *Chem. Senses*, *37*, 65–75.

Milad M., Quirk G. J. (2002). Neurons in medial prefrontal cortex signal memory for fear extinction. *Nature*, *420*, 70–74.

Miller, N. E. (1948). Studies of Fear as an Acquirable Drive: I. Fear as Motivation and Fear-Reduction as Reinforcement in the Learning of New Responses. *Journal of Experimental Psychology*.

Mizrahi, A., Shalev, A., & Nelken, I. (2014). Single neuron and population coding of natural sounds in auditory cortex. *Current Opinion in Neurobiology*, *24*(1), 103–110.

Moga, M. M., Herbert, H., Hurley, K. M., Yasui, Y., Gray, T. S., & Saper, C. B. (1990). Organization of cortical, basal forebrain, and hypothalamic afferents to the parabrachial nucleus in the rat. *Journal of Comparative Neurology*, *295*(4), 624–661.

Mostany, R., Anstey, J. E., Crump, K. L., Maco, B., Knott, G., & Portera-Cailliau, C. (2013). Altered Synaptic Dynamics during Normal Brain Aging. *Journal of Neuroscience*, *33*(9), 4094 – 4104.

Nakayama, D., Baraki, Z., Onoue, K., Ikegaya, Y., Matsuki, N., & Nomura, H. (2015). Frontal association cortex is engaged in stimulus integration during associative learning. *Current Biology : CB*, *25*(1), 117–23.

Olsson, A., & Phelps, E. A. (2004). Learned Fear of Unseen'' Faces After Pavlovian, Observational, and Instructed Fear. *Psychological Science*, *15*(12), 822–828.

Otis, J. M., Namboodiri, V. M. K., Matan, A. M., Voets, E. S., Mohorn, E. P., Kosyk, O., … Stuber, G. D. (2017). Prefrontal cortex output circuits guide reward seeking through divergent cue encoding. *Nature*, *543*(7643), 103–107.

Pai, S., Erlich, J. C., Kopec, C., & Brody, C. D. (2011). Minimal impairment in a rat model of duration discrimination following excitotoxic lesions of primary auditory and prefrontal cortices. *Frontiers in Systems Neuroscience*, *5*, 74.

Palmer, L. M., Shai, A. S., Reeve, J. E., Anderson, H. L., Paulsen, O., & Larkum, M. E. (2014). NMDA spikes enhance action potential generation during sensory input. *Nature Neuroscience*, *17*(3), 383–390.

Pastalkova, E., Itskov, V., Amarasingham, A., & Buzsáki, G. (2008). Internally generated cell assembly sequences in the rat hippocampus. *Science (New York, N.Y.)*, *321*(5894), 1322–7.

Pavlov. (1927). Conditioned Reflexes, an investigation of the psychological activity of the cerebral cortex. *Oxford University Press, New York*.

Paxinos, G., & Watson, C. (2007). *The rat brain in stereotaxic coordinates*. Elsevier.

Peri, T., Ben-Shakhar, G., Orr, S. P., & Shalev, A. Y. (2000). Psychophysiologic assessment of aversive conditioning in posttraumatic stress disorder. *Biological Psychiatry*, *47*(6), 512–9.

Portera-Cailliau, C., Pan, D. T., & Yuste, R. (2003). Activity-Regulated Dynamic Behavior of Early Dendritic Protrusions: Evidence for Different Types of Dendritic Filopodia. *Journal of Neuroscience*, *23*(18), 7129–7142.

Pouchelon, G., Gambino, F., Bellone, C., Telley, L., Vitali, I., Lüscher, C., … Jabaudon, D. (2014). Modality-specific thalamocortical inputs instruct the identity of postsynaptic L4 neurons. *Nature*, *511*(7510), 471–474.

Quirk, G. J., & Armony, J. L. (1997). Fear Conditioning Enhances Different Temporal Components of Tone-Evoked Spike Trains in Auditory Cortex and Lateral Amygdala. *Neuron*, *19*, 613–624.

Quirk, G. J., & Mueller, D. (2008). Neural Mechanisms of Extinction Learning and Retrieval. *Neuropsychopharmacology Reviews*, *33*, 56–72.

Quirk, G. J., Repa, J. C., & Ledoux, J. E. (1995). Fear Conditioning Enhances Short-Latency Auditory Responses of Lateral Amygdala Neurons: Parallel Recordings in the Freely Behaving Rat. *Neuron*, *15*, 1029–1039.

Rajasethupathy, P., Sankaran, S., Marshel, J. H., Kim, C. K., Ferenczi, E., Lee, S. Y., Deisseroth, K. (2015). Projections from neocortex mediate top-down control of memory retrieval. *Nature*, *526*(7575), 653–9.

Reijmers, L. G., Perkins, B. L., Matsuo, N., & Mayford, M. (2007). Localization of a Stable Neural Correlate of Associative Memory. *Science*, *317*(5842), 1230–1233.

Rescorla, R. A., & Solomon, R. L. (1967). Two-process learning theory: relationships between pavlovian conditioning and instrumental learning. *Psychlogical Review*, *74*(3).

Resnik, J., Sobel, N., & Paz, R. (2011). Auditory aversive learning increases discrimination thresholds. *Nature Neuroscience*, *14*(6), 791–796.

Rioult-Pedotti, M. S., Friedman, D., & Donoghue, J. P. (2000). Learning-induced LTP in neocortex. *Science (New York, N.Y.)*, *290*(5491), 533–6.

Rogerson, T., Cai, D. J., Frank, A., Sano, Y., Shobe, J., Lopez-Aranda, M. F., & Silva, A. J. (2014). Synaptic tagging during memory allocation. *Nature Reviews Neuroscience*, *15*(3), 157–169.

Romanski, L. M., Clugnet, M.-C., Bordi, F., & Ledoux, J. E. (1993). Somatosensory and Auditory Convergence in the Lateral Nucleus of the Amygdala. *Behavioral Neuroscience*, *107*(3), 444–450.

Rudy, B., Fishell, G., Lee, S., & Hjerling-Leffler, J. (2011). Three groups of interneurons account for nearly 100% of neocortical GABAergic neurons. *Developmental Neurobiology*, *71*(1), 45–61.

Russchen, F. T., Amaral, D. G., & Price, J. L. (1987). The Afferent Input to the Magnocellular Division of the Mediodorsal Thalamic Nucleus in the Monkey, Macaca fascicularis. *The Journal of Comparative Neurology*, *256*, 175–210.

Sacchetti, B., Baldi, E., Lorenzini, C. A., & Bucherelli, C. (2002). Differential contribution of some cortical sites to the formation of memory traces supporting fear conditioning. *Exp Brain Res, 146*, 223–232.

Sacchetti, B., Baldi, E., Lorenzini, C. A., & Bucherelli, C. (2003). Role of the neocortex in consolidation of fear conditioning memories in rats. *Exp Brain Res, 152*, 323–328.

Sachidhanandam, S., Sreenivasan, V., Kyriakatos, A., Kremer, Y., & H Petersen, C. C. (2013). Membrane potential correlates of sensory perception in mouse barrel cortex. *Nature Neuroscience*, *16*(11), 6–7.

Sahay, A., Scobie, K. N., Hill, A. S., O 'carroll, C. M., Kheirbek, M. A., Burghardt, N. S., … Hen, R. (2011). Increasing adult hippocampal neurogenesis is sufficient to improve pattern separation. *Nature*, *472*.

Sahay, A., Wilson, D. A., & Hen, R. (2011). Pattern Separation: A Common Function for New Neurons in Hippocampus and Olfactory Bulb. *Neuron*, *70*, 582–588.

Salzman, C. D., & Fusi, S. (2010). Emotion, cognition, and mental state representation in amygdala and prefrontal cortex. *Annual Review of Neuroscience*, *33*, 173–202.

Sangha, S., Chadick, J. Z., & Janak, P. H. (2013). Safety Encoding in the Basal Amygdala. *Journal of Neuroscience*, *33*(9), 3744–3751.

Sato, M., Ito, M., Nagase, M., Sugimura, Y. K., Takahashi, Y., Watabe, A. M., & Kato, F. (2012). The lateral parabrachial nucleus is actively involved in the acquisition of fear memory in mice. *Molecular Brain*, *5*, 9.

Sau, C., Lai, W., Franke, T. F., & Gan, W.-B. (2012). Opposite effects of fear conditioning and extinction on dendritic spine remodelling. *Nature*, *482*.

Scala, G. DI, Mana, M. J., Jacobs, -w J, PHILLIPSt, A. G., Scala, D., Mana, M. J., … Phillips, A. G. (n.d.). Evidence of Pavlovian Conditioned Fear Following Electrical Stimulation of the Periaqueductal Grey in the Rat I. *Physiology & Behavior*, *40*, 55–63.

Schiller, D., Cain, C. K., Curley, N. G., Schwartz, J. S., Stern, S. A., Ledoux, J. E., & Phelps, E. A. (2008). Evidence for recovery of fear following immediate extinction in rats and humans. *Learning & Memory*, *15*, 394–402.

Schiller, J., Major, G., Koester, H. J., & Schiller, Y. (2000). NMDA spikes in basal dendrites, *1261*(1997), 285–289.

Schiller, J., Schiller, Y., Stuart, G., & Sakmann, B. (1997). Calcium action potentials restricted to distal apical dendrites of rat neocortical pyramidal neurons. *Journal of Physiology*, *505*(3), 605–616.

Senn, V., Wolff, S. B. E., Herry, C., Grenier, F. O., Ehrlich, I., Grü Ndemann, J., … Lü Thi, A. (2014). Long-Range Connectivity Defines Behavioral Specificity of Amygdala Neurons. *Neuron*, *81*, 428–437.

Serge Campeau and Michael Davis. (1995). Involvement of the Central Nucleus and Basolateral Complex of the Amygdala in Fear Conditioning Measured with Fear-Potentiated Startle in Rats Trained Concurrently with Auditory and Visual Conditioned Stimuli. *Journal of Neuroscience, 15(3)*, 2301–2311.

Shi, C., & Davis, M. (1999). Pain Pathways Involved in Fear Conditioning Measured with Fear- Potentiated Startle: Lesion Studies. *Journal of Neuroscience*, *19(1)*, 420–430.

Shi, S., Li, Y., & Mcnally, G. P. (2014). The conditions that promote fear learning: Prediction error and Pavlovian fear conditioning. *Neurobiology of Learning and Memory*, *108*, 14–21.

Sierra-Mercado, D., Padilla-Coreano, N., & Quirk, G. J. (2011). Dissociable roles of prelimbic and infralimbic cortices, ventral hippocampus, and basolateral amygdala in the expression and extinction of conditioned fear. *Neuropsychopharmacology*, *36*(2), 529–38.

Sorra, K. E., & Harris, K. M. (2000). Overview on the Structure, Composition, Function, Development, and Plasticity of Hippocampal Dendritic Spines. *Hippocampus*, *10*, 501–511.

Stujenske, J. M., Likhtik, E., Topiwala, M. A., & Gordon, J. A. (2014). Fear and Safety Engage Competing Patterns of Theta-Gamma Coupling in the Basolateral Amygdala. *Neuron*, *83*(4), 919–933.

Sul, J. H., Jo, S., Lee, D., & Jung, M. W. (2011). Role of rodent secondary motor cortex in value-based action selection. *Nature Neuroscience*, *14*(9), 1202–1208.

Sullivan, G. M., Apergis, J., Bush, D. E. A., Johnson, L. R., Hou, M., & Ledoux, A. J. E. (2004). Lesions in the bed nucleus of the stria terminalis disrupt corticosterone and freezing responses elicited by a contextual but not by a specific cue-conditioned fear stimulus. *Neuroscience*, *128*, 7–14.

Sun, N., & Cassell, M. D. (1993). Intrinsic GABAergic Neurons in the Rat Central Extended Amygdala. *The journal comparative neurology*, *0*, 33–381.

Svoboda, K. (2004). Do spines and dendrites distribute dye evenly? *Trends Neuroscience*, *27*, 445–446. Tang, J., Ko, S., Ding, H.-K., Qiu, C.-S., Calejesan, A. A., & Zhuo, M. Pavlovian fear memory induced by activation in the anterior cingulate cortex.

Swanson and Petrovich. (1998). What is the amygdala? *Trends Neuroscience*, *21*, 323–331.

Thorndike, E. L. (1898). Animal Intelligence: An Experimental Study of the Associative Processes in Animals. *Psychological Review, Vol 5(5)*, 551–553.

Tian, L., Hires, S. A., & Looger, L. L. (2012). Imaging Neuronal Activity with Genetically Encoded Calcium Indicators. *Cold Spring Harbor Protocols*, *6*, 647–656.

Tonegawa, S., Liu, X., Ramirez, S., & Redondo, R. (2015). Perspective Memory Engram Cells Have Come of Age. *Neuron*, *87*, 918–931.

Tovote, P., Fadok, J. P., & Lüthi, A. (2015). Neuronal circuits for fear and anxiety. *Nature Reviews Neuroscience*, *16*(6), 317–331.

Tropea, D., Majewska, A. K., Garcia, R., & Sur, M. (2010). Development/Plasticity/Repair Structural Dynamics of Synapses in Vivo Correlate with Functional Changes during Experience-Dependent Plasticity in Visual Cortex. *Journal of Neuroscience*, *30*(33), 11086–11095.

Uylings, H. B. M., Groenewegen, H. J., & Kolb, B. (2003). Do rats have a prefrontal cortex? *Behavioural Brain Research*, *146*, 3–17.

Van De Werd, G. R., & P Evers, H. B. U. (2010). Cytoarchitectonic and chemoarchitectonic characterization of the prefrontal cortical areas in the mouse. *Brain Struct Funct*, *214*, 339–353.

Van der Kooy, D., Koda, L. Y., McGinty, J. F., Gerfen, C. R., & Bloom, F. E. (1984). The organization of projections from the cortex, amygdala, and hypothalamus to the nucleus of the solitary tract in rat. *The Journal of Comparative Neurology*, *224*(1), 1–24.

Vidal-Gonzalez, I., Vidal-Gonzalez, B., Rauch, S. L., & Quirk, G. J. (2006). Microstimulation reveals opposing influences of prelimbic and infralimbic cortex on the expression of conditioned fear. *Learning & Memory (Cold Spring Harbor, N.Y.)*, *13*(6), 728–33.

Watson, J. B., & Rayner, R. (1917). Conditioned Emotional Reactions. *American Journal of Psychology*, *28*, 163–174.

Weinberger, N. M. (2011). The medial geniculate, not the amygdala, as the root of auditory fear conditioning. *Hearing Research*, *274*, 61–74.

Wiechert, M. T., Judkewitz, B., Riecke, H., & Friedrich, R. W. (2010). Mechanisms of pattern decorrelation by recurrent neuronal circuits. *Nature Neuroscience*, *13*(8), 1003–1010.

Wilson, D. A. (2009). Pattern Separation and Completion in Olfaction. *Ann. N.Y. Acad. Sci.*, *1170*, 306–312.

Xu, N., Harnett, M. T., Williams, S. R., Huber, D., O'Connor, D. H., Svoboda, K., & Magee, J. C. (2012). Nonlinear dendritic integration of sensory and motor input during an active sensing task. *Nature*, *492*(7428), 247–51.

Xu, T., Yu, X., Perlik, A. J., Tobin, W. F., Zweig, J. A., Tennant, K., … Zuo, Y. (2009). Rapid formation and selective stabilization of synapses for enduring motor memories. *Nature*, *462*, 915–919.

Yang, G., Pan, F., & Gan, W.-B. (2009). Stably maintained dendritic spines are associated with lifelong memories. *Nature*, *462*, 920–924.

Zhou, Q., Homma, K. J., & Poo, M.-M. (2004). Report Shrinkage of Dendritic Spines Associated with Long-Term Depression of Hippocampal Synapses. *Neuron*, *44*, 749–757.

Zhou, Y., Won, J., Karlsson, M. G., Zhou, M., Rogerson, T., Balaji, J., … Silva, A. J. (2009). CREB regulates excitability and the allocation of memory to subsets of neurons in the amygdala. *Nature Neuroscience*, *12*(11), 1438–1443.

10. Annexes

10.1 *Manuscript 1*

Mattia Aime, Elisabete Augusto, Christelle Martin, Yann Humeau, and Frédéric Gambino.

Association of convergent inputs in frontal circuits enhances perceptual discrimination.

Nature Neuroscience, In review

Title: Association of convergent inputs in frontal circuits enhances perceptual discrimination

Authors: Mattia Aime[1,3], Elisabete Augusto[1,3], Christelle Martin[1,2,3], Yann Humeau[1,3], and Frédéric Gambino[1,3]*

Affiliations:

[1] Interdiscliplinary Institute for NeuroScience (IINS), Centre Broca Nouvelle-Aquitaine, 146, rue Léo-Saignat, 33076 Bordeaux, France.

[2] Pole In Vivo.

[3] UMR5297 CNRS and University of Bordeaux.

* Corresponding author. E-mail: frederic.gambino@u-bordeaux.fr

ABSTRACT

The ability of an organism to predict forthcoming events is crucial for self-preservation, and depends on accurate internal representations to discriminate among similar sensory inputs. However, the circuit and synaptic mechanisms by which the brain learns to detect and disambiguate cues predicting threat from safety noise remain largely ignored. Here, we demonstrate that discrimination of safe and fear-conditioned stimuli is an active learning process that depends on full activity of the frontal association cortex (FrA), and is associated with the formation of cue-specific neuronal assemblies therein. During learning, prefrontal pyramidal neurons were potentiated through specific sensory-driven non-linearities supported by the activation of non-specific long-range inputs from the basolateral amygdala (BLA). Taken together, our data provide evidence for a new active dendritic mechanism that associates during learning features of perceived experience with BLA-mediated emotional state into prefrontal memory assemblies.

INTRODUCTION

Discriminative learning is an evolutionary important survival strategy that depends on the repeated contingency and contiguity between sensory cues (conditioned stimuli, CS) and the events (i.e. danger) they must predict (unconditioned stimuli, US)[1,2]. The resulting learned association provides an accurate representation of the environment by increasing discriminative skills between aversive (threat) and non-aversive (safety) environmental signals[1,2]. Many anxiety-related behaviors such as post-traumatic stress disorder (PTSD) are associated with a loss of cue discrimination that may result in fear overgeneralization to harmless environment[1,3]. Therefore, further exploration of the neural circuits that encode and compare aversive *vs.* non-aversive signals is critical for our understanding of PTSD and related affective disorders. However, while previous work has mostly revealed how the CS generate fear responses (e.g.[4–6]), it remains unclear how the brain learns to encode similar though different cues and thus discriminates between threatening and safe environments[7,8].

The medial prefrontal cortex (mPFC) appeared over the past decade as a critical region that shapes behaviors in response to both aversive and non-aversive environmental cues[2,9,10]. These antagonistic effects of mPFC possibly develop through specific interaction between its different subdivisions (i.e prelimbic (PL) and infralimbic (IL) cortices) and the basolateral complex of the amygdala (BLA)[9,11–14]. However, the idea that higher-order neuronal networks above the mPFC might encode opposing memories that are later preferentially selected during recall together with its downstream cortical (e.g. PL or IL mPFC) or subcortical structures (e.g. BLA)[15–20] has never been challenged. In keeping with this idea, it has been shown that the superficial frontal association cortex (FrA) contributes to memory formation during associative learning in rodents[21–25]. This region of the lateral part of the agranular cortex (AGl)[26,27] is reciprocally connected with the mPFC, the BLA, and the mediodorsal thalamic nucleus[17,23,28,29], and its inactivation alters both fear learning and extinction[23,25]. Recently, fear conditioning and extinction have been shown to induce in FrA dendritic spine elimination and formation, respectively[23]. Importantly, this occurred within the same dendrite supporting the idea that a unique FrA circuit might be well suited to control discrimination by computing opposite memories.

Theoretically, the existence of a dynamic high-dimensional cortical state could increase memory storage capabilities and facilitate perceptual acuity[6,30,31]. Whether such a learned discriminative representation is wired within discrete FrA circuits during conditioning and by which synaptic mechanisms remain unknown. To address these questions, we used *in vivo* whole-cell recordings[32] and optogenetic conditional strategies[17,18], together with two-photon (2P) calcium imaging in head-restrained mice to explore the dynamics of layer (L) 2/3 FrA pyramidal neurons[17,18,21,33] and long-range projections from the BLA[32] during the acquisition and recall of discriminative memories. We found that classical fear conditioning is associated with the creation of cue-specific FrA activity patterns whose decorrelation predicted the level of discrimination between threat and safety signals. In naive mice, sensory auditory stimulation produced frequency-specific, NMDARs-dependent, plateau-like depolarizations that potentiated FrA L2/3 neurons when combined with the channelrhodopsin-2-mediated activation of BLA neurons projecting to the FrA. During conditioning, those long-range projecting BLA neurons conveyed integrated information about the CS/US association that were critical to threat *vs.* safety discriminative learning. In conclusion, our study reveals a new circuit and synaptic mechanism for cue discrimination and provides a new cortical framework for our understanding of predictive learning and related disorders.

RESULTS

Chronic imaging of FrA pyramidal neurons during auditory cues discrimination

To examine whether cue discrimination might be encoded within specific prefrontal circuits, mice were injected with a virus encoding the calcium indicator GCaMP5 and implanted with a cranial window[32,33] above the FrA (**Fig. 1 and Supplementary Fig. 1b**). The same population of putative pyramidal neurons was imaged longitudinally in head-fixed awake mice before (sessions 1-3) and after (sessions 4-6) differential fear conditioning (**Fig. 1a, e**), while discriminative performance was tested at least 6 hours after each imaging session (**Fig. 1f and Supplementary Fig. 1c**). During conditioning, five auditory stimuli (each consisting of 27 pure (8 kHz)-tone or white noise pips, 50 ms, 0.9 Hz for 30 s) were positively (CS+, 8 kHz) or negatively (CS-, gaussian noise) paired with the delivery of a mild electrical shock (0.6 mA) to the paws in a pseudorandom order (**Supplementary Fig. 1d**). During recall in a new context, mice froze significantly more in response to CS+ as compared to the habituation period (session 3: 10.1 ± 3 % *vs.* session 4: 64.5 ± 2.4 %; n=5; p<0.001; *paired t-test*) while freezing responses upon CS- presentation remained unchanged (session 3: 11.7 ± 5 % *vs.* session 4: 10.5 ± 2.9 %; n=5; p=0.827; *paired t-test*) (**Fig. 1f**). Fear conditioning eventually resulted in increased behavioral cue discrimination (session 3: +0.064 ± 0.14 *vs.* session 4: +0.73 ± 0.04, n=5; p=0.013; *paired t-test*) (**Supplementary Fig. 1d**). Importantly, when all experimental conditions were pooled together, most animals froze less to the presentation of CS- as compared to the habituation period (**Supplementary Fig. 2**), indicating that sensory cues that were not explicitly paired to the footshock might acquire relative safety properties[2,9,10].

FrA computes both fear and safety sensory cues during learning

We recorded simultaneously over 6 imaging sessions the activity ($\Delta F/F_0$) of ~100 identified neurons per mouse (n=4 mice), among which ~40 % displayed significant calcium transient evoked by the presentation of CS+ and/or CS- stimuli (8 trials per CS with pseudo-random delay) (**Fig. 2 and Supplementary Fig. 3a, b**). Intriguingly, we found that fear learning increased non-specifically the activity of neurons in response to both CS+ and CS- (pooled sessions; CS+, before: 0.93 ± 0.16 Hz, after: 2.82 ± 0.51 Hz; CS-, before: 0.96 ± 0.10 Hz, after: 2.48 ± 0.49 Hz; *2-ways anova: before vs. after*, p<0.001; *CS+*

vs. CS-, p=0.684) without altering the proportion of active neurons nor the neuronal selectivity (**Fig. 2a and Supplementary Fig. 3**), indicating that the global tuning properties of active networks were not affected. In addition, the temporal activity patterns during cue presentation were highly heterogeneous and we did not observe any stable gains in coincident activity between pairs of neurons that were reported previously[17,21,34] (**Fig. 2b, c**). Instead, we found that learning reduced the similarity between activity patterns evoked by the CS+ and the CS- (Pearson correlation coefficient; session 3: 0.13 ± 0.06 *vs.* session 4: -0.022 ± 0.04; n=4; p=0.048 *paired t-test*), indicating that learning may create specific cortical representations by increasing the separation of activity patterns evoked by similar yet distinct sensory inputs (**Fig. 2d,e**). Because activity decorrelation has been proposed to facilitate memory storage[35] and to predict learning performance[36,37], we plotted the Pearson correlation coefficient computed in sessions 3 to 6 as a function of perceptual discrimination (**Fig. 2f**). We observed a linear negative relation between the level of CS+ *vs.* CS- correlated activity and the behavioral performance (r^2 = 0.63; n=4; p<0.01), indicating that the degree of activity separation in the FrA might predict the ability to discriminate between fear and relative safe sensory cues.

To test whether population activity in the FrA was indeed required for cue discrimination rather than for fear acquisition[23], we injected mice bilaterally with an AAV expressing the light-activated proton pump *archaerhodopsin* (AAV9-CAG-ArchT-GFP, or AAV9-CamKII-eGFP) into the FrA and suppressed the activity of L2/3 neurons with light through implanted optical fibers during the presentation of US[38] (**Fig. 3a**). *Ex-vivo* slice recordings confirmed that photostimulation of ArchT-GFP-expressing FrA pyramidal neurons reliably suppressed action potentials (**Supplementary Fig. 4**). The light-driven inactivation of FrA during CS+/US pairings (**Fig. 3b**) significantly impaired the ability to discriminate sensory cues during recall as compared to controls (GFP: 0.67 ± 0.11, n=5; ArchT: 0.08 ± 0.13, n=5; p=0.008; *t-test*) (**Fig. 3c**). FrA inactivation did not affect CS+-evoked fear behavior (normalized to habituation; GFP: 2.2 ± 0.4, n=5; ArchT: 2.04 ± 0.6, n=5; p=0.828; *t-test*) (**Fig. 3d**), confirming that the decrease in cue discrimination performance was not due to a deficit in fear learning acquisition. Rather, we observed an overgeneralization of fear learning with excessive freezing behaviors in response to the neutral CS- (normalized to habituation; GFP: 0.42 ± 0.26, n=5; ArchT: 1.81 ± 0.47, n=5;

p=0.032; *t-test*) (**Fig. 3d**), confirming that safety detection is an active process that develops during conditioning[9] and requires FrA L2/3 pyramidal neurons.

Auditory stimulation generates frequency-specific plateau potentials

The above results (**Fig. 2 and Fig. 3**) indicate that the FrA actively participates in learning-induced cue discrimination and guides behaviors by computing both paired (fear) and unpaired (safety) stimuli during conditioning. To further explore the underlying circuit and synaptic mechanisms, we performed somatic whole-cell recordings of FrA L2 pyramidal cells *in vivo* during anesthesia to limit the effects of attention (**Fig. 4 and Fig. 5**). Consistent with previous *in vivo* recordings of L2/3 pyramidal neurons in anesthetized animals[39], membrane potential spontaneously fluctuated between up and down states (**Fig. 4a, b**). In contrast to a pure auditory tone (CS+) that failed to activate frontal pyramidal neurons, gaussian tone (CS-) alone evoked a long-lasting subthreshold depolarization in naive animals (i.e. before conditioning; **Fig. 4c, d**). It indicates that FrA pyramidal neurons are capable to categorize auditory stimuli based on their spectral properties during anesthesia (**Supplementary Fig. 3a**). The gaussian tone-evoked increase in cumulative potential was essentially supra-linear (**Fig. 4e, f and Supplementary Fig. 5**) and bore similarities with evoked cortical up-states which were shown to depend on NMDA receptors (NMDARs)[32]. Consequently, the topic application of the specific NMDAR antagonist D(-)-2-Amino-5-phosphonovaleric acid (dAP5; 1 mM) efficiently and selectively suppressed the sustained depolarization evoked by the gaussian auditory stimulation (CS-: 36.3 ± 8 mV, CS+: 3.5 ± 8 mV, n=10; CS-/dAP5: -5.6 ± 3 mV, CS+ /dAP5: -4.1 ± 4 mV, n=13; p<0.001, *anova*) (**Fig. 4e, f and Supplementary Fig. 5**). In line with previous studies *in vivo*[32,40], it suggests that auditory-evoked sustained depolarizations recorded at the soma were likely to be mediated by local dendritic Ca^{2+} events through the recruitment of active NMDARs-dependent conductances. Importantly, those auditory-evoked plateau potentials were strongly attenuated in conditioned animals (naive: 36.3 ± 8 mV, n=10; conditioned: 5.4 ± 9 mV, n=8; p=0.008; *anova*) and correlated with learned behaviors (**Supplementary Fig. 6**), suggesting that they might overlap mechanistically with learning-dependent plasticities during memories acquisition[41,42]. Altogether, our data suggest that specific synaptic mechanisms within the FrA might associate salient value to sensory cues that they were not explicitly paired with the footshock during conditioning.

Co-activation of convergent inputs reinforces FrA L2/3 pyramidal neurons

Given that the activation of BLA neurons instructs prefrontal circuits during conditioning and memory recall[2,9,24,43], we hypothesized that BLA axons, along with the synaptic non-linearities evoked by gaussian auditory stimuli, could reinforce L2/3 FrA pyramidal neurons through their projections in L1[23,29,44] (see **Fig. 5f**). To address this question, we expressed the recombinant light-gated ion channel *channelrhodopsin*-2-YFP (ChR2; AAV9-CamKIIa-hChR2-eYFP) into the BLA and performed intracellular recordings in L2/3 FrA neurons of naive mice (n=6) (**Fig. 5**). First, we confirmed that BLA neurons were projecting to the superficial layers of the prefrontal cortex (**Fig. 5a, b and Supplementary Fig. 7a-d**). Local photostimulation of ChR2-BLA axons in acute slices produced excitatory postsynaptic current (EPSC) in FrA pyramidal neurons with short latencies (3.5 ± 0.36 ms, n=9) and low jitter (0.289 ± 0.04 ms, n=9), suggesting that a fraction of BLA neurons are directly and monosynaptically connected to FrA pyramidal neurons (**Supplementary Fig. 7e-g**)[45]. Similar to the cortical responses evoked by long-range thalamic projections[32], we found that the *in vivo* photostimulation of BLA neurons with an implanted optical fiber produced plateau-like depolarizations in all recorded neurons (averaged integral: 6.5 ± 1 mV*sec, n=13) (**Fig.5 c, d**) that were suppressed by artificial hyperpolarization (pre: 6.15 ± 1.6 mV*sec, hyper: 3.9 ± 1.5 mV*sec, post: 5.56 ± 1.4 mV*sec; n=4; p=0.004; *anova repeated measures*) or ectopic dAP5 application (Ctrl: 6.5 ± 1 mV*sec, n=13: dAP5: 1.57 ± 0.7 mV*sec, n=3; p=0.022; *Mann-Whitney test*) (**Fig. 5e**).

BLA-mediated plateau-like depolarizations likely emerge from dendritic NMDARs-mediated conductances which might facilitate the potentiation of coincident sensory-driven inputs[32,40,46–48]. Therefore, we next investigated the effect of BLA activation during auditory cue presentation (**Fig. 5f**). ChR2-expressing BLA neurons were photo-stimulated during 30 s at 0.9 Hz with 27 square light pulses (50 ms), a protocol that precisely overlapped the pattern of auditory stimuli (**Fig. 5g-i**). The coincident activation of BLA[49] produced no difference during the stimulation as compared to the presentation of the CS- alone (CS-: 12.4 ± 13 mV *vs.* CS-/light: 32 ± 10 mV; n=6; p=0.245; *paired t-test*), but significantly altered later on-going spontaneous slow-wave fluctuations (**Fig. 5g-i**). The increase in cumulative potential observed 30 sec after the end of the co-stimulation (CS-: 9.5 ± 14 mV *vs.* CS-/light: 76 ± 20 mV; n=6; p=0.023; *paired t-test*) (**Fig.**

5h, i) possibly reflects synaptic plasticity and might be critical for shaping future sensory perception and learning[50]. Together, our data confirmed the existence of functional and relevant BLA synaptic inputs to frontal L2/3 pyramidal neurons.

Activation of BLA-to-PFC long-range axons is required for discriminative learning

The results above provide a possible cooperative, *Hebbian*-like mechanism for safety encoding that temporally integrates converging inputs from both BLA and cortex into neuronal assemblies during associative learning (**Fig. 5f**)[24,44,49–51]. To test this hypothesis, we questioned the functions of BLA projecting axons to FrA during fear conditioning (**Fig. 6 and Fig. 7**). First, we injected a virus expressing GCaMP5 into the right BLA and imaged axonal Ca^{2+} responses[32] in superficial L1 of the right FrA of awake head-restrained mice during fear conditioning (**Fig. 6a-c**). GCaMP5 calcium transients ($\Delta F/F_0$) provided a direct measure of the activation of BLA neurons projecting to the FrA. Then, we conditioned awake mice under the 2-photon microscope with a modified version of the conditioning test in which each CS+/US pairing was followed by the presentation of the CS- with a pseudo-random delay (**Fig. 6c, d**). While the activity of 242 individual BLA boutons (n=3 mice) was relatively low at rest, it increased significantly upon successive CS+/US pairings (baseline: 1.1 ± 0.5 Hz; pairings: 1.73 ± 0.63 Hz; n=3; +71 ± 20 %; p=0.0042, χ^2=8.2) (**Fig. 6d-f**). Importantly, the activation of BLA axons was non-specific and independent of the nature of the CS presented (CS+: 1.46 ± 0.14 Hz; CS-: 1.72 ± 0.26 Hz; n=3; p=0.19, χ^2=1.7)[2,43]. However, it never occurred before the end of the first CS+/US pairing (baseline: 1.1 ± 0.5 Hz; first CS+: 1.02 ± 0.02Hz; n=3; p=0.49, χ^2=0.46) (**Fig. 6f**). Altogether, it supports the idea that BLA projecting axons likely passively conveyed information about the learning, i.e. the CS+/US association itself rather than (or in addition to) auditory cues alone[24], that must be further combined in the FrA with auditory-evoked non-linearities to recruit prefrontal neurons into cue-specific memories.

This hypothesis was tested by specifically silencing BLA-to-FrA axons during fear conditioning but only during the presentation of the unpaired CS- (**Fig. 7**). Mice were injected bilaterally with a retrograde Cav-2-CMV-Cre[52] into the FrAs together with an AAV9-flex-CBA-ArchT-GFP (or AAV1-CAG-flex-eGFP) into both BLAs (**Fig. 7a**). This resulted in the expression of the light-driven inhibitory proton pump ArchT in a limited but target-specific fraction of BLA neurons that project to the FrA (**Fig. 7b**). Similar to the effect of FrA photo-inhibition (**Fig. 3**), the specific inactivation of BLA-to-FrA neurons

during the presentation of the CS- (**Fig. 7a**) increased freezing behaviors during recall in response to the CS- while leaving the CS+-evoked fear behaviors unaltered (**Fig. 7c**). Consequently, discriminative performance was strongly attenuated as compared to controls (GFP: 0.98 ± 0.08 *vs.* ArchT: 0.33 ± 0.17; n=4; p=0.016; *paired t-test*) (**Fig. 7d**). Taken together, our data revealed that the coincident and time-locked activation of BLA projecting neurons and FrA pyramidal neurons during conditioning drives cue discrimination most likely by encoding safety.

DISCUSSION

Our data describe a new critical role for the prefrontal cortex during behavioral discrimination of threat *vs*. safety environmental signals. Compared to the other prefrontal regions, the frontal association area (FrA) of rodents has long been neglected presumably because of a lack of a standardized anatomical definition[26]. However, despite different names accross the literature (e.g. Fr2[26], PrCm[14], agranular medial and lateral cortices[22], frontal cortex[25], dorsal frontal cortex[53], secondary motor area[29]), the implication of FrA in classical conditioning has constantly been reported[14,23,25,53]. For example, the pharmacological inactivation of FrA before fear conditioning or extinction impaired the consolidation of fear or extinction memories, respectively[23,25], indicating that FrA promotes both the expression and suppression of fear memory traces. Here, we provide the first experimental evidence that the formation of segregated FrA neuronal assemblies that are specific for threatening and non-threatening cues is associated upon learning with increased discriminative performance (**Fig. 2**), providing a possible circuit mechanism for the opposing behavioral output of FrA.

Over the last decade, neuronal assemblies have become the favorite physical substrate for memory traces in brain circuits[20]. They are supposed to be formed during learning and further consolidated into long-term memories through the strengthening of synaptic connections between pairs of neurons with similar input selectivity[20]. For instance, increased temporal correlated activity among similar neurons has been recently reported in the hippocampus during learning[34], which might help subsequent *Hebbian*-like synaptic plasticity mechanisms and promote the selection of the same pattern of neural activity upon memory recall of a particular event[17,20,21,34]. In contrast, in FrA we found that fear learning increased non-specifically the activity evoked by distinct auditory stimulations (**Fig. 2a**). In addition, neither the auditory-cue selectivity nor the temporal correlation between the activity of FrA pyramidal neurons evoked by the same auditory stimulus were affected (**Fig. 2d,e and Supplementary Figure 3f**). Instead, we observed a decrease in the correlation of activity patterns evoked by paired and unpaired CS after learning (**Fig. 2d,e and Supplementary Figure 3g**), suggesting the formation of an higher-order ensemble between paired and unpaired CS that might differ from the formation of individual CS assemblies. Likewise, our data are consistent with the increase of sparse population coding reported in the somatosensory cortex after fear learning[54],

which might support activity pattern decorrelation[35]. Pattern decorrelation has been observed in different divergent neuronal networks. It has been proposed to make stimulus representations more distinct, which in turn may facilitate learning performance[35–37]. In agreement, we observed that the level of fear learning-induced separation of CS activity patterns was associated with a better discrimination of paired (aversive) *vs.* non-paired (non-aversive) auditory stimuli (**Fig. 2f**).

The above results imply that sensory cues that were not positively or explicitly paired with the delivery of the footshock must have been encoded within FrA into safety-related representation. In agreement with this hypothesis, we showed that optogenetic inactivation of the FrA during learning resulted in fear overgeneralization with bias towards encoding neutral, unpaired cues as threat (**Fig. 3**). This indicates that the FrA is required for safety *vs.* threat discrimination rather than for fear acquisition. It contrasts however with previous lesion studies[23,25], which might be explained by the high temporal and spatial precision of our optogenetic inhibition. Besides, our data are consistent with recent studies showing an increase of theta synchronization between mPFC and BLA during safety and CS discrimination that possibly inhibits fear response and anxiety-related behaviors[2,9,10].

The learning-driven synaptic mechanisms that underlie the encoding of unpaired sensory cue into safety-related cortical assembly remain unclear. Beyond its classical role during CS+/US association[1,2,55], the BLA has emerged as a key structure during recall of the CS-[11,43]. In addition it provides massive cortical inputs that critically influence safety encoding and long-lasting memory consolidation[2,9,10,29] presumably through synaptic plasticity[55]. Here, we confirmed that BLA neurons projecting to the FrA participated in the acquisition of safety memory traces as well (**Fig. 7**). However, only a limited fraction of BLA neurons were required[15,51] (**Fig. 7**) and their activation during conditioning was not cue-specific (**Fig. 6**), indicating that neuronal target specificity of BLA-to-FrA long-range projections is likely to be necessary though not sufficient for cue discrimination[11]. Indeed, we showed that, in addition to the presumed spatial specificity, temporal coincident activation of convergent inputs from both BLA and cortex was required to potentiate FrA pyramidal responses evoked by unpaired, gaussian auditory stimulation (**Fig. 5f-i**). This possibly occurred at the level of distal dendrites with the help of BLA-induced NMDARs-dependent dendritic plateau potentials[32,40,46–48] (**Fig. 5a-e**). Together, it indicates that long-range BLA projections in superficial layer of FrA might produce

strong and non-linear dendritic depolarization and gain control over synaptic plasticity of coincident cortical, sensory-related inputs and thus recruit neurons into safety-related assembly[32,44,55].

Taken together, our results provide a new *Hebbian* cortical framework for our understanding of classical conditioning, during which BLA long-range inputs actively instruct cue-specific intra-cortical inputs, likely resulting in the emergence of a discriminative neuronal ensemble that is associated during recall with normal cue-discrimination behaviors, in particular during the non-threat (safe) periods. Whether a similar synaptic mechanism is involved during the formation of fear-related assembly remains to be determined. We found that during anesthesia only gaussian tone (CS-) evoked long-lasting subthreshold depolarization in naive animals (i.e. before conditioning) while pure auditory tones had no effect (**Fig. 4**), suggesting a frequency-specific mechanism. Although convergent inputs from successive or parallel cortical regions that are involved in complex sound processing (e.g. auditory cortex) likely drive this process[1,56], we cannot exclude an effect of anesthesia and future experiments in awake animals will further clarify the synaptic role of tone frequencies in the formation of cue-specific assemblies.

REFERENCES

1. LeDoux, J. E. Emotion Circuits in the Brain. *Annu. Rev. Neurosci.* **23,** 155–184 (2000).
2. Likhtik, E. & Paz, R. Amygdala-prefrontal interactions in (mal)adaptive learning. *Trends in Neurosciences* **38,** 158–166 (2015).
3. Peri, T., Ben-Shakhar, G., Orr, S. P. & Shalev, A. Y. Psychophysiologic assessment of aversive conditioning in posttraumatic stress disorder. *Biol. Psychiatry* **47,** 512–9 (2000).
4. Courtin, J. *et al.* Prefrontal parvalbumin interneurons shape neuronal activity to drive fear expression. *Nature* **505,** 92–6 (2014).
5. Karalis, N. *et al.* 4-Hz oscillations synchronize prefrontal?amygdala circuits during fear behavior. *Nat. Neurosci.* **19,** 605–612 (2016).
6. Dejean, C. *et al.* Prefrontal neuronal assemblies temporally control fear behaviour. *Nature* **535,** 420–4 (2016).
7. Li, W., Howard, J. D., Parrish, T. B. & Gottfried, J. A. Aversive Learning Enhances Perceptual and Cortical Discrimination of Indiscriminable Odor Cues. *Science (80-.).* **319,** 1842–1845 (2008).
8. Resnik, J., Sobel, N. & Paz, R. Auditory aversive learning increases discrimination thresholds. *Nat. Neurosci.* **14,** 791–796 (2011).
9. Likhtik, E., Stujenske, J. M., Topiwala, M. A., Harris, A. Z. & Gordon, J. A. Prefrontal entrainment of amygdala activity signals safety in learned fear and innate anxiety. *Nat. Neurosci.* **17,** 106–13 (2014).
10. Stujenske, J. M., Likhtik, E., Topiwala, M. A. & Gordon, J. A. Fear and Safety Engage Competing Patterns of Theta-Gamma Coupling in the Basolateral Amygdala. *Neuron* **83,** 919–933 (2014).
11. Senn, V. *et al.* Long-range connectivity defines behavioral specificity of amygdala neurons. *Neuron* **81,** 428–37 (2014).
12. Sierra-Mercado, D., Padilla-Coreano, N. & Quirk, G. J. Dissociable roles of prelimbic and infralimbic cortices, ventral hippocampus, and basolateral amygdala in the expression and extinction of conditioned fear. *Neuropsychopharmacology* **36,** 529–38 (2011).
13. Courtin, J. *et al.* Prefrontal parvalbumin interneurons shape neuronal activity to drive fear expression. *Nature* **505,** 92–96 (2013).
14. Vidal-Gonzalez, I., Vidal-Gonzalez, B., Rauch, S. L. & Quirk, G. J. Microstimulation reveals opposing influences of prelimbic and infralimbic cortex on the expression of conditioned fear. *Learn. Mem.* **13,** 728–33 (2006).
15. Reijmers, L. G., Perkins, B. L., Matsuo, N. & Mayford, M. Localization of a Stable Neural Correlate of Associative Memory. *Science (80-.).* **317,** 1230–1233 (2007).
16. Manita, S. *et al.* A Top-Down Cortical Circuit for Accurate Sensory Perception. *Neuron* **86,** 1304–1316 (2015).
17. Rajasethupathy, P. *et al.* Projections from neocortex mediate top-down control of memory retrieval. *Nature* **526,** 653–9 (2015).
18. Kitamura, T. *et al.* Engrams and circuits crucial for systems consolidation of a memory. *Science* **356,** 73–78 (2017).
19. Otis, J. M. *et al.* Prefrontal cortex output circuits guide reward seeking through divergent cue encoding. *Nature* **543,** 103–107 (2017).
20. Holtmaat, A. & Caroni, P. Functional and structural underpinnings of neuronal assembly formation in learning. *Nat. Neurosci.* **19,** 1553–1562 (2016).
21. Komiyama, T. *et al.* Learning-related fine-scale specificity imaged in motor cortex

circuits of behaving mice. *Nature* **464,** 1182–6 (2010).
22. Sul, J. H., Jo, S., Lee, D. & Jung, M. W. Role of rodent secondary motor cortex in value-based action selection. *Nat. Neurosci.* **14,** 1202–8 (2011).
23. Lai, C. S. W., Franke, T. F. & Gan, W.-B. Opposite effects of fear conditioning and extinction on dendritic spine remodelling. *Nature* **483,** 87–91 (2012).
24. Nakayama, D. *et al.* Frontal association cortex is engaged in stimulus integration during associative learning. *Curr. Biol.* (2015). doi:10.1016/j.cub.2014.10.078
25. Sacchetti, B., Baldi, E., Lorenzini, C. A. & Bucherelli, C. Differential contribution of some cortical sites to the formation of memory traces supporting fear conditioning. *Exp. brain Res.* **146,** 223–32 (2002).
26. Uylings, H. B. M., Groenewegen, H. J. & Kolb, B. Do rats have a prefrontal cortex? *Behavioural Brain Research* (2003). doi:10.1016/j.bbr.2003.09.028
27. Paxinos, G. & Watson, C. *The rat brain in stereotaxic coordinates*. (Elsevier, 2007).
28. McDonald, A. J. Organization of amygdaloid projections to the mediodorsal thalamus and prefrontal cortex: a fluorescence retrograde transport study in the rat. *J. Comp. Neurol.* **262,** 46–58 (1987).
29. Mátyás, F., Lee, J., Shin, H.-S. & Acsády, L. The fear circuit of the mouse forebrain: connections between the mediodorsal thalamus, frontal cortices and basolateral amygdala. *Eur. J. Neurosci.* **39,** 1810–23 (2014).
30. Briggman, K. L. & Kristan, W. B. Multifunctional pattern-generating circuits. *Annu. Rev. Neurosci.* **31,** 271–94 (2008).
31. Harvey, C. D., Coen, P. & Tank, D. W. Choice-specific sequences in parietal cortex during a virtual-navigation decision task. *Nature* **484,** 62–8 (2012).
32. Gambino, F. *et al.* Sensory-evoked LTP driven by dendritic plateau potentials in vivo. *Nature* **515,** (2014).
33. Harvey, C. D., Coen, P. & Tank, D. W. Choice-specific sequences in parietal cortex during a virtual-navigation decision task. *Nature* **484,** 62–8 (2012).
34. Cheng, S. & Frank, L. M. New experiences enhance coordinated neural activity in the hippocampus. *Neuron* **57,** 303–13 (2008).
35. Wiechert, M. T., Judkewitz, B., Riecke, H. & Friedrich, R. W. Mechanisms of pattern decorrelation by recurrent neuronal circuits. *Nat. Neurosci.* **13,** 1003–1010 (2010).
36. Leutgeb, J. K., Leutgeb, S., Moser, M.-B. & Moser, E. I. Pattern Separation in the Dentate Gyrus and CA3 of the Hippocampus. *Science (80-.).* **315,** 961–966 (2007).
37. Gschwend, O. *et al.* Neuronal pattern separation in the olfactory bulb improves odor discrimination learning. *Nat. Neurosci.* **18,** 1474–1482 (2015).
38. Chow, B. Y. *et al.* High-performance genetically targetable optical neural silencing by light-driven proton pumps. *Nature* **463,** 98–102 (2010).
39. Gambino, F. & Holtmaat, A. Spike-timing-dependent potentiation of sensory surround in the somatosensory cortex is facilitated by deprivation-mediated disinhibition. *Neuron* **75,** 490–502 (2012).
40. Palmer, L. M. *et al.* NMDA spikes enhance action potential generation during sensory input. *Nat. Neurosci.* **17,** 383–390 (2014).
41. Rioult-Pedotti, M. S., Friedman, D. & Donoghue, J. P. Learning-induced LTP in neocortex. *Science* **290,** 533–6 (2000).
42. Basu, J. *et al.* Gating of hippocampal activity, plasticity, and memory by entorhinal cortex long-range inhibition. *Science (80-.).* **351,** aaa5694-aaa5694 (2016).
43. Sangha, S., Chadick, J. Z. & Janak, P. H. Safety Encoding in the Basal Amygdala. *J. Neurosci.* **33,** 3744–3751 (2013).

44. Larkum, M. A cellular mechanism for cortical associations: an organizing principle for the cerebral cortex. *Trends Neurosci.* **36,** 141–51 (2013).
45. Klavir, O., Prigge, M., Sarel, A., Paz, R. & Yizhar, O. Manipulating fear associations via optogenetic modulation of amygdala inputs to prefrontal cortex. *Nat. Neurosci.* **20,** 836–844 (2017).
46. Lavzin, M., Rapoport, S., Polsky, A., Garion, L. & Schiller, J. Nonlinear dendritic processing determines angular tuning of barrel cortex neurons in vivo. *Nature* **490,** 397–401 (2012).
47. Xu, N. *et al.* Nonlinear dendritic integration of sensory and motor input during an active sensing task. *Nature* **492,** 247–51 (2012).
48. Brandalise, F., Carta, S., Helmchen, F., Lisman, J. & Gerber, U. Dendritic NMDA spikes are necessary for timing-dependent associative LTP in CA3 pyramidal cells. *Nat. Commun.* **7,** 13480 (2016).
49. Johansen, J. P. *et al.* Optical activation of lateral amygdala pyramidal cells instructs associative fear learning. *Proc. Natl. Acad. Sci.* **107,** 12692–12697 (2010).
50. Buzsaki, G. & Draguhn, A. Neuronal Oscillations in Cortical Networks. *Science (80-.).* **304,** 1926–1929 (2004).
51. Johansen, J. P. *et al.* Hebbian and neuromodulatory mechanisms interact to trigger associative memory formation. *Proc. Natl. Acad. Sci.* **111,** E5584–E5592 (2014).
52. Hnasko, T. S. *et al.* Cre recombinase-mediated restoration of nigrostriatal dopamine in dopamine-deficient mice reverses hypophagia and bradykinesia. *Proc. Natl. Acad. Sci. U. S. A.* **103,** 8858–63 (2006).
53. Barrett, D., Shumake, J., Jones, D. & Gonzalez-Lima, F. Metabolic mapping of mouse brain activity after extinction of a conditioned emotional response. *J. Neurosci.* **23,** 5740–9 (2003).
54. Gdalyahu, A. *et al.* Associative fear learning enhances sparse network coding in primary sensory cortex. *Neuron* **75,** 121–32 (2012).
55. McGaugh, J. L. Making lasting memories: remembering the significant. *Proc. Natl. Acad. Sci. U. S. A.* **110 Suppl 2,** 10402–7 (2013).
56. Mizrahi, A., Shalev, A. & Nelken, I. Single neuron and population coding of natural sounds in auditory cortex. *Curr. Opin. Neurobiol.* **24,** 103–110 (2014).

ACKNOWLEDGEMENTS

We thank C. Mulle and A. Charlet for advice on optogenetic experiments, and A. Holtmaat and P. Fossat for their critical reading of our manuscript, and all the members of the Gambino laboratory for technical assistance and helpful discussions. We thank K. Deisseroth and the Standford University, E. Boyden and the MIT, E.J. Kremmer and the IGMM BioCampus Montpellier, L.L. Looger and D. Kim of the GENIE project, and K. Svoboda at the Janelia Farm Research Campus (HHMI) for distributing the ChR2, ArchT, Cav2-Cre, GCaMP5G and GCaMP6S vectors respectively.

This work was supported by the following grants (to FG): FP7 Marie-Curie Career Integration grant 631044, ANR JCJC grant 14-CE13-0012-01, University of Bordeaux and Initiative of Excellence (IdEx) senior chair 2014, Fondation NRJ/Institut de France grant 2015, Laboratory of Excellence (LabEx) Brain grant 2015, and the European Research Council grant ERC-StG-2015-677878.

AUTHOR CONTRIBUTION

MA and EA performed the experiments. YH and CM provided technical assistance. MA and FG conceived the studies and analyzed the data. FG supervised the research and wrote the manuscript with the help from MA and EA. Correspondence and requests for materials should be addressed to FG (frederic.gambino@u-bordeaux.fr). The authors declare no competing financial interests.

FIGURES AND LEGENDS

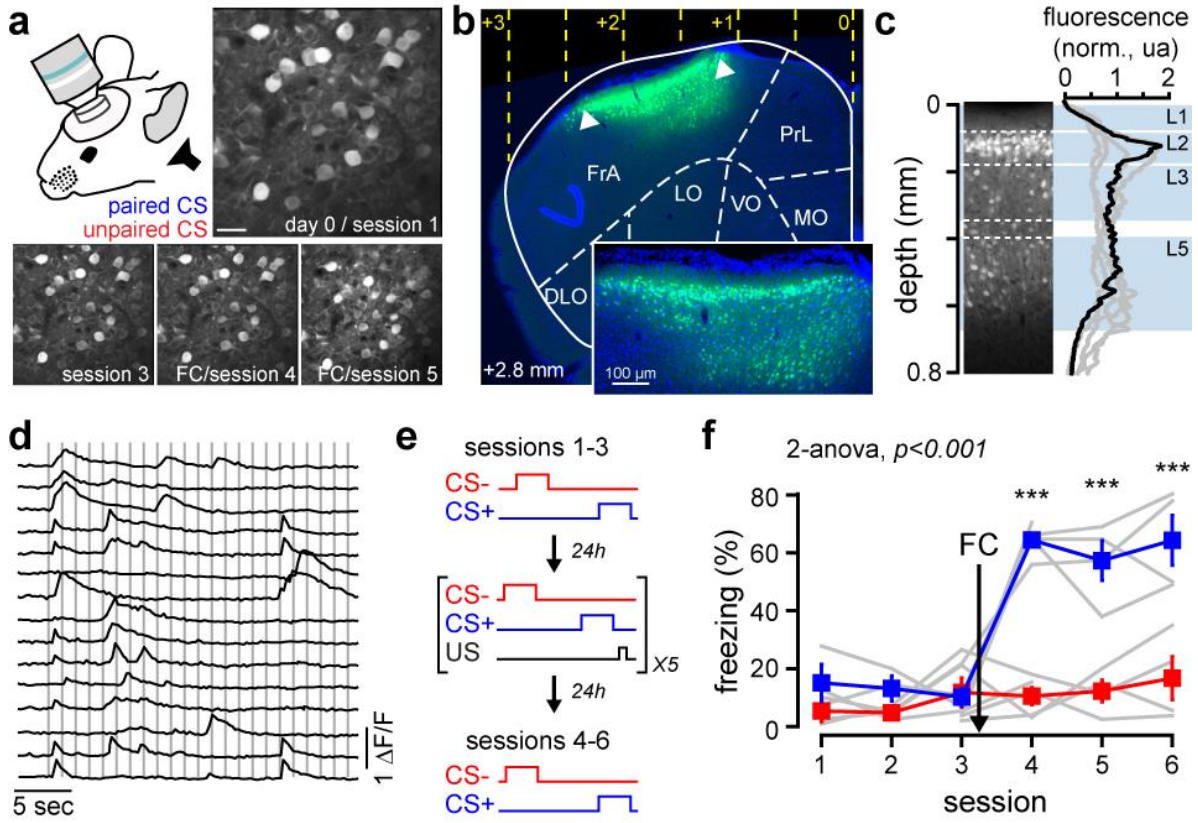

Figure1. Chronic 2-photon calcium imaging of FrA pyramidal neurons

a, Chronic 2P imaging of GCaMP5-expressing FrA neurons over 6 sessions during the presentation of paired (CS+, 8kHz) and unpaired (CS-, gaussian) auditory tones. CS, conditioned stimulus. Scale bar, 30 µm. –**b**, Representative example of the GCaMP5G expression profile in the mouse FrA (+2.8 mm from bregma). FrA, *frontal association cortex*; PrL, *prelimbinc cortex*; MO, *medial orbital cortex*; VO, *ventral orbital cortex*; LO, *lateral orbital cortex*; DLO, *dorsolateral orbital cortex*. **c**, Plot comparing the intensity profiles as a function of cortical depth of 5 different animals (4 mice were used for imaging experiments). Black line represents the example from the left (same as in **b**). Putative layers (L) are indicated in light blue. **d**, Examples of somatic calcium transients ($\Delta F/F_0$) from individual neurons recorded during one CS composed of 27 pips (grey bars: 50 ms, 0.9 Hz for 30 s). **c**, Fear conditioning protocol. US, unconditioned stimulus (footshock). **e**, Fear conditioning protocol. US, unconditioned stimulus (footshock). **f**, Fear behaviors (mean ± sem) in response to CS+ (blue) and CS- (red) were measured as percentage of freezing after each imaging session. Fear conditioning (FC) was induced between sessions 3 and 4 (arrow). Grey lines represent individual mice.

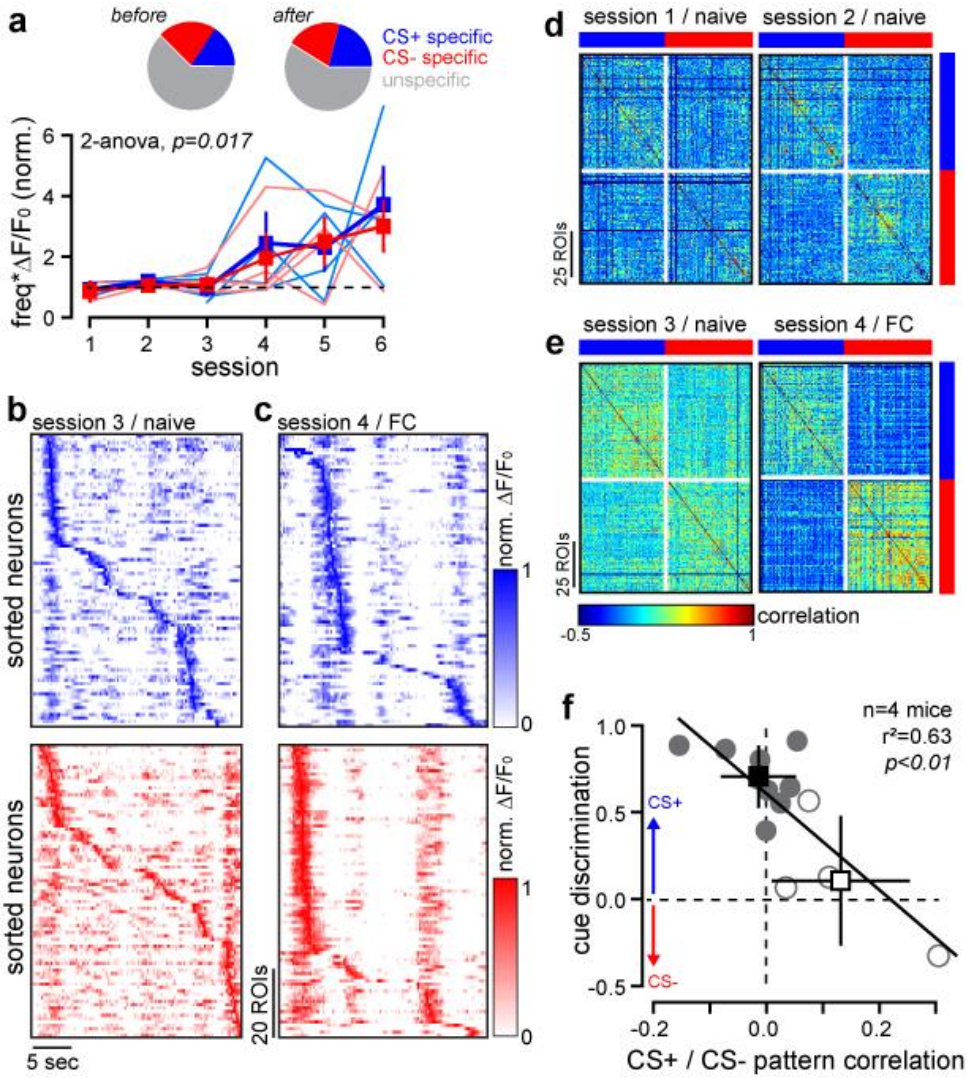

Figure 2. Learning-dependent neuronal assemblies in the FrA are associated with improved cue discrimination

a, Fear learning does not affect the global tuning properties of FrA network (top, CS+ *vs.* CS- specific, before *vs.* after, p=0.7103, χ^2=0.1380) but significantly increases the activity (bottom, frequency*$\Delta F/F_0$ of detected events normalized to the baseline activity before auditory stimulation) of individual neurons in response to both CS+ (blue) and CS- (red) (n=4; p=0.017; two way analysis of variance (anova). Error bars, sem **b, c**, Color-coded $\Delta F/F_0$ of sorted neurons from one example mouse before (**b**) and after (**c**) fear conditioning (FC). Each raw $\Delta F/F_0$ trace during CS presentation (30 s; CS+, blue; CS-, red) was normalized to the peak and sorted by its relative peak time. **d, e**, Example of correlation matrices (same mouse as in **b** and **c**). Blue, CS+; Red, CS-. To minimize bias, neurons were not categorized according to their tuning properties and matrices were computed over 30 s time window based on detected events rather than on raw fluorescence. **f**, Linear relationship (n=4 mice; r^2=0.63; p<0.01; anova) between mean Pearson correlation coefficients and behavioral performance before (session 3, white

circles) and after (sessions 4-6, grey circles) fear conditioning. Each circle represents a mouse. Squares represent averages. Error bars, sd.

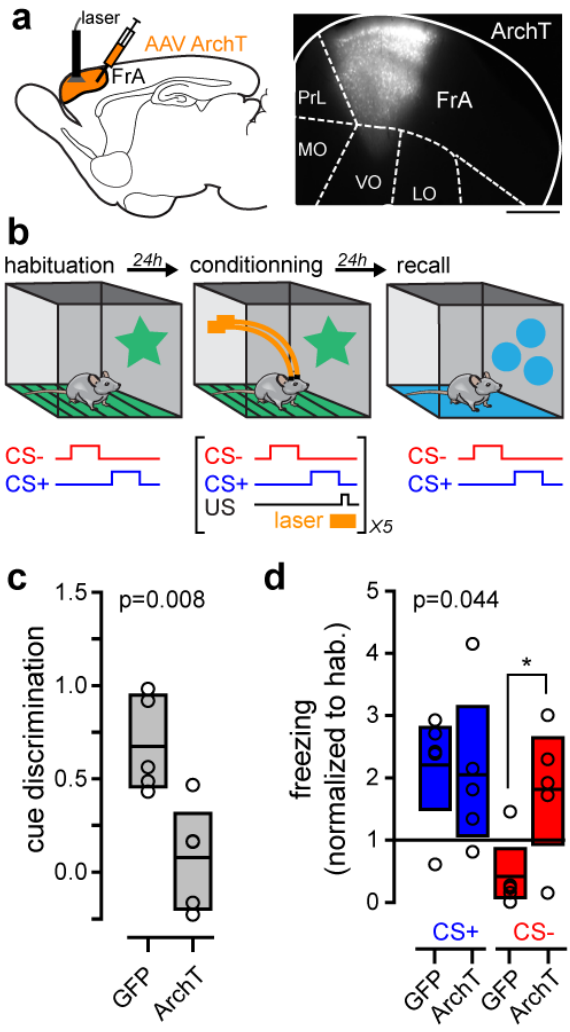

Figure 3. Optogenetic inhibition of FrA during conditioning decreases cue discrimination

a, Schematic of fear conditioning with ArchT (n=5) and GFP (n=5) expressing mice. Virus injections and optical fibers implantations in the FrA (left) were confirmed *post-hoc* with coronal brain sections (right). Scale bar, 500 µm **b**, Modified fear conditioning protocol. FrA neurons were photo-inhibited during the delivery of the footshock. **c, d**, Effect of light on cue discrimination (**c**) and freezing responses (**d**) upon auditory stimuli (GFP, n=5; ArchT, n=5; one way anova; *,p<0.05, post-hoc Holm-Sidak test). Boxplots represent mean and interquartile range. Open circles indicate individual mice.

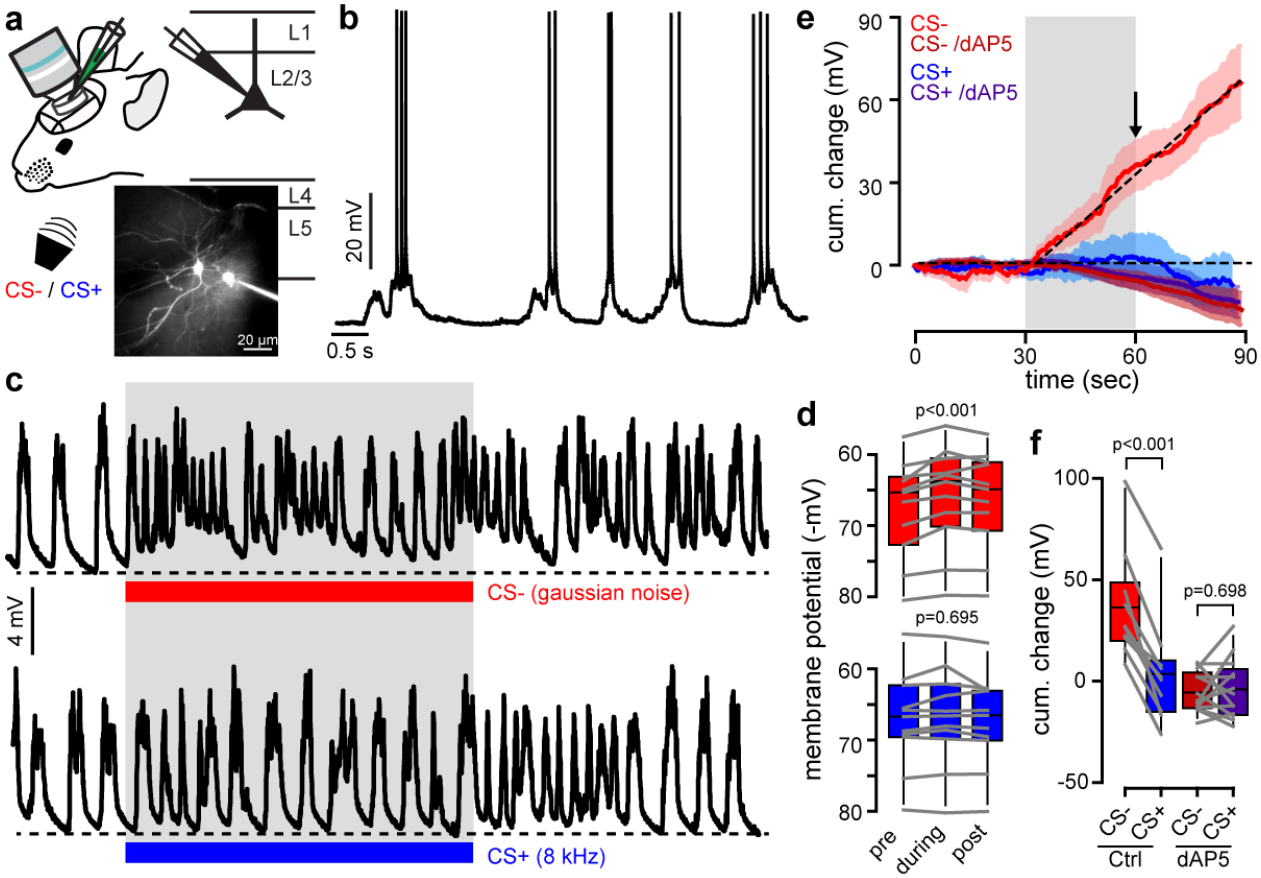

Figure 4. Gaussian stimulation evokes NMDAR-dependent, plateau potentials

a, Sensory-evoked postsynaptic potentials (PSPs) were recorded from L2/3 FrA pyramidal neuron obtained under urethane anesthesia with 2P visual guidance. **b**, Typical spontaneous slow wave fluctuations. Spontaneous overshooting spikes were occasionally observed only during up states. **c**, Example traces of postsynaptic membrane potential recorded from an individual FrA L2/3 pyramidal neuron upon gaussian (top, CS-, red) and pure (bottom, CS+, blue) auditory stimulation (27 pips, 50 ms, 0.9 Hz, 30 s). The effect of both stimuli was tested on the same cell. **d**, 30 s-averaged membrane potential before, during, and after auditory stimulation (top, gaussian noise, n=11, $p<0.001$, one way repeated measures anova; bottom, 8 kHz tone, n=10, $p=0.695$, one way repeated measures anova on ranks). Grey lines between bars indicate pairs. **e**, Averaged change (± sem) in cumulative postsynaptic membrane potential with or without the blockade of NMDARs (dAP5). Grey bar, auditory stimulation; arrow, analysis time point. **f**, Effect of dAP5 on cumulative PSPs change at the end of the stimulation (Ctrl, n=10, $p<0.001$, paired t-test; dAP5, n=13, $p=0.698$, paired t-test). Grey lines between bars indicate pairs. Boxplots represent mean and interquartile range.

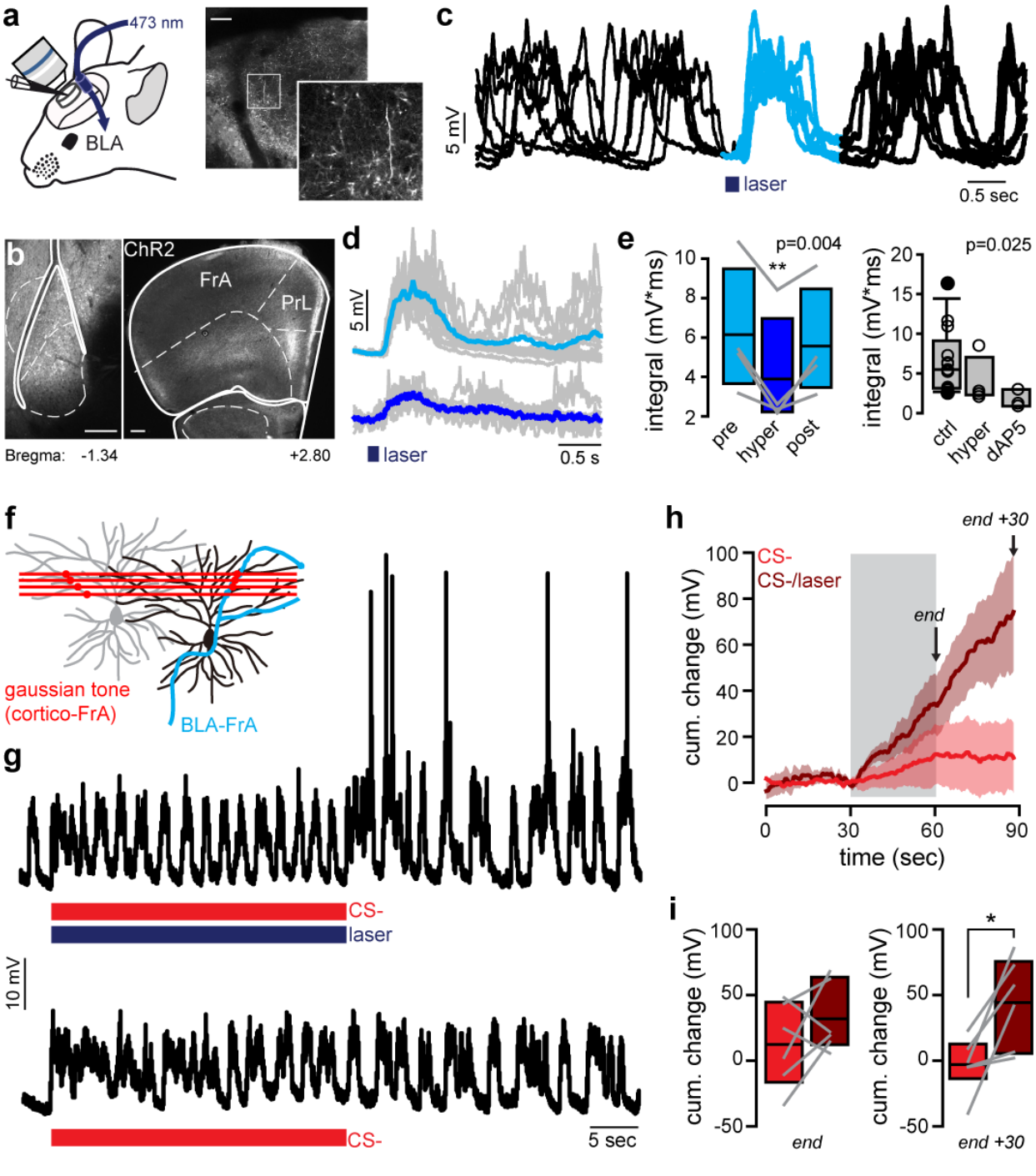
a
473 nm
BLA
c
5 mV
laser
0.5 sec
b
ChR2
FrA
PrL
Bregma: -1.34
+2.80
d
5 mV
laser
0.5 s
e
p=0.004
**
integral (mV*ms)
pre
hyper
post
p=0.025
ctrl
hyper
dAP5
f
gaussian tone
(cortico-FrA)
BLA-FrA
g
CS-
laser
10 mV
CS-
5 sec
h
end +30
CS-
CS-/laser
end
cum. change (mV)
time (sec)
i
cum. change (mV)
end
*
end +30

Figure 5. Coincident activation of BLA excitatory inputs to the FrA reinforces L2/3 pyramidal neurons

a, BLA neurons were transfected with AAV9-CamKIIa-hChR2-eYFP. Left, schematic of the *in vivo* DPSSL-mediated photostimulation (λ = 473 nm) of ChR2-expressing BLA neurons through an optical fiber. Right, examples of ChR2-expressing axons imaged before whole-cell recordings. Scale bar, 50 µm. **b**, The expression profiles of ChR2-eYFP in the BLA (left) and cortex (right) were confirmed *post-hoc*. Scale bars, 200 µm. **c**, Photostimulation of BLA neurons evoked sustained depolarizations in FrA neurons (left, blue) that shared similarities with cortical up-states (e.g decreased spontaneous variability). **d**, Examples of photostimulus-evoked PSPs in a single L2/3 cortical neuron at resting membrane potential (top) and upon cell-autonomous hyperpolarization (bottom). Grey, single trials; blue, averaged traces; blue bar, light duration. **e**, Right, BLA-mediated PSP integrals before (pre), during (hyper) and after (post) hyperpolarization (n=4, p=0.004, one way repeated measures anova; **, p=0.002, post-hoc Holm-Sidak test). Boxplots represent mean and interquartile range. Grey lines between bars indicate pairs. Left, Effect of hyperpolarization (n=4) and dAP5 (n=3) on *in vivo* FrA PSPs evoked by the photostimulation of BLA (control, n=13; p=0.025, Kruskal-Wallis one way anova on ranks). Boxplots represent median and interquartile range. Open circles indicate individual mice. Filled circles indicate outliers **f**, Co-activation protocol. ChR2-expressing BLA neurons were photo-stimulated during auditory stimulation. **g**, Example traces of postsynaptic membrane potential recorded from individual FrA L2/3 pyramidal neuron upon gaussian (CS-) auditory stimulation paired (top) or not (bottom) with BLA photoactivation. Red and blue bars below the traces indicate the duration of the stimulation. **h**, Averaged change (± sem) in cumulative postsynaptic membrane potential (n=6) upon paired (dark red, CS-/laser) and unpaired (red, CS-) auditory stimulation. The analysis was restricted to the end of the (co-) stimulation (end arrow) and 30 s later (end+30 arrow). **i**, Effect of photostimulation on CS-evoked cumulative change at the end of the stimulation (left; n=6, p=0.245, paired t-test) and 30 s later (right; n=6, *, p=0.023, paired t-test). Boxplots represent mean and interquartile range. Grey lines between bars indicate pairs.

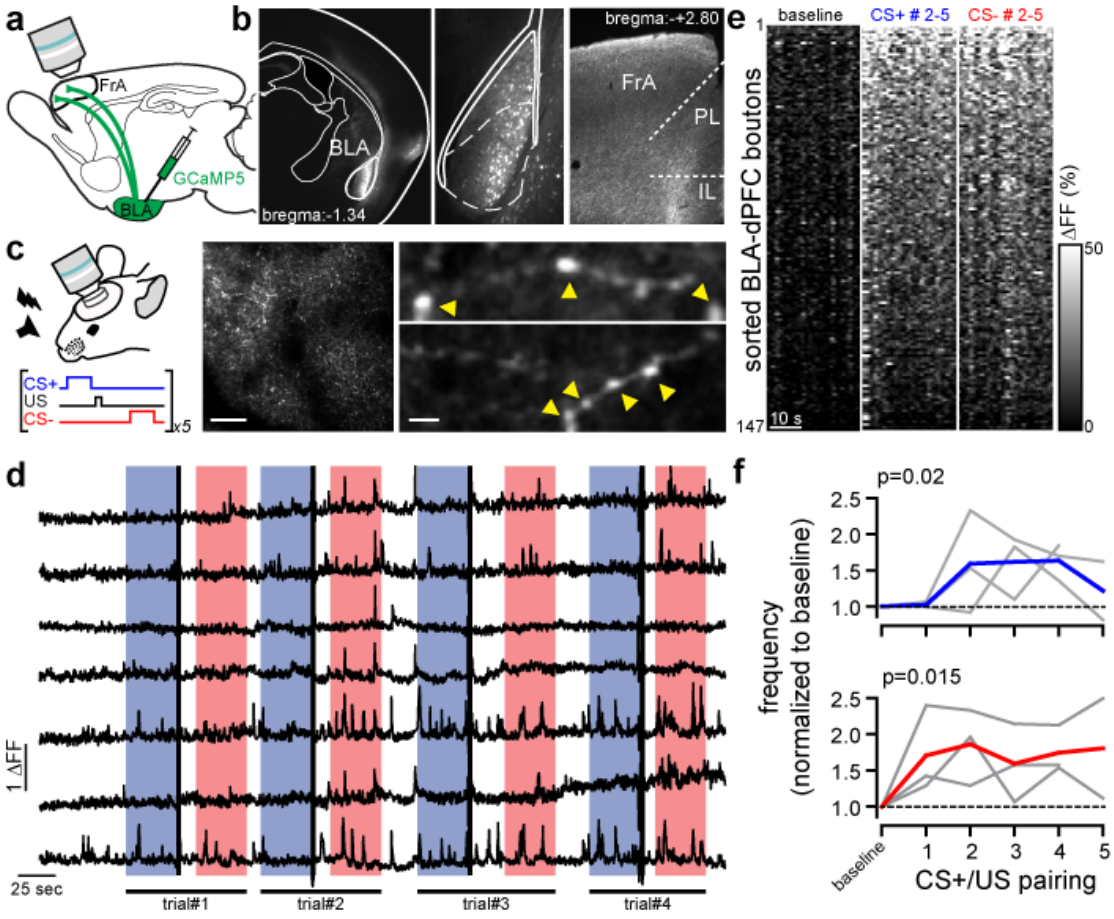

Figure 6. Activation of BLA-to-FrA projecting axons during conditioning

a, Schematic of the experimental protocol. BLA neurons were transfected with AAV1-hSyn-GCAMP5G and their boutons were imaged in the superficial layer of the FrA. **b**, Expression profiles of GCaMP5 in the BLA (left) and FrA (right). PL, prelimbic cortex; IL, infralimbic cortex. **c**, GCaMP5-expressing mice were fear conditioned under the microscope (left), and GCaMP5-expressing axons (middle) and individual presynaptic boutons (right, yellow arrowheads) were imaged in the FrA during conditioning. Scale bars, 50 µm (middle), 2 µm (right). **d**, Examples of calcium transients ($\Delta F/F_0$) from individual boutons recorded from one mouse upon 4 consecutive CS+ / US pairings. Blue bars, CS+; red bars, CS-; black bars, footshock (US). Each CS is composed of 27 pips (50 ms in duration at 0.9 Hz for 30 s). **e**, Color-coded $\Delta F/F_0$ of 147 individual boutons from one example mouse during baseline, CS+ (blue) and CS- (red) auditory stimuli. $\Delta F/F_0$ from trials 2 to 5 were averaged. **f**, Frequency of detected calcium events during CS+ (top, blue; baseline *vs.* CS+#2-4, p=0.019, χ^2=5.5) and CS-(bottom, red; baseline *vs.* CS-#2-4, p=0.0153, χ^2=5.8) presentation. Grey lines indicate individual mouse. Color lines represent mean.

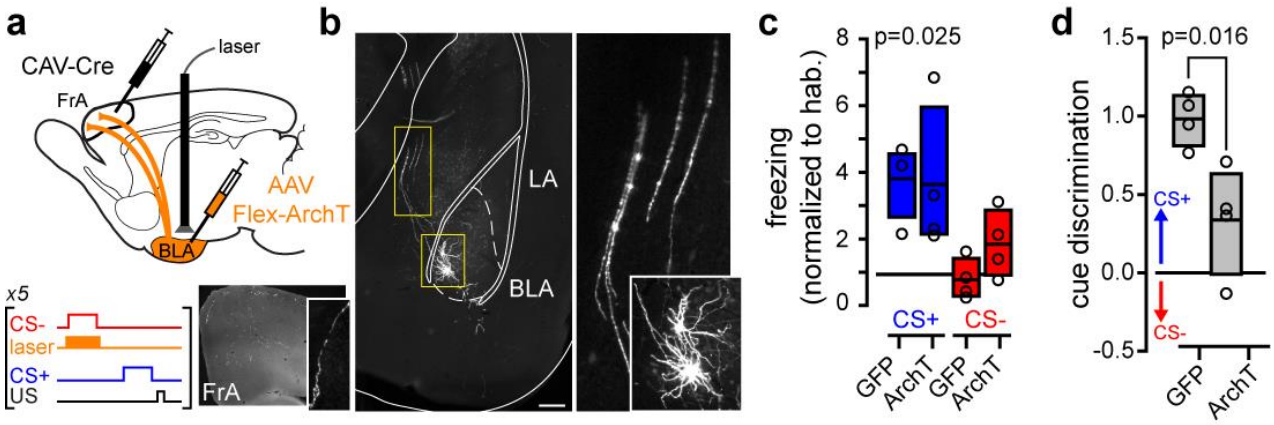

Figure 7. BLA-to-FrA projecting neurons mediate discriminative learning

a, Schematic of fear conditioning with ArchT (n=4) and GFP (n=4) BLA-to-FrA expressing mice. BLA axons were visible in the FrA (bottom right). BLA neurons that project to FrA were specifically photo-inhibited during the presentation of the CS- (bottom left). **b**, Examples of neurons and axons projecting from the BLA to the FrA. LA, lateral amygdala. Scale bar, 200 µm. **c, d**, Effect of light on freezing responses (**c**) and cue discrimination (**d**) upon auditory stimuli (GFP, n=4; ArchT, n=4; one way anova). Boxplots represent mean and interquartile range. Open circles indicate individual mice.

METHODS

Animals

All experiments were performed in accordance with the Guide for the Care and Use of Laboratory Animals (National Research Council Committee (2011): Guide for the Care and Use of Laboratory Animals, 8th ed. Washington, DC: The National Academic Press.) and the European Communities Council Directive of September 22th 2010 (2010/63/EU, 74). Experimental protocols were approved by the institutional ethical committee guidelines for animal research (N°50DIR_15-A) and by the French Ministry of Research (N°02169.01). We used male C57Bl6/J 6-weeks old mice from Charles River that were housed with littermates (3-4 mice per cage) in a 12-h light-dark cycle. Cages were enriched and food and water were provided *ad libitum*.

Surgery and virus injection

Mice were anesthetized with an intraperitoneal (i.p.) injection of a mix containing medetomidine (sededorm, 0.27 mg kg^{-1}), midazolam (5 mg kg^{-1}) and fentanyl (0.05 mg kg^{-1}) in sterile NaCl 0.9% (MMF-mix). Analgesia was achieved by local application of 100 µl of lidocaine (lurocaine, 1%) and subcutaneous (s.c.) injection of buprenorphine (buprécare, 0.05 mg kg^{-1}). 40 µl of dexamethasone (dexadreson, 0.1mg ml^{-1}) was administrated intramuscularly (i.m.) in the quadriceps to prevent inflammation potentially caused by the friction of the drilling. A heating-pad was positioned underneath the animal to keep the body temperature at 37ºC. Eye dehydration was prevented by topical application of ophthalmic gel. The skin above the skull was disinfected with modified ethanol 70% and betadine before an incision was made. Stereotaxic injections were done as previously described[32] . Briefly, the bregma and lambda were aligned (x and z) and a hole for injection was made using a pneumatic dental drill (BienAir Medical Technologies, AP-S001). The injections were targeted either to the layer 2/3 of the FrA (from bregma: AP, +2.8 mm; DV, -0.2-0.3 mm; ML ±1.0 mm) or to the BLA (from bregma: AP, -1.3 mm; DV, -4.5 to 4.8 mm; ML, ±2.9 mm), or to both at the same time. 200 nl of virus were injected at a maximum rate of 60 nl/min, using a glass pipette (Wiretrol, Drummond) attached to an oil hydraulic manipulator (MO-10, Narishige).

The following viruses were used depending on the experiments. AAV-ChR2 (AAV9.CamKIIa.hChR2(H134R).eYFP.WPRW.SV40, 1.03 x 10^{14} GC ml^{-1}, Penn Vector Core, provided by K. Deisseroth) was unilaterally injected in the right BLA, whereas AAV-

ArchT (AAV9.CAG.ArchT.GFP.WPRE.SV40, 5.66 x 10^{12} GC ml^{-1}, Penn Vector Core, provided by Ed Boyden and the MIT), AAV-ArchT-Flex (AAV2/9.CBA.flex.Arch-GFP.WPRE.SV40, Penn Vector Core, provided by Ed Boyden and the MIT), Cav-Cre (Cav2.CMV.Cre, IGMM BioCampus Montpellier) were bilaterally injected into the BLA or FrA. Control experiments were performed using an AAV containing the DNA construct for only GFP (AAV9.CamKII0.4.eGFP.WPRE.rBG, 5.27 x 10^{13} GC ml^{-1}, Penn Vector Core) or GFP-DIO (AAV2/9.EF1a.DIO.eYFP.WPRE.hGH 2.46 x 10^{13} GC ml^{-1}, Penn Vector Core, provided by K. Deisseroth). For somatic calcium imaging, AAV-GCaMP5G (AAV1.hSyn.GCAMP5g.(GCAMP3-T302L.R303P.D380Y).WPRE.SV40, Penn Vector Core, 2.13x10^{13} GC ml^{-1}, Penn Vector Core) was injected to the FrA immediately after the craniotomy was made. The same virus was used for the calcium imaging of BLA-FrA boutons, but the injection was targeting the right BLA. After injections, the viruses were allowed to diffuse for at least 10 min before the pipette was withdrawn. Mice were then either prepared for cranial window implantation or waked-up by a sub-cutaneous injection of a mixture containing atipamezole (revertor, 2.5 mg kg^{-1}), flumazenil (0.5 mg kg^{-1}), and buprenorphine (buprécare, 0.1 mg kg-1) in sterile NaCl 0.9% (AFB-mix).

To evaluate the viral expression profiles in BLA and dPFC, fixed brain slices were imaged post-hoc using a wide-field epifluorescence microscope (Nikon, Eclipse N-iU). Illumination was set such that the full dynamic range of the 16-bit images was utilized. A two-dimensional graph of the intensities of pixel was plot using Fiji Software. 16-bit images' brightness was processed and masks were registered to the corresponding coronal plates (ranging from -1.94 to -2.70 mm) of the mouse brain atlas[27] using Illustrator (Adobe), at various distances antierior (FrA) or posterior (BLA) to the bregma.

Behavior

At least 5 days before starting behavior, mice went through handling with the same experimenter that performed the experiments in order to decrease stress. On the first day of the protocol, mice were placed on the conditioning compartment (context A, consisting on a squared box with grid floor that allows the release of a foot shock and with home cage litter under; cleaned between individuals with 70% ethanol) for habituation, where two conditional stimuli (CS) (CS+: 8 kHz; CS-: white noise pips; composed of 27 pips, 50 ms, 0.9 Hz for 30 s) were presented 4 times with a 80 dB sound pressure level and variable inter stimulus interval (ISI). The freezing time during each CS

presentation was measured and the mice returned to their home cage. 24 hours later mice were exposed to context A and 5 CS+ were paired with the unconditional stimulus (US, 1s foot shock at 0.6 mA) with the onset coinciding with the CS+ offset. 5 CS- presentations were intermingled with CS+ presentations with a variable (10-60 s) ISI during the test (Fig. S2). Recall tests were carried out 24 hours after the conditioning phase by measuring the freezing time during the presentation of 2 CS+ and 2 CS- in a new context (context B, consisting of a cylindrical white compartment with home cage litter on the floor; cleaned between individuals with septanios MD 2%). Freezing behavior was quantified automatically in each behavioral session using a fire-wire CCD-camera connected to automated freezing detection software (AnyMaze, Ugo Basile, Italy).

For the experiments in which the conditioning phase was taken place under the 2 photon microscope (Fig. 4), the behavior context consisted on the microscope box in which the mice were head-restrained in a custom tube containing with a shocking grid at the bottom. CS and US presentations were triggered by a MATLAB routine, associated to a pulse-stimulator (Master-8, A.M.P.I) capable of triggering the foot shock. For optogenetic experiments using *archeorhodopsin* (ArchT) or GFP controls (Fig. 1), mice were subjected to the same behavioral protocol described above, but light-induced neuronal network inhibition of the FrA during conditioning phase was obtained by applying a 3 second-lasting yellow laser stimulation during the pairings between CS+ and US (since the last second of CS+ presentation until 2 seconds after US termination). Optogenetic inhibition of BLA-to-FrA projections during the CS- presentation of the conditioning phase (Fig. 4) was achieved by synchronizing the 50 ms laser pulses with the 50 ms pip of the CS- presentations.

2-photon laser-scanning microscope (2PSLM)-based calcium imaging.

The cranial windows were made as previously described[32]. Briefly, after skull's exposure a ~5 mm plastic chamber was attached on the area of interest and a 3 mm craniotomy was made on the right hemisphere above FrA and M2, with a pneumatic dental drill, leaving the dura intact. The craniotomy was covered with sterile saline (0.9% NaCl) and sealed with a 3 mm glass cover slip after viral injection (for imaging experiments). The chamber, the cover slip and a custom-made stainless steel head stage

were well attached to the skull using dental acrylic and dental cement (Jet Repair Acrylic, Lang Dental Manufacturing).

Head-fixed awake mice were placed and trained under the microscope every day for at least 7 days prior to the experiment, and then imaged 21 to 35 days after virus injection using an *in vivo* non-descanned FemtoSmart 2PLSM (Femtonics, Budapest, Hungary) equipped with a ×16 objective (0.8 NA, Nikon). The MES Software (MES v.4.6; Femtonics, Budapest, Hungary) was used to control the microscope, the acquisition parameters, and the TTL-driven synchronization between the acquisition and auditory/footshock stimuli. The GCaMPs were excited using a Ti:sapphire laser operating at λ=910 nm (Mai Tai DeepSee, Spectra-Physics) with an average excitation power at the focal point lower than 50 mW. Time-series images were acquired within a field-of-view of 300 x 300 µm (for axons and somas, 256 lines, 1ms/line). Each imaging session consisted of 30 s of baseline recording followed by 8 gaussian and 8 pure (8kHz)-tone auditory stimuli delivered in a pseudorandom order. We imaged on average 3500 frames (~900 s) per session, and no visible photo-bleaching was observed. Images were then analyzed as previously described[32] using custom routines written in Fiji and Matlab (Mathworks). We registered images over time and corrected XY motion artifacts within a single imaging session by using cross-correlation based on rigid body translation (Stack aligner, Image J, NIH, USA). Motion corrections were then assessed by computing pair-wise 2D correlation coefficient (Image correlation, Image J, NIH, USA), and frames were discarded from the analysis if lower than 0.7. Similar rigid body translation was used to align inter-sessions images with the session 4 (first session post learning) selected as a reference template. Regions of interest (ROIs) for pyramidal neurons and putative axonal boutons were selected and drawn manually. All pixels within each ROI were first averaged providing a single time-series of raw fluorescence. To limit the effect of fluorescence drift over time, peaks of fluorescence were first detected, and the baseline fluorescence (F_0) was calculated as the mean of the lower 50% of previous 10 s fluorescence values. Change in fluorescence ($\Delta F_t/F_0$) was defined as $(F_t-F_0)/F_0$, were F_t is the fluorescence intensity at time *t (*time of the first pixel in each frame). Calcium events were then detected using a template-based method with a custom library of calcium transients. Each detected event was inspected visually and analysis was restricted to detected events rather than on raw fluorescence. To measure correlations between neurons within a single population, the activity of each recorded neuron was normalized

to the activity during baseline prior to auditory stimulation. Detected events ($\Delta F/F_0$) upon 30 s-lasting auditory stimulation were binned (1 sec), averaged over 8 trials, and organized in a *n* x 30 two-dimensional matrix (n=number of ROIs per animal). Pearson's coefficient of correlations were then computed between CS+ and CS- related matrices.

In vivo whole cell recordings

Isoflurane (4% with ~0.5 l min^{-1} O_2) combined with an i.p. injection of urethane (1.5 g kg^{-1}, in lactated ringer solution containing in [mM] 102 NaCl, 28 Na L Lactate, 4 KCl, 1.5 $CaCl_2$) was used to induce anesthesia and prolonged by supplementary urethane (0.15 g kg^{-1}) if necessary. To prevent risks of inflammation, brain swelling and salivary excretions, 40 µl of dexamethasone (dexadreson, 0.1 mg ml^{-1}, i.m.) and glycopyrrolate (Robinul-V, 0.01 mg kg^{-1}, s.c.) were injected before the surgery. Adequate anesthesia (absence of toe pinch and corneal reflexes, and vibrissae movements) was constantly checked and body temperature was maintained at 37°C using a heating-pad positioned underneath the animal. Ophthalmic gel was applied to prevent eye dehydration. Analgesia was provided as described for viral injection (with lidocaine and buprenorphine). After disinfection of the skin (with modified ethanol 70% and betadine), the skull was exposed and a ~3mm plastic chamber was attached to it above the prefrontal cortex using a combination of super glue (Loctite) and dental acrylic and dental cement (Jet Repair Acrylic, Lang Dental Manufacturing). A small ~1 x 1 mm craniotomy centered above the FrA (+2.8 mm from bregma, ±1.0 mm midline) was made using a pneumatic dental drill, leaving the dura intact.

Whole-cell patch-clamp recordings of L2/3 pyramidal neurons were obtained as previously described[32] Briefly, high-positive pressure (200–300 mbar) was applied to the pipette (5–8 MΩ) to prevent tip occlusion, when passing the pia. Immediately after, the positive pressure was reduced to prevent cortical damage. The pipette resistance was monitored in the conventional voltage clamp configuration during the descendent pathway through the cortex (until -200 µm from the surface) of 1 µm steps. When the pipette resistance abruptly increased, the 3–5 GΩ seal was obtained by decreasing the positive pressure. After break-in, Vm was measured, and dialysis was allowed to occur for at least 5 min before launching the recording protocols. Current-clamp recordings were made using a potassium-based internal solution (in mM: 135 potassium gluconate, 4 KCl, 10 HEPES, 10 Na2-phosphocreatine, 4 Mg-ATP, 0.3 Na-GTP, and 25 µM, pH adjusted

to 7.25 with KOH, 285 mOsM), and acquired using a Multiclamp 700B Amplifier (Molecular Devices). Spontaneous activity was recorded prior, during and after the presentation of the CS- and the CS+. Spiking pattern of patched cells was analyzed to identify pyramidal neurons. dAP5 (1 mM, Tocris) was topically applied to the dura mater, before whole cell recordings. Offline analysis was performed using custom routines written in Sigmaplot (Systat), IGOR Pro (WaveMetrics) and Matlab (Mathworks).

In vivo optogenetics

After virus injection for ChR2 or ArchT expression, mice were subsequently implanted with fiber optic cannula for optogenetics (CFML22U, Thorlabs) in the FrA or BLA. The optic fibers were previously cleaved with a fiber optic scribe (S90R, Thorlabs) at 4.5mm for BLA, or 0.4-0.5 mm for superficial implantation in FrA. The cannula were guided and stereotaxically inserted inside the brain with the help of a cannula holder (XCL, Thorlabs) through the same burr hole used for the viral injections (FrA coordinates from bregma: AP, +2.8 mm; DV, -0.5 mm; ML, ±1.0 mm; BLA coordinates from bregma: AP, -1.3mm; DV, -4.5 mm; ML, ±2.9mm) and secured in place with a mix of super glue (Loctite) and dental acrylic and dental cement (Jet Repair Acrylic, Lang Dental Manufacturing). Anesthesia was reversed using AFB-mix for mice assigned to behavioral experiments. For *in vivo* photostimulation of ChR2-expressing BLA neurons, the fiber optic cannula and the optogenetic patch cable (M83L01, Thorlabs) were connected through a ceramic split mating sleeve (ADAL1, Thorlabs). The patch cable was then coupled to a blue DPSS laser (SDL-473-050MFL, Shanghai Dream Lasers Technology) which was triggered by a pulse-stimulator (Master-9, A.M.P.I), able to synchronize 50 ms laser pulses with 50 ms sound pips composing the CS. For inhibition of FrA or BLA-to-FrA projections during learning, *in vivo* bilateral optic stimulation of ArchT-expressing neurons was achieved by coupling the optic fibers implanted in FrA or BLA, respectively to a multimode fiber optic coupler (FCMH2-FCL, Thorlabs), with a ceramic split mating sleeve, and subsequently connected to a yellow DPSS laser (SDL-LH-1500, Shanghai Dream Lasers Technology).

In vitro whole-cell recordings

Mice were anesthetized with a mixture of ketamine/xylazine (100mg/kg and 10mg/kg respectively) and cardiac-perfused with ice-cold, oxygenated (95% O2, 5%

CO2) cutting solution (NMDG) containing (in mM): 93 NMDG, 93 HCl, 2.5 KCl, 1.2 NaH2PO4, 30 NaHCO3, 25 Glucose, 10 MgSO4, 0.5 CaCl2, 5 Sodium Ascorbate, 3 Sodium Pyruvate, 2 Thiourea and 12mM N-Acetyl-L-cysteine (pH 7.3-7.4, with osmolarity of 300-310 mOsm). Brains were rapidly removed and placed in ice-cold and oxygenated NMDG cutting solution (described above). Coronal slices (300 μm) were prepared using a Vibratome (VT1200S, Leica Microsystems, USA) and transferred to an incubation chamber held at 32°C and containing the same NMDG cutting solution. After this incubation (9-11 min), the slices were maintained at room temperature in oxygenated modified ACSF containing (mM): 92 NaCl, 2.5 KCl, 1.2 NaH2PO4, 30 NaHCO3, 20 HEPES, 25 Glucose, 2 MgSO4, 2 CaCl2, 5 Sodium Ascorbate, 3 Sodium Pyruvate, 2 Thiourea and 12mM N-Acetyl-L-cysteine (pH 7.3-7.4, with osmolarity of 300-310 mOsm) until recording.

Whole-cell recordings of layer 2/3 FrA principal neurons were performed on coronal slices (from bregma: +2.58 mm to +3.08 mm) at 30-32ºC in a superfusing chamber. Patch electrodes (3-5 MΩ) were pulled from borosilicate glass tubing and filled with a K-gluconate-based intracellular solution (in mM: 140 K-gluconate, 5 QX314-Cl, 10 HEPES, 10 phosphocreatine, 4 Mg-ATP and 0.3 Na-GTP (pH adjusted to 7.25 with KOH, 295 mOsm). BLA-to-dPFC monosynaptic EPSCs were elicited by 1-50 ms light stimulations delivered by an ultrahigh power 460 nm LED (Prizmatix Ltd, Israel). Data were recorded with a Multiclamp700B (Molecular Devices, USA), filtered at 2 kHz and digitized at 10 kHz. Data were acquired and analysed with pClamp10.2 (Molecular Devices).

Data availability and Statistics

All data generated or analysed during this study are included in the manuscript. Data are presented as the mean ± interquartile range, except where stated differently. All statistics were performed using Matlab (Mathworks) and Sigmaplot (Systat) with an α significant level set at 0.05. Normality of all value distributions and the equality of variance between different distributions were first assessed by the Shapiro-Wilk and Levene median tests, respectively. Standard parametric tests were only used when data passed the normality and equal variance tests ($p>0.05$). Non-parametric tests were used otherwise. Only two-sided tests were used. When applicable, pair-wise multiple post-hoc comparisons were done by using the Holm-Sidak method. Randomization and blinding

methods were not used. No statistical methods were used to estimate sample size, but β-power values were calculated for parametric tests and are provided in the tables below.

Figure 1f

Group	N	Missing	Mean	Standard deviation	Standard error
CS+, Session1	5	2	15.111	11.108	6.413
CS+, Session2	5	2	13.167	7.485	4.322
CS+, Session3	5	0	10.100	6.866	3.071
CS+, Session4	5	0	64.467	5.275	2.359
CS+, Session5	5	1	57.333	13.738	6.869
CS+, Session6	5	1	64.333	17.159	8.580
CS-, Session1	5	2	5.333	6.405	3.698
CS-, Session2	5	2	4.778	2.417	1.396
CS-, Session3	5	0	11.733	11.267	5.039
CS-, Session4	5	0	10.500	6.669	2.982
CS-, Session5	5	1	12.250	7.377	3.688
CS-, Session6	5	1	16.667	14.875	7.438

Shapiro-Wilk test : p=0.805 (normality passed)	**Levene median test: p=0.312 (equality of variance passed)**

Two-way analysis of variance (general linear model):

Source of variation	Degrees of freedom	Sum of squares	Mean squares	F-ratio	*P-value*	Significant?	β power
CS	1	8505.499	8505.499	82.427	<0.001	yes	1
Session	5	9082.340	1816.468	17.603	<0.001	yes	1
Interaction	5	6308.417	1261.683	12.227	<0.001	yes	1
Residual	36	3714.765	103.188				
Total	47	28942.981	615.808				

Multiple comparison procedures (Holm-Sidak method):

Comparison	Difference of means	t-value	*P-value*	Significant?
CS+, session 4 vs session 3	54.367	8.462	<0.001	yes
CS+, session 5 vs session 3	47.233	6.932	<0.001	yes
CS+, session 6 vs session 3	54.233	7.959	<0.001	yes
CS-, session 4 vs session 3	1.233	0.192	0.849	no
CS-, session 5 vs session 3	0.517	0.0758	0.940	no
CS-, session 6 vs session 3	4.933	0.724	0.474	no

Figure 2a

Group	N	Missing	Mean	Standard deviation	Standard error
CS+, Session1	4	2	0.919	0.339	0.240
CS+, Session2	4	1	1.195	0.0721	0.0416
CS+, Session3	4	0	0.971	0.443	0.221
CS+, Session4	4	0	2.443	1.987	0.994
CS+, Session5	4	0	2.301	1.517	0.758
CS+, Session6	4	0	3.723	2.437	1.219
CS-, Session1	4	2	0.858	0.453	0.320
CS-, Session2	4	1	1.053	0.0454	0.0262
CS-, Session3	4	0	1.092	0.428	0.214
CS-, Session4	4	0	1.951	1.587	0.793
CS-, Session5	4	0	2.503	1.558	0.779
CS-, Session6	4	0	2.999	1.625	0.812

Shapiro-Wilk test : p<0.05 (normality failed)	**Levene median test: p=0.503 (equality of variance passed)**

Two-way analysis of variance (general linear model):

Source of variation	Degrees of freedom	Sum of squares	Mean squares	F-ratio	*P-value*	Significant?	β power
CS	1	0.327	0.327	0.161	0.691	no	-
Session	5	33.402	6.680	3.296	0.017	yes	-
Interaction	5	1.273	0.255	0.126	0.985	no	-
Residual	30	60.800	2.027				
Total	41	95.878	2.338				

Multiple comparison procedures (Holm-Sidak method):

Comparison	Difference of means	t-value	*P-value*	Significant?
session 3 vs session 1	0.143	0.164	0.871	no
session 3 vs session 2	0.0926	0.120	0.905	no
session 3 vs session 4	1.165	1.637	0.112	no
session 3 vs session 5	1.371	1.926	0.064	no
session 3 vs session 6	2.330	3.273	0.003	yes
session 3 vs session 1	0.143	0.164	0.871	no

Figure 2f

Group	[pearson correlation coefficient; cue discrimination]	
Session 3	[0.3047;0.3298], [0.1111;0.1233], [0.0351;0.0638], [0.0753; 0.5636]	**Shapiro-Wilk test : p=0.8771**
Session 4	[0.0543; 0.9087], [0.0422; 6427], [-0.0134; 0.6883], [-0.1544; 0.8835]	
Session 5	[0.0254; 0.5506], [2.7958e-3; 0.6242]	**Levene median test: p=0.2212**
Session 6	[-6.9924e-4; 0.3931], [-0.0725; 0.8608], [-0.0112; 0.8018]	

Non-linear regression (polynomial, y = a*x+b):

	Coefficient	Standard error	t-value	*P-value*
a	-2.7852	0.6341	-4.3925	0.0011
b	0.6065	0.0674	9.0003	<0.0001
R	0.7981	0.2326		

Analysis of variance (corrected for the mean of the observations):

Source of variation	Degrees of freedom	Sum of squares	Mean squares	F-ratio	*P-value*	Significant?	β power
Regression	1	1.0442	1.0442	19.2937	0.0011	yes	-
Residual	11	0.5954	0.0541				-
Total	12	1.6396	0.1366				

Figure 3c

Group	N	Missing	Mean	Standard deviation	Standard error
GFP	5	0	0.674	0.255	0.114

ArchT	5	0	0.0785	0.282	0.126
Shapiro-Wilk test : p=0.277			**Levene median test: p=0.932**		

Student t-test							
Source of variation	**Degrees of freedom**	**Difference of means**	**t-value**	**95% confidence interval**	***P-value***	**Significant?**	**β power**
GFP vs ArchT	8	0.596	3.499	0.203 to 0.988	0.044	yes	0.845

Figure 3d

Group	**N**	**Missing**	**Mean**	**Standard deviation**	**Standard error**
CS+ GFP	5	0	2.204	0.923	0.413
CS+ ArchT	5	0	2.046	1.278	0.571
CS- GFP	5	0	0.418	0.587	0.262
CS- ArchT	5	0	1.813	1.053	0.471
Shapiro-Wilk test : p=0.671			**Levene median test: p=0.667**		

One-way analysis of variance (general linear model):							
Source of variation	**Degrees of freedom**	**Sum of squares**	**Mean squares**	**F-ratio**	***P-value***	**Significant?**	**β power**
Between Groups	3	10.022	3.341	3.394	0.044	yes	0.486
Residual	16	15.750	0.984				
Total	19	25.772					

Multiple comparison procedures (Holm-Sidak method):				
Comparison	**Difference of means**	**t-value**	***P-value***	**Significant?**
CS+ GFP vs CS- GFP	1.786	2.846	0.012	yes
CS+ ArchT vs CS- GFP	1.628	2.594	0.020	yes
CS- ArchT vs CS- GFP	1.395	2.223	0.041	yes
CS+ GFP vs CS- ArchT	0.391	0.624	0.542	no
CS+ ArchT vs CS- ArchT	0.233	0.372	0.715	no
CS+ GFP vs. CS+ ArchT	0.158	0.252	0.804	no

Figure 4d (top)

Treatments	N	Missing	Mean	Standard deviation	Standard error
CS- pre	11	0	67.556	6.869	2.071
CS- during	11	0	65.966	7.160	2.159
CS- post	11	0	66.432	6.955	2.097
Shapiro-Wilk test : p=0.506				**Levene median test: p=0.792**	

One-way repeated measures analysis of variance (general linear model):							
Source of variation	**Degrees of freedom**	**Sum of squares**	**Mean squares**	**F-ratio**	***P-value***	**Significant?**	**β power**
Between Subjects	10	1460.046	146.005				
Between Treatments	2	14.716	7.358	18.109	<0.001	yes	1
Residual	20	8.127	0.406				

Multiple comparison procedures (Holm-Sidak method):				
Comparison	**Difference of means**	**t-value**	***P-value***	**Significant?**
pre vs during	1.591	5.853	<0.001	yes
pre vs post	1.125	4.139	<0.001	yes
post vs during	0.466	1.714	0.102	no

Figure 4d (bottom)

Treatments	N	Missing	Median	25%	75%
CS- pre	11	0	66.711	63.108	69.482
CS- during	11	0	66.604	62.517	69.525
CS- post	11	0	66.522	63.077	69.912
Shapiro-Wilk test : p<0.05					

Friedman repeated measures analysis of variance on ranks:					
Source of variation	**Degrees of freedom**	**χ^2**	***P-value***	**Significant?**	**β power**
Between treatments	2	0.725	0.698	no	-

Figure 4f

Group	N	Missing	Mean	Standard deviation	Standard error
CS- ctrl	10	0	36.268	26.714	8.448
CS+	10	0	3.485	25.384	8.027
Difference ctrl	10	0	32.783	12.934	4.090
CS- dAP5	13	0	-5.592	9.972	2.766
CS+ dAP5	13	0	-4.122	14.737	4.087
Difference dAP5	13	0	-1.471	13.324	3.695
Shapiro-Wilk test : p=0.345 (ctrl); p=0.858 (dAP5)					

Student paired t-test							
Source of variation	**Degrees of freedom**	**Difference of means**	**t-value**	**95% confidence interval**	***P-value***	**Significant?**	**β power**
CS- vs CS+ ctrl	9	32.783	8.016	23.531 to 42.035	<0.001	yes	1
CS- vs CS+ dAP5	12	-1.471	-0.398	-9.522 to 6.581	0.698	no	0.05

Figure 5e (left)

Treatments	N	Missing	Mean	Standard deviation	Standard error
pre	4	0	6.138	3.291	1.645
hyper	4	0	3.891	3.021	1.510
post	4	0	5.566	2.822	1.411
Shapiro-Wilk test : p=0.950			**Levene median test: p=0.674**		

One-way repeated measures analysis of variance:							
Source of variation	**Degrees of freedom**	**Sum of squares**	**Mean squares**	**F-ratio**	***P-value***	**Significant?**	**β power**
Between Subjects	3	81.651	27.217				
Between Treatments	2	10.910	5.455	15.563	0.004	yes	0.964
Residual	6	2.103	0.351				
Total	11	94.664					

Multiple comparison procedures (Holm-Sidak method):				
Comparison	**Difference of means**	**t-value**	***P-value***	**Significant?**
Pre vs hyper	2.247	5.368	0.002	yes
Pre vs post	0.573	1.369	0.220	no

Figure 5e (right)

Treatments	N	Missing	Median	25%	75%
Area-CTRL	13	0	5.400	3.121	8.088
Area-HYPER	13	9	2.488	2.268	5.514
Area-DAP5	3	0	0.951	0.863	2.432
Shapiro-Wilk test : p<0.05					

Kruskal-Wallis one way analysis of variance on ranks:					
Source of variation	**Degrees of freedom**	**H**	***P-value***	**Significant?**	**β power**
Between treatments	2	7.358	0.025	yes	-

Figure 5i

Group	N	Missing	Mean	Standard deviation	Standard error
CS- / end	6	0	12.336	32.015	13.070
CS- laser / end	6	0	31.804	26.351	10.758
Difference end	6	0	-19.468	36.246	14.797
CS- / end+30	6	0	9.333	36.675	14.973
CS- laser / end+30	6	0	75.969	50.697	20.697
Difference end+30	6	0	-66.636	50.398	20.575
Shapiro-Wilk test : p=0.66 (endl); p=0.24 (end+30)					

Student paired t-test							
Source of variation	**Degrees of freedom**	**Difference of means**	**t-value**	**95% confidence interval**	***P-value***	**Significant?**	**β power**
CS- vs CS- laser End	5	-19.468	-1.31	-57.505 to 18.570	0.245	no	0.105
CS- vs CS- laser End+30	5	-66.636	-3.23	-119.525 to -13.747	0.023	yes	0.698

Figure 7c

Group	N	Missing	Mean	Standard deviation	Standard error
CS+ GFP	4	0	3.800	1.127	0.563
CS+ ArchT	4	0	3.630	2.200	1.100
CS- GFP	4	0	0.772	0.614	0.307
CS- ArchT	4		1.842	1.009	0.505
Shapiro-Wilk test : p=0.236			**Levene median test: p=0.578**		

One-way analysis of variance (general linear model):							
Source of variation	**Degrees of freedom**	**Sum of squares**	**Mean squares**	**F-ratio**	***P-value***	**Significant?**	**β power**
Between Groups	3	25.547	8.516	4.538	0.024	yes	0.633
Residual	12	22.519	1.877				
Total	15	48.066					

Multiple comparison procedures (Holm-Sidak method):				
Comparison	**Difference of means**	**t-value**	***P-value***	**Significant?**
CS+ GFP vs CS- GFP	3.028	3.126	0.009	yes
CS+ ArchT vs CS- GFP	2.858	2.951	0.012	yes
CS+ GFP vs CS- ArchT	1.958	2.022	0.066	no
CS+ ArchT vs. CS- ArchT	1.788	1.846	0.090	no
CS- ArchT vs CS- GFP	1.070	1.105	0.291	no
CS+ GFP vs CS- ArchT	0.170	0.175	0.864	no

Figure 7d

Group	N	Missing	Mean	Standard deviation	Standard error
GFP	4	0	0.982	0.168	0.0839
ArchT	4	0	0.337	0.348	0.174
Shapiro-Wilk test : p=0.765			**Levene median test: p=0.494**		

Student t-test							
Source of variation	**Degrees of freedom**	**Difference of means**	**t-value**	**95% confidence interval**	***P-value***	**Significant?**	**β power**
GFP vs ArchT	6	0.645	3.340	0.172 to 1.117	0.016	yes	0.763

Supplementary Figure 1d

Group	N	Missing	Mean	Standard deviation	Standard error
Session 1	5	2	0.571	0.247	0.143
Session 2	5	2	0.375	0.488	0.282
Session 3	5	0	0.0641	0.330	0.148
Session 4	5	0	0.727	0.167	0.0747
Session 5	5	1	0.679	0.140	0.0699
Session 6	5	1	0.652	0.218	0.109
Shapiro-Wilk test : p=0.991			**Levene median test: p=0.100**		
One-way analysis of variance (general linear model):					
Source of variation	**Degrees of freedom**	**Sum of squares**	**Mean squares**	**F-ratio**	***P-value***	**Significant?**	**β power**
Between Groups	5	1.491	0.298	3.987	0.013	yes	0.731
Residual	18	1.347	0.0748				
Total	23	2.838					
Multiple comparison procedures (Holm-Sidak method):					
Comparison	**Difference of means**	**t-value**	***P-value***	**Significant?**
Session 3 vs. Session 4	0.663	3.834	0.001	yes
Session 3 vs. Session 5	0.615	3.354	0.004	yes
Session 3 vs. Session 6	0.588	3.204	0.005	yes
Session 3 vs. Session 1	0.507	2.540	0.021	yes
Session 3 vs. Session 2	0.311	1.556	0.137	no

Supplementary Figure 2b

Group	N	Missing	Mean	Standard deviation	Standard error
CS+ naive	25	0	11.630	7.735	1.547
CS+ FC	25	0	37.025	23.654	4.731
Difference CS+	25	0	-25.395	24.488	4.898
CS- naive	25	0	9.617	7.479	1.496
CS- FC	25	0	7.067	6.806	1.361
Difference CS-	25	0	2.550	9.850	1.970
Shapiro-Wilk test : p=0.157 (CS+); p=0.721 (CS-)					
Student paired t-test							
Source of variation	**Degrees of freedom**	**Difference of means**	**t-value**	**95% confidence interval**	***P-value***	**Significant?**	**β power**
CS+ Naive vs FC	24	-25.395	-5.185	-35.503 to -15.286	<0.001	yes	0.999
CS- Naive vs FC	24	2.550	1.294	-1.516 to 6.616	0.023	no	0.116

Supplementary Figure 2d (left)

Treatments	N	Missing	Median	25%	75%
CS+ naive	21	0	8.750	5.662	10.958
CS+ FC	21	0	40.000	19.700	64.750
Shapiro-Wilk test : p<0.05					
Wilcoxon Signed Rank Test:						
Source of variation	**W**	**T+**	**T-**	**Z-statistic (positive ranks)**	***P-value***	**Significant?**
Between treatments	231	231	0	4.015	<0.001	yes

Supplementary Figure 2d (right)

Group	N	Missing	Mean	Standard deviation	Standard error
CS+ naive	4	0	22.667	5.569	2.785

CS+ FC	4	0	13.750	10.043	5.021
Difference	4	0	8.917	10.857	5.429
Shapiro-Wilk test : p=0.282					

Student paired t-test							
Source of variation	**Degrees of freedom**	**Difference of means**	**t-value**	**95% confidence interval**	***P-value***	**Significant?**	**β power**
CS+, naive vs FC	3	8.917	1.643	-8.360 to 26.193	0.199	no	0.153

Supplementary Figure 2e

Group	**N**	**Missing**	**Mean**	**Standard deviation**	**Standard error**
CS- naive (increase)	9	0	4.981	3.798	1.266
CS+ FC (increase)	9	0	13.148	6.286	2.095
Difference (increase)	9	0	-8.167	5.659	1.886
CS- naive (decrease)	16	0	12.224	7.853	1.963
CS+ FC (decrease)	16	0	3.646	4.286	1.072
Difference (decrease)	16	0	8.578	5.521	1.380
Shapiro-Wilk test : p=0.501 (increase); p=0.319 (decrease)					

Student paired t-test							
Source of variation	**Degrees of freedom**	**Difference of means**	**t-value**	**95% confidence interval**	***P-value***	**Significant?**	**β power**
naive vs FC (increase)	8	-8.167	-4.330	-12.516 to -3.817	0.003	yes	0.965
naive vs FC (decrease)	15	8.578	6.215	5.636 to 11.520	<0.001	yes	1

Supplementary Figure 3f

Treatments	**N**	**Missing**	**Median**	**25%**	**75%**
session 1	4	1	0.0949	0.00108	0.149
session 2	4	1	0.0107	-0.0249	0.0155
session 3	4	0	-0.123	-0.130	-0.0684
session 4	4	0	0.0837	-0.0210	0.164
session 5	4	1	0.140	0.129	0.166
session 6	4	0	0.0504	0.0330	0.134
Shapiro-Wilk test : p<0.05					

Friedman repeated measures analysis of variance on Ranks				
Source of variation	**Degrees of freedom**	**χ^2**	***P-value***	**Significant?**
Between treatments	5	5.714	0.335	no

Supplementary Figure 4b

Treatments	N	Missing	Mean	Standard deviation	Standard error
Frequency before	3	0	7.046	2.609	1.506
Frequency during	3	0	0.393	0.301	0.174
Frequency after	3	0	4.566	2.603	1.503
Shapiro-Wilk test : p=0.817			**Levene median test: p=0.649**		

One-way repeated measures analysis of variance:							
Source of variation	**Degrees of freedom**	**Sum of squares**	**Mean squares**	**F-ratio**	***P-value***	**Significant?**	**β power**
Between Subjects	2	16.867	8.434				
Between Treatments	2	67.812	33.906	12.943	0.018	yes	1
Residual	4	10.479	2.620				
Total	8	95.158					

Multiple comparison procedures (Holm-Sidak method):				
Comparison	**Difference of means**	**t-value**	***P-value***	**Significant?**
Before vs during	6.652	5.034	0.007	yes
Before vs after	2.480	1.876	0.134	no

Supplementary Figure 5e (left)

Group	N	Missing	Mean	Standard deviation	Standard error
End, control	10	0	1.176	0.110	0.0349
End, dAP5	13	0	0.944	0.102	0.0284
End+30, control	10	0	1.063	0.0361	0.0114
End+30, dAP5	13	0	0.895	0.151	0.0418
Shapiro-Wilk test : p=0.324			**Levene median test: p<0.05**		

One-way analysis of variance (general linear model):							
Source of variation	**Degrees of freedom**	**Sum of squares**	**Mean squares**	**F-ratio**	***P-value***	**Significant?**	**β power**
Between Groups	3	0.532	0.177	14.355	<0.001	yes	1
Residual	42	0.519	0.0124				
Total	45	1.051					

Multiple comparison procedures (Holm-Sidak method):				
Comparison	**Difference of means**	**t-value**	***P-value***	**Significant?**
End, control vs dAP5	0.233	4.972	<0.001	yes
End+30, control vs dAP5	0.168	3.590	<0.001	yes

Supplementary Figure 5 (right)

Treatments	N	Missing	Median	25%	75%
End, control	10	0	1.014	0.951	1.033
End, dAP5	13	0	0.929	0.838	1.056
End+30, control	10	0	0.977	0.947	1.004
End+30, dAP5	13	0	0.945	0.917	0.986
Shapiro-Wilk test : p<0.05					
Kruskal-Wallis one way analysis of variance on ranks:					
Source of variation	**Degrees of freedom**	**H**	***P-value***	**Significant?**	**β power**
Between treatments	3	2.468	0.481	no	-

Supplementary Figure 6a

Group	N	Missing	Mean	Standard deviation	Standard error
CS- naive	10	0	36.268	26.714	8.448
CS- FC	8	0	5.410	26.650	9.422
CS+ FC	8	0	1.441	14.016	4.955
Shapiro-Wilk test : p=0.268			**Levene median test: p=0.305**		
One-way analysis of variance (general linear model):					
Source of variation	**Degrees of freedom**	**Sum of squares**	**Mean squares**	**F-ratio**	***P-value***	**Significant?**	**β power**
Between Groups	2	6700.554	3350.277	6.034	0.008	yes	0.767
Residual	23	12769.564	555.198				
Total	25	19470.118					
Multiple comparison procedures (Holm-Sidak method):					
Comparison	**Difference of means**	**t-value**	***P-value***	**Significant?**
CS- (naive) vs. CS+ (FC)	34.826	3.116	0.005	yes
CS- (naive) vs. CS- (FC)	30.858	2.761	0.011	yes
CS- (FC) vs. CS+ (FC)	3.969	0.337	0.739	no

Supplementary Figure 6b

Group	N	Missing	Mean	Standard deviation	Standard error
Naive	10	0	0.436	0.327	0.104
Naive+dAP5	13	0	-0.0977	0.383	0.106
FC	8	0	-0.0235	0.449	0.159
Shapiro-Wilk test : p=0.086			**Levene median test: p=0.880**		
One-way analysis of variance (general linear model):					
Source of variation	**Degrees of freedom**	**Sum of squares**	**Mean squares**	**F-ratio**	***P-value***	**Significant?**	**β power**
Between Groups	2	1.756	0.878	5.944	0.007	yes	0.770
Residual	28	4.137	0.148				
Total	30	5.893					
Multiple comparison procedures (Holm-Sidak method):					
Comparison	**Difference of means**	**t-value**	***P-value***	**Significant?**
Naive vs Naive + dAP5	0.533	3.300	0.003	yes
Naive vs FC	0.459	2.519	0.018	yes
FC vs Naive + dAP5	0.0742	0.430	0.671	no

Supplementary Figure 6c

Group	**[cell discrimination index; % of freezing]**						
Mouse 1	[0.0784; 49.5000], [0.1364 ; 49.5000]					**Shapiro-Wilk test : p=0.0653**	
Mouse 2	[0.3764; 3.6667]						
Mouse 3	[-0.2504; 83.1667]					**Levene median test: p=0.05**	
Mouse 4	[-1.0000; 70.1667], [-0.0266; 70.1667], [0.0743; 70.1667]						
Mouse 5	[0.4235; 16.6667]						
Non-linear regression (polynomial, y = a*x+b):							
	Coefficient		**Standard error**		**t-value**		***P-value***
a	-94.0741		17.5060		-5.3738		0.0126
b	51.0207		5.5140		9.2530		0.0027
R	0.9518		12.0397				
Analysis of variance (corrected for the mean of the observations):							
Source of variation	**Degrees of freedom**	**Sum of squares**	**Mean squares**	**F-ratio**	***P-value***	**Significant?**	**β power**
Regression	1	4185.9899	4185.9899	28.8778	0.0126	yes	-
Residual	3	434.8657	144.9552				-
Total	4	4620.8556	1155.2139				

SUPPLEMENTARY FIGURES AND LEGENDS

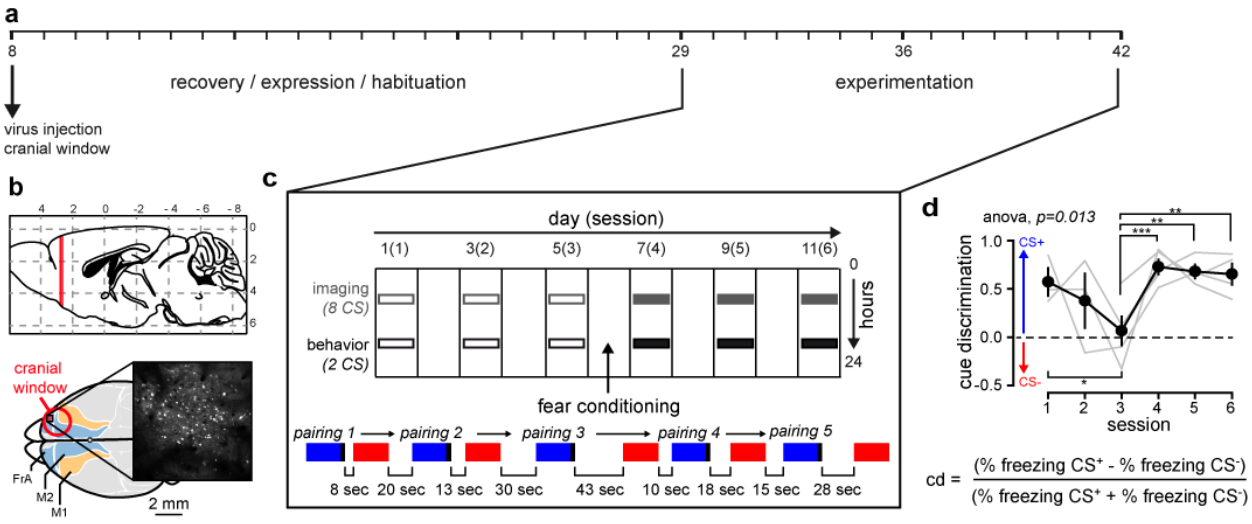

Supplementary Figure 1. FrA neuronal activity and behavioral performance of GCaMP5-expressing mice

a, Schedule of experiments. Head-fixed awake mice were placed and trained under the microscope every day for at least 7 days prior to the experiment, and then imaged 21 to 35 days after virus injection. **b**, Injection sites and position of cranial window are depicted in red. **c**, Imaging-behavior protocol. Mice were imaged in the morning upon the presentation of 8 CS- and 8 CS+. Behavior was assessed at least 6 hours later (only 2CS+ and 2CS- were presented). Fear conditioning occurred on day 6 between sessions 3 and 4. Fear conditioning protocol is represented below. Five auditory stimuli (each consisting of 27 pure (8 kHz)-tone or white noise pips, 50 ms, 0.9 Hz for 30 s) were positively (blue, CS+, 8 kHz) or negatively (red, CS-, gaussian noise) paired with the delivery of a mild electrical shock (black, 0.6 mA) to the paws in a pseudorandom order. Delays between stimuli are indicated below. **d**, Fear conditioning increases the index of cue discrimination (cd, equation below the graph) between CS+ and CS-. Only GCaMP5 mice that went through 6 imaging sessions are represented (n=4; p=0.013, one-way anova; *p<0.05, **p<0.01, ***p<0.001; post-hoc Holm-Sidak test). Grey lines indicate individual mice. Black line and circles indicate mean ± sem.

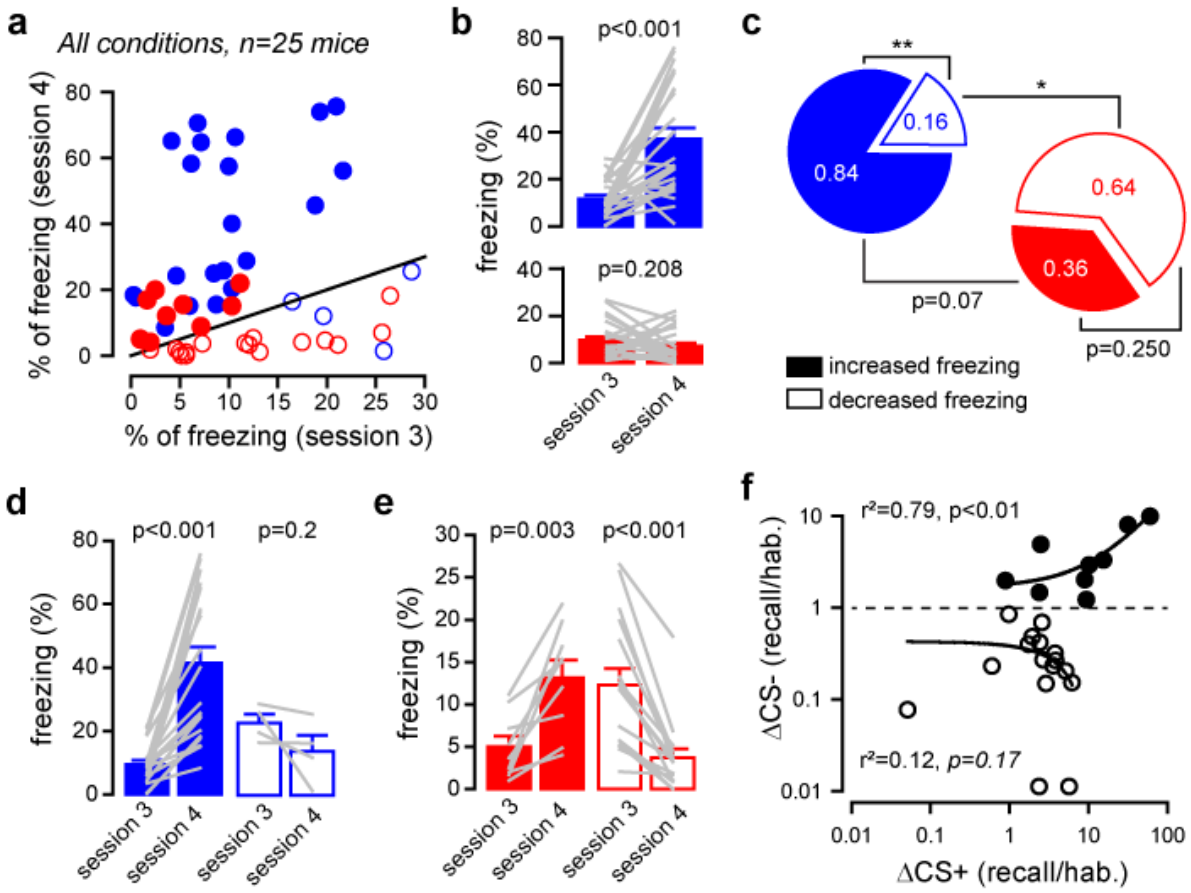

Supplementary Figure 2. Effect of fear conditioning on behavioral parameters among all mice

a, Relation between the level of freezing before (session 3) and after (session 4) fear conditioning. Each circle represents the freezing response upon CS+ (blue) and CS- (red) stimuli. Filled and open circles indicate increased and decreased freezing responses, respectively (*i.e* above and below the unity black line). **b**, Effect of fear conditioning on fear responses evoked by the presentation of CS+ (top, blue; n=25; p<0.001; paired t-test) and CS- (bottom, red; n=25; p=0.208; paired t-test). Grey lines indicate pairs. **c**, Proportions of mice with increased (filled pie, n=21 and 9) or decreased (open pie, n=4 and 16) fear responses evoked by CS+ (blue, n=25; **p=0.0044; χ^2=8.12) and CS- (red, n=25; p=0.25; χ^2=1.32). The proportion of mice that showed decreased fear responses are significantly different between CS+ and CS- (n=4 and 16; *p=0.0213; χ^2=5.23). **d**, Mice were categorized depending on whether they showed increased (filled bars, n=21; p<0.001; Wilcoxon Signed Rank Test) or decreased (open bars; n=4; p=0.199; paired t-test) fear responses evoked by the presentation of CS+. **e**, Same presentation as in **d** but for CS- (increase, n=9, p=0.003; decrease, n=16, p<0.001; paired t-test). **f**, Relation

between fear index (ΔCS) upon CS+ and CS- (freezing responses after learning were normalized to freezing responses before learning). Each circle represents a mouse. Learning-dependent decreased freezing behaviors in response to CS- do not depend on the freezing behaviors observed upon CS+ (white circle, ΔCS- <1; n=16; r^2=0.12; p=0.1758; one way anova). Error bars, sem.

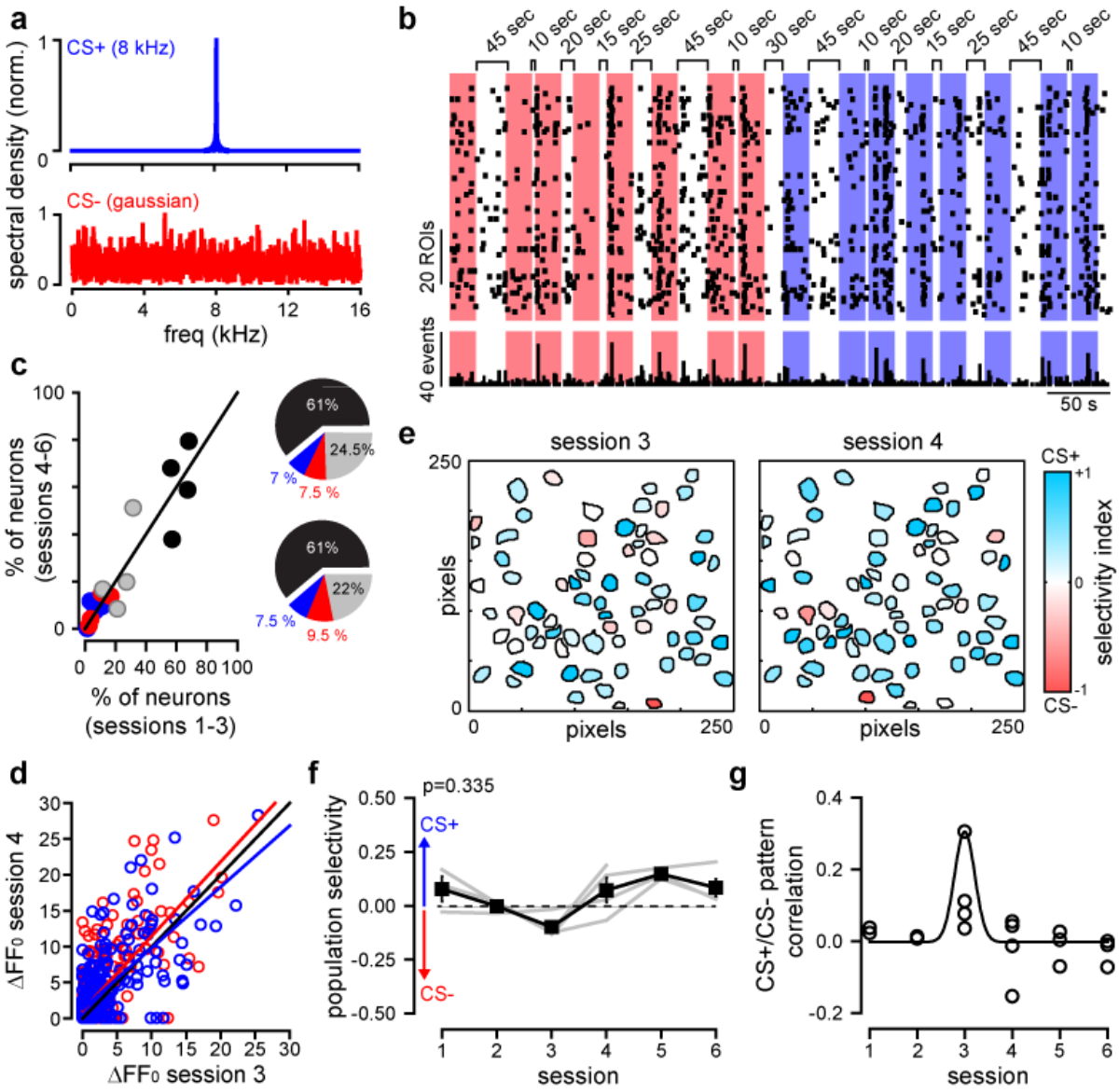

Supplementary Figure 3. Fear conditioning does not alter neuronal network selectivity

a, Spectral properties of auditory stimulation. **b**, Example raster plots (top) and peri-stimulus time histograms (bottom, bin size: 1 s) showing the heterogeneity of neuronal activity among successive auditory stimuli. Each square represents a detected calcium transient. Red and blue bars represent CS- and CS+ epochs, respectively. Pseudo-random delays between epochs are indicated. **c**, Relationship between the proportion of neurons in different categories before (sessions 1-3) and after (sessions 4-6) fear conditioning. Neurons were categorized as non responding (black), CS+ specific (blue), CS- specific (red), and non-specific (grey, responding to both CS+ and CS-). Neurons were considered

responding if at least one calcium transient was detected in at least 1 out of 8 trials. All neurons from all recorded mice (n=4) were pooled. **d**, Relationship between the activity before and after fear conditioning. For each responding neuron, all detected ΔFF_0 events within a single trial were first summed and then averaged among all trials. Blue and red circles represent the activity of neurons in response to CS+ and CS-, respectively. Blue and red lines represent linear regression line. Black line represents the identity line. **e**, Example of FrA population selectivity. Responding neurons are outlined and color-coded as a function of their selectivity index. Values close to 1 (blue) and -1 (red) indicate higher activity upon CS+ and CS- presentation, respectively. Values close to 0 indicate equal activity. For each neuron, we first computed the weighted responding probabilities (w*P*(CS) = averaged responding probabilities over 8 consecutive trials weighted by the mean of peaks of detected ΔFF_0). The selectivity index was then defined as : [w*P*(CS+)-w*P*(CS-) / (w*P*(CS+)+w*P*(CS-)]. (**F**) Average selectivity index as a function of imaging session. Grey lines represent individuals (n=4), black line and squares, mean ± sem. Fear conditioning occurred between sessions 3 and 4 (p=0.335; n=4; Friedman repeated measures anova on ranks). **g**, Pearson's coefficients of correlation among all imaging sessions. Error bars, sem.

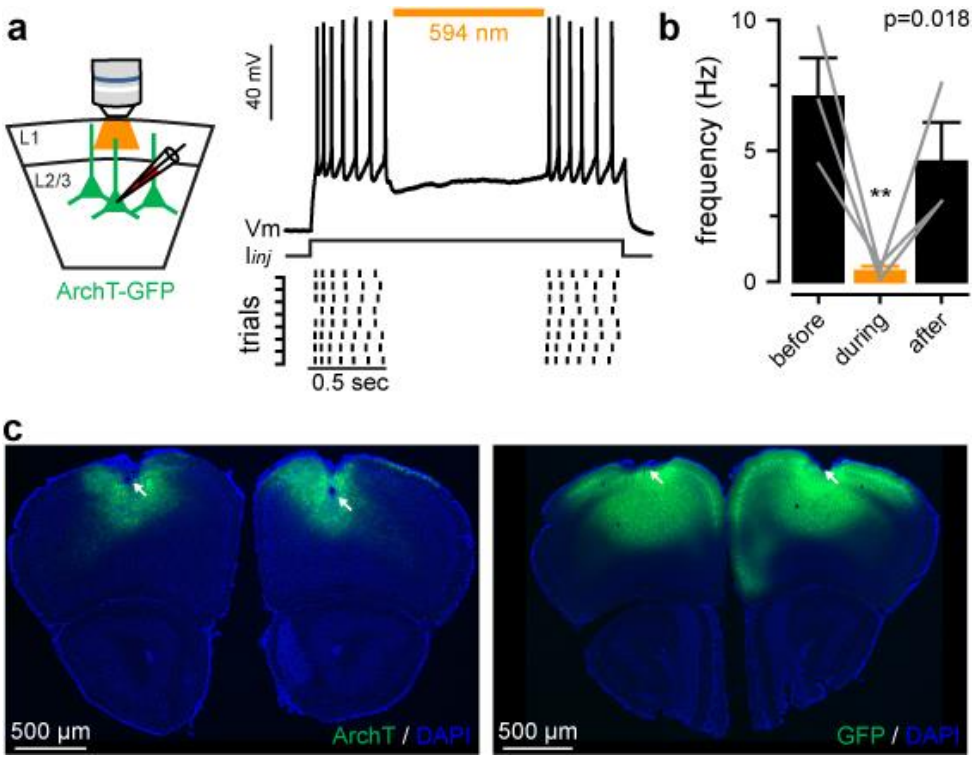

Supplementary Figure 4. Expression of ArchT-GFP in the FrA.

a, Left, schematic of the slice experiment. L2/3 pyramidal neurons expressing ArchT were photo-inhibited through the objective with a ultrahigh power 597 nm LED . Right, example of the effect of photo-inhibition on the spiking pattern evoked through current injection. **b**, Average spike frequency before, during and after illumination (n=3; p=0.018, one way repeated measures anova; **p=0.007, Holm-Sidak method multiple comparisons versus condition "before"). **c**, Examples of mice expressing bilaterally ArchT (left) and GFP (right) in FrA. Mice were used for behavioral experiments (see Fig.1). Arrows, positions of cannulas. Error bars, sem.

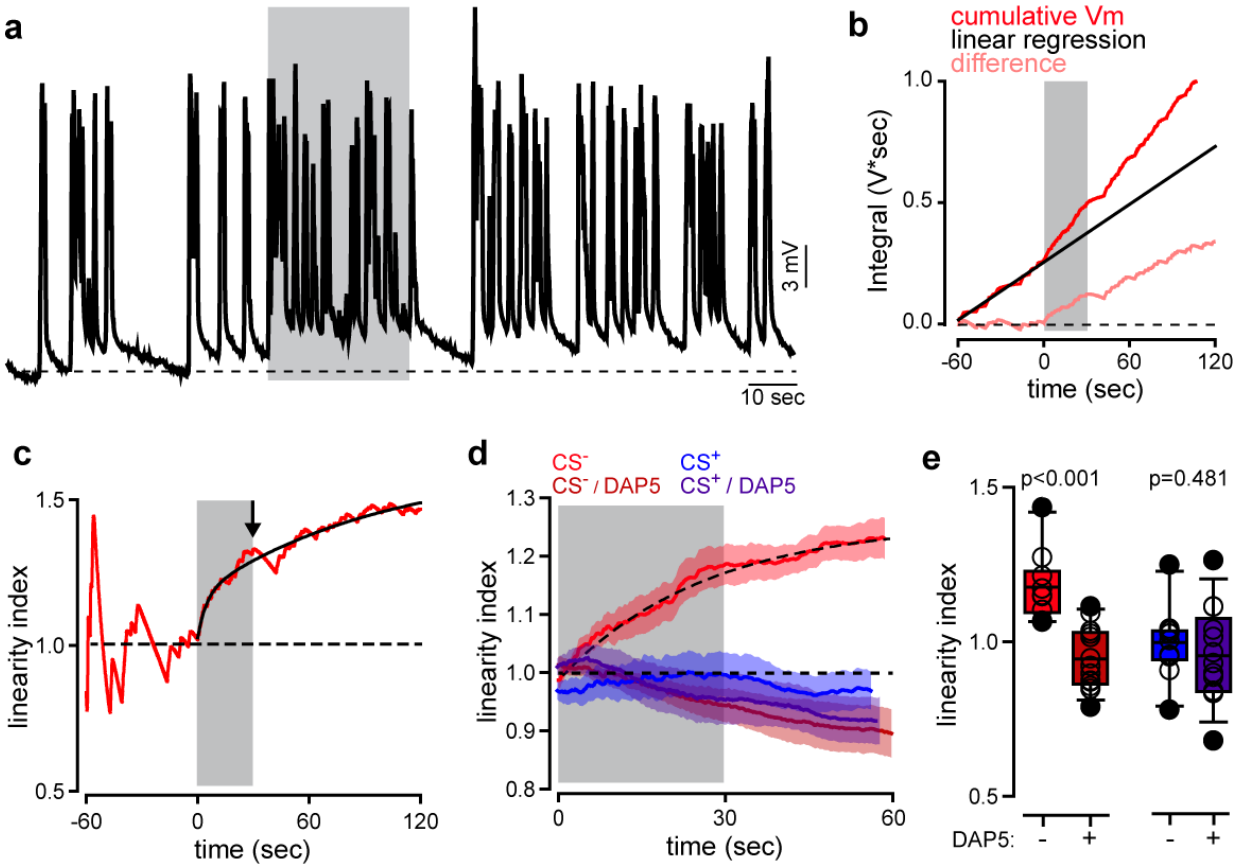

Supplementary Figure 5. Gaussian auditory stimulation evokes non-linear, NMDARs-dependent depolarization

a, Example traces of postsynaptic membrane potential recorded from an individual FrA L2/3 pyramidal neuron upon gaussian auditory stimulation (grey bar, CS-: 27 pips, 50 ms, 0.9 Hz, 30 s). **b**, Cumulative depolarization (red). To reduce the variability related to spontaneous activity, the cumulative PSPs were subtracted by the linear regression (black line) during the baseline period prior to auditory stimulation (grey bar). The difference (pink) represents stimulus-induced cumulative change. **c**, Linearity was computed by dividing cumulative depolarization by the linear regression. Grey bar, auditory stimulation; arrows, analysis time points. **d**, Averaged linearity (± sem) without (control) or with the blockade of NMDARs (dAP5). Grey bars, auditory stimulation. **e**, Effect of dAP5 on CS- (left) and CS+ (right) evoked membrane potential linearity at two different time points (end and end+30 s) (CS-, $p<0.001$, one-way anova, ***$p<0.001$, *$p<0.05$, Holm-Sidak post-hoc multiple comparisons; CS+, $p=0.484$, Kruskal-Wallis one way anova on ranks). Boxplots represent mean and interquartile range. Open circles, individual mice; filled circles, outliers.

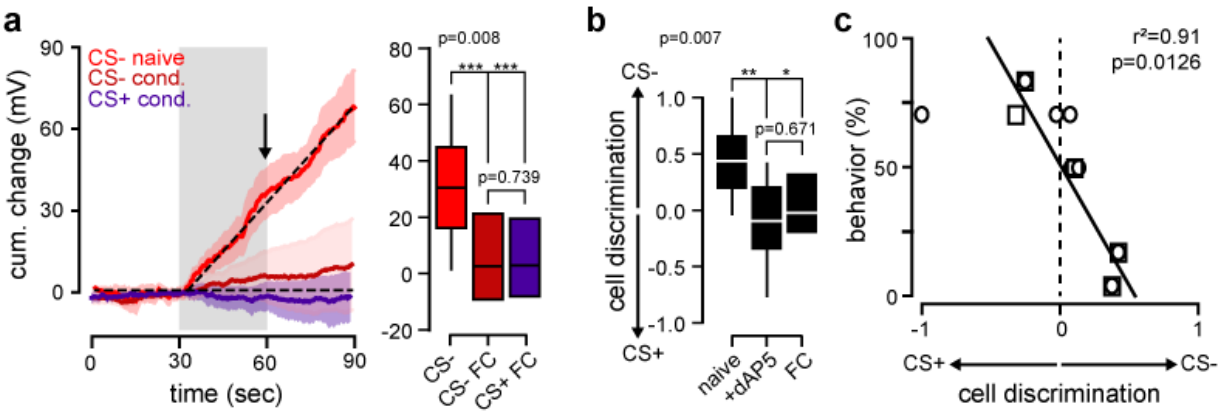

Supplementary Figure 6. Fear conditioning occludes auditory-evoked plateau potentials

a, Effect of fear conditioning (FC) on cumulative PSPs change. Same representation as in e (left) and f (right). (CS- naive, n=10; CS- FC, n=8; CS+ FC, n=8; p=0.005, one way anova; ***, p<0.001, post-hoc Holm-Sidak test). Left, error bars, sem. **b**, Effect of dAP5 and fear conditioning (FC) on cellular discrimination between CS- and CS+ (naive, n=10; naive+dAP5, n=13; FC, n=8; p=0.007, one way anova; *, p<0.05, **, p<0.001, post-hoc Holm-Sidak test). **c**, Linear relationship between mean cellular discrimination and CS+ evoked freezing response following fear conditioning (n=5 mice; r^2=0.91; p=0.0126; anova). Each circle represents a cell (n=8), each square represents a mouse (n=5). Boxplots represent mean and interquartile range.

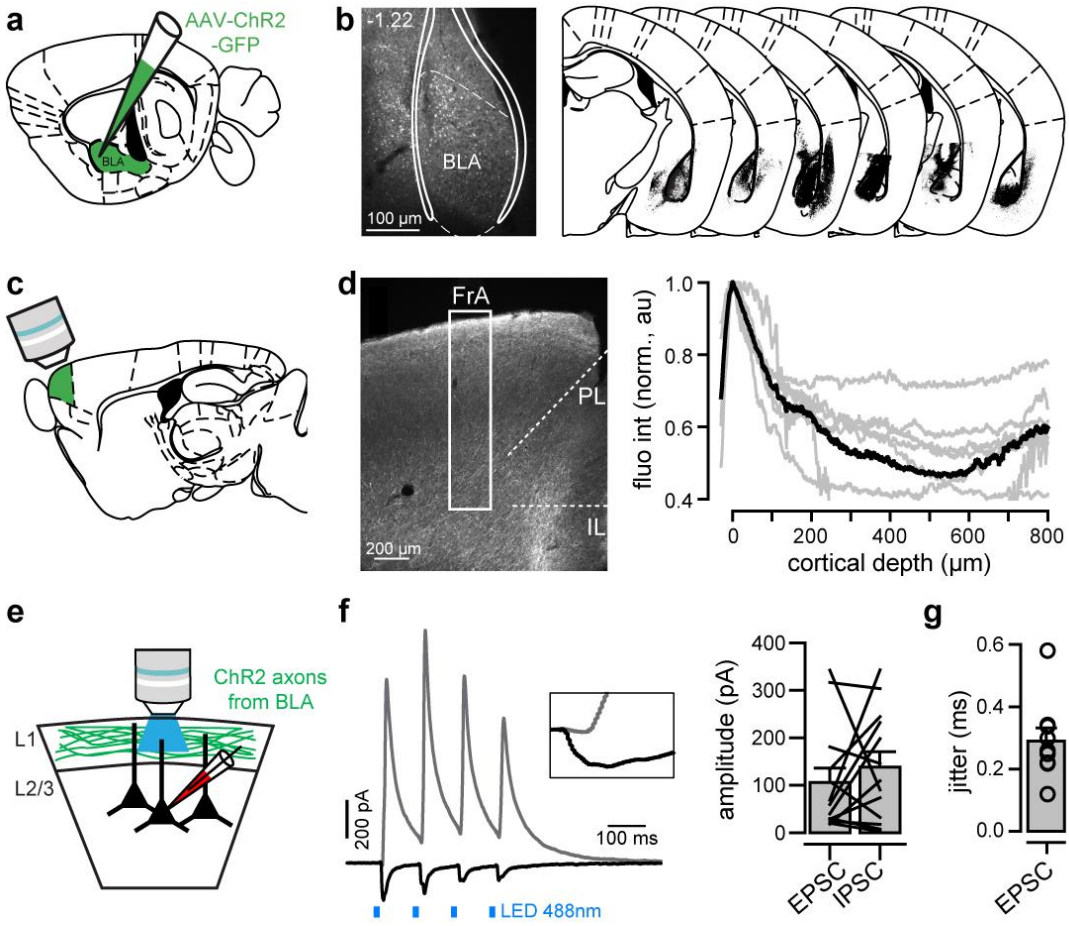

Supplementary Figure 7. Expression of ChR2-GFP in the BLA and its afferents

a, Schematic of the viral injection in the BLA. Neurons were transfected with AAV9-CamKIIa-hChR2-eYFP. **b**, Representative example of the ChR2-GFP expression profile in the mouse BLA (Left). The coronal diagrams of the brains from 6 mice showing the expression profiles (in black) of ChR2-GFP are depicted on the right. Diagrams were adapted from the Paxinos atlas. **d**, Left, example of a cortical slice with ChR2-GFP fluorescence in the FrA. *PL, prelimbic cortex; IL, infralimbic cortex*. Right, plot comparing the intensity profiles measured in the FrA (white bow on the left) of 6 different animals in which injections targeted BLA. **e**, schematic of the slice experiment. L2/3 pyramidal neurons expressing ChR2 were photo-activated through the objective. **e**,**f,** Excitatory post-synaptic current (EPSCs) and feed-forward inhibitory post-synaptic currents (IPSCs) were evoked with a ultrahigh power 488 nm LED. Black lines indicate pairs. **g**, jitter of light-evoked EPSCs. Open circles indicate indiviual cells.

10.2 *Manuscript 2*

Chunlei Zhang, Mattia Aime, Emilie Laheranne, Xander Houbaert, Hajer El Oussini, Christelle Martin, Marilyn Lepleux, Elisabeth Normand, Jamel Chelly, Etienne Herzog, Pierre Billuart and Yann Humeau.

Protein Kinase A deregulation in the medial prefrontal cortex impairs working memory in murine Oligophrenin1 deficiency.

Journal of Neuroscience, accepted

Protein Kinase A deregulation in the medial prefrontal cortex impairs working memory in murine Oligophrenin1 deficiency.

Short title: Tuning PKA levels rescues *Ophn1*$^{-/y}$ pathophysiology.

Chun-Lei Zhang[5], Mattia Aime[1], Emilie Laheranne[1], Xander Houbaert[1], Hajer El Oussini[1], Christelle Martin[1], Marilyn Lepleux[1], Elisabeth Normand[2], Jamel Chelly[3,4], Etienne Herzog[1], Pierre Billuart[3] and Yann Humeau[1§]

[1] *Team synapse in cognition, institut Interdisciplinaire de Neuroscience, Centre National de la Recherche Scientifique CNRS UMR5297, Université de Bordeaux, Bordeaux, France.*

[2] *Pole in vivo, institut Interdisciplinaire de Neuroscience, Centre National de la Recherche Scientifique CNRS UMR5297, Université de Bordeaux, Bordeaux, France.*

[3] *Centre National de la Recherche Scientifique, Université Paris Descartes, Institut National de la Santé et de la Recherche Médicale, UMR8104, Institut Cochin, 75014 Paris, France.*

[4] *Team médecine « translationnelle et neurogénétique » IGBMC - CNRS UMR 7104 - Inserm U 964, Université de Strasbourg, Illkirch, France.*

[5] *Neural circuits for spatial navigation and memory, Department of Neuroscience, Institut Pasteur, Paris, France*

§ Corresponding author.

Yann Humeau
UMR5297 Institut interdisciplinaire de neuroscience
Bâtiment Neurocampus, 146 rue Léo Saignat,33077, Bordeaux cedex, France
Email: yann.humeau@u-bordeaux.fr

Number of pages: 26
Number of figures and tables: 8 Figures, 2 tables.
Number of words: Abstract (228); Introduction (491) Discussion (1311)

Acknowledgments and Disclosures

We would like to thanks Dr. Pierre Trifilieff for fruitful discussions, Dr. Frédéric Gambino for helping with statistics, Dr Andrew Penn for text improvement, and Prof. Benjamin K. Yee for technical advices on setting up the Y-maze experiments. This

work has been supported by grants from Agence Nationale de la Recherche to YH (ANR-2010-BLAN-1434-01), and the program investissement d'avenir (Labex Brain).

Authors declare that they have no conflict of interest.

Abstract

Classical and systems genetics have identified wide networks of genes associated with cognitive and neurodevelopmental diseases. In parallel to deciphering the role of each of these genes in neuronal or synaptic function, evaluating the response of neuronal and molecular networks to gene loss-of-function could reveal some pathophysiological mechanisms potentially accessible to non-genetic therapies. Loss of function of the Rho-GAP Oligophrenin-1 is associated with cognitive impairments in both human and mouse. Up-regulation of both PKA and ROCK has been reported in *Ophn1*$^{-/y}$ mice, but it remains unclear if kinase hyperactivity contributes to the behavioural phenotypes. In this study, we thoroughly characterized a prominent perseveration phenotype displayed by *Ophn1* deficient mice using a Y-maze spatial working memory (SWM) test. We report that *Ophn1* deficiency in the mouse generated severe cognitive impairments, characterized by both a high occurrence of perseverative behaviours and a lack of deliberation during SWM test. *In vivo* and *in vitro* pharmacological experiments suggest that PKA dysregulation in the mPFC underlies cognitive dysfunction in *Ophn1* deficient mice, as assessed using a delayed spatial alternation task results. Functionally, mPFC neuronal networks appeared to be affected in a PKA-dependent manner, whereas hippocampal-PFC projections involved in SWM were not affected in *Ophn1*$^{-/y}$ mice. Thus, we propose that discrete gene mutations in intellectual disability might generate "secondary" pathophysiological mechanisms, which are prone to become pharmacological targets for curative strategies in adult patients.

Significance Statement

Here we report that *Ophn1* deficiency generates severe impairments in performance at spatial working memory tests, characterized by a high occurrence of perseverative behaviours and a lack of decision making. This cognitive deficit is consecutive to PKA deregulation in the mPFC that prevents *Ophn1* KO mice to exploit a correctly acquired rule. Functionally, mPFC neuronal networks appear to be affected in a PKA-dependent

manner, whereas behaviourally important hippocampal projections were preserved by the mutation. Thus, we propose that discrete gene mutations in intellectual disability can generate “secondary” pathophysiological mechanisms prone to become pharmacological targets for curative strategies in adults.

Introduction

Loss of function of the Rho-GAP Oligophrenin 1 is associated with cognitive impairments (Billuart et al., 1998; van Bokhoven, 2011) and more rarely to autism spectrum disorder (ASD) and schizophrenia (Piton et al., 2011). Mice with a null *Ophn1* mutation also display a number of behavioural and learning deficits (Khelfaoui et al., 2007). Ophn1 is a synaptic protein controlling synaptic vesicle trafficking, AMPAR recruitment, and mGluR1 dependent Long-term Depression (LTD) (Nadif Kasri et al., 2009; Nakano-Kobayashi et al., 2009; Nadif Kasri et al., 2011; Di Prisco et al., 2014; Nakano-Kobayashi et al., 2014). *Ophn1* deficiency in mice has been associated with hyperactivity of Rho-associated protein kinase (ROCK) and cAMP-dependent Protein Kinase (PKA) (Khelfaoui et al., 2009, 2014), possibly due to the loss of function of Rho-GAP activity and phosphorylation-based feedback controlling Rho A (Nusser et al., 2006). Interestingly, acute and chronic pharmacological treatments suggested that inhibition of PKA/ROCK activities by the ROCK inhibitors Y27632 improve some of the functional and behavioural deficits observed in *ophn1* KO mice (Powell et al., 2012; Khelfaoui et al., 2014; Meziane et al., 2016). However, actual data do not establish how hyper-phosphorylation in discrete neuronal networks generates specific behavioural deficits.

Medial prefrontal cortex (mPFC) and its connections with other brain regions play a crucial role in allowing meta-cognitive actions such as working memory, behavioural flexibility (Kesner and Churchwell, 2011) and capacities that are impaired in mental disorders (Geurts et al., 2004; Rolls et al., 2008; Sumiyoshi et al., 2011). In rodents, researchers use a delayed spatial alternation task (DSA) to test spatial working memory (SWM), of which connections between the hippocampus and mPFC have been shown to play a fundamental role (Laroche et al., 2000; Wang and Cai, 2006). Also, *in vivo* electrophysiological recordings during the DSA task revealed a decision point prior to the bifurcation area of the maze, where synchronization of hippocampus-PFC neuronal activities occurs in the theta (4-10 Hz) range (Benchenane et al., 2010).

It has been proposed that this would allow animals to deliberate in order to choose the rewarding arm. Interestingly this deliberation process is characterized by “vicarious trial and errors” (VTE) behaviours, the occurrence of which strongly correlate with the success rate (Wikenheiser and Redish, 2015; Redish, 2016).

Computational studies proposed that working memory impairment could be consecutive to aberrant signal-to-noise ratios within PFC networks (Rolls et al., 2008). In rodents, SWM performance is altered in excessive, but not in depressed PKA activity (Taylor et al., 1999; Arnsten et al., 2005). Meanwhile, some form of PKA-dependent plasticity has been described at hippocampus-PFC projections (Jay et al., 1998). It was also suggested that PKA activity could influence the signal-to-noise ratio within PFC networks, physiologically relaying the dopaminergic activation (Rolls et al., 2008).

Here, we observed that *Ophn1*-deficient mice performed poorly in Y-maze based SWM tests. We then combined *in vivo* and *in vitro* strategies to test whether the poor behavioural performance results from the hyper-activity of PKA in the PFC region.

Material and methods

Subjects

A total of 73 *Ophn1* WT and 73 *Ophn1* KO male littermates were used in this study. All animals are on C57BL/6N background, selected from 2-3 months old, and housed in 12/12 LD with ad libitum feeding. Every effort was made to minimize the number of animals used and their suffering. The experimental design and all procedures were in accordance with the European guide for the care and use of laboratory animals and the animal care guidelines issued by the animal experimental ethics committee of Bordeaux Universities (CE50) (APAFIS n°2572)

Behavioural protocols

Our Y-maze consists of three arms (40 cm long, 10 cm wide, 15 cm high, 120° between) made of white PVC material. Between trials, the maze was wiped by 4% acetic acid to avoid odor-based bias. Allocation of the starting arm was varied and counterbalanced within groups. The room light was weak and balanced, and a digital camera located 2 meters above the maze was used to record animal trajectories.

- Spontaneous alternation

A cohort of mice was placed in the room for 30 min before that each mouse was positioned at the end of one starting arm and allowed to freely explore the maze for 10 minutes. The Y-maze was located on the ground with prominent surrounding visual cues. Instinctively, mice are willing to explore the new environment, thus naturally alternating between arms. Scoring of spontaneous alternation is made as described before [1]. An entry occurs when all four paws of the animals were within the arm.

- Spatial novelty test

Another cohort of mice was habituated to the room for 30 minutes. Mice were then assigned to explore two arms for 5 minutes: the “starting” arm and another that will become the “familiar” arm. The third arm - that will become the “novel” arm - was blocked by a sliding door. After returning back to the home cage for 10 minutes, mice were then allowed to explore the entire maze for 2 minutes. The time spent in each of the three arms was measured and the number of entries were counted.

Delayed Spatial Alternation task (DSA test). Delayed spatial alteration task (DSA) task is a delayed non-matching-to-place (DNMP) task extensively described and used to assess for prefrontal cortex function (Taylor et al., 1999; Wang and Cai, 2006). To improve animal motivation, mice were handled and food restricted to maintain around

85% weight. In the initial week, mice would perform two periods of habituation. In the 1st step, on a daily basis each mouse was allowed to explore the maze twice for 10 minutes with 3 hours interval. The food wells in the three-arm ends were baited with rewards, and mice were trained until they were capable of quickly obtaining the food reward. Then in the 2nd step, one arm was set as the "starting" arm, the two others as the "baited" ones. A total of 10 runs were performed in two days (5 runs per day, at least 30 minutes interval between each run). The mice had to learn to alternate between "right-left or left-right" to get the bait with a time limit of 1 minute. To avoid a rewarding odor-based bias to mice choices, three bigger pieces of reward were positioned behind each arm end outside of the maze.

In the second week, the learning phase lasts 4 consecutive days. During this phase, the mice received two sessions per day (3 hours interval between sessions), each composed of 10 trials (Figure 1). From trial 0, mice run from a starting arm. One of two food-rewarded arms was closed, and mice were forced to get the reward in the opposite arm. In the next 9 successive trials, mice must alternate between right and left arm to find the reward. A trial may include up-to 6 runs (30 second delay between runs, 5 consecutive errors allowed, before being forced to enter the rewarding arm). The success rate is calculated as the number of successful choices / the total number of choices. We also ranked the errors from #1 to #5 to evaluate the perseveration of mice in repeating wrong choices (Wang and Cai, 2006). Food wells were changed in each trail, and arms were wiped by 4% acetic acid after each run. Between sessions, the maze was rotated, and starting arm was randomly chosen and balanced between animals.

Cannula implantation.

At first, mice were treated with buprenorphine (0.1 mg/kg, i.p) and positioned in a stereotaxic apparatus (David Kopf Instruments, Tujunga, CA), on a 33-35°C heating pad, and maintained under continuous Isoflurane anesthesia. Stainless steel guide cannula (26 gauge; Plastics-One, Roanoke, VA, USA) were bilaterally implanted above the medial PFC: [AP] +1.9-2.1 mm, [ML] ±2.1-2.3 mm, [DV] -1.5 mm, with ±30° angle, and/or dorsal hippocampus: [AP] -1.8-2.0 mm, [ML] ±2.2-2.5 mm, [DV] -0.5 mm, with ±30° angle. The cannula was fixed to the skull using dental cement (Super-Bond, Sun Medical Co. Ltd, Moriyama, Shiga, Japan). A dummy cannula was inserted into the guide cannula to reduce the risk of infection. A delay of 3-4 weeks for surgery

recovery was respected before the food deprivation began, during which the body weight of mice was checked daily.

Drug Administration.

To reduce stress during drug injection, mice were trained on a daily basis for dummy cannula removal/insertion. To perform freely moving drug injection, the dummy cannula was replaced by an infusion cannula (33 gauge; connected to a 1 µl Hamilton syringe via polyethylene tubing) projecting out of the guide cannula with 1.5-2 mm to target mPFC or dHPC. Drug doses have been used previously (Taylor et al., 1999): cAMPS-Rp, triethylammonium salt (10 µg/µl in saline), cAMPS-Sp triethylammonium salt (1µg/µl) and 6-BNZ-cAMP N^6-Benzoyladenosine-3′,5′-cyclic monophosphate sodium salt (10 µg/µl in saline) were obtained from Tocris (Illisville, MO) and were infused bilaterally at a rate of 0.15 µl/min and a volume of 300–400 nl per side by an automatic pump (Legato 100, Kd Scientific), 30 min before testing. To allow the penetration of drug, the injector was maintained for an additional 3 min. After the injection procedure, animals were placed back in their home-cage.

***In vitro* Electrophysiological recordings**

Acute slice preparation. Fresh slices were obtained from 4-5 month-old *Ophn1* WT and KO mice as described previously (Houbaert et al., 2013). All recordings were performed on mPFC-containing coronal slices ([AP] +1.3-2 mm). Briefly, mice were anesthetized by intra-peritoneal injection of a mixture of Ketamine (10mg/ml)/Xylazine (1mg/ml) before an intra-cardiac perfusion with a refrigerated bubbled (carbogen: 95% O2/5% CO2) sucrose solution containing (in mM): 2.7 KCl, 26 NaHCO3, 1.25 NaH2PO4, 10 glucose, 220 sucrose, 0.2 CaCl2, 6 MgCl2. Then, the brain was sliced (300µm thickness) with a vibratome (Leica VT1200s; Germany) at 4°C in sucrose solution. Slices were then maintained for 45 min at 37°C in an interface chamber with artificial cerebrospinal fluid (ACSF) containing (in mM): 124 NaCl, 2.7 KCl, 2 CaCl2, 10 MgSO4.7H2O, 26 NaHCO3, 1.25 NaH2PO4, 18.6 glucose and 2.25 ascorbic acid and equilibrated with 95% O_2/5% CO_2. Recordings were performed with standard ACSF (Humeau et al., 2005).

Electrophysiological Recordings. Synaptic activities and cellular properties of mPFC neuronal cells were recorded using classical whole cell patch-clamp techniques previously described (Humeau et al., 2005; Houbaert et al., 2013; Zhang et al., 2015). Cells were recorded in current clamp (spiking activities, spontaneous EPSPs) or

voltage-clamp mode (synaptic conductances) respectively using K-gluconate-based (in mM: 140 K-gluconate, 5 QX314-Cl, 10 HEPES, 10 phosphocreatine, 4 Mg-ATP and 0.3 Na-GTP (pH adjusted to 7.25 with KOH, 295 mOsm) and Cs-methylsulfonate based (in mM: 140 Cs-methylsulfonate, 5 QX314-Cl, 10 HEPES, 10 phosphocreatine, 4 Mg-ATP and 0.3 Na-GTP (pH adjusted to 7.25 with CsOH, 295 mOsm)) intracellular recording solutions.

- Optogenetic based experiments.

Adeno-associated viruses (AAV2/9.CAG.ChR2-Venus.W.SV40-p1468, ref Addgene-20071, $5.82E^{12}$ vector genomes (vg)/ml)) were packaged at the University of Pennsylvania Vector Core. Around 2 months old mice (over 20g) were prepared for the stereotaxic injection. Beforehand, mice were treated with buprenorphine (0.1 mg/kg, i.p), and positioned in a stereotaxic apparatus (David Kopf Instruments, Tujunga, CA) under continuous anaesthesia with isoflurane. During the surgery, the mice were warmed on a 33-35°C heating pad. The virus was bilaterally pressure-injected through glass pipettes (Hirschmann Laborgerate, ringcaps, tips pulled O.D 30-40 µm) using a Picosprizer (Parker Co). The positions of Bregma and Lambda points were defined and adjusted to the same horizontal level. The used coordinates for caudal HPC were: [AP] -3.1-3.3 mm, [ML] ±3.2-3.4 mm, [DV] -4.0 mm. In mPFC containing acute slices (see above), Hippocampo-mPFC monosynaptic EPSCs and di-synaptic IPSCs were elicited by 1 ms light pulse delivered by an ultrahigh power 460 nm LED (Prizmatix Ltd, Israel) at maximal intensity. All included cells were recorded in layer V of the IL region, as they consistently receive more excitatory inputs from the hippocampal region (Humeau lab, data not shown). As for above-mentioned experiments, data were recorded with a Multiclamp700B (Molecular Devices, USA), filtered at 2 kHz and digitized at 10 kHz. Data were acquired and analysed with pClamp10.2 (Molecular Devices).

PKA phosphorylation in mPFC tissues

Animals were sacrificed by cervical dislocation and their brains were rapidly dissected out and processed further at 4°C. The PFC were isolated and immediately homogenized (Figure 4A1) or snap-frozen in liquid nitrogen (Figure 4B1). The PFC tissues were homogenized in TPS buffer (0,32M sucrose, 4mM Hepes) containing 1X protease inhibitor cocktail (Calbiochem, CA) alone (Figure 4A1) or added with 1X phosphatase inhibitor cocktail (Figure 4B1)(Pierce biotechnology, IL). Protein was

quantified by Bradford assay. An equal amount of protein (10µg) was separated on 12% (Figure 4A1) or 4-20% SDS-polyacrylamide gels (Figure 4B1) and transferred to nitrocellulose membranes at 4°C for Western blot analysis. The membranes were blocked in 5% BSA in phosphate-buffered saline containing 0.1% Tween-20 for 1 hour at room temperature and incubated with the relevant antibody. The blots were incubated over night at 4°C with the primary antibodies diluted in blocking solution: 1/1000 dilution of anti-Phospho-(Ser/Thr) PKA Substrate antibody (Cell Signaling Technology, MA), and 1/1000 dilution of anti-oligophrenin 1 27. Membranes were also probed with 1/5000 dilution of anti-βtubuline (Sigma, MO), used as a loading control, allowing signal normalization. The membranes were washed and incubated in the appropriate Alexa Fluor® 488/647 coupled secondary antibodies diluted 1/2000 for 1 h followed by direct reading membranes on Bio-Rad Pharos FX plus. The density of immune-blots was measured using ImageJ software. Phosphorylation rate was determined by ratios between phosphorylated proteins and the β-tubuline loading control.

Statistics.

Detailed statistics are described in each figure legend, and are accessible in Table 1. For all tests, statistical difference was considered at $p<0.05$.

Results

Ophn1 deficiency in mice leads to aberrant perseverative behaviours in a spatial working memory test.

Based on previous observations unravelling a lack of cued fear extinction behaviour in *Ophn1* deficient mice (Khelfaoui et al., 2014), we embarked on a more specific investigation to test the executive functions supported by the mPFC. Thus, we assessed the ability of *Ophn1* WT and KO mice to learn an alternation rule with a time delay in the Y-maze. This task is known to mobilize spatial working memory in the medial PFC and hippocampus (Benchenane et al., 2010; Gordon, 2011) (Figure 1A). All along the training phase, *Ophn1* WT progressively improved their performance, reaching a success rate close to 0.7 (70%), which was maintained during a remote test (success rate $WT_{\#1}$ *VS* $WT_{\#5}$: p<0,001; Figure 1C1). In stark contrast, all along the training and the testing phases *Ophn1* KO mice did not perform better than a random score rate (50%) (success rate $KO_{\#1}$ *VS* $KO_{\#5}$: p<0,447; $WT_{\#5}$ *VS* $KO_{\#5}$: p<0,001; Figure 1C1), thus not displaying apparent sign of alternation rule learning. Beside this poor performance, *Ophn1* KO mice displayed another characteristic phenotype: the increased occurrence of repetitive errors – i.e. when the animal kept choosing the wrong arm several times in a row (Figure 1B and 1C2). This was scored as high rank errors – which normally disappear with training in WT mice (high rank errors: $WT_{\#1}$ *VS* $WT_{\#5}$, p<0,001; Figure 1C2). High rank errors were strikingly and consistently present in KO mice (high rank errors: $KO_{\#1}$ VS $KO_{\#5}$, p<0,683; $WT_{\#5}$ *VS* $KO_{\#5}$: p<0,001; Figure 1C2). Control spatial preference tests showed that these high rank mistakes were not due to turning preferences (Figure 2B) and argued against navigation abnormalities in the maze (Figure 2A) or short-term spatial reference memory preferences (Figure 2C). Interestingly, decreased spontaneous alternation was found in *Ophn1* KO mice (Figure 2D). Together with previous reports from our lab (Khelfaoui et al., 2014), these results confirmed that *Ophn1* deficiency in mice leads to behavioural perseveration, a phenotype classically attributed to mPFC dysfunction.

Ophn1 deficient mice display low occurrence of deliberative behaviours and cognitive impairments.

Interestingly, when mice make a choice prior to the bifurcation area (Figure 3A), they display VTE behaviour, reflecting a deliberative process (Redish, 2016). We first characterized VTE behaviour in WT mice. During VTE behaviour, the trajectory of mice appears to waver on approaching the bifurcation area, which is easily detectable in videos. Specifically, we observe a slower and less linear displacement at the crossing point as compared to the starting or ending arm (Figure 3A1). Importantly, the occurrence of VTE during trials ("VTE trials") was associated with high choice accuracy (success rate: "VTE trials": 0.82 ± 0.04; "no VTE trial": 0.49 ± 0.05, p<0,001, Figure 3B2-B3). In stark contrast, in *Ophn1* KO mice, the occurrence of VTE behaviours was lower ("VTE trials": WT *VS* KO p<0,001; Figure 3A2) and the success rate of "VTE trials" was lower and close to random (success rate "VTE": 0.66 ± 0.04; WT *VS* KO p=0,002; Figure 3B3). From these results, we conclude that the deterioration of *Ophn1* KO mice performance in Y-maze resides both in cognitive impairment and the low occurrence of deliberation-driven decision making.

Neurophysiology of mPFC networks in *Ophn1* deficient mice.

Next we examined the physiology of some of the neuronal circuits known to support spatial working memory, namely mPFC neuronal circuits and the long range hippocampal projections that are likely to allow the synchronization between hippocampal and mPFC neuronal networks (Laroche et al., 2000; Benchenane et al., 2010). To achieve this, we performed whole-cell patch clamp recordings from mPFC neurons in acute slices of *Ophn1* WT and KO mice (Figure 4 and 5). First, we compared various passive cellular properties of recorded mPFC neurons, but failed in identifying any genotype-based differences (see table 2) with one noticeable exception: the holding current was found to be higher in KO cells, suggesting that mPFC neurons were slightly more depolarized (see statistical values in table 1). The spiking pattern activities were also comparable between WT and KO mice (Figure 4B). Next, we tested the functionality of hippocampal projections to layer V IL cells (see methods) using an optogenetic approach based on the stereotaxic injection of an AAV-ChR2-GFP within caudal hippocampus (Figure 4C) (Zhang et al., 2015). We then photo-stimulated long-range hippocampal fibres carrying channel-rhodopsin in mPFC slices to allow the recording of direct monosynaptic excitatory transmission (Figure 4C2) and the feed-forward recruitment of local mPFC interneurons. Their activation by

hippocampal inputs lead to a GABAA-mediated outward current at a holding potential of 0 mV and that is delayed by a few milliseconds (Figure 4C3). Importantly, these two synaptic conductance are thought to be involved in the control of behaviourally relevant neuronal assemblies and in their synchronization during spatial working memory dependent tasks (Rolls et al., 2008). Interestingly, these projections appeared to be functionally preserved when *Ophn1* is mutated in mice (Figure 4C). Although some hippocampal projections towards specific mPFC cell populations may be impacted by *Ophn1* deletion, it suggested us that behavioural deficits must reside from local neuronal networks defects either in hippocampus or in mPFC.

PKA increases synaptic noise in the prefrontal cortex of Ophn1 KO mice.

Neuronal networks have to extract meaningful sensory evoked signal from background synaptic noise, the level of which depends on several neuromodulators and signalling pathways, including those involving PKA (Geurts et al., 2004; Arnsten et al., 2005; Rolls et al., 2008). We therefore recorded the spontaneous excitatory synaptic events in mPFC neurons from WT and KO mice. In control conditions, both in voltage and current-clamp mode, we detected a strong increase in the frequency of spontaneous excitatory events in *Ophn1* KO preparations, without any effect on event amplitudes (sEPSP frequency WT *VS* KO: p=0,004, Figure 5A2; sEPSC frequency WT *VS* KO: p<0,001, Figure 5B2).

Next, we tested for possible involvement of PKA activity in controlling spontaneous excitatory transmission in mPFC slices (Figure 5C). Beforehand, we wanted to confirm our previous results that PKA activity was increased in some but not all brain regions in *Ophn1* KO mice {Khelfaoui:2014bi}. To this aim, we run biochemical analysis of PKA-mediated phosphorylation in homogenates from *Ophn1* WT and KO prefrontal cortices (material and methods and Figure 5B). Using an anti phospho-PKA-target antibody, we compared PKA mediated phosphorylation levels between WT and KO mice (Figure 5B1-B3): A moderate but significant increase of phosphorylation levels of PKA targets was observed in *Ophn1* KO samples (Total labeling WT vs KO, p<0,05, Figure 5B3), confirming previous results obtained with enzymatic assay in mouse cerebral cortex homogenates.

Then, sEPSC frequency was assessed in WT and KO slices in presence of PKA-signaling antagonist cAMPS-Rp (100µM) or PKA-signalling agonist cAMPS-Sp (50µM)(Figure 5B). Interestingly, PKA modulators were efficient in affecting sEPSC frequency recorded in mPFC neurons in both genotypes, but measured frequencies in low-PKA (cAMP-Rp) and high-PKA (cAMP-Sp) conditions were indistinguishable between genotypes (cAMPS-Sp: sEPSC frequency WT *VS* KO: p=0,798, Figure 5B2). Thus the increased "synaptic noise" observed in *Ophn1* KO mPFC preparations may result from higher endogenous PKA activity level, and possibly to neuronal cell depolarization (see above). Interestingly, under the presence of the well-tolerated and permeable PKA pathway antagonist cAMPS-Rp, the sEPSC frequency in *Ophn1* KO preparations was comparable to the one found in WT mice (cAMPS-Rp: sEPSC frequency WT *VS* KO: p=0.289, Figure 5B2), akin to a process of normalisation of synaptic noise levels *in vivo* in *Ophn1*-deficient mice (Taylor et al., 1999).

Increasing PKA activity in mPFC of WT mice mimicked Ophn1 KO phenotype.

At first, we tested whether PKA activity changes in mPFC were necessary and sufficient to mimic the SWM deficits observed in *Ophn1* KO mice. To achieve this, we manipulated PKA activity levels in the mPFC of WT and KO mice running the DSA test. To that end, mice were implanted to allow intra-mPFC delivery of PKA modulators prior to the DSA test sessions (Figure 6). We first tried to reproduce previous experiments showing that an increase of PKA levels in PFC impacts SWM performance in WT mice (Taylor et al., 1999). Here, as in Figure 3, the success rate scoring was sorted according to the absence or presence of a "VTE" behaviour. A first group of WT animals were implanted within mPFC or dorsal hippocampus (Figure 6B) and submitted to DSA learning (Figure 6A). After accomplishment of the DSA learning, animal performance was collected the day before, during and the day after (Taylor et al., 1999) intra-mPFC injection of the well-tolerated PKA agonist (cAMPS-Sp, 1µg/µl) (Taylor et al., 1999), The results showed that increased PKA activity in mPFC affected not only the local network activity (Figure 5C) but also animal performances (success rate: WT drug cAMP-Sp *VS* before or *VS* after: p<0,001, Figure 6C1 and 6C2) with a pronounced decrease in the occurrence of VTE behaviours (VTE: drug *VS* before or *VS* after: p<0,001, Figure 6F, left panel), and a non-significant difference in the success rate with VTE behaviour (Success rate with VTE: drug *VS* before or *VS* after:

p=0.784, Figure 6F, right panel). In addition, we also noticed the appearance of high rank errors (high rank errors: drug *VS* before or *VS* after: p=0.002, Figure 6C2), indicating perseveration behaviour. Interestingly, similar results were obtained following mPFC injections of 6-BNZ-cAMP (10µg/µl), a PKA activator with a strong selectivity for PKA over Epac (see discussion section) (high rank errors: drug *VS* before or *VS* after: p<0,001, Figure 6E). Thus, an increase of PKA activity in mPFC - but not dorsal hippocampus, see Figure 6D - is sufficient to mimic the deficit in SWM tests that we observed in *Ophn1* KO mice.

Decreased PKA activity in PFC of KO mice restores cognitive performance

We then directly tested whether PKA hyperactivity in mPFC of *Ophn1* KO mice is the primary cause for DSA performance and perseveration behaviour. For this, we scored KO animals performance while PKA activity was decreased in the PFC through local infusion of cAMPS-Rp (10 µg/µl; Figure 7). As a control, we analysed the effect of a similar treatment performed in WT animals (Figure 7C, left panels) or in the dorsal hippocampus of KO mice (Figure 7D). In KO - but not WT animals (Figure 7C) - decreasing PKA activity in the mPFC significantly improved SWM performance: indeed, all treated KO mice displayed a noticeable increase of success rate (success rate WT drug *VS* before or *VS* after: p=0.684, success rate KO drug *VS* before or *VS* after: p<0.001, Figure 7C1) accompanied with a decrease of high rank errors (high rank errors KO before *VS* drug *VS* after: p<0.001, Figure 7C2). The same pharmacological treatment applied in dHPC of KO mice had no positive effect on DSA test (Figure 7D) as for lower dose of cAMPS-Rp in mPFC of KO mice (1 µg/µl; data not shown).

Finally, to determine if we achieved a real normalization of animal VTE behaviour, we also scored VTE/wavering occurrence and its relation to success rates. The tested group of mice were bilaterally implanted in both in mPFC and dHPC, in which cAMPS-Rp could be allowed to diffuse successively in dHPC and mPFC with a five day protocol (Figure 7E1): As shown in Figure 7, mPFC – but not dHPC - infusion was associated with a significant increase of VTE (VTE occurrence KO: mPFC drug *VS* all other conditions: p<0.001, Figure 7E2), which was observed together with an increase in the choice accuracy in VTE trials (choice accuracy KO: mPFC drug *VS* all other conditions: p<0.001, Figure 7E3).

Therefore, our results collectively lead us to propose that PKA hyperactivity associated with *Ophn1* deficiency in mice is necessary and sufficient to explain the spatial alternation deficit.

Discussion

In the present work, we thoroughly characterized a pronounced behavioural phenotype displayed by *Ophn1* deficient mice in a Y-maze based spatial working memory test. Our results led us to conclude that the poor performance of KO mice results from a lack of deliberation (VTE/wavering) during decision-making and to cognitive (low choice accuracy even when VTE/wavering is present) and adaptive (no self-correction leading to perseverative behaviour) deficits. Meanwhile, we could establish that *Ophn1* deficiency is accompanied by an increase of excitatory synaptic noise in the mPFC. Interestingly, we could phenocopy *Ophn1* deficiency phenotype in the DSA test through the local activation of PKA in WT mPFC. Finally, our attempts to inhibit the pathological PKA hyperactivity in KO mPFC corrected all observed behavioural deficits (Figure 8).

PKA activity and synaptic noise in absence of *Ophn1*.

Peak performance at a DSA test has been shown to depend on mobilization of neuronal assemblies in the mPFC following hippocampal instructions, that synchronizes circuit activities in the theta range (Benchenane et al., 2010). Importantly, computational studies suggest that activation of mPFC networks, that have been proposed to allow pattern completion during cognitive processes such as working memory, is sensitive to synaptic noise (Rolls et al., 2008). In line with a previous study (Khelfaoui et al., 2014), the present data obtained using electrophysiological approaches support the notion that hyperactivity of PKA in *Ophn1*-deficient mice generated synaptic noise in mPFC region (see Figure 5). If it is well known that PKA-mediated phosphorylation of RhoA and ROCK could inhibit RhoA pathway (Newell-Litwa et al., 2011), yet the origin for the increased PKA activity in *Ophn1* deficient mice remains to be understood. It may result from the loss of function of its Rho-GAP activity and translational and/or post-translational driven feedback mechanism controlling RhoA activity (Nusser et al., 2006). To our knowledge, no evidences are available for a direct link between PKA and Ophn1. Some answers may be provided by a more detailed analysis of AKAPs (A Kinase-Anchoring Proteins; a family of scaffold proteins that regulate PKA activity) in neuronal populations (Diviani et al., 2006; Wang et al., 2006).

Synaptic noise in mPFC region is thought to cause some of the phenotypes observed in schizophrenic patients, that typically exhibited reduced signal-to-noise ratio and reduced phase locking in the prefrontal cortex (Winterer et al., 2000). Among many mechanisms, cAMP/PKA signaling pathway seems well-positioned to finely tune the signal-to-noise ratio. Indeed, dopamine release in the PFC is thought to mimic the reward prediction signal and efficiently modulate PFC-HPC synchrony during DSA test (Benchenane et al., 2010), as well as tune the signal-to-noise ratio within mPFC networks (Rolls et al., 2008). Furthermore, DA release within the mPFC involves cAMP/PKA-dependent signalling (Arnsten et al., 2005), opening the possibility that the hyperactivity of PKA in *Ophn1*-deficient mice could shunt the ability of dopaminergic inputs to provide rewarding signals within the mPFC. This absence could contribute to the absence of self-correction during the DSA test, thus generating the perseverative behaviour. Interestingly, because a normalization of KO animal behaviour is obtained even after training is completed, the reward circuits allowing rule learning and reinforcement must be maintained in absence of *Ophn1*. Future experiments will be required to test how *Ophn1* deletion may disrupt dopaminergic modulation by changing cAMP/PKA signaling activity.

Separating cognitive and deliberative deficits using DSA test.

Interestingly, Benchenane and collaborators showed that the level of PFC-HPC synchrony prior to the entrance of the crossroad point in the Y-maze was correlated with choice accuracy and hence renamed as the “decision point”. We here show that choice accuracy at the decision point is also highly correlated with the occurrence of a VTE/wavering behaviour, typified by deceleration at the crossroad point and slow motion sequence preceded by a subsequent acceleration (Figure 3A1), thereby reproducing pioneer studies describing VTE behaviours (see (Redish, 2016)). Therefore, VTE/wavering at the decision point is considered as a reliable indication of working memory processing and deliberation leading to decision making (Figure 3B). If combined with choice accuracy determination, it could help in characterizing real SWR-related decisions (VTE *VS* no VTE) and cognitive-related choices (accuracy of “VTE trials”). This further dissection of the behavioural sequence allowed a better understanding of the poor performance of *Ophn1* KO mice. Thus, the incorrect choices

could be attributed both to a deliberation deficit adding onto cognitive-based failures even when they do pay attention to the task (Figure 3). Strikingly, all these parameters were completely normalized following pharmacological PKA activity correction within the mPFC but not in the dHPC (Figure 7), thus shedding light onto the crucial role of PKA deregulation associated with *Ophn1* deficiency within the prefrontal cortex in this cognitive task. An interesting observation is the normalization of high accuracy-related VTE behaviours in PKA-manipulated KO mice, thus showing the capacity of prefrontal circuits in establishing relevant cognitive actions even though *Ophn1* expression is absent in this structure.

Pharmacological correction of behaviour in trained OPHN1 deficient adult mice.

We believe that our findings are opening a new avenue in the understanding of the pathophysiology of intellectual disabilities by showing that some of very handicapping consequences of monogenic mutations may be largely accessible to pharmacological treatment in affected adults. Another interesting finding reported here is that the poor performance of *Ophn1* mutated animals in the Y-maze test was not due to defective learning capabilities, but rather due to a lack of behavioural control normally assumed by the prefrontal cortex during the DSA task. Indeed, we could phenotypically normalize animal behaviour after the training procedure was terminated, demonstrating that the KO mice acquired the DSA rule during the learning phase. Together with the observation that dHPC PKA modulations in WT and KO mice did not display strong effects (Figures 6 and 7), we propose that the described increase in PKA activity in the hippocampus of *Ophn1* KO mice (Khelfaoui et al., 2014) and the related lack of PKA dependent LTP at DG-CA3 synapses did not play major role in DSA coding in mice. Similarly, synaptic deficits were previously reported in hippocampal circuits due to *Ophn1* deletion (Nadif Kasri et al., 2009; Nakano-Kobayashi et al., 2009; Nadif Kasri et al., 2011; Powell et al., 2012; Nakano-Kobayashi et al., 2014). Even though these may reflect important direct cellular and molecular consequences to the deletion, they may not be central to the presently described cognitive impairment.

Recent studies have shown that in addition to PKA, cAMP activates the guanine nucleotide exchange factor cAMP-GEF (Epac) (Kawasaki et al. 1998; de Rooij et al. 1998) thereby controlling HCN channels (see Wang et al., 2007). However, in contrast

to PKA, Epac do not seems to activate CREB in vitro. (ref). We first measured HCN channels activity in mPFC cells from Ophn1 WT and KO mice, but could not find any difference in the outward current generated during hyperpolarizing steps (ref method, data not shown) in both conditions. Next, we used conditional Ophn1 animals to test if deletion of Ophn1 was sufficient to lead to P-CREB increase in a cell autonomous way. Indeed when compared to non-transfected cells, mPFC cells in which Ophn1 was deleted exhibited higher P-CREB levels as their un-transfected neighbours, as assessed by P-CREB immunochemistry (see methods, data not shown). Although not definitively excluding any effect of Ophn1 condition on Epac signaling, these experiments strongly support that a cell-specific increase in PKA activity is associated with the loss of function of Ophn1 in the mPFC, at the origin of an increase in synaptic noise in this structure.

To conclude, we report here that *Ophn1* deficiency in mice leads to an unanticipated destabilization of the cAMP/PKA signaling pathway that is causing a major incapacity to access working memories. As pharmacological approaches successfully restored normal performance and physiological parameters, we think that our report is opening a new therapeutic avenue for *Ophn1*-related syndromes. Beyond this, it should contribute to the heterogeneity of pathological consequences of *Ophn1* deficiencies in humans.

REFERENCES

Arnsten AFT, Ramos BP, Birnbaum SG, Taylor JR (2005) Protein kinase A as a therapeutic target for memory disorders: rationale and challenges. Trends Mol Med 11:121–128.

Benchenane K, Peyrache A, Khamassi M, Tierney PL, Gioanni Y, Battaglia FP, Wiener SI (2010) Coherent theta oscillations and reorganization of spike timing in the hippocampal- prefrontal network upon learning. Neuron 66:921–936.

Billuart P, Bienvenu T, Ronce N, Portes des V, Vinet MC, Zemni R, Roest Crollius H, Carrié A, Fauchereau F, Cherry M, Briault S, Hamel B, Fryns JP, Beldjord C, Kahn A, Moraine C, Chelly J (1998) Oligophrenin-1 encodes a rhoGAP protein involved in X-linked mental retardation. Nature 392:923–926.

Di Prisco GV, Huang W, Buffington SA, Hsu C-C, Bonnen PE, Placzek AN, Sidrauski C, Krnjević K, Kaufman RJ, Walter P, Costa-Mattioli M (2014) Translational control of mGluR-dependent long-term depression and object-place learning by eIF2α. Nat Neurosci 17:1073–1082.

Diviani D, Baisamy L, Appert-Collin A (2006) AKAP-Lbc: a molecular scaffold for the integration of cyclic AMP and Rho transduction pathways. Eur J Cell Biol 85:603–610.

Geurts HM, Geurts HM, Verté S, Verté S, Oosterlaan J, Oosterlaan J, Roeyers H, Roeyers H, Sergeant JA, Sergeant JA (2004) How specific are executive functioning deficits in attention deficit hyperactivity disorder and autism? J Child Psychol Psychiatry 45:836–854.

Gordon JA (2011) Oscillations and hippocampal-prefrontal synchrony. Curr Opin Neurobiol 21:486–491.

Houbaert X, Zhang CL, Gambino F, Lepleux M, Deshors M, Normand E, Levet F, Ramos M, Billuart P, Chelly J, Herzog E, Humeau Y (2013) Target-Specific Vulnerability of Excitatory Synapses Leads to Deficits in Associative Memory in a Model of Intellectual Disorder. Journal of Neuroscience 33:13805–13819.

Humeau Y, Herry C, Kemp N, Shaban H, Fourcaudot E, Bissière S, LUthi A (2005) Dendritic Spine Heterogeneity Determines Afferent-Specific Hebbian Plasticity in the Amygdala. Neuron 45:119–131.

Jay TM, Gurden H, Yamaguchi T (1998) Rapid increase in PKA activity during long-term potentiation in the hippocampal afferent fibre system to the prefrontal cortex in vivo. Eur J Neurosci 10:3302–3306.

Kesner RP, Churchwell JC (2011) An analysis of rat prefrontal cortex in mediating executive function. Neurobiol Learn Mem 96:417–431.

Khelfaoui M, Denis C, van Galen E, de Bock F, Schmitt A, Houbron C, Morice E, Giros B, Ramakers G, Fagni L, Chelly J, Nosten-Bertrand M, Billuart P (2007) Loss of X-linked mental retardation gene oligophrenin1 in mice impairs spatial

memory and leads to ventricular enlargement and dendritic spine immaturity. J Neurosci 27:9439–9450.

Khelfaoui M, Gambino F, Houbaert X, Ragazzon B, Müller C, Carta M, Lanore F, Srikumar BN, Gastrein P, Lepleux M, Zhang C-L, Kneib M, Poulain B, Reibel-Foisset S, Vitale N, Chelly J, Billuart P, LUthi A, Humeau Y (2014) Lack of the presynaptic RhoGAP protein oligophrenin1 leads to cognitive disabilities through dysregulation of the cAMP/PKA signalling pathway. Philos Trans R Soc Lond, B, Biol Sci 369:20130160.

Laroche S, Davis S, Jay TM (2000) Plasticity at hippocampal to prefrontal cortex synapses: dual roles in working memory and consolidation. Hippocampus 10:438–446.

Meziane H, Khelfaoui M, Morello N, Hiba B, Calcagno E, Reibel-Foisset S, Selloum M, Chelly J, Humeau Y, Riet F, Zanni G, Herault Y, Bienvenu T, Giustetto M, Billuart P (2016) Fasudil treatment in adult reverses behavioural changes and brain ventricular enlargement in Oligophrenin-1 mouse model of intellectual disability. Human Molecular Genetics 25:2314–2323.

Nadif Kasri N, Nakano-Kobayashi A, Malinow R, Li B, Van Aelst L (2009) The Rho-linked mental retardation protein oligophrenin-1 controls synapse maturation and plasticity by stabilizing AMPA receptors. Genes Dev 23:1289–1302.

Nadif Kasri N, Nakano-Kobayashi A, Van Aelst L (2011) Rapid synthesis of the X-linked mental retardation protein OPHN1 mediates mGluR-dependent LTD through interaction with the endocytic machinery. Neuron 72:300–315.

Nakano-Kobayashi A, Kasri NN, Newey SE, Van Aelst L (2009) The Rho-linked mental retardation protein OPHN1 controls synaptic vesicle endocytosis via endophilin A1. Curr Biol 19:1133–1139.

Nakano-Kobayashi A, Tai Y, Kasri NN, Van Aelst L (2014) The X-linked mental retardation protein OPHN1 interacts with Homer1b/c to control spine endocytic zone positioning and expression of synaptic potentiation. Journal of Neuroscience 34:8665–8671 Available at: http://eutils.ncbi.nlm.nih.gov/entrez/eutils/elink.fcgi?dbfrom=pubmed&id=24966368&retmode=ref&cmd=prlinks.

Newell-Litwa KA, Newell-Litwa KA, Horwitz AR, Horwitz AR (2011) Cell migration: PKA and RhoA set the pace. Curr Biol 21:R596–R598.

Nusser N, Gosmanova E, Makarova N, Fujiwara Y, Yang L, Guo F, Luo Y, Zheng Y, Tigyi G (2006) Serine phosphorylation differentially affects RhoA binding to effectors: implications to NGF-induced neurite outgrowth. Cell Signal 18:704–714.

Piton A et al. (2011) Systematic resequencing of X-chromosome synaptic genes in autism spectrum disorder and schizophrenia. Mol Psychiatry 16:867–880.

Powell AD, Gill KK, Saintot P-P, Jiruska P, Chelly J, Billuart P, Jefferys JGR (2012) Rapid reversal of impaired inhibitory and excitatory transmission but not spine

dysgenesis in a mouse model of mental retardation. The Journal of Physiology 590:763–776.

Redish AD (2016) Vicarious trial and error. Nat Rev Neurosci 17:147–159.

Rolls ET, Rolls ET, Loh M, Loh M, Deco G, Deco G, Winterer G, Winterer G (2008) Computational models of schizophrenia and dopamine modulation in the prefrontal cortex. Nat Rev Neurosci 9:696–709.

Sumiyoshi C, Kawakubo Y, Suga M, Sumiyoshi T, Kasai K (2011) Impaired ability to organize information in individuals with autism spectrum disorders and their siblings. Neurosci Res 69:252–257.

Taylor JR, Birnbaum S, Ubriani R, Arnsten AF (1999) Activation of cAMP-dependent protein kinase A in prefrontal cortex impairs working memory performance. Journal of Neuroscience 19:RC23.

van Bokhoven H (2011) Genetic and epigenetic networks in intellectual disabilities. Annu Rev Genet 45:81–104.

Wang G-W, Cai J-X (2006) Disconnection of the hippocampal–prefrontal cortical circuits impairs spatial working memory performance in rats. Behav Brain Res 175:329–336.

Wang Y, Chen Y, Chen M, Xu W (2006) AKAPs competing peptide HT31 disrupts the inhibitory effect of PKA on RhoA activity. Oncol Rep 16:755–761.

Wikenheiser AM, Redish AD (2015) Hippocampal theta sequences reflect current goals. Nat Neurosci 18:289–294.

Winterer G, Ziller M, Dorn H, Frick K, Mulert C, Wuebben Y, Herrmann WM, Coppola R (2000) Schizophrenia: reduced signal-to-noise ratio and impaired phase-locking during information processing. Clin Neurophysiol 111:837–849.

Zhang C-L, Houbaert X, Lepleux M, Deshors M, Normand E, Gambino F, Herzog E, Humeau Y (2015) The hippocampo-amygdala control of contextual fear expression is affected in a model of intellectual disability. Brain Struct Funct 220:3673–3682.

FIGURE LEGENDS

Figure 1: *Ophn1*-deficient mice are incompetent at spatial working memory tests, and exhibit perseverative behaviour.

A: protocol used for testing for spatial working memory performance in Ophn1 WT and KO mice. After habituation, the learning phase includes 80 trials separated into 4 sessions of 20 trials (10+10, with 3 hours delay) conducted in 4 consecutive days. A retrieval test (10+10 trials) is run 2-3 days after learning. High rank errors are defined as errors repeated more than twice (attempt#2-#5). **B:** Example of individual scoring exhibited by a WT or a KO mouse during the protocol. **C1**: Time course of the success rate in WT and KO mice during the learning and retrieval phases. The dashed line denotes a 0.5 success rate dictated by random choice. **C2**: Bar graphs showing the evolution of the different choices occurrence (marked in colors in accordance with individual scoring in panel B) along the spatial working memory procedure in WT (top) and KO (bottom) mice.

Figure 2: *Ophn1*-deficient mice show deficit in spontaneous alteration task, but not in other Y-maze based tasks.

A: The exploration activity and spatial preference of *Ophn1* WT and KO mice were tested by counting the total number of arm entries (left panel) or entries into each arm (right panel). **B:** Natural tendency of mice in turning left or right was also tested. **C:** Spatial reference memory was tested using spatial novelty task (see methods), and was not impaired in *Ophn1* KO mice. Number of animals is indicated. **D:** Based on the innate tendency of mice to explore a prior unvisited arm, regular/irregular choices were defined. KO mice displayed less such tendency than their WT littermate in spontaneous alteration task, which indicates a spatial working memory problem.

Figure 3: *Ophn1* KO mice display deliberation and cognitive deficits at spatial working memory tests.

A1: Examples of mouse video-tracking in the Y-maze showing typical “wavering” as VTE or “no wavering” NO VTE trajectories at the bifurcation (choice) area of the maze (zoom in insert). Speed of motion is color-coded from blue (low) to red (high). **A2**: Bar

graph showing the occurrence of VTE/wavering in WT and KO mice. **B1-B3**: Detailed analysis of the success rates depending on the occurrence of VTE. Note that when no VTE/wavering is measured, the success rate is random in both genotypes (B2), whereas upon VTE behaviour high success rates are observed (B3). However, KO mice performance upon VTE remains lower than that of WT mice. Number of analyzed trials is indicated.

Figure 4: *In vitro* electrophysiological recordings did not reveal a functional impact of the mutation on hippocampo-mPFC interconnections.

A: Scheme of the acute slice preparation in which IL and PL neurons were recorded using whole cell patch clamp technique. **B:** Spiking activities of mPFC neurons in WT and KO preparations were indistinguishable. Numbers of recorded cells is indicated. **C**: Study of hippocampal-mPFC feed-forward circuits using optogenetic stimulation. An AAV-ChR2-YFP vector was injected into caudal hippocampus to allow stimulating direct hippocampal projections to the mPFC following delivery of flashes of blue light (1ms, 470 nm). mPFC neurons were recorded at -70 and 0 mV to allow detecting monosynaptic EPSCs (C2-C3) and di-synaptic IPSCs (C3). **C2**: Input/output curves of light evoked EPSCs in both genotypes. C3: Relative amplitude of light-evoked di-synaptic IPSCs in both genotypes. Numbers of recordings is indicated. Typical recordings are shown in inserts.

Figure 5: *Ophn1* deficiency leads to a PKA-dependent increase of synaptic noise in the mPFC.

A1: typical recordings of spontaneous excitatory potentials, and KO preparations show more frequent events. **A2**: Bar graphs showing the sEPSP frequency in mPFC neurons in WT (grey) and KO (orange) preparations. **B**: PKA-mediated phosphorylation was tested using western blots and anti-phospho-PKA target antibodies. **B1-B3**: Ophn1 KO samples showed increased signal intensities as compared to WT homogenates. Number of animals is indicated. *:$p<0.05$. **C:** Modulation of spontaneous EPSCs frequency by pharmacological manipulations of PKA activity. **C1**: typical electrophysiological recordings in the various tested conditions. cAMPS-Rp: competitive inhibiting cAMP-dependent PKA; cAMPS-Sp: competitive activating cAMP-dependent PKA (for further details see text). **C2**: Bar

graph showing the average excitatory drives received by mPFC neurons in control conditions and following application of cAMPS-Rp or cAMPS-Sp. Numbers of recordings is indicated.

Figure 6: Increasing PKA activity in mPFC phenocopies *Ophn1* KO performance drop at the DSA test.

A: Experimental scheme includes cannula implantation, learning of DSA rule, and 3 sessions of testing before, during and after delivery of the PKA activators cAMPS-Sp or 6-BNZ-cAMP in the mPFC or in the dHPC of WT animals. **B:** injection loci for all included animals. **C, D** and **E:** Scoring of the success rate of WT animal performance at the DSA test before, upon and after drug delivery in the mPFC (C, E) or dHPC (D). **F:** VTE/wavering expression and consecutive choice accuracy was analyzed in the cAMP-sp/mPFC condition. Numbers of analyzed trials is indicated.

Figure 7: Complete phenotypic normalization of *Ophn1 KO* mice following pharmacological inactivation of PKA in the mPFC.

A: Description of our protocol that includes cannula implantation, learning of DSA rule, and 3 testing sessions done before, during and after delivery of the PKA blocker cAMPS-Rp in mPFC or dHPC of KO and WT animals. **B:** Injection loci for all included animals. **C:** Scoring of the success rate of WT and KO animal performance at the DSA test before/during/after cAMPS-Rp application in mPFC. Number of animals is indicated. Note that upon cAMPS-Rp infusion, success rate of KO animals improves, and high rank error rate strongly decreases. **D:** A similar cAMPS-Rp infusion within dHPC of KO animals did not reproduce the effects within mPFC. **E1:** a group of mice was implanted both bilaterally in dHPC and mPFC in order to assess for VTE/wavering occurrence and choice accuracy (as in figure 2). cAMPS-Rp was successively injected in dHPC and then in mPFC. **E2:** Effect of cAMPS-Rp injection on the occurrence of VTE. Note the strong increase observed following mPFC injection. **E3:** Scoring of the choice accuracy following a VTE/wavering behaviour. Number of trials is indicated.

Figure 8: Results Summary.

A: Pharmacological tools acting on various kinases that have been used or discussed in *in vivo* experiments on *Ophn1*-deficient mice in the present study. **B:** Scheme

describing the proposed sequence of molecular, cellular, network events leading to behavioral perseveration in *Ophn1* KO mice.

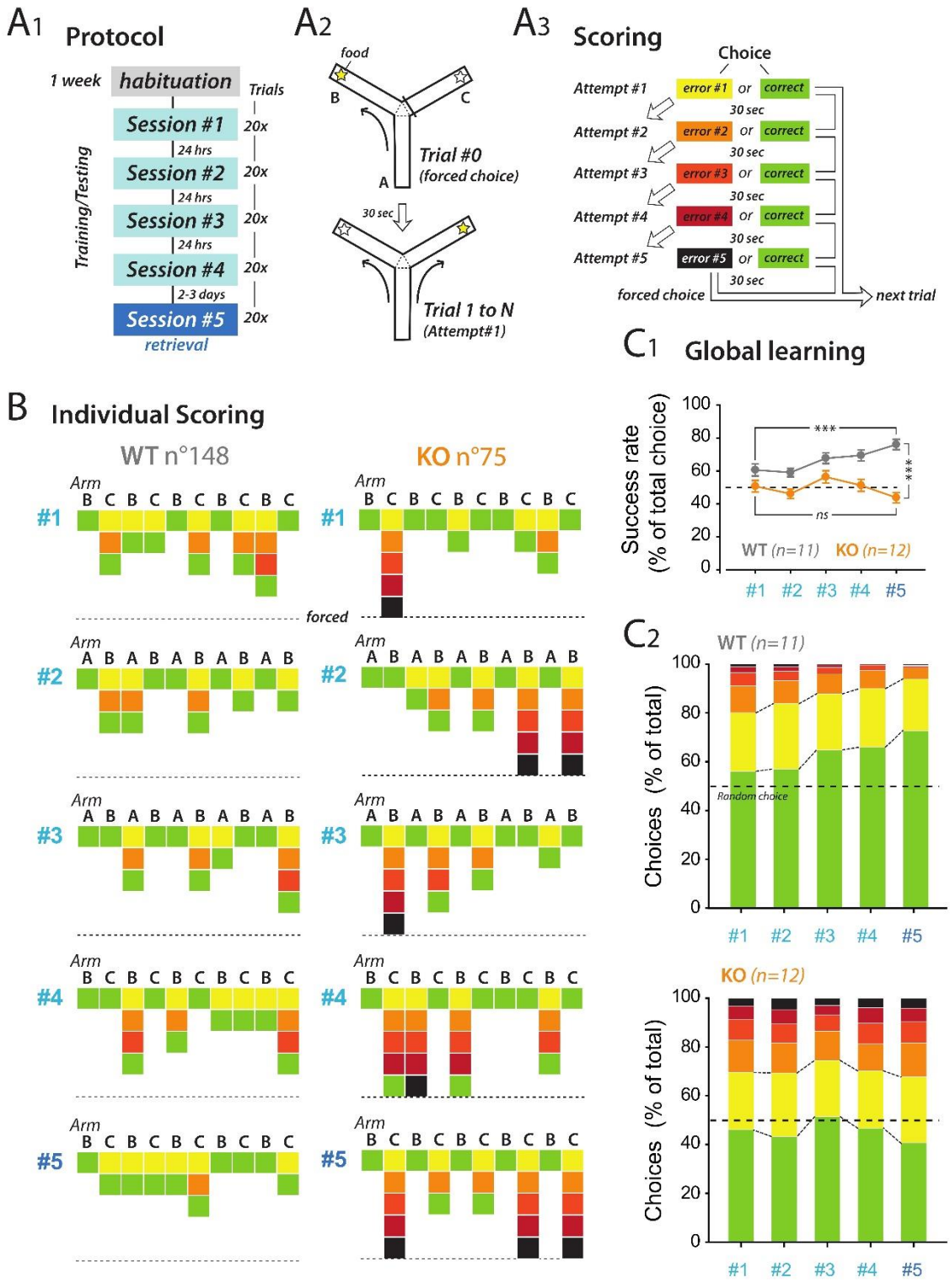
A1 Protocol
1 week
habituation
Trials
Training/Testing
Session #1
20x
24 hrs
Session #2
20x
24 hrs
Session #3
20x
24 hrs
Session #4
20x
2-3 days
Session #5
20x
retrieval
A2
food
B
C
A
Trial #0
(forced choice)
30 sec
Trial 1 to N
(Attempt#1)
A3 Scoring
Choice
Attempt #1
error #1
or
correct
30 sec
Attempt #2
error #2
or
correct
30 sec
Attempt #3
error #3
or
correct
30 sec
Attempt #4
error #4
or
correct
30 sec
Attempt #5
error #5
or
correct
30 sec
forced choice
next trial
B Individual Scoring
WT n°148
KO n°75
Arm
#1
#2
#3
#4
#5
forced
C1 Global learning
Success rate
(% of total choice)
***
***
ns
WT (n=11)
KO (n=12)
C2
WT (n=11)
KO (n=12)
Choices (% of total)
Random choice

Figure 1.

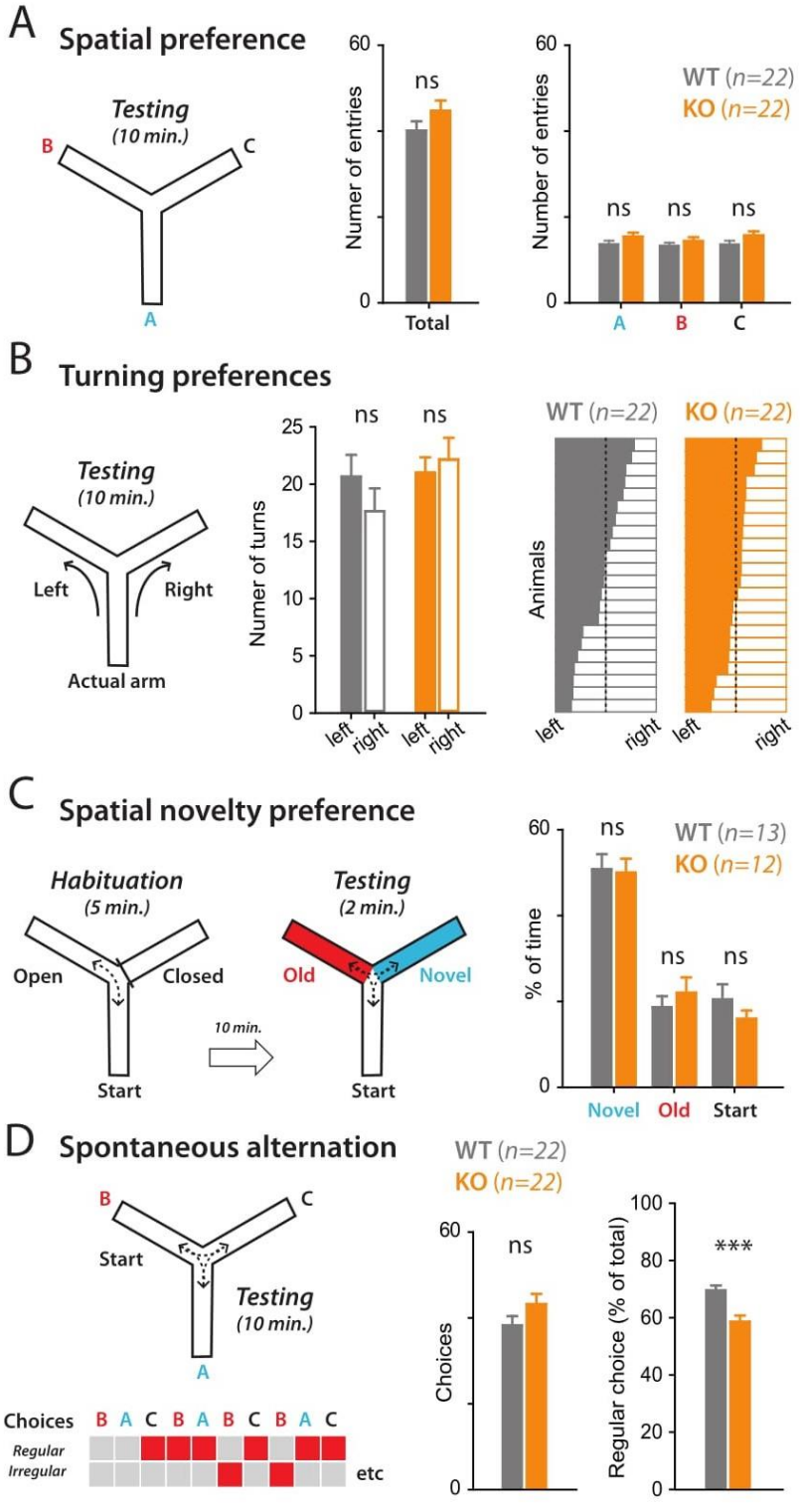
A
Spatial preference
Testing
(10 min.)
B
C
A
Numer of entries
60
0
ns
Total
Number of entries
WT (n=22)
KO (n=22)
ns ns ns
A B C
B
Turning preferences
Testing
(10 min.)
Left
Right
Actual arm
Numer of turns
25
20
15
10
5
0
ns ns
left right left right
WT (n=22)
KO (n=22)
Animals
left right left right
C
Spatial novelty preference
Habituation
(5 min.)
Open
Closed
Start
10 min.
Testing
(2 min.)
Old
Novel
Start
% of time
60
0
ns ns ns
WT (n=13)
KO (n=12)
Novel Old Start
D
Spontaneous alternation
B
C
Start
Testing
(10 min.)
A
Choices B A C B A B C B A C
Regular
Irregular
etc
WT (n=22)
KO (n=22)
Choices
60
0
ns
Regular choice (% of total)
100
80
60
40
20
0
***

Figure 2.

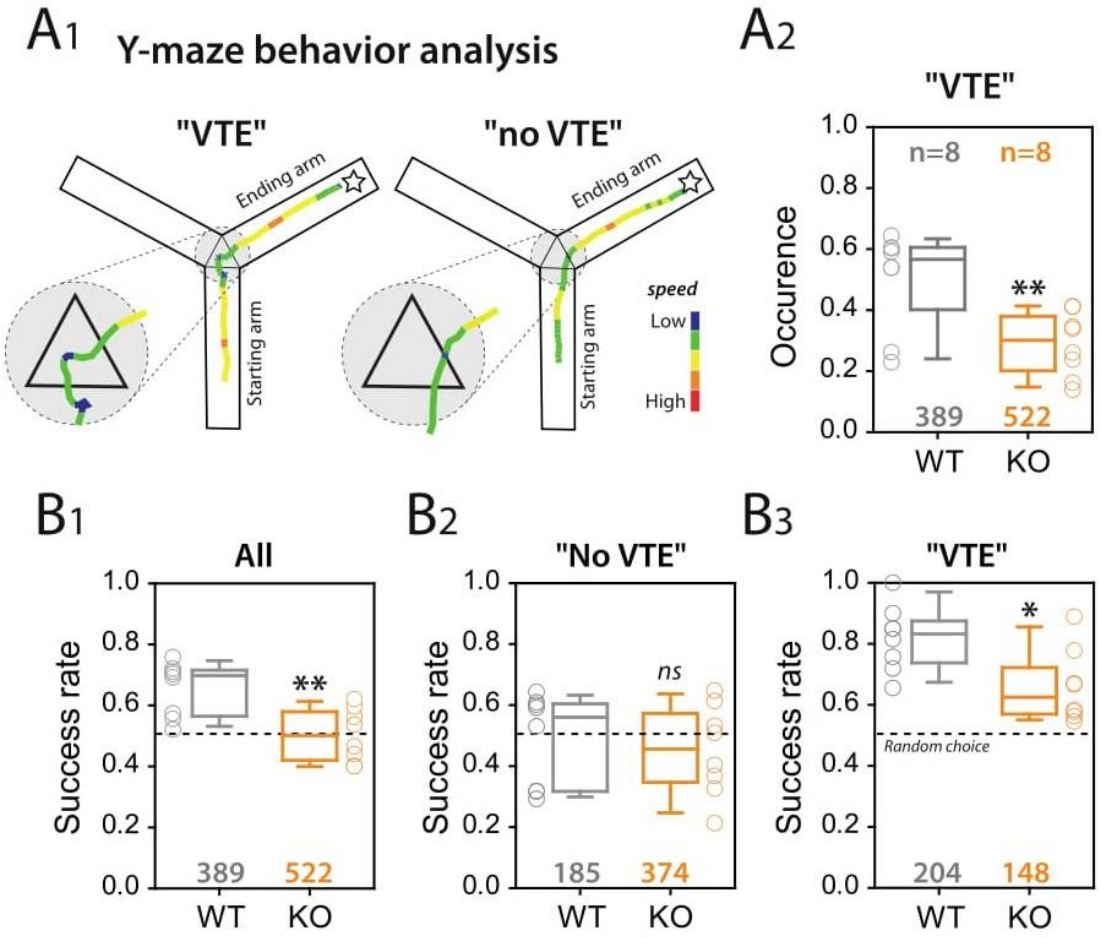
A1
Y-maze behavior analysis
"VTE"
"no VTE"
Ending arm
Starting arm
speed
Low
High
A2
"VTE"
n=8
n=8
Occurence
**
389
522
WT
KO
B1
All
Success rate
**
389
522
WT
KO
B2
"No VTE"
ns
185
374
WT
KO
B3
"VTE"
*
Random choice
204
148
WT
KO

Figure 3.

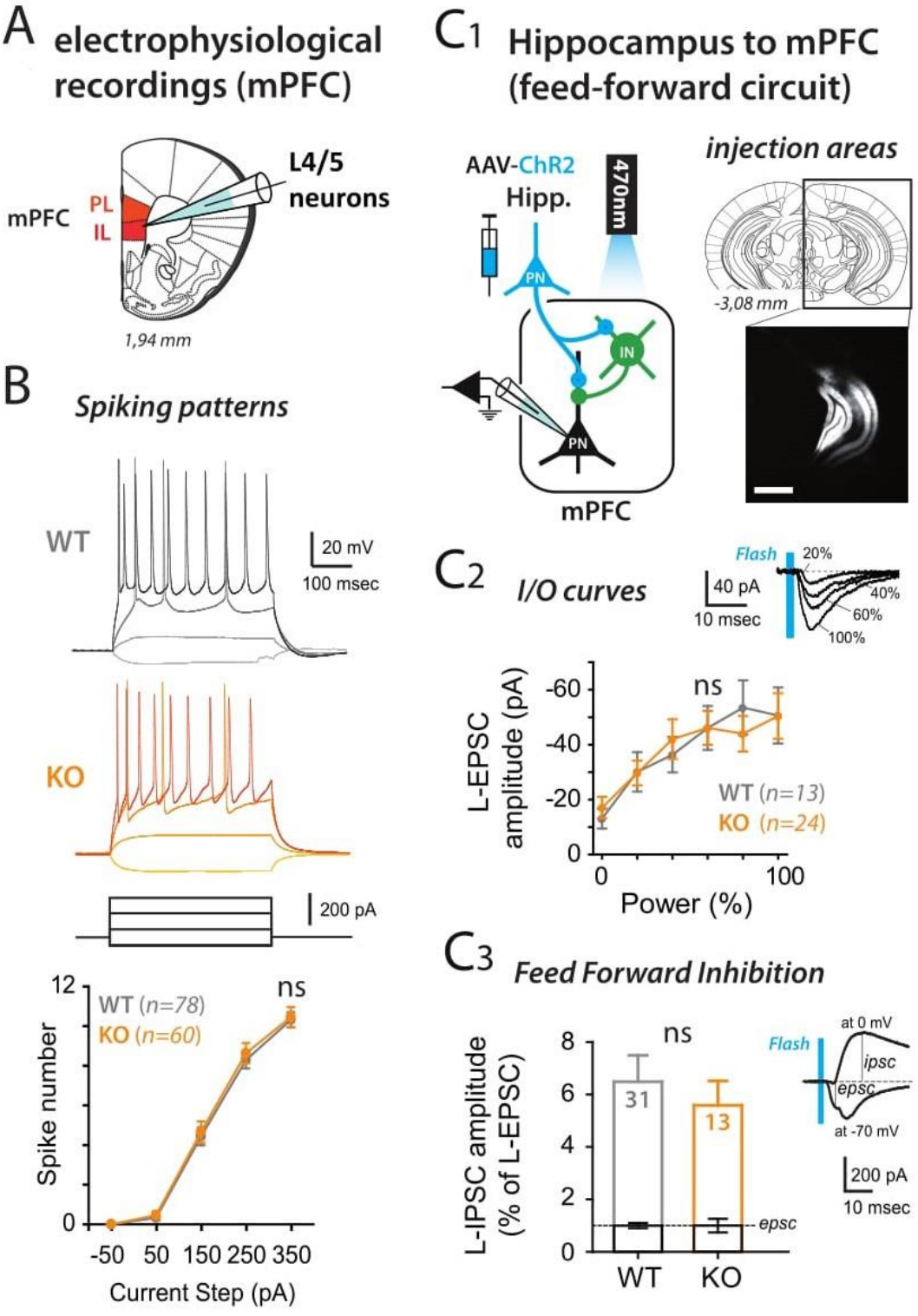
A
electrophysiological recordings (mPFC)
mPFC
PL
IL
L4/5 neurons
1,94 mm
B
Spiking patterns
WT
20 mV
100 msec
KO
200 pA
12
WT (n=78)
KO (n=60)
ns
Spike number
0
-50 50 150 250 350
Current Step (pA)
C1
Hippocampus to mPFC (feed-forward circuit)
AAV-ChR2
Hipp.
470nm
PN
IN
PN
mPFC
injection areas
-3,08 mm
C2
I/O curves
Flash
20%
40%
60%
100%
40 pA
10 msec
L-EPSC amplitude (pA)
-60
-40
-20
0
ns
WT (n=13)
KO (n=24)
0
100
Power (%)
C3
Feed Forward Inhibition
L-IPSC amplitude (% of L-EPSC)
8
6
4
2
0
ns
31
13
epsc
WT
KO
Flash
at 0 mV
ipsc
epsc
at -70 mV
200 pA
10 msec

Figure 4.

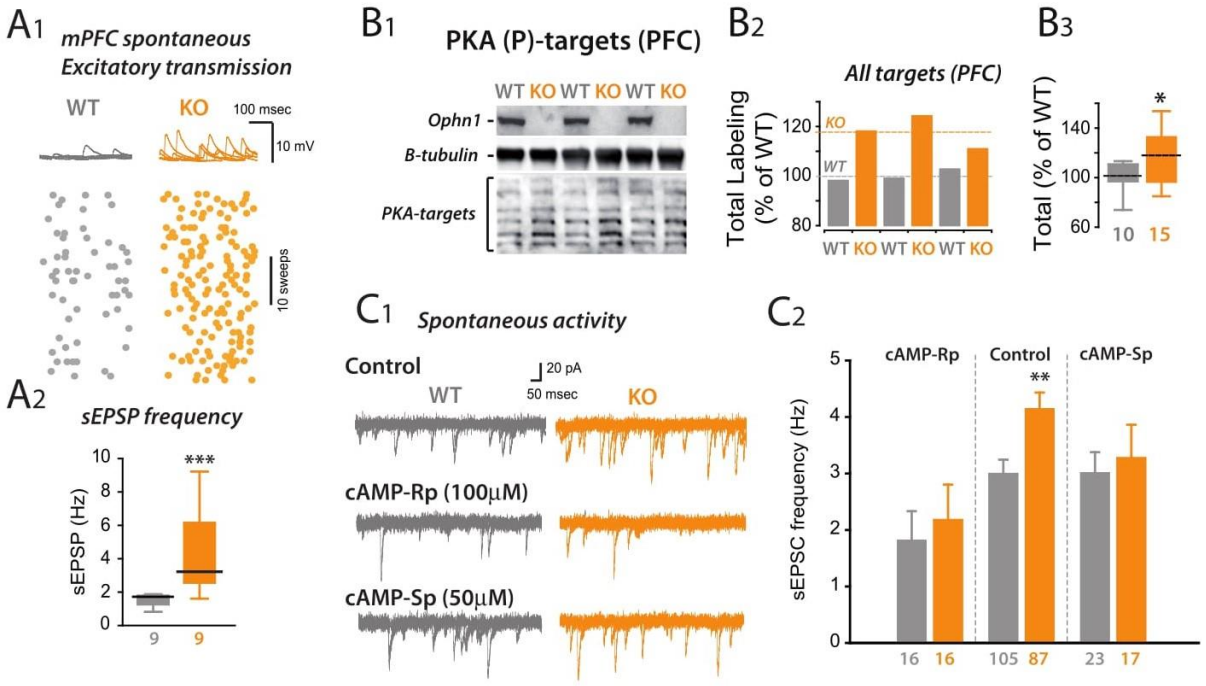
A1
mPFC spontaneous
Excitatory transmission
WT
KO
100 msec
10 mV
10 sweeps
A2
sEPSP frequency
sEPSP (Hz)
***
9
9
B1
PKA (P)-targets (PFC)
WT KO WT KO WT KO
Ophn1
B-tubulin
PKA-targets
B2
All targets (PFC)
Total Labeling
(% of WT)
KO
WT
WT KO WT KO WT KO
B3
Total (% of WT)
*
10
15
C1
Spontaneous activity
Control
20 pA
50 msec
WT
KO
cAMP-Rp (100μM)
cAMP-Sp (50μM)
C2
cAMP-Rp
Control
cAMP-Sp
sEPSC frequency (Hz)
**
16
16
105
87
23
17

Figure 5.

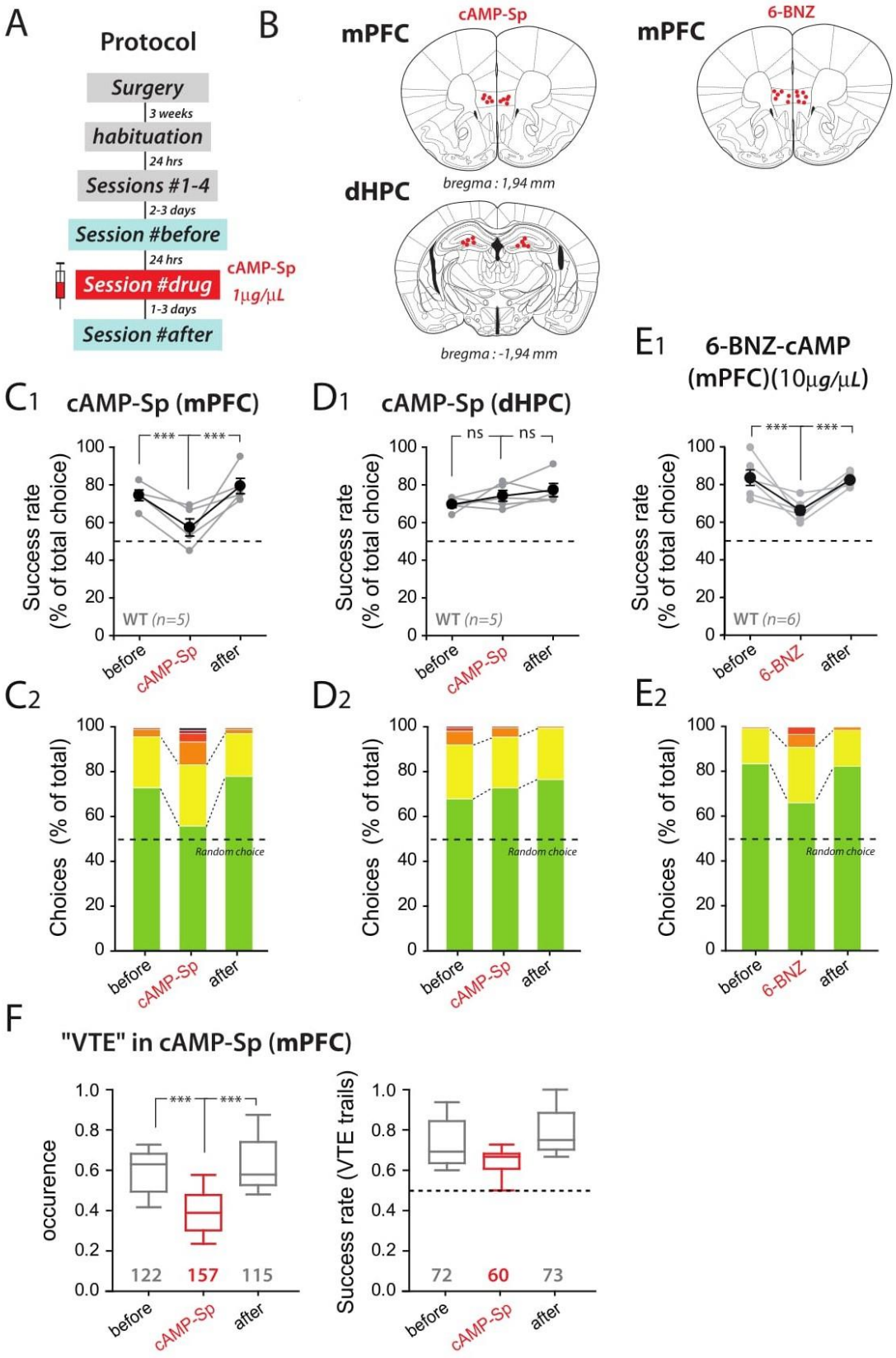
A
Protocol
Surgery
3 weeks
habituation
24 hrs
Sessions #1-4
2-3 days
Session #before
24 hrs
Session #drug
cAMP-Sp
1µg/µL
1-3 days
Session #after
B
mPFC
cAMP-Sp
bregma : 1,94 mm
dHPC
bregma : -1,94 mm
mPFC
6-BNZ
C1
cAMP-Sp (mPFC)
Success rate (% of total choice)
WT (n=5)
before
cAMP-Sp
after
D1
cAMP-Sp (dHPC)
ns
WT (n=5)
E1
6-BNZ-cAMP (mPFC)(10µg/µL)
WT (n=6)
6-BNZ
C2
Choices (% of total)
Random choice
D2
E2
F
"VTE" in cAMP-Sp (mPFC)
occurence
122
157
115
Success rate (VTE trails)
72
60
73

Figure 6.

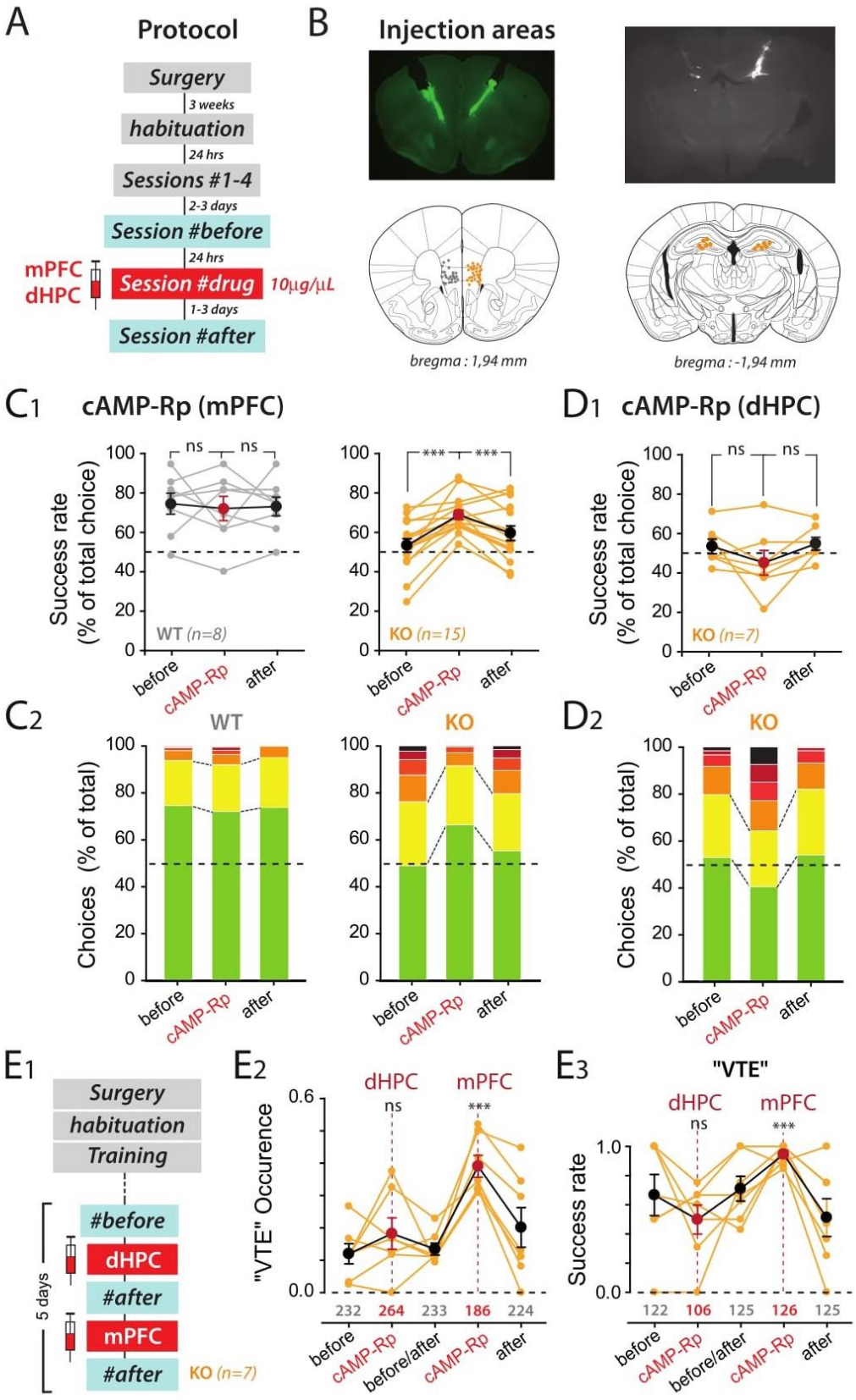
A
Protocol
Surgery
3 weeks
habituation
24 hrs
Sessions #1-4
2-3 days
Session #before
24 hrs
mPFC
dHPC
Session #drug
10µg/µL
1-3 days
Session #after
B
Injection areas
bregma : 1,94 mm
bregma : -1,94 mm
C1
cAMP-Rp (mPFC)
Success rate (% of total choice)
WT (n=8)
KO (n=15)
D1
cAMP-Rp (dHPC)
KO (n=7)
before
cAMP-Rp
after
ns
***
C2
WT
KO
Choices (% of total)
D2
E1
Surgery
habituation
Training
5 days
#before
dHPC
#after
mPFC
#after
KO (n=7)
E2
dHPC
mPFC
"VTE" Occurence
232
264
233
186
224
before/after
E3
"VTE"
122
106
125
126
125

Figure 7.

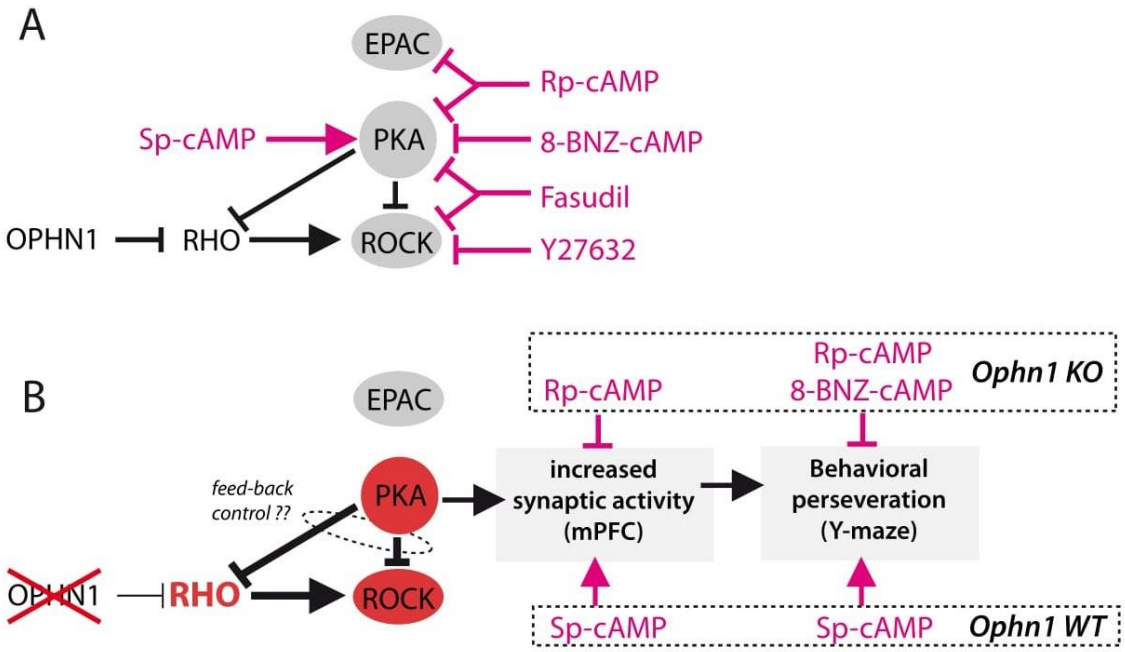
A
EPAC
Rp-cAMP
Sp-cAMP
PKA
8-BNZ-cAMP
Fasudil
OPHN1
RHO
ROCK
Y27632
B
Rp-cAMP
Rp-cAMP
8-BNZ-cAMP
Ophn1 KO
EPAC
feed-back
control ??
PKA
increased
synaptic activity
(mPFC)
Behavioral
perseveration
(Y-maze)
OPHN1
RHO
ROCK
Sp-cAMP
Sp-cAMP
Ophn1 WT

Figure 8.